| | |
|---|---|
| **Titre:** Title: | Localization of Solid Micro and Nano-Inclusions in Heterophase Bioplastic Blends |
| **Auteur:** Author: | Ebrahim Jalali Dil |
| **Date:** | 2015 |
| **Type:** | Mémoire ou thèse / Dissertation or Thesis |
| **Référence:** Citation: | Jalali Dil, E. (2015). Localization of Solid Micro and Nano-Inclusions in Heterophase Bioplastic Blends [Thèse de doctorat, École Polytechnique de Montréal]. PolyPublie. https://publications.polymtl.ca/1821/ |

UNIVERSITÉ DE MONTRÉAL

# LOCALIZATION OF SOLID MICRO AND NANO-INCLUSIONS IN HETEROPHASE BIOPLASTIC BLENDS

EBRAHIM JALALI DIL

DÉPARTEMENT DE GÉNIE CHIMIQUE

ÉCOLE POLYTECHNIQUE DE MONTRÉAL

THÈSE PRÉSENTÉE EN VUE DE L'OBTENTION

DU DIPLÔME DE PHILOSOPHIAE DOCTOR

(GÉNIE CHIMIQUE)

AOÛT 2015

UNIVERSITÉ DE MONTRÉAL

ÉCOLE POLYTECHNIQUE DE MONTRÉAL

Cette thèse initulée:

# LOCALIZATION OF SOLID MICRO AND NANO-INCLUSIONS IN HETEROPHASE BIOPLASTIC BLENDS

présentée par : JALALI DIL Ebrahim

en vue de l'obtention du diplôme de : Philosophiae Doctor

a été dûment acceptée par le jury d'examen constitué de :

M. VIRGILIO Nick, Ph. D., président

M. FAVIS Basil, Ph. D., membre et directeur de recherche

M. AJJI Abdellah, Ph. D., membre

Mme KONTOPOULOU Marianna, Ph. D., membre

# DEDICATION

*To my family and my wife*

# ACKNOWLEDGMENTS

First and foremost, praise and thanks to Almighty God for his guidance and blessing throughout my life.

I would like to express my deepest gratitude to my supervisor, Professor Basil Favis, for his support, patience, immense knowledge and for providing me with a friendly and comfortable atmosphere for doing research. His vision and motivation have deeply inspired me and it was a great privilege to work and study under his guidance.

I also would like to thank Professor Pierre Carreau for his insightful comments and suggestions on the first part of the project.

A special word of thanks is owed to Dr. Vahid Khoshkava, Dr. Amir Saffar, Dr. Amirhossein Maani and Dr. Hesam Ghasemi for their help during this study.

I also would like to thank Professor Uttandaraman Sundararaj, Dr. Mohammad Arjman and Yan Li for their help and comments on the collaborative part of the project.

I would like to extend my gratitude to my friends Arash, Richard, Ali, Vahid and Jun for the fruitful discussions we have had. I greatly value their friendship and I deeply appreciate their help.

I also would like to thank the technical and administrative staff of the Chemical Engineering Department of École Polytechnique de Montréal.

Last but not least, I would like to thank my parents and sisters, who have always supported me throughout my life. A special thanks to my wife, Zahra, who has always stood by me and supported me through the good times and bad.

# RÉSUMÉ

Le mélange de poly (acide lactique), PLA, et autres bioplastiques à haute résistance à l'impact a été introduit en tant que méthode efficace pour améliorer la ténacité du PLA. Toutefois, cette stratégie réduit considérablement le module d'Young et la résistance mécanique du PLA. L'ajout de particules solides est une méthode bien connue pour réconcilier l'équilibre rigidité / ténacité des matrices polymères. Bien que l'importance de contrôler la localisation des inclusions solides dans des mélanges de polymères soit mise en évidence, la littérature échoue à fournir une analyse détaillée des mécanismes de migration et n'identifie pas en détail les conséquences des paramètres thermodynamiques et cinétiques relatifs à la localisation de particules solides dans des mélanges de polymères.

Dans ce mémoire, la localisation et la migration des particules de micro- et nano-silice sphériques dans deux mélanges de bioplastiques, soit : PLA / polyéthylène basse densité (LDPE) et PLA / poly (butylène adipate-co-téréphtalate), PBAT, ont été étudiés.

Dans la première partie de ce travail, une étude détaillée de la miscibilité et du développement de la morphologie dans le mélange PLA / PBAT a été réalisée. Une tension interfaciale de 0,6 ± 0,15 mN / m a été déterminée pour le couple PLA et PBAT en ajustant le modèle de Palierne sur les données rhéologiques. La miscibilité du PLA / PBAT a ensuite été examinée en étudiant le décalage de la température de transition vitreuse (Tg) des phases de polymère à différentes compositions. Les résultats obtenus indiquent une miscibilité partielle unidirectionnelle limitée des molécules de PBAT dans la phase riche en PLA. Cette miscibilité partielle dépend significativement du poids moléculaire du PBAT, qui reflète son caractère entropique. L'analyse de la morphologie des échantillons a montré que la phase dispersée dans les mélanges de PLA / PBAT existe sous la forme de fibres, même à basse composition de 1% en vol. de la phase dispersée. Enfin, la région de co-continuité dans les mélanges de PLA / PBAT a été déterminée en utilisant une approche rhéologique. Il a été montré que le mélange PLA / PBAT a une région de co-continuité symétrique large située entre 30 à 40 et 60 à 70 vol.% de PBAT.

Dans la deuxième partie de ce projet, la localisation et la migration des particules de silice dans les mélanges de PLA / PBAT ont été étudiés. Basé sur les énergies de surface mesurées du PLA et PBAT, le modèle d'Young prédit que la position d'équilibre thermodynamique des particules de silice se situe dans la phase de PBAT. Suite à l'ajout de particules de silice au PLA / PBAT

fondu, les particules de micro- et nano-silice ont été localisées dans la phase de PBAT quelle que soit la viscosité de la phase de PLA. Il a été démontré que cette localisation sélective se produit lors des premières étapes de mélange et a été attribuée à la tension interfaciale inférieure du couple PBAT / silice par rapport au couple PLA / silice. L'influence des paramètres cinétiques a été étudié en effectuant le pré-mélange des particules de silice avec la phase PLA, ainsi, les particules étaient localisées dans la phase thermodynamiquement défavorable. Il a été constaté que la migration des particules de micro-silice à partir de la phase PLA à l'interface dépend fortement de la viscosité de la phase PLA, du taux de cisaillement lors du mélange et de la taille des particules de silice. Ces résultats mettent en évidence le rôle critique de l'étape du retrait du film de PLA entre les particules de micro-silice et l'interface. Suite au pré-mélange de particules de nano-silice dans la phase PLA, une localisation stable à l'interface PLA/PBAT a été constatée, quel que soit la viscosité de la phase PLA. En utilisant un modèle semi-empirique récemment mis au point pour déterminer la vitesse de migration de particules sphériques à l'interface, il a été montré que la localisation stable des particules de silice à l'interface est dû à la vitesse de migration très lente à l'interface, qui provient de la faible tension interfaciale entre le PLA et le PBAT.

Dans la dernière partie de cette thèse, les effets des paramètres thermodynamiques et cinétiques sur la migration et la localisation des particules de micro- et nano-silice dans un mélange à haute tension interfaciale de PLA / LDPE ont été étudiés. La surface des particules de micro-silice a été modifié par greffage de (2-Dodecen-1-yl) d'anhydride succinique en utilisant une nouvelle approche de réaction en phase gazeuse. Les localisations d'équilibre thermodynamique de particules de silice non-modifiées et modifiées ont été déterminées comme étant dans la phase PLA et à l'interface, respectivement. Il a été constaté que l'addition de particules de silice non-modifiées et modifiées à une masse fondue de PLA et de LDPE haute viscosité (H-LDPE) résulte en l'encapsulation préférentielle des particules de la phase avec laquelle ils ont la plus faible tension interfaciale. Les effets des paramètres cinétiques ont été étudiés en pré-mélangeant des particules de silice avec la phase H-LDPE suivi du mélange avec le PLA. Il a été constaté que le retrait du film de LDPE entre les particules et l'interface joue un rôle critique dans l'inhibition de la migration des particules de micro-silice non-modifiées et modifiées vers le PLA et l'interface, respectivement. D'autre part, lorsque les particules de nano-silice ont été utilisées, les particules individuelles de nano-silice ont pu migrer vers la phase PLA , tandis que les agrégats de nano-

silice sont restés dans la phase H-LDPE. Ces résultats indiquent que la localisation de nanoparticules bien dispersées dans un mélange de polymères à haute tension interfaciale est peu susceptible d'être influencée par les effets cinétiques.

En comparant les résultats obtenus pour la localisation des particules de silice dans les mélanges PLA/PBAT et PLA/LDPE, une perspective générale des paramètres importants dans le contrôle de la migration et de la localisation des particules dans les mélanges de polymères est présenté

# ABSTRACT

Blending poly(lactic acid), PLA, with other high impact bioplastics has been introduced as an effective method for improving the toughness of PLA; however, this strategy considerably reduces the modulus and mechanical strength of PLA. The addition of solid particles is a well-known method for tuning the stiffness/toughness balance in toughened polymer matrices. Notwithstanding the significance of controlling the localization of solid inclusions in polymer blends, the literature is lacking a detailed analysis of the migration mechanisms and the effects of thermodynamic and kinetic parameters on the localization of solid particles in polymer blends.

In this dissertation, the localization and migration of spherical micro- and nano-silica particles in two bioplastic blends of PLA/low density polyethylene (LDPE) and PLA/poly(butylene adipate-co-terephthalate), PBAT, were studied.

In the first part of this work, a detailed study on the miscibility and morphology development in the PLA/PBAT blend was carried out. The interfacial tension between PLA and PBAT was determined to be 0.6 ± 0.15 mN/m by fitting Palierne's model on the rheological data. The miscibility of PLA/PBAT was then examined by studying the shift in the glass transition temperature (Tg) of the polymer phases at different blend compositions. The obtained results indicate a limited one-way partial miscibility of PBAT molecules in the PLA-rich phase. This partial miscibility depends significantly on the molecular weight of PBAT, which underlines its entropic nature. The morphology analysis of the blend samples revealed that the dispersed phase in PLA/PBAT blends exists in the form of fibers, even at low compositions of 1 vol.% of the dispersed phase. Finally, the co-continuity region in PLA/PBAT blends was determined using a rheological approach and it was shown that PLA/PBAT has a wide symmetric co-continuous region located between 30-40 and 60-70 vol.% of PBAT.

In the second part of this project, the localization and migration of the silica particles in PLA/PBAT blends were studied. Based on the measured surface energies of PLA and PBAT, Young's model predicts that the thermodynamic equilibrium localization of the silica particles should be in the PBAT phase. When the silica particles were added to a PLA/PBAT melt, micro- and nano-silica particles were localized in the PBAT phase irrespective of the PLA phase viscosity. This selective localization was shown to occur at the early stages of mixing and was attributed to the lower interfacial tension of PBAT/silica compared to PLA/silica. The influence

of kinetic parameters was imposed by the premixing of the silica particles with the PLA phase, which is the least thermodynamically preferred phase. It was found that the migration of micro-silica particles from the PLA phase to the interface depends strongly on the viscosity of the PLA phase, the shear rate of mixing and the particle size of the silica. These results point to the critical role of the PLA film draining between micro-silica particles and the interface. When nano-silica particles were premixed in the PLA phase, they were localized at the interface in a stable fashion irrespective of the PLA phase viscosity. Using a newly developed semi-empirical model for the migration velocity of spherical particles at the interface, it was shown that the stable localization of silica particles at the interface is due to the very slow migration velocity at the interface, which originates from the low interfacial tension between PLA and PBAT.

In the last part of the thesis, the effects of thermodynamic and kinetic parameters on the migration and localization of micro- and nano-silica particles in a high interfacial tension blend of PLA/LDPE were studied. The surface of the micro-silica particles was modified by the grafting of (2-dodecen-1-yl) succinic anhydride using a new gas phase reaction approach. The thermodynamic equilibrium localizations of unmodified and modified silica particles were determined to be in the PLA phase and at the interface, respectively. It was found that the addition of unmodified and modified silica particles to a melt of PLA and high viscosity LDPE (H-LDPE) results in the preferential encapsulation of the particles by the phase with which they have the lowest interfacial tension. The effects of kinetic parameters were studied by premixing silica particles with the H-LDPE phase followed by mixing with PLA. It was found that the draining of the LDPE film between the particles and the interface plays a critical role in inhibiting the migration of both unmodified and modified micro-silica particles toward the PLA phase and the interface, respectively. On the other hand, when nano-silica particles were used, individual nano-silica particles could migrate to the PLA phase, while the nano-silica aggregates remained in the H-LDPE phase. These results indicate that the localization of well-dispersed nanoparticles in a high interfacial tension polymer blend system is unlikely to be significantly influenced by the kinetic effects.

By comparing the obtained results on the localization of silica particles in PLA/PBAT and PLA/LDPE, a general perspective of the important parameters in controlling the migration and localization of the particles in polymer blends is presented.

# TABLE OF CONTENTS

# LIST OF TABLES

# LIST OF FIGURES

# LIST OF SYMBOLS AND ABBREVIATIONS

***English Letters:***

| | |
|---|---|
| *Ca* | capillary Number |
| $Ca_{crit}$ | critical Capillary Number |
| *G** | complex modulus |
| *G'* | storage Modulus |
| p | dispersed phase/matrix viscosity ratio |
| Tg | glass transition temperature |
| Mw | molecular weight |
| $W_a$ | work of adhesion |
| D | diameter |
| $P_r$ | probability of a successful collision in coalescence |
| $E_{DK}$ | bulk breaking energy of dispersed phase |
| $W_i$ | weight percent of component i |
| $A_f$ | surface area of the film in film draining |
| $F_c$ | contact force of a particle to the interface |

***Greek letters:***

| | |
|---|---|
| $\Delta G_m$ | Gibbs free energy of mixing |
| $\chi_{AB}$ | Flory-Huggins interaction parameter |
| ρ | density |
| φ | volume fraction |
| ΔH | enthalpy of mixing |
| $\gamma_{ij}$ | interfacial tension between component i and j |

| | |
|---|---|
| $\gamma_i$ | surface tension of component i |
| $\gamma_i^d$ | non-polar (dispersive) component of surface energy of component i |
| $\gamma_i^p$ | polar component of surface energy of component i |
| $\alpha$ | amplitude of sinusoidal distortions in breaking thread |
| $\eta_m$ | matrix viscosity |
| $\eta_0$ | zero-shear viscosity |
| $\eta^*$ | complex viscosity |
| $\eta'$ | real part of the complex viscosity |
| $\eta''$ | imaginary part of the complex viscosity |
| $\tau$ | shear stress |
| $\omega$ | wetting parameter |
| $\dot{\gamma}$ | Shear rate |
| $\delta_C$ | critical film thickness in film draining |
| $\delta_C$ | initial film thickness in film draining |

***List of Abbreviations:***

| | |
|---|---|
| PLA | poly(lactic acid) |
| PHA | polyhydroxyalkanoate |
| PE | polyethylene |
| PA | polyamide |
| PBAT | poly(butylene adipate-co-terephthalate) |
| PBS | poly(butylene succinate) |
| PCL | polycaprolactone |
| PLLA | poly(L-lactic acid) |

| | |
|---|---|
| PET | polyethylene terephthalate |
| HDPE | high density polyethylene |
| LDPE | low density polyethylene |
| LLDPE | linear low density polyethylene |
| SAN | styrene–acrylonitrile |
| PS | polystyrene |
| PP | polypropylene |
| EPDM | ethylene propylene diene monomer |
| PC | polycarbonate |
| DMA | dynamic mechanical analysis |
| GMA | glycidyl methacrylate |
| XPS | x-ray photoelectron spectroscopy |
| TPS | thermoplastic starch |
| ABS | acrylonitrile butadiene styrene |
| MA | maleic anhydride |
| EPR | ethylene propylene rubber |
| CB | carbon black |
| CNT | carbon nanotube |
| PBT | polybutylene terephthalate |
| TGA | thermogravimetric analysis |
| POE | polyolefin elastomer |
| MMT | organoclay |
| PEO | polyethylene oxide |
| EOC | poly(ethylene-co-octene) |

| | |
|---|---|
| PA6 | polyamide 6 or nylon 6 |
| PA11 | polyamide 11 |
| PA12 | polyamide 12 |
| PB | polybutadiene |

# CHAPTER 1 INTRODUCTION

Polymers from renewable resources have received an increasing amount of attention over the last two decades due to environmental concerns and finite petroleum resources[1]. As a result, the production of bioplastics has increased significantly in recent years. According to the latest annual report of the European Bioplastic Organization[2], the global production capacity of bioplastics in 2012 reached 1.5 million tons per year and is expected to grow by 400% in 2017. Therefore, in the near future, bioplastics will be a key player in the polymer market.

Among different bioplastics, poly(lactic acid), PLA, has attracted considerable attention as it is not only a bio-based polymer but also can be composted in industrial plants [1, 3]. The most important weaknesses of PLA are its poor impact properties, low heat deflection temperature (HDT), moisture sensitivity and thermal degradation [3]. Different strategies have been used to improve the poor toughness and impact strength of PLA such as plasticization, copolymerization with other polyesters and blending with other bioplastics [4-26]. Among them, the blending of PLA with other bioplastics has received much attention as it is economical and through using this method not only the brittleness but also other properties of PLA can be modified[6]. Among blends of PLA with bioplastics, blends of PLA with polycaprolactone (PCL) and poly(butylene adipate-co-terephthalate) (PBAT) have been studied extensively as these two bioplastics have much higher impact strength and elongation at break compared to most bioplastics. Moreover, PCL and PBAT are produced in an industrial scale and are available in the market, which makes them potential candidates for achieving a high performance PLA blend at a reasonable price. On the other hand, the low melting temperature of PCL limits the application of PLA/PCL blends and, therefore, PLA/PBAT blends can offer a much wider application range. Presenting blends of PLA/PBAT under the trademark of Ecovio® by BASF is clear evidence of this claim. However, many important aspects of PLA/PBAT such as miscibility and morphology have not yet been studied in detail. Therefore, it is necessary to carry out a comprehensive analysis of these aspects of PLA/PBAT. In addition, the commercial production of bio-based polyethylene (bio-PE) using ethylene manufactured from sugar cane ethanol has recently been undertaken. According to the annual report of the European Bioplastics Organization [2], the global production capacity of bio-PE has passed that of PLA in 2013. Currently, bio-based HDPE and bio-based LDPE (bio-LDPE) exist in the market. Considering the higher impact and elongation at break of bio-LDPE, blends

of PLA/bio-LDPE have a significant commercial potential to be introduced as a fully bio-based high performance polymer blend.

Due to all the factors mentioned above, blends of PLA/PBAT and PLA/LDPE were chosen as the bioplastic blends in this study. However, due to the limited access to bio- LDPE, petroleum-based LDPE was used in this research study. It is worth mentioning that the processing and final properties of bio-LDPE are similar to petroleum-based LDPE.

The most important drawback of blending PLA with PBAT or LDPE is the drop in the mechanical strength and stiffness compared to neat PLA. The addition of solid inclusions is a well-known method for achieving a balance between toughness and stiffness in polymer blends [27-29]. Moreover, it has been shown that the addition of conductive solid particles such as carbon nanotubes not only improves the mechanical properties but also can enhance electrical conductivity[30]. However, all previous studies point to the important role of controlling the localization of solid particles in achieving the desired mechanical properties and/or electrical conductivity [31, 32]. Despite previous attempts, little knowledge exists on the mechanism of the migration and localization of solid particles in polymer blends. This can be attributed to the complexity of the analysis of the systems incorporating solid particles. For example, the rheology of these systems can be affected considerably by the addition of the particles. In addition, the complex shape of the particles and particle size distribution increase the complexity of interpreting the results. In addition, the level of the dispersion of the particles can also affect the results.

To eliminate these issues, spherical silica particles with a narrow particle size distribution ($D_{90}/D_{10}$ = 1.3) and a good dispersion were used in this study. Note that $D_{90}$ and $D_{10}$ refer to the particle diameters at 90% and 10% from the cumulative percent curve, respectively. Moreover, the spherical shape of these particles allowed us to use the rheological and thermodynamic equations that have been developed in the field of filled polymers, which are mainly based on the mono-dispersed spherical particle assumption. Two types of spherical silica with individual particle sizes of 100 nm and 300 nm were used to study the effect of the particle size on the migration and localization. These particles will be referred to as nano- and micro-silica, respectively. Note that according to ISO/TS 27687 and ASTM E2456-06, nanoparticles are defined as particles with at least one length dimension smaller than 100 nm. Therefore, in this

study the localization of spherical micro- and nano-silica particles in two bioplastic blends of PLA/PBAT and PLA/LDPE are studied. Considering all the aforementioned, the main objectives of this work are presented in the following section.

## 1.1 Objectives

The main objective of this project is *to control the preferential location of spherical micro- and nano-silica particles in heterophase bioplastic blends.* Thus, the following specific objectives are defined as the main milestones to achieving the main objective of this work:

- Investigate the miscibility and morphology development in PLA/PBAT blends.
- Determine the effect of thermodynamic and kinetic parameters on the localization and migration of micro- and nano-silica in a low interfacial tension system of PLA/PBAT.
- Study the localization and migration of micro- and nano-silica particles in a high interfacial tension PLA/LDPE blend.

# CHAPTER 2 LITERATURE REVIEW

## 2.1 Bioplastics

Each year more than 300 million tons of plastics, mostly non-biodegradable or compostable, are produced. The disposal of plastic waste into landfills has short and long-term negative ecological impacts. Despite the growing demand on the recycling of plastics as a solution, recycling cannot solely resolve this issue due to its cost and limited capacity. In addition, most of the commodity polymers are petroleum–based materials; therefore, limited oil and gas resources underline the need for these materials to be replaced by the plastics produced from renewable resources. Bioplastic materials have emerged as a new class of polymers that are bio-based and/or biodegradable. These unique characteristics of bioplastics have motivated the plastic industries and even consumers to consider them as the next generation of polymer materials. This new class of polymers is generally classified into three main categories:

1) bio-based and biodegradable (or compostable) polymers, such as starch, poly(lactic acid) or PLA, and polyhydroxyalkanoate (PHA).

2) bio-based or partially bio-based but non-biodegradable (or non-compostable) polymers, such as bio-polyethylene (bio-PE) and bio-polyamide 11 (bio-PA11).

3) petroleum-based but biodegradable (or compostable) polymers, such as poly(butylene adipate-co-terephthalate) or PBAT, poly(butylene succinate) or PBS, and polycaprolactone (PCL).

Despite the great potential of bioplastics, they have not been widely used in the plastic industry mainly due to their higher price and poor mechanical properties. Improving the production technology and increasing the production capacity of bioplastics are likely to reduce their final cost; however, the poor mechanical properties of these materials will still be a limiting factor. Figure 2.1 compares the modulus and elongation at break of some bioplastics. As can be seen, almost all bioplastics have either a low modulus or a low elongation at break, which indicates the lack of a balance between stiffness and toughness in these materials.

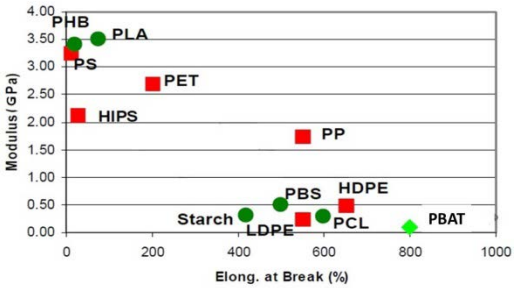


Figure 2.1. Modulus versus elongation at break for bioplastics and commodity polymers. The red symbols and the green symbols indicate synthetic polymers and bioplastics, respectively[33].

### 2.1.1 Poly (lactic acid)

Compared to other biodegradable polyesters, PLA has one of the highest commercial potential due to its availability in the market, its mechanical properties and its price [34]. The molecular structure of PLA is shown in Figure 2.2.

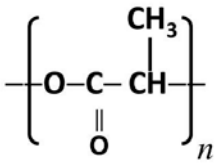


Figure 2.2. The molecular structure of PLA.

The most common method for the production of PLA is the ring opening polymerization (ROP) of cyclic lactide dimers [1]. Therefore, almost all commercial PLAs available in the market are polylactides. The properties of PLA are highly related to the ratio between its D and L mesoforms. At present, 100% L-PLA, PLLA, which is a highly crystalline polymer and copolymers of poly (L-lactic acid) and poly (D -lactic acid), which are rather amorphous, are commercially available. As can be seen in Figure 2.1, PLA is among the few bioplastics that have a mechanical strength comparable with the commodity polymers such as polystyrene (PS) and polyethylene terephthalate (PET). The main weaknesses of PLA are its brittleness, low barrier properties and low crystallization rate [1]. Anderson et al. [6] and Rasal et al. [26] reviewed different strategies for increasing the toughness of PLA including the variation of the ratio of D and L mesoforms, plasticization, copolymerization with other polyesters and blending with other

bioplastics. Among these approaches, blending with other bioplastics has received much attention as it is economical and through using this method not only the brittleness but also other properties of PLA can be improved [6]. The blending of PLA with other bioplastics will be discussed later in this chapter.

### 2.1.2 Poly (butylene adipate-co-terephthalate)

PBAT is a petroleum-based biodegradable aliphatic-aromatic copolyester which was first produced industrially by BASF in 1997. The molecular structure of PBAT consists of butylene terephthalate (BT) and butylene adipate (BA) segments as shown in Figure 2.3.

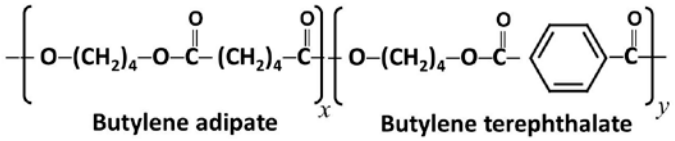


Figure 2.3. The molecular structure of PBAT.

PBAT is mainly manufactured for packaging applications and has processability, impact strength and elongation at break comparable to low density polyethylene (LDPE) [19]. On the other hand, unlike LDPE, the polyester nature of PBAT provides good compatibility with hydrophilic materials. Witt et al.[35] studied the biodegradability of PBAT and found no sign of environmental risk (eco-toxicity) after degradation.

### 2.1.3 Bio-Based Polyethylene

The low price, excellent chemical resistance, easy processing, high elongation at break and electrical insulation make polyethylene (PE) an excellent candidate for a wide range of applications. Recently, Braskem started the commercial production of bio-based high density polyethylene (bio-HDPE) and bio-based low density polyethylene (bio-LDPE) using ethylene manufactured from sugar cane ethanol. It is worth mentioning that the mechanical properties and performance of bio-PE are similar to those of petroleum-based PE. Braskem has also announced that they will use this approach to produce bio-based polypropylene (bio-PP). Therefore, it can be seen that bio-based polyolefins will soon be an important component of the bioplastics market.

### 2.1.4 Blends of PLA and Other Bioplastics

As mentioned before, the blending of PLA with other bioplastics has been introduced as an effective approach for improving the toughness of PLA. Blends of PLA with PCL [9, 36-38] and PBAT [10-12, 14-21, 39-42] have received much attention due to their high impact strength and elongation at break of PCL and PBAT. Moreover, the polyester nature of these polymers provides good compatibility with PLA. However, considering the low melting temperature of PCL (~60 $^{o}$C), PLA/PBAT blends can offer a much wider range of applications as a high performance compostable bioplastic material. On the other hand, the high impact strength and renewable resource of bio-PE indicate the potential of the PLA/bio-PE blend as a fully bio-based blend with improved mechanical properties [5, 7, 8, 43, 44]. Before reviewing the literature on PLA/PBAT and PLA/PE blends, some general concepts of polymer blends will first be reviewed in the next section.

## 2.2 Polymer Blends

### 2.2.1 Thermodynamics of Polymer Blends

The thermodynamics of mixing in binary polymer mixtures can be expressed by the Gibbs free energy of mixing:

$$\Delta G_m = RT\chi_{AB}.\varphi_A\varphi_B + RT\left[\frac{\rho_A\varphi_A \ln \varphi_A}{Mw_A} + \frac{\rho_B\varphi_B \ln \varphi_B}{Mw_B}\right]$$

Here, $\Delta G_m$ is Gibbs mixing energy, $\chi_{AB}$ is the Flory-Huggins interaction parameter, $\varphi_i$ is the volume fraction of the polymer components, $\rho_i$ is the density of polymers, and $Mw_i$ is the molecular weight of the polymers. The first term on the right side of this equation shows the enthalpy of mixing, $\Delta H_m$, according to Hilbrand-Scatchard-van Lard theory and the terms in the brackets represent the combinational entropy of mixing based on Flory-Huggins lattice theory. Based on Gibbs free energy of mixing, binary polymer blends are categorized into three main groups: (i) miscible polymer blends: when $\Delta G_m < 0$ and $\frac{\partial^2 \Delta G}{\partial \varphi^2} > 0$ over the full composition range;

(ii) partial miscible polymer blends when $\Delta G_m < 0$ but $\frac{\partial^2 \Delta G}{\partial \varphi^2} < 0$ in some compositions; (iii) immiscible polymer blends when $\Delta G_m > 0$ over the full composition range. In miscible polymer blends, both components are miscible down to the molecular scale while in immiscible polymer blends, two separate phases of the polymers are formed. In partially miscible systems, again, two phases are formed but each phase is a miscible mixture of both polymer components. The negligible entropy of mixing in polymers mixtures (due to their high molecular weights) and the positive enthalpy of mixing (in the absence of any specific interaction) results in the immiscibility of most polymer mixtures. However, achieving miscibility in polymer blends is not always desired as some unique properties can only be obtained in immiscible polymer systems. The final properties of immiscible polymer blends strongly depend on their morphology. Figure 2.4 shows the different morphologies of binary polymer blends with their potential properties.

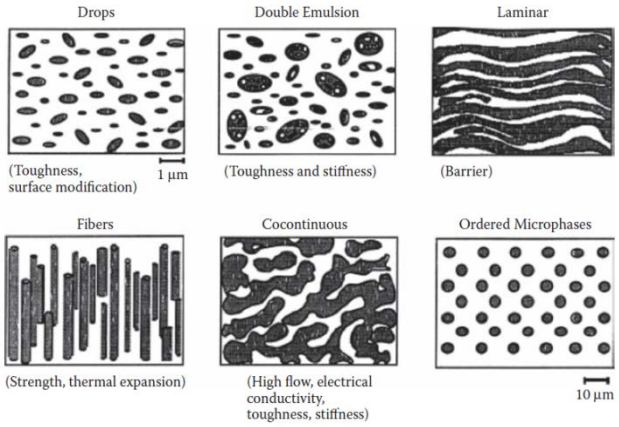


Figure 2.4. Different morphologies of immiscible polymer blends with their potential properties [45].

It has been shown that the morphology of immiscible polymer blends depends strongly on the interfacial tension between the phases [46]. On the other hand, the interfacial tension between two polymers is directly related to their surface tension (energy). The surface tension and interfacial tension will be discussed below.

### 2.2.2 Surface Tension

Surface tension is defined as the work required to increase the surface area of a solid or a liquid by the unit of area [47]. The unit of the surface tension is $J/m^2$ or N/m. The surface tension

originates from the imbalanced molecular forces at the surface compared to the bulk. Among different techniques, the contact angle method [48] is the most common method used to measure the surface tension of polymers in the solid state. On the other hand, the pendant drop technique has been widely used in determining the surface tension of polymer melts [49, 50]. This method can be used for both Newtonian and viscoelastic fluids and provides a high accuracy and small range of error [51].

### 2.2.3 Interfacial Tension

The interface is the boundary between two phases and plays a critical role in the morphology and final properties of heterophase polymer blends [52]. The interfacial tension is defined as the reversible work required to increase the interfacial area by the unit of area[47]. The interfacial tension can also be defined as the rate of the change in the interfacial energy of a system by increasing the interfacial area. The interfacial tension has the same unit as the surface tension ($J/m^2$ or N/m) and originates from the imbalanced forces at the interface. Different techniques that have been used to determine the interfacial tension between polymer pairs will be reviewed below.

#### 2.2.3.1 Estimation of the Interfacial Tension from the Surface Energy Data

The interfacial tensions between two polymer melts or a polymer melt and a solid can be estimated from the surface energy of the components. Good and Girifalco [53] estimated the interfacial tension using the work of adhesion concept as:

$$\gamma_{12} = \gamma_2 + \gamma_1 - W_a$$

Where $\gamma_{12}$ is the interfacial tension between the components, $\gamma_1$ is the surface tension of the component 1, $\gamma_2$ is the surface tension of the component 2 and $W_a$ is the work of adhesion between the components. Wu [54] applied the energy additivity concept and estimated the contributions of polar and nonpolar interactions in the work of adhesion using the Harmonic Mean approach:

$$W_a = 4\left(\frac{\gamma_2^d \gamma_1^d}{\gamma_2^d + \gamma_1^d} + \frac{\gamma_2^p \gamma_1^p}{\gamma_2^p + \gamma_1^p}\right)$$

Here $\gamma_i^d$ and $\gamma_i^p$ are the nonpolar (or dispersive) and polar components of the surface energy, respectively. On the other hand, Wu [55] found that the Harmonic Mean equation cannot accurately estimate the interfacial tension between two materials with highly different polarity (such as the interfacial tension between mercury and organic polymers) and showed that the estimation of the work of adhesion by the Geometric Mean approach results in much better predictions of the interfacial tension in those systems. The work of adhesion by the Geometric Mean equation is defined as:

$$W_a = 2\left(\sqrt{\gamma_2^d \gamma_1^d} + \sqrt{\gamma_2^p \gamma_1^p}\right)$$

#### 2.2.3.2 The Breaking Thread Method

If a high aspect ratio thread of a liquid is embedded in another liquid, in the absence of flow, sinusoidal distortions form and grow exponentially at the interface of the liquids and finally cause the thread to break up into a number of smaller droplets. The formation and growth of the sinusoidal distortions occur due to the tendency of two immiscible liquids to minimize their interfacial area. The breakup of a nylon 6 (PA6) thread embedded in a polystyrene (PS) matrix is shown in Figure 2.5. According to Tomotika's model, the amplitude of the sinusoidal distortions grows exponentially over time as:

$$\alpha = \alpha_0 . e^{qt}$$

where $\alpha_0$ is the amplitude of the initial distortions and q is defined as[56]:

$$q = \frac{\gamma_{12\Omega}}{\eta_0 D_0}$$

here $\gamma_{12}$ is the interfacial tension between the liquids, $\eta_0$ is the zero-shear viscosity of the matrix, $D_o$ is the initial thread diameter and $\Omega$ is a tabulated function.

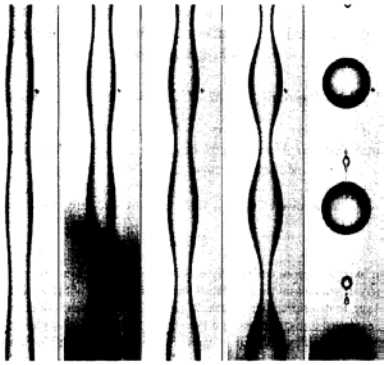

Figure 2.5. From left to right: the breakup process of a PA6 thread with a diameter of 55 μm embedded in a PS matrix at 230 ℃ [56].

The interfacial tension can be determined from the slope (q) of the log-log plot of the amplitude of the distortions (α) versus time. It should be considered that the breaking thread method can only be used if both polymers exhibit a Newtonian plateau at low frequencies.

#### 2.2.3.3 Rheological Analysis

Palierne [57] presented a model to predict the rheological properties of viscoelastic emulsions with a narrow droplet size distribution in the small amplitude oscillation shear (SAOS). According to his model, the complex modulus of a polymer blend can be written as:

$$G^* = G_m^* \frac{1 + 3\varphi H}{1 - 2\varphi H}$$

In this equation, H is defined as:

$$H = \frac{(G_d^* - G_m^*)(19\,G_d^* + 16\,G_m^*) + 4\frac{\gamma_{12}}{R}(5\,G_d^* + 2\,G_m^*)}{(2\,G_d^* + 3\,G_m^*)(19\,G_d^* + 16\,G_m^*) + 40\frac{\gamma_{12}}{R}(G_d^* + \,G_m^*)}$$

here G*is the complex modulus of the blend, $G^*_m$ is the complex modulus of the matrix, $G^*_d$ is the complex modulus of the dispersed phase, $\gamma_{12}$ is the interfacial tension between the matrix and the dispersed phase, R is the volume average dispersed phase diameter and φ is the volume fraction of the dispersed phase. In this method, $\frac{\gamma_{12}}{R}$ is obtained from fitting Plaierne model on the

rheological data. The estimation of the interfacial tension by the rheological method is limited to systems where the second plateau in the storage modulus is experimentally accessible.

## 2.2.4 Morphology Development in Heterophase Polymer Blends

The final morphology in a heterophase polymer blend is a result of the competition between the disintegration and breakup on one hand and the coalescence of the dispersed phase on the other. These two processes will be briefly reviewed below.

### 2.2.4.1 Droplet Breakup

Droplet breakup in a Newtonian emulsion under the elongation and shear flow was first studied by Taylor [58]. He found that by increasing the elongation rate, the shape of the dispersed droplet changed from a sphere to a thread and finally broke down into a number of smaller droplets after the secession of the flow. This is similar to the thread breakup experiment that was discussed in 2.2.3.2. On the other hand, the droplet in the shear flow was stretched and oriented in a plane of $45^o$ with respect to the flow direction. Taylor also found that by increasing the deformation, the droplet breakup occurred when the ratio of the viscous force to the interfacial force was greater than a critical value. The ratio of the viscous force to the interfacial force is known as the Capillary number and is defined as:

$$\mathrm{Ca} = \frac{\eta_m \dot{\gamma}}{\gamma_{12}/\mathrm{R}}$$

where $\dot{\gamma}$ is the shear rate, $\eta_m$ is the matrix viscosity, $\gamma_{12}$ is the interfacial tension and R is the droplet radius. Figure 2.6 shows the critical capillary number ($Ca_{crit}$), at which the droplet breakup occurs, as a function of the viscosity ratio (p) a Newtonian emulsion under the elongation and shear flow fields [59]. Note that the viscosity ratio is defined as the ratio of the dispersed phase viscosity to the viscosity of the matrix. As can be seen, $Ca_{crit}$ for the shear flow is always greater than that of the elongation flow and shows a minimum at $0.25 < p < 1$. This indicates much enhanced droplet breakup in the elongation flow compared to the shear flow. Favis and Chalifoux [60] studied the effect of viscosity ratio on the droplet breakup in the blends of polycarbonate (PC) PC and PP. Figure 2.7 shows the average dispersed phase diameter in PC/PP blends as a function of the torque ratio of the neat dispersed phase to the neat matrix. Note

that they observed a similar effect of the torque ratio and the viscosity ratio on the dispersed phase morphology.

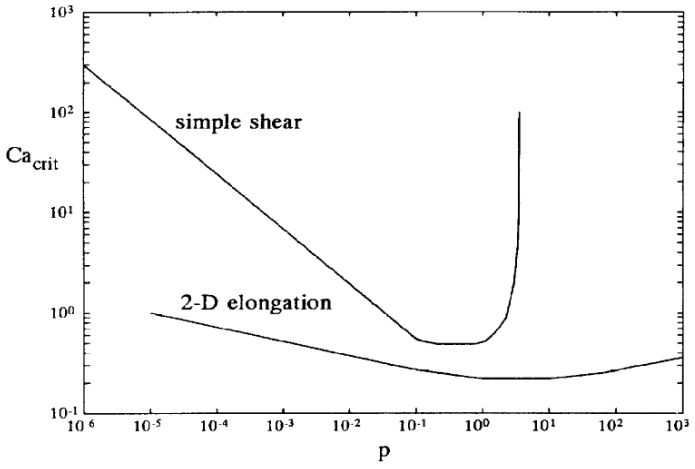


Figure 2.6. $Ca_{crit}$ versus viscosity ratio (p) in the shear and elongation flows [61]

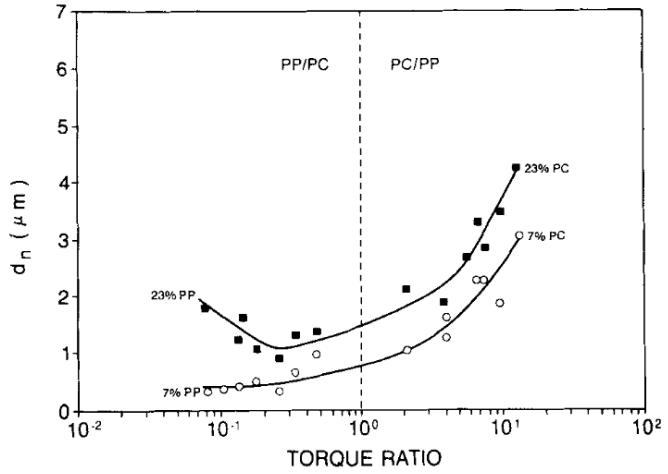


Figure 2.7. The effect of the torque ratio on the number average diameter (Dn) of the dispersed phase in the blends of PC/PP [60]

By increasing the torque ratio from 2 to 13, they observed that the dispersed phase size increased by a factor of about 2. Moreover, they found that the dispersed phase size decreased when the torque ratio was less than 1 with a minimum in the particle size occurring at the torque ratio of 0.25. This value is in good agreement with the one observed by Taylor in a Newtonian emulsion under shear flow, Figure 2.6. Wildes et al. [62] also studied the effect of the viscosity ratio on the dispersed phase size in a blend of PC and styrene–acrylonitrile (SAN) and found that in the absence of a compatibilizer, the minimum droplet size occurred at a viscosity ratio of 0.4.

Bhadane et al. [63] examined the effect of viscosity ratio on dispersed phase size in a low interfacial tension blend of PP and ethylene propylene diene monomer (EPDM) and found that a small change in the viscosity ratio did not influence the dispersed phase size but a seven-fold increase in the viscosity ratio increased the dispersed EPDM phase size by a factor of 3 to 4.

As mentioned previously, Taylor[58] found that the droplet breakup is enhanced in the elongation flow. Favis and Therrien [52] compared the dispersed phase size/viscosity ratio dependency in a high viscosity polycarbonate (PC)/PP blend in an internal batch mixer and a twin screw extruder. They found that the dispersed phase size was much less dependent on the viscosity ratio in the twin-screw extruder. Considering that elongation flow is very dominant in the twin screw extruder, the observed difference can be related to the highly effective droplet breakup in the extruder. These results are in agreement with the results of Wildes et al. [62] who found that in a PC/SAN blend processed by a twin-screw extruder, the phase size of the dispersed SAN particles was independent of the viscosity ratio.

Therefore, the previous studies have shown that: (a) shear flow has a limitation in droplet breakup when the viscosities of the phases are very different; (b) elongation flow is highly efficient.

#### 2.2.4.2 Coalescence

The coalescence of two droplets in an emulsion can be assumed as a three-step process: (i) two droplets are brought together by the flow field, (ii) A film of the matrix between two droplets is drained until the thickness of the film reaches a critical value, (iii) The rupture of the film occurs, which results in the coalescence and merging of the droplets [64]. At equilibrium, Tokita derived the following equation for the phase size of the dispersed phase [52]:

$$D_e \approx \frac{24 P_r \gamma_{12}}{\pi \tau} (\varphi + \frac{4 P_r E_{DK}}{\pi \tau} \varphi^2)$$

where $\tau$ is the shear stress, $P_r$ is the probability that a collision results in the coalescence and $E_{DK}$ is the bulk breaking energy of the dispersed phase. Tokita's model predicts that the phase size decreases linearly by increasing the shear stress and by decreasing the interfacial tension. Favis and Willis [65] obtained a master curve of the phase size as a function of composition for several immiscible polymer blends and found that the phase size dependency on compositions follows $\varphi+k\varphi^2$ but Tokita`s theory overestimates the effect of shear stress on the dispersed phase size.

Therefore, it can be seen that the coalescence and coarsening of the dispersed phase increases significantly by increasing the amount of the dispersed phase.

#### 2.2.4.3 Continuity Development in Polymer Blends

By increasing the amount of the dispersed phase, at a certain volume fraction, a 3D inter-connected continuous structure of the dispersed phase is formed in the blend. This volume fraction is known as the onset of the continuity of the dispersed phase. When both phases exist in the form of the 3D interconnected structures, the morphology is known as the co-continuous morphology. It has been shown that the formation of the continuous structure of the dispersed phase is promoted when the dispersed phase exists in the form of a stable highly elongated phase [63, 66, 67]. According to Tomotika's model [56], increasing the viscosity of the matrix and decreasing the interfacial tension result in the formation of a more stable thread of the dispersed phase and, therefore, these factors should enhance the formation of the co-continuous morphology. Previous studies confirmed the broadening of the co-continuity region by decreasing the interfacial tension [67, 68].

### 2.2.5 Compatibilization of Polymer Blends

The addition or in-situ generation of compatibilizers in immiscible polymer blends is a well-known method for enhancing the interfacial adhesion between polymeric phases and improving the final mechanical properties. The features of the compatibilization of polymer blends can be listed as: 1) decreasing the interfacial tension; (2) reducing the dispersed phase size; (3) preventing either partially or completely both dynamic and static coalescence processes; (4) improves the adhesion between the phases; (5) stabilizing the microstructure and (6) ultimately allowing much more control over the various processing parameters and final properties of the material [69]. The compatibilization process is generally carried out through two methods: a) the addition of a copolymer which has parts that are miscible or highly compatible with either phases, (b) formation of a compatibilizer at the interface by reactive processing. In the second method, the third component either has functional groups that can react with both phases at the interface or has a tail compatible with one of the phases and a functional group that can react with the other phase.

In the first method, different types of the copolymers can be used such as a di-block copolymer, tri-block copolymer or branched or grafted copolymers. Fayt et al. [70] showed that among the different types of block copolymers, di-block copolymers are the most effective at enhancing the interfacial adhesion and final mechanical properties. More recently, Harrats [71] found that a tapered copolymer of hydrogenated butadiene-styrene (SEB) can offer even better compatibilization properties than a pure di-block copolymer in an LDPE/PS blend.

By the addition of the compatibilizer, the compatibilizer molecules situate themselves at the interface and reduce the interfacial free energy of the system. By increasing the compatibilizer content, at a certain amount of the compatibilizer, the interface becomes saturated with the compatibilizer and increasing the compatibilizer content does not have a considerable effect on the interfacial adhesion between polymer pairs. However, higher concentration of the compatibilizer causes micelle formation in the system. This effect is clearly shown in Figure 2.8, in which the measured interfacial tension between PS and polybutadiene (PB) decreased by the addition of a styrene-butadiene (SB) block copolymer and reached a plateau at high compatibilizer contents.

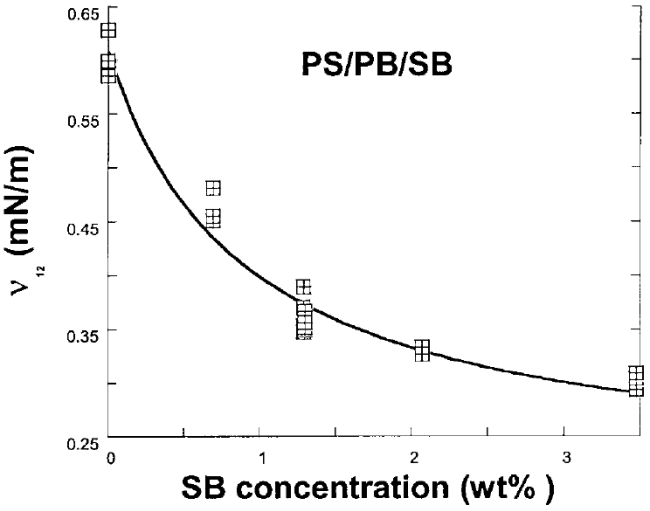


Figure 2.8.Effect of the addition of a SB copolymer on the interfacial tension ($\upsilon_{12}$) between PS and PB [72].

Considering the direct influence of the interfacial tension on the phase size of polymer blends, this effect can also be seen by studying the particle size of the blend as a function of compatibilizer content, Figure 2.9.

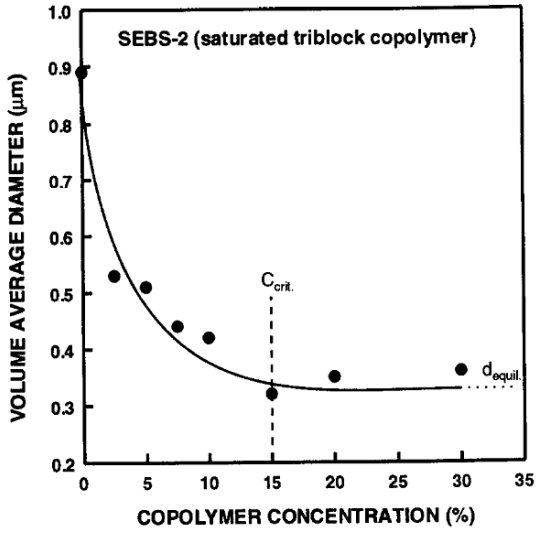


Figure 2.9. The effect of the addition of a hydrogenated styrene-butadiene-styrene tri-block copolymer on the phase size of PS/Ethylene-propylene rubber (EPR) (90/10%) [73].

As these curves are similar to the emulsification curves, they are being referred to as the emulsification curve of compatibilizers in polymer blends [69, 73].

In the case of reactive compatibilization, the main requirements are [74]: 1) Short reaction time (< 3 minutes) which means that the chemical functionalities should be very reactive; 2) the reaction should not generate a significant amount of heat; 3) as the reaction takes place at the interface, rigorous mixing is required to increase the interfacial area; 4) the reaction product should be stable. An example of reactive compounding is the compatibilization of polyolefin/polyamide blends by the addition of polyethylene grafted maleic anhydride and/or polypropylene grafted maleic anhydride. In this case, maleic anhydride reacts with amine groups of polyamide resulting in the formation of a graft copolymer. In this case, maleic anhydride was grafted to PE prior to the reactive compounding.

## 2.3 PLA/PBAT and PLA/PE Blends

### 2.3.1 PLA/PBAT Blends

Jiang et al. [12] studied the miscibility of PLA/PBAT by examining the shift in the glass transition temperature (Tg) of the phases in dynamic mechanical analysis (DMA) results. They

observed two distinct Tgs of PLA and PBAT phases over the studied composition range and concluded that PLA/PBAT is an immiscible polymer blend. Yeh et al. [19] used the same approach and observed two Tgs at compositions above 2.5 wt.% of PBAT (which indicates immiscibility in this composition range). On the other hand, they only observed one Tg close to the Tg of the PLA phase at 2.5 wt.% of PBAT. They finally concluded that a PLA/PBAT blend is a miscible system below 2.5 wt.% of PBAT. However, the amplitude of the response of the PBAT phase in the DMA results at 2.5 wt.% of PBAT is expected to be very small and, therefore, achieving a solid conclusion about the presence of the PBAT phase at this composition is challenging. Therefore, it can be seen that the miscibility of the PLA/PBAT blend is still a controversial issue that has not yet been studied in detail. Previous studies on the mechanical properties of PLA/PBAT indicate that the addition of PBAT reduces the tensile strength and modulus and enhances the elongation at break compared to the neat PLA [12, 19, 41]. For example, Figure 2.10 shows these trends in the mechanical properties of PLA/PBAT reported by Jiang et al. [12]. On the other hand, as can be seen in Figure 2.10, the addition of PBAT does not improve the impact properties of PLA considerably, which is attributed to an insufficient interfacial adhesion between the phases to transfer the stress from PLA to the PBAT phase [12, 20, 21, 39].

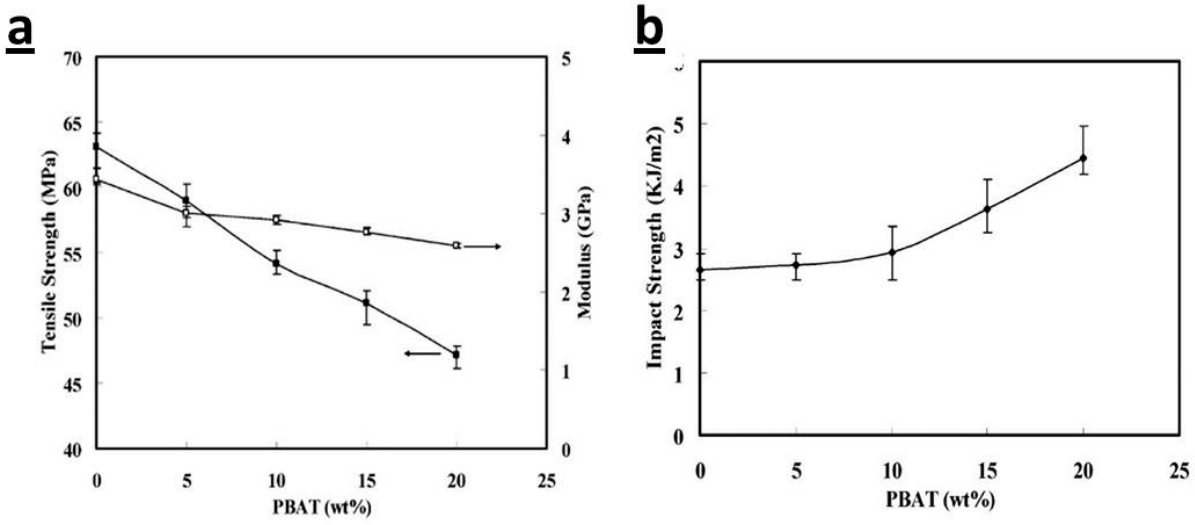


Figure 2.10. The mechanical properties of PLA/PBAT blends at different compositions: (a) tensile strength and modulus, (b) impact strength [12].

Some authors have used the compatibilization approach to enhance the interfacial adhesion between PLA and PBAT. Lin et al. [39] added tetrabutyl titanate (TBT) to a PLA/PBAT blend and reported that TBT enhanced the tensile and impact strength by the formation of a PLA-PBAT copolymer through a trans-esterification reaction at the interface. However, the authors did not provide any morphological and/or elemental analysis to prove the formation of the copolymers at the interface. Zheng et al. [20] added glycidyl methacrylate (GMA) to a PLA/PBAT blend and observed an increase in the elongation at break and impact strength compared to the neat blend. They also attributed this observation to the formation of a PLA-PBAT copolymer at the interface but did not present any evidence to prove the presence of the copolymer. Al-Itry et al. [75] proposed a mechanism to demonstrate how multi-functional epoxy chain extenders such as Joncryl can bind PLA and PBAT molecules at the interface. However, as the multi-functional epoxy components are not selectively localized at the PLA/PBAT interface, they can also react with either phase and form branched molecules, which considerably increases the elasticity and viscosity [75, 76]. Therefore, it can be seen that despite previous attempts to compatibilize the PLA/PBAT interface, an effective compatibilization strategy for PLA/PBAT blends is lacking in the literature.

### 2.3.2 PLA/PE Blends

Despite the commercial potential of a PLA/PE blend, this blend has been studied by few authors. A set of systematic studies on the mechanical properties and compatibilization of the interface in this blend was carried out by the research group of Professor Hillmyer at the University of Minnesota [5, 77, 78]. They studied the mechanical properties of blend samples prepared by solution blending [78] and melt blending [5, 77] and found that in both cases the blending enhanced the elongation at break but reduced the tensile modulus and impact properties. They studied the effect of the addition of di-block copolymers of PLA-b-PE on the morphology and mechanical properties of PLA/LDPE, Figure 2.11. As can be seen, the addition of PLA-b-PE copolymers reduced the dispersed phase and enhanced considerably the elongation at break. In another interesting work from the same group, the effect of the microstructure of PLA-PE copolymers on the final properties of PLA/linear low density polyethylene (LLDPE) blends was

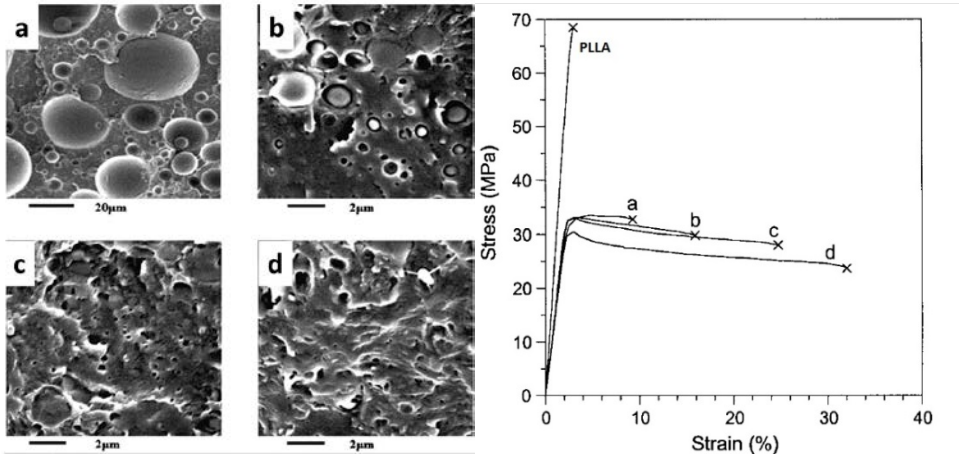


Figure 2.11. (Left) the effect of the addition of a PLLA-b-PE copolymer on the morphology of PLLA/LDPE (80/20) blends at (a) 0, (b) 2, (c) 5 and (d) 10 wt.% of the copolymer (based on the total weight of the blend); (right) the tensile properties of the blends [78].

studied and it was found that the presence of high crystalline blocks in the copolymer increased the impact strength from 20 J/m, for the neat PLA, up to 760 J/m [5].On the other hand, the elongation at break of the same sample was only enhanced from 4% to 31%. However, the authors did not discuss the observed limited improvement in the elongation at break. They also studied the effect of the compatibilizer content on the phase size and impact properties and showed that the interface saturation occurred at about 1 wt.% of the copolymer, Figure 2.12.

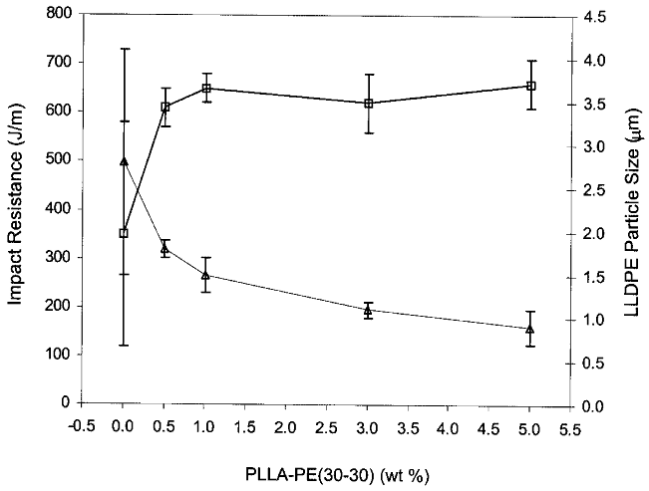


Figure 2.12. The effect of PLLA-b-PE content on the dispersed phase size and impact strength of PLLA/LLDPE (80/20)[77].

## 2.4 Polymer Nanocomposites

As shown in the previous section, the blending of PLA with PBAT or PE enhances the elongation at break but, at the same time, reduces the mechanical strength and modulus considerably. The addition of solid inclusions to polymer blends is an effective method for achieving a balance between stiffness and toughness [27-29, 79-82]. The addition of nanoparticles to polymer blends in particular has received much attention due to their potential in enhancing the mechanical properties at much lower solid contents. Moreover, with the discovery of the double and multiple percolation phenomena, the addition of conductive nanoparticles to polymer blends to produce conductive and semi-conductive materials has been studied extensively [83, 84]. Previous studies clearly indicate that the key parameter in achieving a balance between stiffness and toughness and/or increasing conductivity in the systems incorporating nanoparticles is the ability to control the localization of solid inclusions[27, 79, 85-87]. Therefore, understanding the mechanisms involved in the localization of solid particles in polymer blends is crucial in achieving the final blend with the desired properties. In the following sections, the effects of the most important thermodynamic and kinetic parameters on the localization of solid particles in polymer blends will be reviewed.

### 2.4.1 Thermodynamic of the Localization of Solid Inclusions in Polymer Blends

The thermodynamic equilibrium localization of solid particles in a polymer blend can be predicted by Young's model or the wetting parameter which is defined as[31]:

$$\omega = \frac{\gamma_{1s} - \gamma_{2s}}{\gamma_{12}}$$

Where $\gamma_{1s}$, $\gamma_{2s}$ and $\gamma_{12}$ are the interfacial tension between: polymer 1 and a solid, polymer 2 and a solid and polymer 1 and 2. Figure 2.13 schematically shows the different predicted localizations of solid particles based on the different values of ω. As can be seen in Young's model, the interfacial tension between solid particles and polymers has a determining role in the final thermodynamic localization of the particles. Elias et al. [88] showed that in a PP/PS blend, by the simultaneous addition of all components, hydrophobic silica particles were located in the

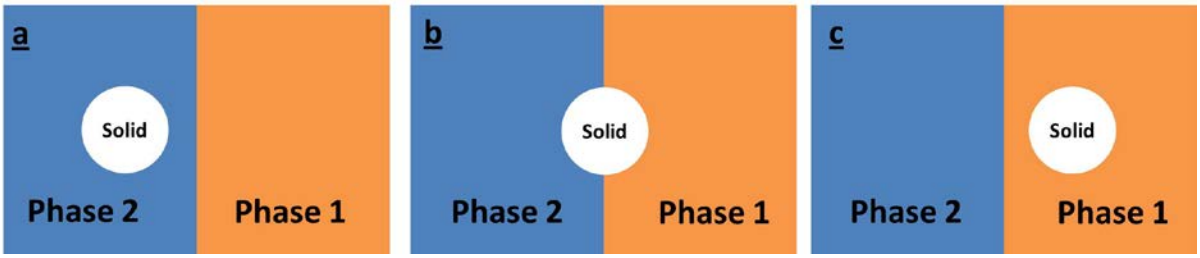


Figure 2.13. Different localizations of solid inclusions based on the wetting parameter(ω): (a) in Phase 2 when ω > 1; (b) at the interface when -1 < ω < 1; (c) in phase 1 when ω <-1.

PP phase and at the interface while hydrophilic silica particles were localized into the PS phase. These localizations were in agreement with the predicted localizations from Young's equation.However, some authors found that the localization predicted by Young's model did not match with their observation [89-92]. The uncertainty in the surface energy data of the components as well as the difference between the melting temperatures of the polymeric phases have been mentioned as the main reasons for these observations. The uncertainty in the reported values of the surface energies of solid particles can be seen inTable 2-1.

Table 2-1. The surface energy of different nano-particles reported in the literature.

| Solid particle | grade | γ (mN/m) | $\gamma^d$ (mN/m) | $\gamma^p$ (mN/m) | T ($^oC$) | Reference |
|---|---|---|---|---|---|---|
| CB | NC7000 from Nanocyl | 55 | 51-49 | 4-6 | 190 | [93] |
| CB | From Denki-kagaku Co. Japan | 108.8 | 108.1 | 0.8 | 180 | [94] |
| CB | Printex XE 2B from Degussa | 42 | 3-5 | 37-39 | 210 | [95] |
| Silica | Aerosil A200 from Degussa | 80 | 29.4 | 50.6 | 25 | [88] |
| | | - | 79<br>38 | - | 0<br>100 | [96] |
| Silica | Aerosil R805 From Degussa | 32 | 30 | 2 | 25 | [88] |
| Montmorillonite | Cloisite®30B from Rockwood additives | 24.3 | 17.4 | 6.9 | 260 | [97] |
| | | 35 | 22.4 | 12.6 | 250 | [98] |
| MWCNT | from Dynamic Enterprises | 27.8 | 17.6 | 10.2 | 25 | [99] |
| MWCNT | from Nanolab | 45.3 | 18.4 | 26.9 | - | [100] |
| MWCNT | from Arkema and Nanocyl | - | 81-115 | - | 100 | [101] |

The difference in the reported values is mainly due to the differences in purity, surface crystallinity and functionality of the solid particles. Therefore, all these factors should be considered when selecting surface energy data from the literature. For example, in the case of silica particles, the density of the SiOH groups on the surface can be used as a criterion to select the most proper surface energy data. Hydrophilic silica particles have SiOH density of 2-6 SiOH/nm$^2$, while this value is usually less than 1 SiOH/nm$^2$ in hydrophobic silica [96]. In addition to the above-mentioned factors, the different techniques that have been used in the measurements of the surface energy of solid particles can also result in different surface energy data. Moreover, in most of the previous studies, the surface energy of polymers at room temperature was taken from the literature and then was extrapolated to higher temperatures. This common strategy increases errors in the prediction of the thermodynamic localization as the surface energy and its temperature coefficient depend on the molecular weight and molecular weight distribution of polymers [47, 102, 103].

It should be mentioned that, in addition to the surface energy of the components, any specific interaction between polymer components and solid particles should also be considered in analysing the localization of the particles. These interactions can be in the form of a chemical reaction with the surface of the solid or strong adsorption of polymer molecules on the surface of the particles. Taghizadeh and Favis [104] found that in a thermoplastic starch (TPS)/ PCL blend, Young's model predicts that CNT particles should be localized at the interface; however, they found that the particles had a significant tendency toward the TPS phase. Using X-ray Photoelectron spectroscopy (XPS) analysis, they found that TPS molecules react with the carboxylic groups on the surface of the CNT particles. As a result, the CNT particles are drawn from their thermodynamic localization at the interface into the TPS phase. Specific interactions can be used as an effective tool to alter the thermodynamic equilibrium localization of solid particles in multiphase systems. For example, Gultner et al. [105] found that the addition of amino functionalized CNT particles to a PC/SAN blend resulted in the localization of CNT particles in the PC phase. By premixing N-phenylmaleimide styrene maleic anhydride with the SAN phase, they could successfully change the thermodynamic localization of the particles to the SAN phase. They attributed the change in the localization to the reaction of N-phenylmaleimide styrene maleic anhydride with the functional amino groups on the surface of CNT. In another study, Chen et al. [106] found that the addition of CNT particles to a blend of PC and

acrylonitrile butadiene styrene (ABS) resulted in the localization of the particles in the PC phase. However, with the addition of 5 wt.% of ABS-graft-maleic anhydride (ABS-g-MA) to the ABS phase, the localization of the particles changed to the ABS/ABS-g-MA phase. Liu et al.[107] also showed that in a blend of PP/ethylene propylene rubber (EPR), nano-silica particles were localized in the PP phase. On the other hand, when they used EPR-graft-Maleic Anhydride (EPR-g-MA), the silica particles were selectively localized in the EPR-g-MA phase.

Therefore, it can be seen that in addition to the surface energy of the components, the specific interactions can also be used to control the localization of solid particles in multiphase systems.

## 2.4.2 Kinetics of the Migration and Localization

Although the thermodynamic equilibrium localization of solid particles in polymer blends can be predicted by Young's model, kinetic effects can interrupt the migration of the particles toward their preferred thermodynamic equilibrium location. In this section, the effect of different kinetic parameters on the migration and localization of solid particles in polymer blends will be reviewed.

### 2.4.2.1 The Effect of Mixing Strategy

The effect of the sequence of the addition of components is the most studied kinetic parameter in the literature. Most of the previous studies found that the addition of all the components to the mixing chamber or the addition of solid particles to a melt of polymers result in the localization of the particles in their thermodynamic equilibrium localization[29, 85, 88-91, 94, 105, 108-117]. On the other hand, when solid particles are premixed with a phase with which they have the lowest thermodynamic affinity, different observations have been reported. Some authors observed that, even by changing the mixing strategy, the particles migrated to their thermodynamic equilibrium localization[85, 88, 105, 106, 113] while in some other systems, the migration of solid particles was inhibited and a non-equilibrium localization was observed [89, 104, 115]. For example, Baudouin et al.[90] found that when CNT particles were added to a blend of polyamide 12 (PA12) and ethylene–acrylate (EA) copolymer, they were localized at their thermodynamic equilibrium localization at the interface. However, when the particles were premixed in a high viscosity PA12 phase, they remained in the PA12 phase. Therefore, it can be seen that premixing particles with a low affinity phase increases the effect of kinetic parameters.

Viscosity is the most mentioned kinetic barrier for the migration of solid particles in the literature. The effect of this parameter will be reviewed in the next section.

#### 2.4.2.2 The Effect of Viscosity

Austin et al. [111] studied the effect of the viscosity of EPR-g-MA on the localization of organoclay in a blend of PP/EPR-g-MA and found that the particles were localized in the EPR-g-MA phase irrespective of its viscosity. It should be mentioned that they carefully eliminated the effect of the difference between the melting temperatures of the phases by the addition of the particles to a PP/EPR-g-MA melt.

Persson and Bertilsson [118] studied the effect of the viscosity of phases on the localization of aluminum whiskers in a low interfacial tension blend of PE and polyisobutylene (PIB). They found that the aluminum whiskers were always localized in the more viscous phase irrespective of the mixing strategy. This observation was attributed to the minimization of the viscous energy of the system by the localization of aluminum whiskers in the more viscous phase. On the other hand, they also found that in a polyamide (PA)/SAN blend, the aluminum borate whiskers were localized in the less viscous PA phase. Finally, they concluded that the role of the viscosity is only important in low interfacial tension systems and the thermodynamic interactions control the localization in high interfacial tension blends. However, some other authors observed considerable effects of viscosity in high interfacial tension systems. Feng et. al. [119] studied the effect of the viscosity of poly(methyl methacrylate), PMMA, on the localization of carbon black (CB) in a PP/PMMA blend. They found that by the addition of all the components to the mixing chamber, CB particles were localized in the less viscous PMMA phase, while by increasing the viscosity of the PMMA phase, CB particles were only localized at the interface and in the PP phase. Considering that the thermodynamic localization of CB particles was determined to be in the PMMA phase, they concluded that increasing the viscosity of the PMMA phase prevented the migration of CB particles to the PMMA phase. Figure 2.14 shows the localization of CB particles in the samples with low and high viscosity PMMA.

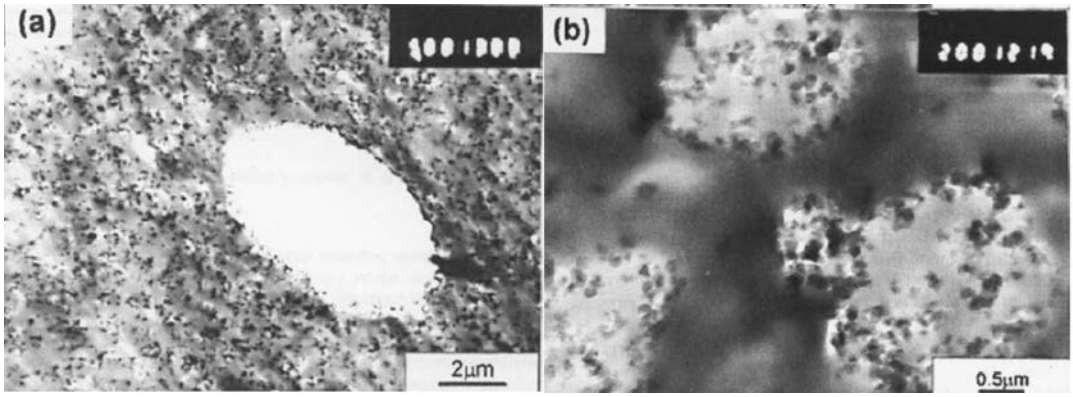


Figure 2.14. The effect of the viscosity of the PMMA phase in PP/PMMA(73/27): (a) high viscosity PMMA, (b) low viscosity PMMA. PMMA is always the brighter phase[119].

Plattier et al. [120] studied the effect of the viscosity ratio of the phases on the localization of CB particles in a blend of PP and PCL. Although the thermodynamic localization of CB particles was predicted to be in the PCL phase the particles were always localized in the more viscous phase irrespective of whether it was PP or PCL. They attributed this observation to the higher drag force that the more viscous phase applied to the particles at the interface. However, as can be seen in Figure 2.15, they based their conclusion on the assumption that the drag forces always tend to pull the particles out of the interface, which is not necessarily a valid assumption.

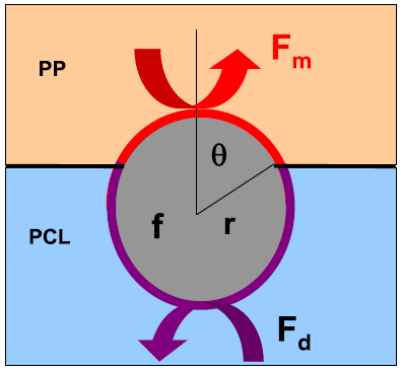


Figure 2.15. Schematic representation of a CB particle at the PP/PCL blend interface. $F_d$ and $F_m$ are the drag forces applied by PCL and PP, respectively[120].

Chen et al. [106] found that in a blend of PC/ABS/ABS-g-MA (55/40/5), the premixing of CNT particles with a high viscosity PC phase prevents the migration of the particles to their thermodynamic equilibrium localization in the ABS/ABS-g-MA phase. Elias et al. [91] also studied the localization of fumed silica in a PP/ethylene-co-vinyl acetate (EVA) blend and found

that when hydrophobic fumed silica, PP and a low viscosity EVA were added simultaneously to a micro-compounder, all silica particles were located at the interface and in the PP phase, which was the predicted thermodynamic equilibrium localization. On the other hand, when a high viscosity EVA phase was used in the experiments, the silica particles were localized in the EVA phase and at the interface. Figure 2.16 shows the different localizations of silica particles in these samples.

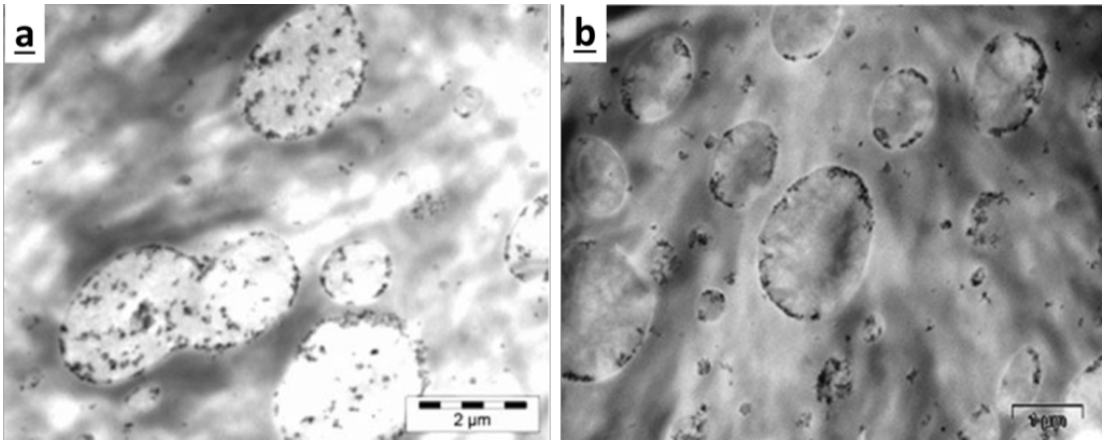


Figure 2.16. The localization of hydrophobic silica in PP/EVA blends by the simultaneous addition of components: (a) high viscosity EVA, (b) low viscosity EVA[91].

Considering the much lower melting temperature of EVA (~75 $^{o}$C) compared to PP (~165 $^{o}$C), it is likely to expect that at the early stages of the mixing, EVA melted first and encapsulated silica particles. As a result, when the high viscosity EVA phase was used, the particles could not migrate from the EVA phase to their thermodynamic equilibrium localization (at the interface and in PP). Taghizadeh and Favis [104] compared the localization of carboxylic acid functionalized CNT in a blend of PCL and TPS prepared by a twin-screw extruder and an internal batch mixer. As can be seen in Figure 2.17, they found that by mixing a PCL/CNT masterbatch with TPS in the twin-screw extruder, CNT particles completely migrated to the TPS phase. However, when the sample was prepared by the internal batch mixer, CNT particles were located in the PCL phase and at the interface. Using rheological analysis, they showed that the TPS phase viscosity drops significantly by increasing the shear rate. They concluded that, in addition to the different flow fields that exist in these instruments, the higher shear rate of mixing in the twin-screw extruder dropped the viscosity of the TPS phase and allowed CNT particles to migrate into

the TPS phase. On the other hand, the viscosity of TPS was much higher in the internal batch mixer (due to the lower shear rate) which prevented the migration of CNT particles to the TPS phase.

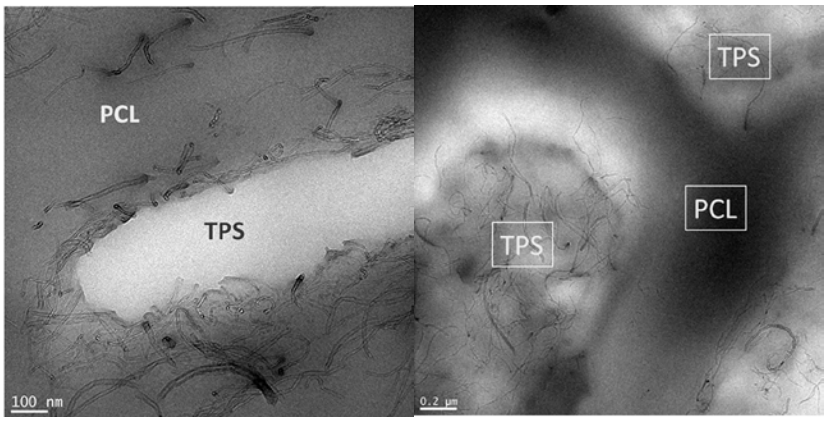


Figure 2.17. TEM images of PCL/TPS/CNT nanocomposites prepared by premixing CNT with PCL. (Left) sample prepared in the internal batch mixer; (right) sample prepared in the twin-screw extrude [104].

From all the aforementioned, it can be seen that the viscosity can prevent or delay the migration of solid particles in polymer blends. However, the origin of the effect of viscosity has not been discussed yet.

#### 2.4.2.3 Effect of Mixing Time

Gubbels [121] showed that when CB particles were initially dispersed in the PS phase in a PS/PE blend, electrical resistivity was reduced and reached a minimum after 2 minutes, Figure 2.18(a), and increased again by further processing. Further investigations revealed that after 2 minutes of mixing (the minimum in the resistivity curve), the particles were localized temporarily at the interface. The localization of the particles at the interface formed a conductive network of the particles at the interface and significantly reduced the electrical resistivity of the blend. Further processing resulted in the complete migration of the particles to the PS phase, which increases the electrical resistivity,

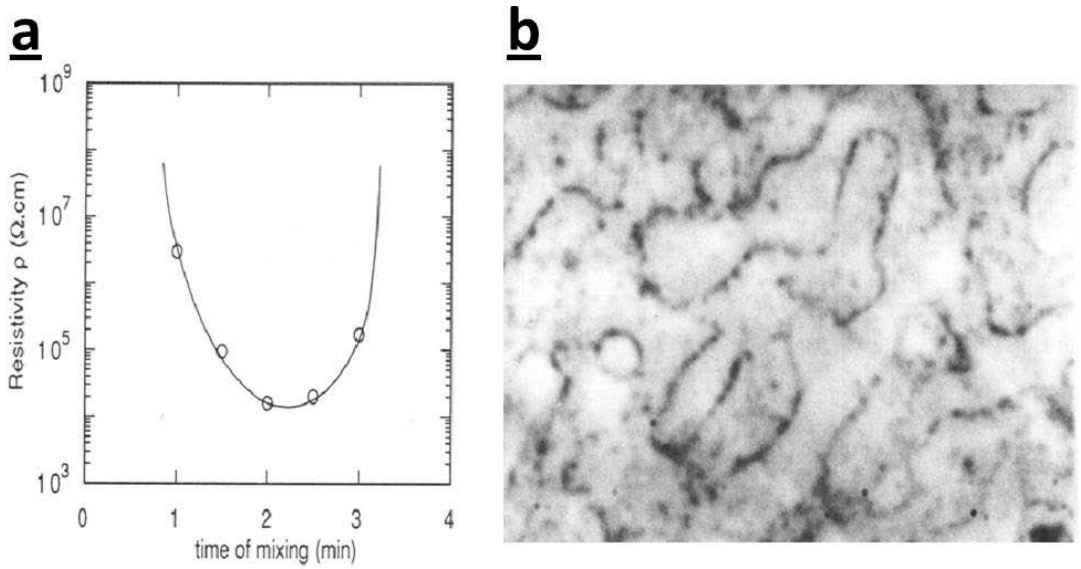


Figure 2.18. (a) Electrical resistivity of the PS/PE (55/45) blend with 1 wt.% CB particles as a function of mixing time, (b) the localization of CB particles after 2 minutes of mixing. [121].

Hunag et al. [113] studied the localization of CNT particles in a PLA/PCL blend and showed that, according to Young's model, CNT particles should be localized in the PCL phase. By premixing CNT with PLA followed by mixing with PCL they found that after 20 minutes of mixing, all CNT particles completely migrated to the PCL phase. Figure 2.19 shows the TEM images of PLA/PCL blends with the CNT particles at different mixing times.

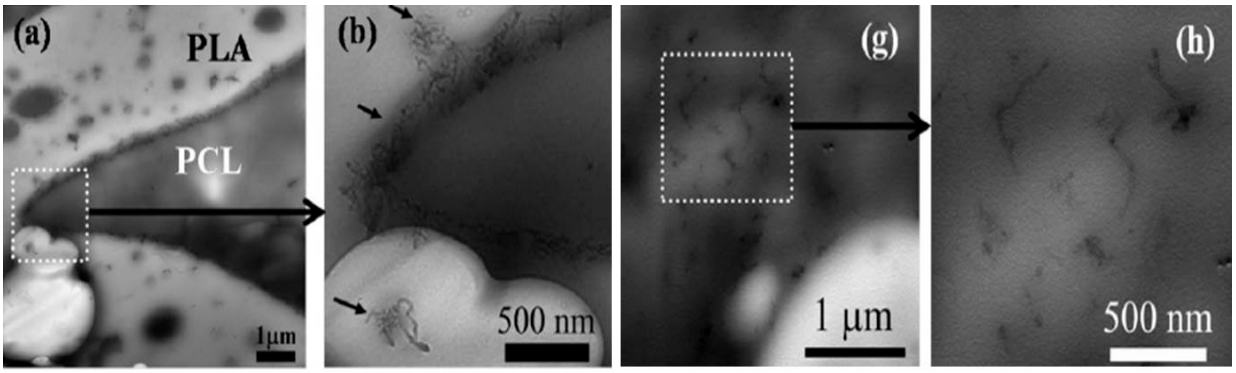


Figure 2.19. TEM images of the PLA/PCL(50/50) blend with 0.25 wt% CNT premixed with: (a) after 1 min of processing, (g) after 20 min of processing. (b) and (h) show higher magnifications of (a) and (g) respectively[113].

Hong et al. [122] studied the effect of mixing time on the migration of organoclay from a PS phase to Poly(butylene terephthalate) PBT. To this aim, they prepared multilayer disks of PBT and PS/organoclay (organoclay was premixed initially with PS) and studied the migration of organoclay particles under steady shear flow in a rheometer with parallel plate geometry. As can be seen in Figure 2.20, they found that after 300 s at the shear rate of 1 $s^{-1}$, most of the organoclay particles were localized in the PS phase. By increasing the time, more particles migrated to the interface and finally after 1800 s, all organoclay particles either migrated to the PBT phase or were localized at the interface.

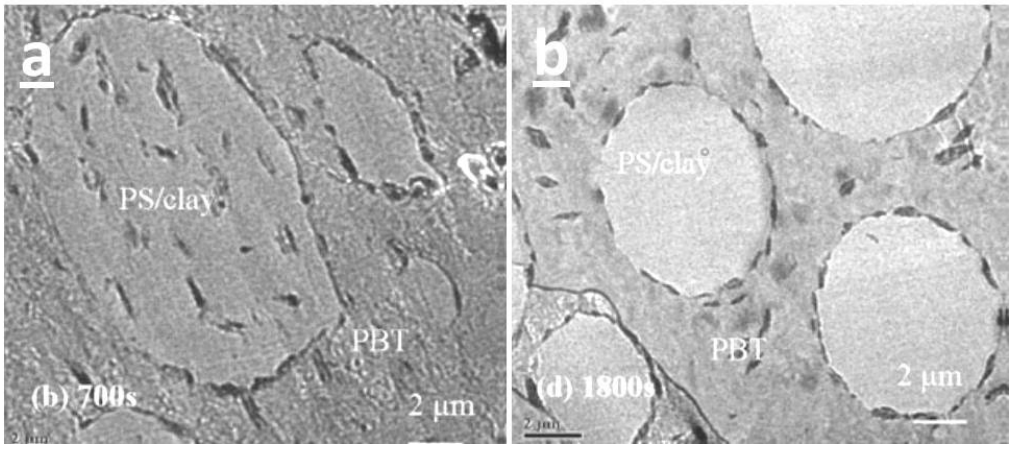


Figure 2.20. TEM images of PBT/PS disk samples showing the migration of organoclay in a PBT/PS nanocomposite at a shear rate of 1 $s^{-1}$ at different times: a) 700 s; b) 1800 s [122].

In conclusion, it can be seen that the previous studies in the literature show that increasing the mixing time can enhance the migration of the particles to their thermodynamic equilibrium localization.

#### 2.4.2.4 Effect of Shear Rate

The shear rate of mixing is another kinetic parameter that can influence the migration and final localization of solid particles in polymer blends. The effect of shear rate was studied by Hong et al. [122] in a PBT/PS blend. They studied the effect of shear rate on the migration of organoclay from PS layers to PBT layers in a multilayer disk of PBT and PS/organoclay. The results are shown in Figure 2.21.

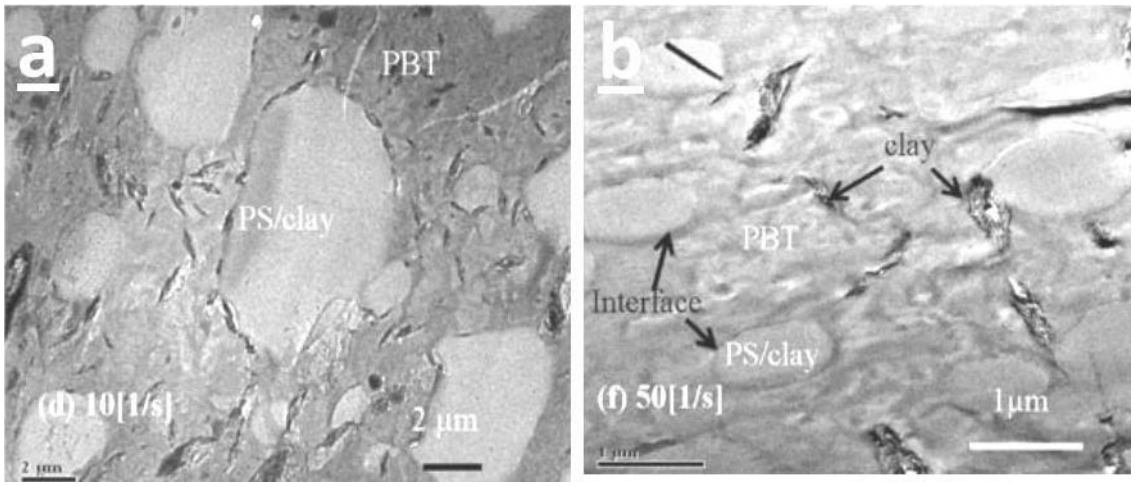


Figure 2.21. TEM images of PBT/(PS/organoclay) after 700 s at shear rates of (a) 10 $s^{-1}$ and (b) 50 $s^{-1}$ [122].

Although the TEM images in Figure 2.21 show that by increasing the shear rate from 10 to 50 $s^{-1}$, all organoclay particles migrated from the PS to PBT phase, but it should be considered that working at the shear rate of 50 $s^{-1}$ or even 10 $s^{-1}$ in a parallel plate geometry results in the leaking of the material out of the disk space. Considering the non-Newtonian behaviour of polymer materials, changing the shear rate can also affect the viscosity of the phases in a polymer blend. As mentioned previously in 2.4.2.2., Taghizadeh and Favis [104] found that in a PCL/TPS blend, increasing the shear rate reduced the viscosity of the TPS phase and enhanced the migration of CNT particles to the TPS phase.

#### 2.4.2.5 Effect of the Aspect Ratio of the Particles

Goldel [110] studied the effect of the aspect ratio of solid particles on the migration by comparing the migration of CNT and CB particles from SAN to PC in a PC/SAN blend. They found that the migration of CB particles at the interface is much slower than the CNT particles. They proposed a mechanism named the “slim-fast-mechanism” or SFM in which the interface curvature is considered as the only driving force for the migration. As is shown in Figure 2.22, they mentioned that during the migration of a low aspect ratio particle through the interface, the interface curvature and the thermodynamic driving force decrease, which can result in the

trapping of the particles at the interface. On the other hand, during the migration of a high aspect ratio particle, the interface cannot relax until the particle completely passes through the interface. Therefore, the driving force for the migration of high aspect ratio particles remains unchanged during the course of the migration and these particles migrate much faster. However, the authors did not consider the difference between the surface energies of CB and CNT particles in their discussions. This can be related to the fact that they assumed the migration to occur only due to the interface curvature.

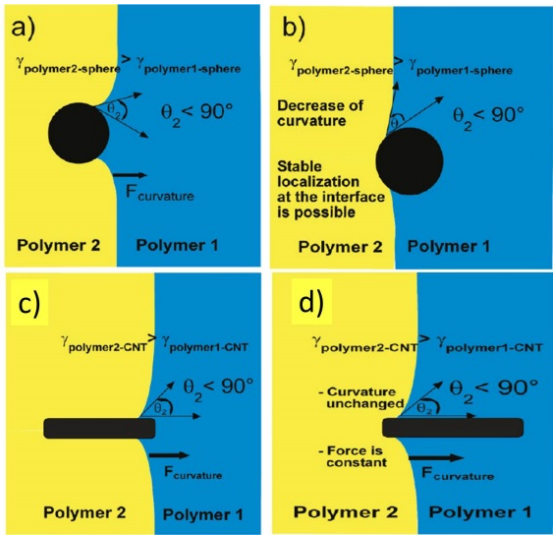


Figure 2.22. The migration of a low and a high aspect ratio particle at the interface: (a,c) at the beginning of the migration, (b,d) at the end of the migration. θ indicates the interface curvature[110].

#### 2.4.2.6 Effect of the Dispersion of the Particles

Achieving a good dispersion of nano-particles is challenging as decreasing the particle size significantly increases the agglomerate strength of solid particles [123]. The presence of the agglomerates or aggregates of solid particles can significantly reduce the reinforcement effect of the particles [28, 81, 82]. The poor dispersion of solid particles can also affect the migration and localization of the particles. Baudouin et al. [90] found that in an EA/PA6 blend, when CNT particles were premixed by the EA phase, aggregates of CNT remained in the EA phase while well-dispersed CNT particles could migrate to their thermodynamic localization at the interface. Goldel et al. [110] proposed that the dispersion-state dependence of the localization of solid particles increases by increasing the aspect ratio of individual nanoparticles. They attributed this

conclusion to the SFM mechanism that was reviewed in the previous section. It can be seen that achieving a goof dispersion can be another limiting parameter in controlling the localization of solid particles in polymer blends.

#### 2.4.2.7 The effect of Molecular Adsorption on the Migration and Localization

Baudouin et al. [90] used extraction followed by thermal gravimetric analysis (TGA) and showed that in an EA/PA12 blend with CNT particles localized in the PA12 phase, some PA12 molecules remained adsorbed to the surface of the particles even after the extraction. Tao et al [124] coated CNT particles with two PS phases with different molecular weights of 2900 and 2900000 g/mol. The coated particles were premixed with PA12 followed by mixing with the EA phase. They found that when CNT is coated with the low molecular weight PS, particles were localized in the PA12 phase while in the case of the high molecular weight PS, the particles migrated and were localized at the interface. The same interface localization was observed when neat PS was added to a EA/PA12 blend. They concluded that, by increasing the molecular weight of the PS, the desorption of the PS molecules from the surface of CNT particles becomes much more difficult and the CNT particles coated by the high molecular weight PS acted the same as the neat PS droplets.

#### 2.4.2.8 Mechanisms of Migration of Solid Inclusions in Polymer Blends

The mechanism of migration and transfer of solid particles in polymer blends are not yet well-understood. All previous works agreed that the diffusion and Brownian motion are not effective mechanisms of particle migration in high viscous polymer matrices [31, 91, 109]. In the shear induced migration, solid particles move randomly under hydrodynamic forces and collide with the interface. The frequency of the collision of mono-dispersed spherical particles moving in a shear flow is estimated as [91]:

$$C = \frac{8}{\pi}\dot{\gamma}\varphi$$

where $\dot{\gamma}$ and φ are the shear rate and the volume fraction of the solid particles. The linear dependency of the collision frequency to the shear rate in this mechanism can explain the enhancement effect of the shear rate on the migration of solid particles. However, this mechanism

cannot explain the observed effects of other kinetic parameters such as the effect of viscosity and particle size of silica. Moreover, this mechanism assumes that when the particles collide with the interface, the transfer of the particles to the other phase occurs instantaneously. Therefore, this mechanism cannot explain the non-equilibrium localization of solid particles reported in the literature [110, 121]. As mentioned in 2.4.2.5, Goldel et al. [110] proposed the SFM mechanism to explain the effect of the aspect ratio of solid particles on their migration velocity at the interface. However, this mechanism does not consider the effect of the surface energy of the components on the migration velocity at the interface.

In addition, some authors proposed that the trapping of solid particles between two colliding dispersed phase droplets can result in the transfer of solid particles from the matrix phase to the dispersed phase [31, 109]. Obviously, this mechanism is not considerable when the particles are initially distributed into the dispersed phase droplets. As can be seen, the present mechanisms in the literature can only limitedly explain the effect of some parameters, but a general mechanism of migration that considers the whole migration process and the kinetic and thermodynamic parameters involved is lacking in the literature.

### 2.4.3 The Effect of Different Localizations of Solid Particles on the Morphology of Polymer Blends

After reviewing the thermodynamic and kinetic aspects of the migration and localization of solid particles, in this section, the effect of different localizations of solid particles on the morphology of polymer blends will be discussed.

#### 2.4.3.1 Localization of Solid Inclusions in the Dispersed Phase

Filippone et al. [125] reported that in HDPE/PA6 blends, the addition of organoclay resulted in an exclusive localization of organoclay particles in the PA6 phase. They showed that by increasing organoclay content, the morphology of PA6 phase changed to an elongated morphology and at higher organoclay contents, a semi-continuous network of PA6 formed in the HDPE matrix, Figure 2.23.

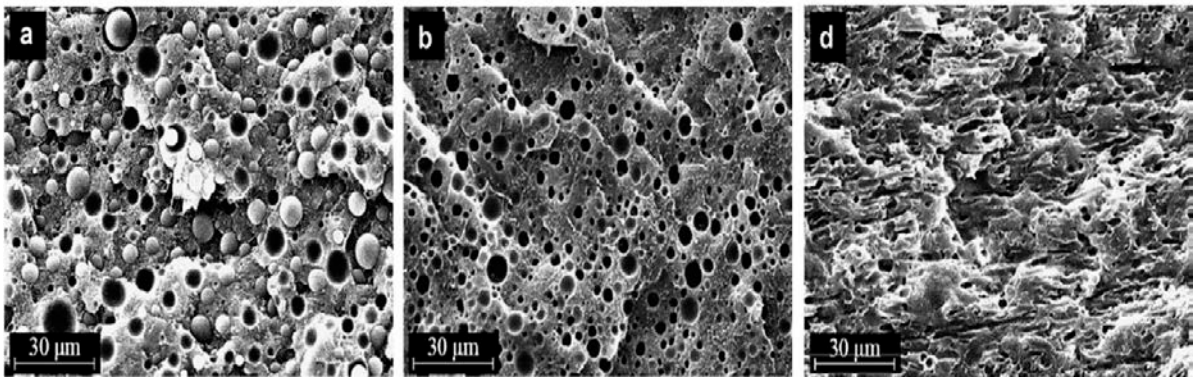


Figure 2.23. The effect of organoclay content on the morphology of HDPE/PA6 (75/25) blends: a) 0 wt.%; b) 1 wt.%; d) 5 wt.% [5].

They also studied the continuity of the PA6 phase in this blend at different solid contents and confirmed that increasing the organoclay content promoted the continuity level of PA6. They proposed that at high solid contents, a double percolating network forms in which PA6 becomes the continuous phase as it encapsulates the 3D formed structure of organoclay, Figure 2.24. Moreover, they observed that increasing the organoclay content up to 2.5 wt.% decreased the dispersed PA6 phase size. This was attributed to the decrease in the coalescence due to the platelet-like geometry of the organoclay; however, the authors did not explain how the confined organoclay particles in PA6 can affect the coalescence rate of PA6 droplets.

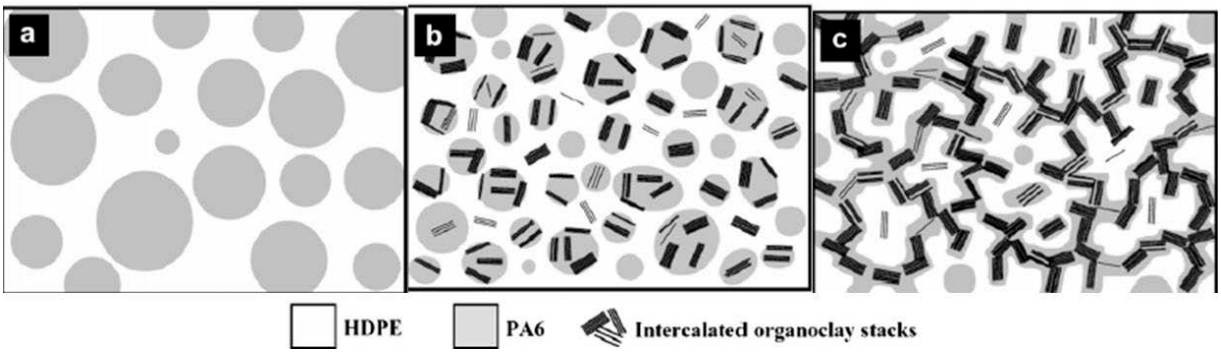


Figure 2.24. Mechanism of the formation of a continuous structure pf PA6 in HDPE/PA6 (75/25) blends: a) without organoclay; b) at low organoclay content; c) at high organoclay content [125].

The development of continuity in polymer blends by the formation of a 3D network of CB particles was also observed by Wu et al.[126] in a blend of ABS/PA6 where the particles were selectively localized in the PA6 phase, Figure 2.25.

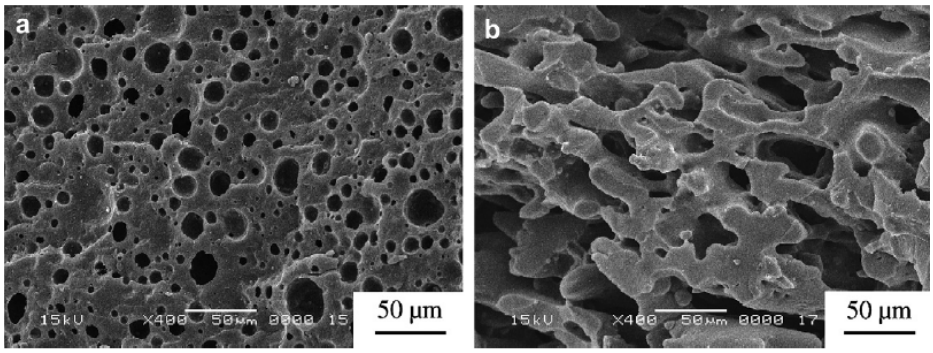


Figure 2.25. SEM images of ABS/PA6 (60/40) blend: (a) without CB particles (PA6 was extracted), (b) with 7.5 phr CB (ABS was extracted)[126].

Hong et al. [127] studied the effect of the localization of organoclay particles in a PE/PBT(90/10) blend. They found that the localization of the particles in the dispersed PBT phase increased the PBT phase size due to the increase in the viscosity of PBT, Figure 2.26.

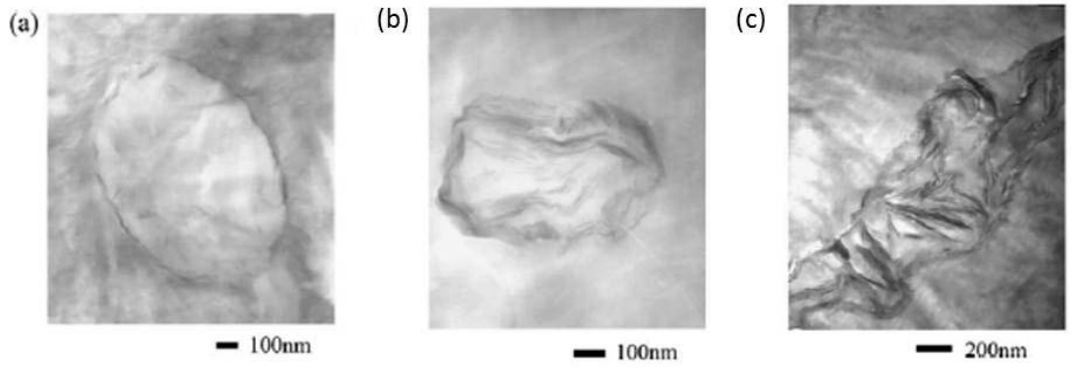


Figure 2.26. TEM images of a PE/PBT (90/10) blend with (a) 1 wt.%, (b) 5 wt.% and (c) 10 wt.% of organoclay [127].

Nuzzo et al.[128] also observed the enhanced continuity development of polyamide 11 (PA11) induced by the selective localization of organoclay, organo-modified sepiolite and CNT particles. They attributed this observation to the increase in the relaxation time of the PA11 dispersed phase due to the formation of a 3D solid structure inside the PA11 phase. Kong et al. [129] studied the effect of the addition of nano-silica in PA6 on the relaxation and breakup of a deformed PA6 droplet in a PS matrix and confirmed that the presence of nano-silica in the PA6 phase increased the relaxation and breakup time of PA6 droplets significantly. It can be

concluded that the previous studies show that the localization of solid inclusions in the dispersed phase promotes the formation of co-continuous structures in polymer blends.

### 2.4.3.2 Localization of Solid Inclusions in the Matrix Phase

The localization of solid inclusions in the matrix phase is a well-known approach to achieving a balance between toughness and stiffness [28, 79, 81, 82, 107]. Lee et al. [79] found that the localization of organoclay (MMT) in the PP phase in blends of PP/ethylene–octene based elastomer (EOR) increased both the modulus and impact strength of the blend, Figure 2.27.

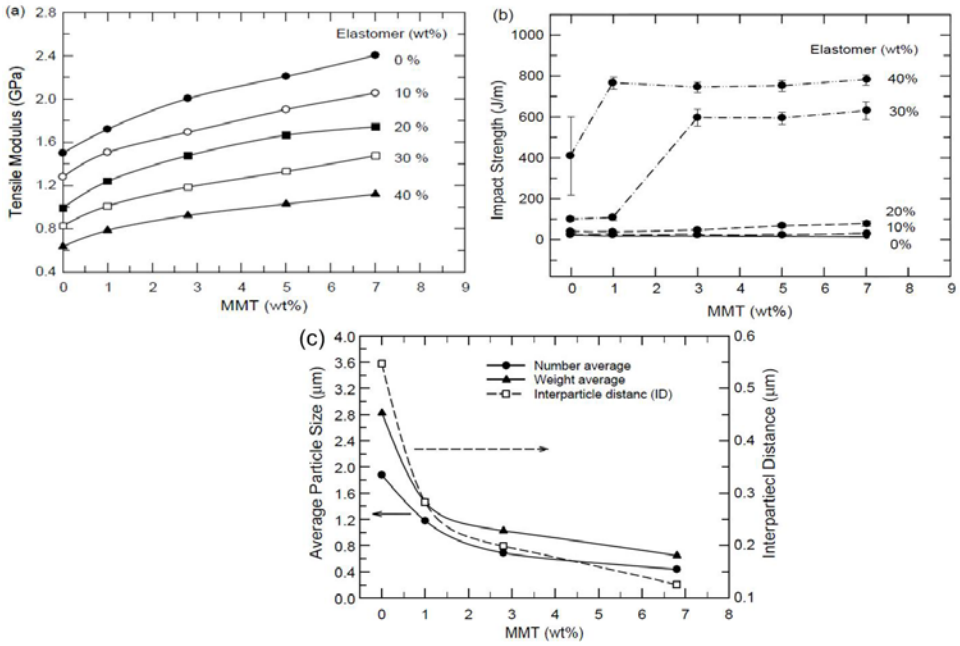


Figure 2.27. The effect of organoclay content on the mechanical properties of PP/EOR blends: (a) tensile modulus, (b) impact strength, (c) average particle size and inter-particle distance [79].

They found that by increasing the organoclay content, the dispersed EOR phase size decreased and finally reached a plateau at high organoclay contents, Figure 2.27(c). The observed onset of the plateau region in the droplet size curve occurs at the same composition as the onset of the plateau region in the impact strength (Figure 2.27 b). Khatua et al.[130] also reported that by increasing the organoclay content in a blend of nylon 6 (PA6) and EPR, the size of the dispersed EPR phase decreased and finally reached a plateau at high organoclay contents, Figure 2.28.

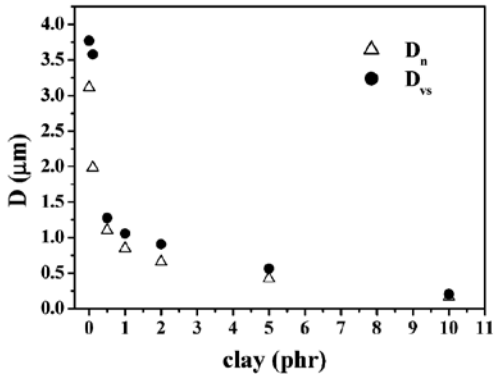


Figure 2.28. Volume ($D_{vs}$) and number ($D_n$) average diameter of EPR dispersed phase in a PA6/EPR blend as a function of organoclay content[130].

Bailly et al.[28] also showed that the selective localization of nano-silica particles in the PP matrix phase in a PP/ethylene-octene copolymer blend reduced the dispersed copolymer phase size and increased the mechanical strength. It can be seen that the reported effect of organoclay on the droplet size of the dispersed phase is similar to the effect of a compatibilizer on the phase size in polymer blends (which was reviewed in 2.2.5). These studies clearly indicate the potential application of nano-particles to reduce the dispersed phase size and improve the mechanical properties of the systems where finding a compatibilizer is challenging. The observed reduction in the dispersed phase size in polymer blends with solid inclusions localized in the matrix phase has been attributed to the decrease in the coalescence due to: (i) the presence of solid particles between droplets at the contact point[31, 32, 88, 131], (ii) reduced mobility of the chains around the particles [28, 29, 31, 32]. According to the first mechanism, during the coalescence of the dispersed phase droplets, solid particles that exist between the droplets can act as a solid barrier and prevent the coalescence. In the second mechanism, decreasing the mobility of the polymer chains around the particles increases the viscosity and the draining time of a thin film of the matrix separating the droplets. On the other hand, increasing the viscosity of the matrix can alter the viscosity ratio and affect the droplet breakup[81]. Lee et al.[132] observed a phase size reduction in PP/polyolefin elastomer (POE). As the presence of the particles did not change the viscosity, they proposed that the presence of the solid particles in the matrix forces the dispersed phase droplets to follow a highly tortuous path which implies a confined flow condition and enhances the droplet breakup. Lee et.al [81] studied the effect of nano-silica on the coarsening of a (PP+PP-g-MA)/poly(ethylene-co-octene), EOC, blend in a quiescent and under shear condition shows the obtained results. As can be seen in Figure 2.29, the presence of the particles in the

matrix phase significantly suppressed the coarsening of the structure in the quiescent annealing. Similar observations have been reported by other authors [132, 133]. Moreover, the coalescence of the blends with and without silica under shear showed a similar stabilization effect.

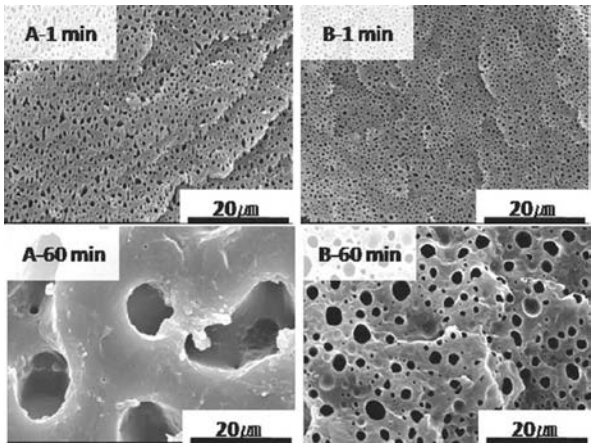


Figure 2.29. The effect of the quiescent annealing on the morphology of (PP+PP-g-MA)/EOC (60/40) in (A) the neat blend, (B) blend with 5 wt.% of nano-silica [81].

#### 2.4.3.3 Localization of Solid Inclusions at the Interface

The localization of solid particles at the interface of emulsions has been shown to reduce the dispersed phase size and stabilize the morphology. Ramsden in 1903 was the first researcher who reported particle stabilized emulsions, but Pickering conducted the first systematic study on solid-stabilized emulsions[134]. This work has been widely recognized as the first study on solid-stabilized emulsions and because of Pickering's contribution in this field solid stabilized emulsions are called "Pickering emulsions". Trifkovic et al.[135] studied the effect of the interface localization of nanoclay on the stability of a co-continuous blend of PE and PEO. They showed that the localization of organoclay at the interface significantly reduced the coalescence and stabilized the morphology against annealing, even with as little as 1 wt.% of organoclay. For lower organoclay contents, they observed that the coarsening of the morphology proceeded until the interface was entirely covered by the organoclay. By changing the surface treatment of organoclay, they found that the effectiveness of organoclay in stabilizing the morphology increases as the wetting parameter ($\omega$) approaches zero. This is a situation in which organoclay particles are predicted to be symmetrically localized at the interface. Elias et al. [88] found that by the addition of 3 wt.% fumed silica to a PP/PS blend, the silica particles were localized at the

interface and reduced the volume average diameter of the dispersed phase from 6.5 µm to 1.7 µm. Figure 2.30 shows the localization and morphology of the blends with and without fumed silica.

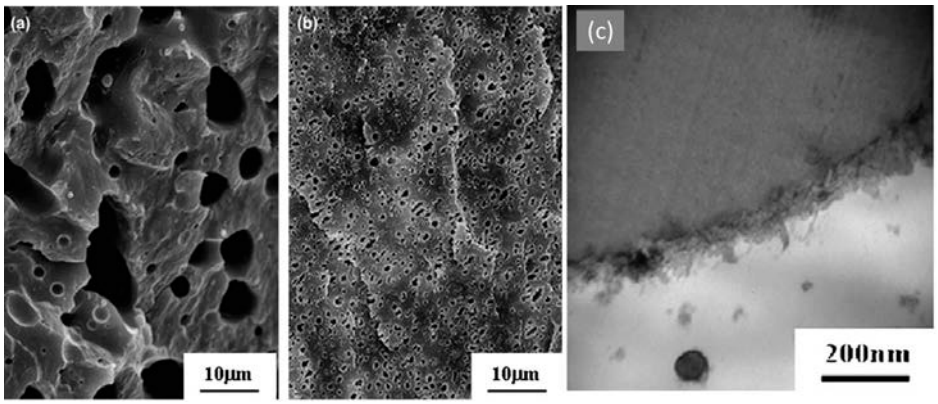


Figure 2.30. SEM images of (a): PP/PS (70/30) blend; (b) the blend with 3 wt.% fumed silica, (c) TEM image showing the localization of fumed silica at the interface[88].

The reduction in the dispersed phase size of polymer blends has been attributed to two main mechanisms [31, 32]: I) the solid barrier effect and II) the effect of solid particles on the interfacial tension. In the solid barrier mechanism, the presence of a solid shell around the dispersed phase prevents the coalescence upon the collision of the dispersed phase droplets. Baoudouin et al. [90] clearly showed the formation of a solid shell of CNT around PA6 droplets in an EA/PA6 blend, Figure 2.31.

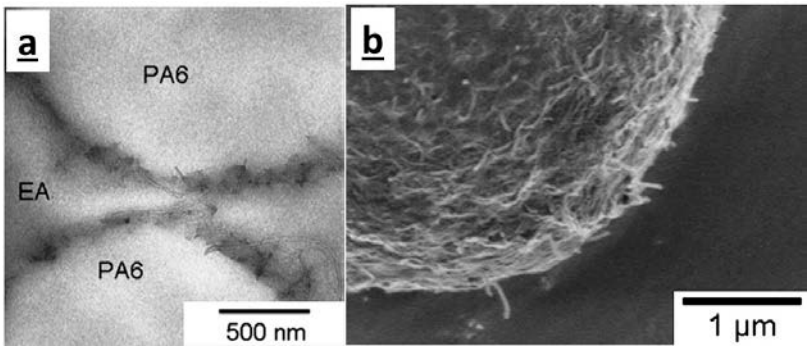


Figure 2.31. TEM (a) and SEM (b) image of the CNT shell around the PA phase in EA/PA6[90].

Elias et al. [91] found that despite the addition of 3 wt.% of hydrophobic silica to PP/EVA(80/20) the interface was not covered completely by the particles but the dispersed phase size was reduced from 1.6 µm to 0.9 µm. Figure 2.32 shows the localization of the silica particles in the

PP/EVA blend. These results confirm that the presence of solid particles at the interface even below the interface saturation can reduce the dispersed phase size. This stabilization is similar to the one observed in Pickering emulsions at low solid contents[136]. The mechanism of the stability of sparsely covered droplets is not well understood but the formation of a layer of solid particles at the contact area of the droplets may be responsible for the stabilization.

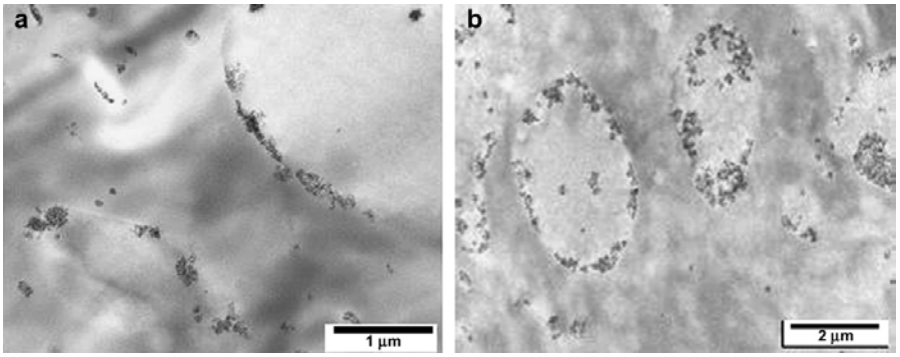


Figure 2.32. TEM images of PP/EVA(80/20) with 3 wt.% silica particles localized at the interface[91].

The effect of solid particles on reducing the interfacial tension has been mentioned frequently as another mechanism responsible for the observed reduction in the dispersed phase size. The idea of decreasing the interfacial tension and improving the compatibility in the presence of solid particles originates from the work of Lipatov [137] who showed that the presence of solid particles can enhance the compatibility of polymers in a blend. Fang et al. [138] proposed three different mechanisms for the enhancement in the compatibility of polymer phases due to the localization of nanoclay at the interface. These mechanisms are schematically shown in Figure 2.33.

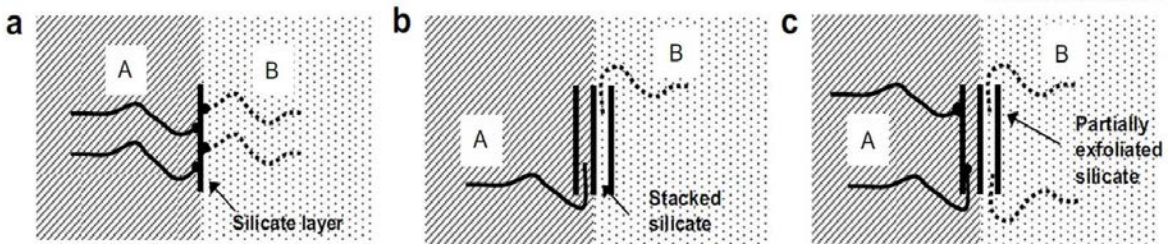


Figure 2.33. The proposed mechanisms for the enhancement of the compatibility of polymers due to the localization of nanoclay particles at the interface [138].

In these mechanisms, polymer chains are immobilized due to their interactions with the surface of nanoclay. As a result, a structure similar to a copolymer is formed which can act as a compatibilizer and enhance the compatibility of the polymer phases. The immobilization can occur as a result of strong interactions (or reactions) such as the one shown in Figure 2.33(a), or by the physical adsorption of the molecules (Figure 2.33 c).

Some authors tried to demonstrate the compatibilization effect of the particles at the interface by the estimation of the interfacial tension using rheological analysis. Elias et al. [88] used Palierne's model to estimate the interfacial tension between PP and PS in the presence of silica particles at the interface. Using this method, they concluded that the localization of 3 wt.% of silica particles at the interface reduced the interfacial tension between PP and PS from 2.3 mN/m to 0.45 mN/m. In another work from the same group [116], they used a new approach where they first separated the effect of composition from the effect of droplet relaxation on a storage modulus in PP/EVA blends and then, by assuming a Newtonian behaviour at low frequencies, they used Taylor theory [139] to estimate the interfacial tension. They found that the interfacial tension decreased from 0.94 mN/m to 0.56 mN/m. Salehyian et al. [140] used Gramespacher and Meissner's model [141] to predict the interfacial tension in a PP/PS(80/20) blend with organoclay localized at the interface and reported that the interfacial tension dropped from 1.9 mN/m for the neat blend to 0.4 mN/m for the system containing 5 wt.% of organoclay.

Despite the above-mentioned results in the literature, the definition of an interface and interfacial tension between two phases that are completely separated by a shell of solid particles should be used with caution. Moreover, the rheological models that were used in the literature to determine the effect of solid particles on the interfacial tension were developed for liquid emulsions with liquid-liquid interfaces and do not consider the effect of solid particles on the interfacial rheology.

# CHAPTER 3 ORGANIZATION OF ARTICLES

The results of the first part of this thesis are presented in Chapter 4 as the first article entitled “Morphology, miscibility and continuity development in poly(lactic acid)/poly(butylene adipate-co-terephthalate) blends”. This chapter is dedicated to the study of the morphology and miscibility of PLA/PBAT blends. The interfacial tension between PLA and PBAT was estimated using a rheological approach. The miscibility of PLA/PBAT was examined using the temperature-modulated DSC. Different microscopy techniques including SEM using lower secondary electron imaging (LEI), SEM using low-angle backscattered electrons (LABE) and atomic force microscopy (AFM) were used to investigate the morphology of this system. The morphology of the blend over the full composition range was studied and, finally, the co-continuity region was determined using a rheological approach.

In the second part of this project, the localization and migration of micro- and nano-silica particles in PLA/PBAT blends were studied. The results of this part are presented in Chapter 5 as the second article entitled “Localization of Micro- and Nano-Silica Particles in Heterophase Poly(lactic acid)/ Poly(butylene adipate-co-terephthalate) Blends”. The thermodynamic localization of silica particles was predicted to be in the PBAT phase. The effect of different mixing strategies was studied and it was found that the kinetic effects are very pronounced when the particles were premixed with the PLA phase. Using this mixing strategy, the effects of the viscosity of the PLA phase, the shear rate and the particle size of silica particles on the migration of silica were studied. The mechanism and parameters involved in each step of the migration were discussed in detail.

The effects of thermodynamic and kinetic parameters on the localization of micro- and nano-silica particles in PLA/LDPE blends were investigated. The results were presented as the third article entitled “Localization of Micro and Nano-Silica Particles in a High Interfacial Tension Poly(lactic acid)/ Low Density Polyethylene System” in Chapter 6. To study the effect of the surface energy of the particles, the surface of micro-silica particles was modified from a high to a low energy surface. The thermodynamic equilibrium localization of the unmodified and modified silica particles were determined to be in the PLA phase and at the interface, respectively. The effect of different mixing strategies was studied and it was found that the kinetic effects were

considerable when the particles were premixed with the LDPE phase. This mixing strategy was used and the effects of the viscosity of LDPE, the shear rate and particle size of silica particles on the migration were studied. The origin of the effects observed was discussed by considering different steps in the migration of the particles.

In addition, in Annex 1, the development of a semi-empirical model proposed for the migration velocity at the interface is presented in detail. The effects of different localizations of micro- and nano-silica particles on the morphology, rheology and mechanical properties of PLA/PBAT are studied in Annex 2. As will be discussed later in this thesis, finding a compatibilizer to enhance the interfacial adhesion in a PLA/PBAT blend is challenging due to the similar nature of PLA and PBAT. In Annex 3 solid state shear pulverization was used to enhance the interfacial adhesion in this system. The effects of silica particles on the morphology and continuity of PLA/PBAT were studied in Annex 4. Finally, Annex 5 presents the results of studying the effects of kinetic parameters on the migration and localization of copper nanowires in PLA/LDPE blends.

# CHAPTER 4 ARTICLE 1: MORPHOLOGY, MISCIBILITY AND CONTINUITY DEVELOPMENT IN POLY(LACTIC ACID)/POLY(BUTYLENE ADIPATE-CO-TEREPHTHALATE) BLENDS*

*Ebrahim Jalali Dil, P. J. Carreau and Basil D. Favis*

*CREPEC, Department of Chemical Engineering, École Polytechnique de Montréal, Montreal, Québec, H3C3A7, Canada.*

## 4.1 Abstract

In this study, the morphology and miscibility of poly(lactic acid), PLA, and poly(butylene adipate-co-terephthalate), PBAT, blends were studied in detail. Three techniques to examine the morphology of PLA/PBAT are compared: SEM using lower secondary electron imaging (LEI), SEM using low-angle back scattered electrons (LABE) and atomic force microscopy (AFM). The interfacial tension of the system was examined by fitting the Palierne model to the rheological data and the results indicate a very low value of 0.6±0.15 mN/m. The miscibility in PLA/PBAT blends was studied by modulated DSC and the results show a limited one-way partial miscibility of PBAT in the PLA-rich phase with the glass transition temperature of the PLA-rich phase in PBAT showing a drop of up to 10 ℃, as compared to the neat PLA. Further investigations reveal that this effect depends significantly on the molecular weight of PBAT and underlines the strong entropic nature of this partial miscibility. The morphology at 1 vol.% of the dispersed phase shows that the dispersed phase exists in a stable fiber form even at these very low concentrations, an observation which is compatible with partial miscibility, with fiber diameters of 300 nm for PLA in PBAT and 150 nm for PBAT in PLA. The influence of composition on the dispersed phase fiber diameter shows a significant increase in fiber diameter with minor phase concentration which is not a result of classic coalescence, but more a result of the partial miscibility phenomenon. The region of dual-phase continuity has been examined by a rheological

*Published in *Polymer* (2015): 68, 202.

approach and is determined to be a wide and highly symmetric region with the lower and upper limits located between 30-40 and 60-70 vol.% of PBAT, respectively.

*Keywords: Poly(lactic acid), Miscibility, Morphology*

## 4.2 Introduction

Bioplastics have received much attention during the past decade predominantly due to environmental concerns related to greenhouse gas production and the end of life scenarios for classic petroleum based polymers [1]. Among bioplastics, poly(lactic acid), PLA, has shown significant commercial growth due to its bio-based and compostable nature, mechanical strength, availability in the market and lower price compared with most other bioplastics [2]. One of the most important weaknesses of PLA is its brittleness. Different methods have been proposed to overcome this drawback and, in this regard, the blending of PLA with other polymers has received much attention [3]. Polymer blends with PLA offer an economically viable approach to overcome the brittleness and also enhance other properties, such as the crystallinity of PLA. Among different blends of PLA, blends with other polyester-based bioplastics such as polycaprolactone (PCL) [4, 5] and poly(butylene adipate-co-terephthalate), a copolymer of butylene adipate (BA) and butylene terephthalate (BT) known as PBAT, [6-21] have been studied more extensively due to their compatibility with PLA, high elongation at break and impact strength and biodegradability/compostability. The PLA/PBAT blend is particularly interesting since it can offer a much wider range of application temperatures and thus has the most significant commercial potential.

Jiang et al. [21] studied PLA/PBAT and showed that the addition of 20 wt.% of PBAT increases the elongation at break by a factor of 50. A number of other studies [6-20] have focused on the mechanical properties and, to some extent, the rheological properties, however many aspects of the morphology and miscibility of PLA/PBAT remain unclear. This can be attributed to the complexity of the characterization of this blend which originates from the very similar polyester nature of both PLA and PBAT. The complex morphology of some polymer blends with similar nature components was previously studied in this group. Ravati et al. [22] studied the

morphology of ternary blends of PLA/PBAT/ poly(butylene succinate), PBS, and PLA/PBS/polycaprolactone,PCL and showed that PLA/PBAT/PBS develops into a tri-continuous morphology while PLA/PCL/PBS has a partially wet morphology with droplets of one phase spread on the interface of two other phases. In previous work from this group, Li et al. [23] studied the continuous and co-continuous morphology development in polymer blends with different types of the interfaces and showed that highly interacting, low interfacial tension systems demonstrate fibrillar morphologies even at low composition. This fibrillar morphology leads to a lower percolation threshold for continuity development and results in a wide region of co-continuous morphology. Marin et al. [24] and Bhadane et al. [25] also studied the morphology development in highly compatible low interfacial tension blends and observed some deviations from the classified features by Li et al. which they attributed to the partially miscible nature of the polymer blends studied. The results of these three studies clearly indicate that the level of interaction between components in low interfacial tension polymer blends and their mutual miscibility/immiscibility can have a determining effect on the morphology development. Jiang et al. [21] used dynamic mechanical analysis, DMA, to study the miscibility of PLA/PBAT blends in the composition range of 5 to 20 wt.% of PBAT and concluded that PLA/PBAT is an immiscible polymer blend. Yeh et al. [16], also using DMA, reported that PLA/PBAT was a miscible binary polymer blend system when PBAT was less than 5 wt.%. The miscibility/immiscibility of PLA/PBAT still remains to a large degree unresolved.

The objective of this work is to carry out a highly detailed examination of the miscibility, interfacial tension and morphology of PLA/PBAT blends. The dispersed phase and co-continuous morphology will be characterized using a variety of microscopic and rheological techniques. Finally a comprehensive conceptual model for the morphological development of these systems will be proposed.

## 4.3 Experimental

### 4.3.1 Materials

PLA 3001D (Natureworks) from Cargill and two commercial grades of PBAT, Ecoflex F BX 7011 and Ecoflex F Blend C1200 from BASF will be referred as PLA, L-PBAT and H-PBAT

respectively. All the materials were dried at 60 ℃ under vacuum overnight before being used in the experiments.

### 4.3.2 Molecular weight and Gel permeation chromatography (GPC)

The molecular weights of the three polymers were obtained from GPC tests carried out on an Agilent 1260 Infinity Multi-Detector GPC/SEC system equipped with two Phenomenex Phenogel columns ($10^3$Å pore size, 5μm bead) and a 1260 Infinity Refractive Index Detector. The solution of polymers (100 μL of 2mg/ml in chloroform) was injected with the flow rate of 1 mL/min.

### 4.3.3 Proton nuclear magnetic resonance ($^1$HNMR)

In order to determine the ratio of butylene adipate (BA) to butylene terephthalate (BT) segments in PBATs, $^1$HNMR spectra of L-PBAT and H-PBAT in $CDCl_3$ were recorded at 25℃ on a Bruker AVII-700, operating at 16.4 Tesla ($^1$H frequency of 700 MHz). 64 scans with a repetition time of 7.8 s were used for all the samples.

### 4.3.4 Blend preparation

All samples were prepared using an internal batch mixer (Plasti-Corder DDR501, Brabender) with a total volume of 30 mL at 50 RPM and 180 ℃ under a nitrogen blanket. The average shear rate at the processing condition used was estimated as 25 $s^{-1}$ [26]. After 10 minutes of mixing, samples were cut and cooled in ice-water to freeze-in the morphology of the samples.

### 4.3.5 Field emission scanning electron microscopy (FE-SEM)

The samples were cut and microtomed under liquid nitrogen using a microtome (Leica-Jung RM 2065). Then, the sample surface was coated with a15 nm thick gold layer and the morphology was observed with a FE-SEM machine (JSM 7600F, JEOL). Two different detectors of lower

secondary electron image (LEI) and low-angle backscattered electron (LABE) were used to examine the morphology of the microtomed sample. Cryo-fractured samples were also coated with a gold layer before determining their morphology by FE-SEM.

### 4.3.6 Atomic force microscopy (AFM)

The samples were microtomed using the same procedure as mentioned for FE-SEM samples. The AFM machine was equipped with a scanning probe microscope Dimension 3100 with a Nanoscope IVa controller from Veeco Instruments. Silicon tips, model ACTA-W from AppNano, with the tip radius less than 10 nm were used in this study. Because of the differences in the modulus of PLA and PBAT, the tapping phase mode was used to determine the morphology of the samples.

### 4.3.7 Image analysis

The AFM images were analyzed by an image analysis software (SigmaScan Pro. V.5, Sigmaplot) equipped with a digitizer table (Wacom) and a pressure sensitive pen for convenient mapping of the dispersed phase. The detailed procedure on how the digitizing table works was described elsewhere [27]. The average dispersed phase fiber or spherical droplet diameter were determined using an average number of 350 measurements from 6 to 8 AFM images (depending on the blend structure) for each sample. In the samples with 1 vol.% of the dispersed phase, the average dispersed phase diameter was determined using an average number of 30-50 measurements. In the disk samples with spherical dispersed phase morphology for the interfacial tension measurement, the Saltikov correction was applied [28] in calculating the dispersed phase diameter to consider the fact that the droplets are not cut exactly at their equator in the microtomed surface. The average dispersed fiber diameter in the samples with fibrillar morphology cannot be determined from the area of the dispersed fibers in the microtomed samples as the cross-sectional area depends considerably on the angle between the microtoming direction and the fiber axis. Figure 4.1 schematically shows how cutting a fiber at different angles in a blend with fibrillar morphology can result in different observed cross-sectional area of the fiber in AFM images.

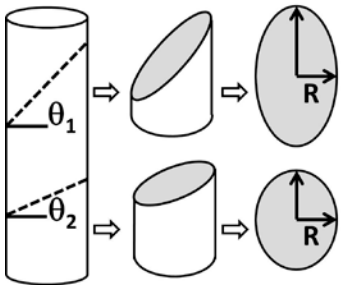


Figure 4.1. The effect of different cutting angles with respect to a fiber axis on the observed cross-sectional area in the microtomed surface. $\theta_i$ is the cut angle with the respect to the fiber axis and R is the fiber radius.

After cutting a fiber, its final geometry becomes a cylindrical segment in which the smallest diameter of the formed ellipse (minor axis) in the microtomed surface is always equal to the diameter of the fiber. Therefore, the average fiber diameter in this work was calculated based on the measured smallest diameter of the dispersed fibers cross-sectional area in the microtomed surfaces. The average fiber diameters are reported as XX±YY where XX denotes the average value and YY represents the standard deviation.

### 4.3.8 Rheological analysis

All the samples were compression moulded at 180 ℃ and at 300 kPa under a nitrogen blanket in the form of 1.2 mm thick disks with 25 mm diameter. The rheological analysis was carried out using a controlled stress rheometer (Physica MCR 301, Anton Paar) with 25 mm parallel plate geometry at 1 mm gap and at a temperature of 180 ℃ under nitrogen atmosphere. All the samples were annealed at 180 ℃ for 5 minutes in the rheometer before performing the rheological tests. Before measuring the rheological properties of the PLA/L-PBAT blends, the stability of PLA and L-PBAT was studied in the test condition using a time sweep test and no degradation was observed in the experimental time scale of 40 minutes. Moreover, the linear viscoelastic region was determined using a strain sweep test for neat polymers and polymer blend samples at different frequencies. According to the obtained results, the frequency sweep tests for the neat polymers and polymer blends were performed at strains of 5% and 1% respectively.

### 4.3.9 Interfacial tension measurement

The interfacial tension between PLA and L-PBAT was determined in this work using a rheological approach developed by Palierne [29, 30]. That model predicts the rheological behaviour of incompressible viscoelastic emulsions with a narrow droplet size distribution ($D_v/D_n \leq 2$) in small amplitude oscillatory shear experiments, SAOS, and relates it to the interfacial tension. According to the Palierne model, the complex modulus of an emulsion can be expressed as:

$$G^* = G_m^* \frac{1 + 3\varphi H}{1 - 2\varphi H}$$

where H is defined as:

$$H = \frac{(G_d^* - G_m^*)(19\,G_d^* + 16\,G_m^*) + 4\frac{\gamma_{md}}{R}(5\,G_d^* + 2\,G_m^*)}{(2\,G_d^* + 3\,G_m^*)(19\,G_d^* + 16\,G_m^*) + 40\frac{\gamma_{md}}{R}(G_d^* + \,G_m^*)}$$

and $G^*$, $G^*_m$, $G^*_d$, $\gamma_{md}$, R and φ are respectively the complex modulus of the blend, complex modulus of the matrix, complex modulus of the dispersed phase, the matrix/dispersed phase interfacial tension, the volume average dispersed phase radius and the volume fraction of the dispersed phase. As the sample preparation for rheological analysis and the annealing of the sample during preheating before the rheological measurements can change the morphology and phase size of the dispersed phase considerably, to increase the precision of the obtained value for the average dispersed phase radius, the phase size of the dispersed phase right before starting the rheological analysis should be determined. To this aim, the disk sample of PLA/L-PBAT(80/20) prepared by compression moulding was placed in the rheometer at 180 ℃ under a nitrogen atmosphere and the gap was set as 1mm. The sample was kept in this condition for 5 minutes (the same period as the preheating step in the rheological measurements) and then, the chamber of the rheometer was opened and the sample was cooled as quickly as possible using an air gun. The disk sample was then cut and microtomed at ½ of the radius of the disk and the morphology of its cross-section was determined by AFM. The volume average dispersed phase diameter was determined using the procedure explained in the image analysis section.

### 4.3.10 Temperature-Modulated dynamic scanning calorimetry (TMDSC)

Modulated DSC was employed to determine the miscibility state of PLA/PBAT blends by studying the variation of the glass transition temperature (*Tg*) of the polymeric phases. TMDSC tests were performed using a DSC Q1000 machine (TA Instruments) in the temperature range of -60 to 70 ℃. To obtain precise results, the calibration of heat capacity was performed by running a standard sapphire sample and comparing the obtained results with the literature value[31]. Moreover, melting peak temperature and cell constant calibrations were carried out using an empty pan and a standard indium sample. In all of the TMDSC experiments, an oscillation amplitude of ±1.27 ℃ and oscillation period of 60 s were used with a heating rate of 2℃/min. The *Tgs* of the phases were determined from the inflection points in the reversible heat flux curves of TMDSC results. The reported values are an average of three different measurements. Due to the high accuracy of TMDSC, the error in the measured *Tgs* was always less than 0.8% (~ 0.3-0.4 ℃) .

## 4.4 Results and Discussion

### 4.4.1 Molecular Weight and Rheological Characterization of the Neat Polymers

The molecular weight and molecular structure of PLA, L-PBAT and H-PBAT were characterized using GPC and $^{1}$HNMR and the results are shown in Table 4-1**.** The ratios of BA to BT co-monomers in both L-PBAT and H-PBAT were determined using the ratio of the integrated peak intensities of chemical shifts at 2.34 ppm and 8.11 ppm in the $^{1}$HNMR spectra of PBAT which correspond to methylene protons adjacent to carbonyl groups in BA segments and protons of the aromatic groups in BT segments, respectively. The $^{1}$HNMR spectra of PLA and L-PBAT (which is identical to H-PBAT) are shown in Figure 4.2. It can be seen that the molecular weight of H-PBAT is about three times higher than L-PBAT, but both of these copolymers have similar molecular structure with the same ratio of BA/BT co-monomers.

Table 4-1. The molecular characteristics of PLA, L-PBAT and H-PBAT.

| | Mn(g/mol)* | Mw(g.mol)* | Degree of polymerization (DP)* | BA/BT ratio** |
|---|---|---|---|---|
| PLA | 72000 | 142000 | 2535 | - |
| L-PBAT | 20000 | 45000 | 214 | 1.08 |
| H-PBAT | 72000 | 126000 | 600 | 1.08 |

*Determined from GPC data

** Determined from $^{1}$HNMR spectrum

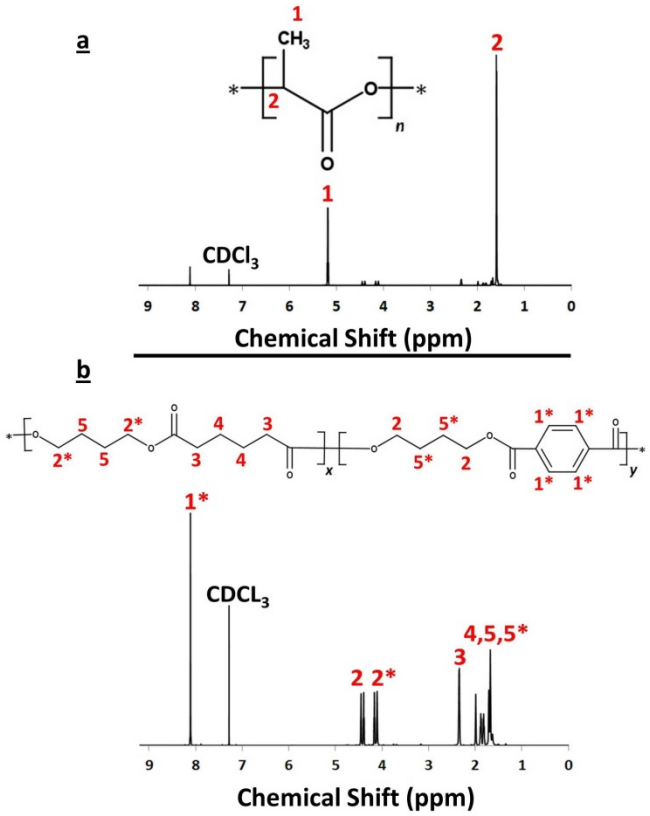


Figure 4.2. The $^{1}$HNMR spectra of (a) PLA, (b) L-PBAT. The red labels indicate the different hydrogen with the associated peaks.

The complex viscosities of the neat polymer components were measured and are shown in Figure 4.3. As expected, increasing the molecular weight of PBAT increases the complex viscosity. However, the increase in the viscosity is much less than what is expected from the empirical model of $\eta \sim M_w^{3.4}$ presented for narrow molecular weight distribution (MWD) of linear homopolymers with the molecular weight ($M_w$) greater than the entanglement molecular weight ($M_e$) [32]. It should be mentioned that the deviation from the empirical relation has also been observed in some other polymers [33, 34]. The observed deviation could be related to the

MWD of the L-PBAT and H-PBAT as well as the difference in their MWDs. In addition, the empirical relation was presented for homopolymers and therefore the copolymer nature of PBAT can also contribute to the observed deviation. All polymer components show a Newtonian plateau at low frequencies (shear rates) and the viscosity ratios of L-PBAT to PLA and H-PBAT to PLA at the shear rate corresponding to the processing conditions used are determined as 0.3 and 1.

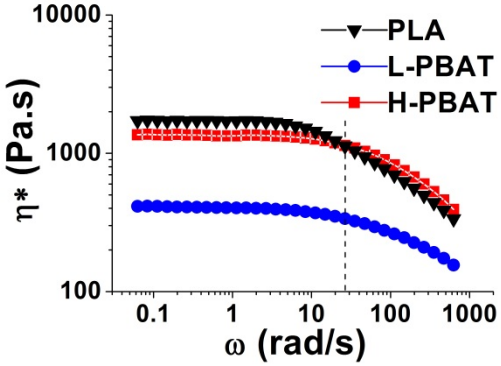


Figure 4.3. The complex viscosity of the polymer components as a function of angular frequency. The dashed line represents the average shear rate of mixing (25 $s^{-1}$) estimated using the equation presented in ref.[26].

### 4.4.2 PLA/PBAT Interfacial Tension

The interfacial tension between polymer components is an important characteristic parameter that significantly influences the morphology of a polymer blend system. The interfacial tension between PLA and PBAT at 185 ℃ was previously estimated using the Harmonic Mean Approach as 0.08 ± 0.1 mN/m by extrapolation of the measured surface energy data at room temperature [22]. The error in the estimated interfacial tension is due to the small differences between the surface energy of PLA and PBAT and the unavoidable errors in the contact angle measurements (such as the roughness of the surface of solid polymer, purity of the liquid probes and the resolution of the droplet images). Since that approach is approximative, it was decided to undertake a more detailed experimental approach for measuring the interfacial tension.

The interfacial tension between PLA and PBAT was estimated by fitting the Palierne model on the complex modulus ($G^*$) of PLA/L-PBAT (80/20) blend sample. The storage modulus ($G'$) of the blend sample was used as the criterion to evaluate the accuracy of the fitting as it is more sensitive to elastic interfacial phenomena such as droplet relaxation. The result of the fitting of the Palierne model on the experimental data is shown in Figure 4.4.

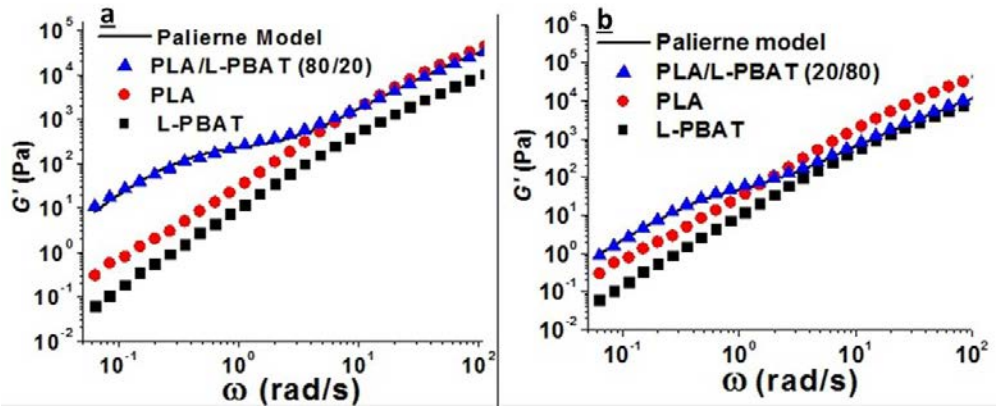


Figure 4.4. Fitting of the Palierne model on the storage modulus of PLA/L-PBAT blends. (a) PLA/L-PBAT (80/20), the solid line shows the Palierne fit with γ/d=444, (b) PLA/L-PBAT (20/80), the solid line shows the Palierne fit with γ/d=232.5.

Using this approach, the ratios of $\frac{\gamma_{md}}{R}$ in PLA/PBAT(80/20) and PLA/L-PBAT(20/80) were determined as 444.45±111.1 and 232.5±23 mN/m$^2$ which are an average of three different measurements. Figure 4.5(a) shows the AFM image of the microtomed surface of the disk sample of PLA/L-PBAT prior to rheological analysis.

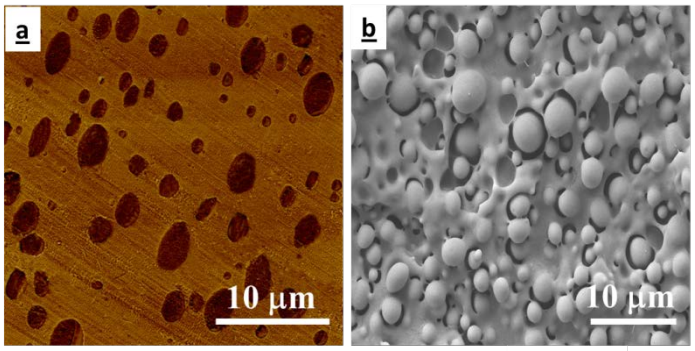


Figure 4.5. The morphology of the cross-section of PLA/L-PBAT(80/20) disk sample after decreasing the gap to 1mm and annealing for 5 minutes at 180 ℃: a) AFM phase image, b) FE-SEM image of the fractured surface. The scale bars show 10 μm.

As can be seen in Figure 4.5(b), the morphology of PLA/L-PBAT (80/20) right before the rheological measurements is a matrix-dispersed phase morphology with a spherical L-PBAT dispersed phase. It should be noted that later in this paper, we will show that the morphology of PLA/L-PBAT demonstrates a fibrillar dispersed phase morphology over a wide composition

range. The spherical morphology shown above is due to the compression molding and annealing times used in preparing the samples for the rheological measurements. That procedure allows dispersed fibers to retract to a spherical form.

The difference in the number of the observed particles in Figure 4.5 (a) and (b) is related to the different sample preparation method of these samples. The AFM sample was microtomed and therefore all the observed dispersed PBAT droplets are in a flat-plane surface. On the other hand, the SEM sample was prepared by cryo-fracture and as the cryo-fracture occurs at the weakest points of the sample, the dispersed phase droplets in the SEM image are not necessarily in the same-plane. This causes more particles to be seen in the SEM images compared with the AFM images. In Figure 4.7, it can be seen that when the SEM samples were prepared by microtoming, the particle density of SEM and AFM images are similar.

The volume average diameter of L-PBAT droplets in the annealed samples of PLA/L_PBAT(80/20) and PLA/L-PBAT(20/80) were determined from AFM images as 2.7± 0.6 and 4.3 ± 0.9 μm, respectively. Using the $\frac{\gamma_{md}}{R}$ ratio obtained from the fitting of the Palierne model on *G'*data, the interfacial tension between PLA and L-PBAT was determined as 0.60±0.15 mN/m for PLA/L-PBAT(80/20) and 0.5±0.1 mN/m for PLA/L-PBAT(20/80). It is important to note that the same interfacial tension was observed for the blends of PBAT dispersed in PLA and for PLA dispersed in PBAT.

Recently, Al-Itry et al. [20] and Nofar et al. [35] also used the Palierne rheological analysis to determine the interfacial tension between PLA and PBAT and reported values of 6.0 and 1.25 mN/m, respectively. The high interfacial tension reported by Al-Itry et al.[20] could be related to the fact that they fit their experimental data to loss modulus (*G"*) rather than the storage modulus (*G'*) and that the data fit to their *G'* data at low frequencies, where the droplet relaxation occurs, is very poor. Nofar et al. [35] report a low interfacial tension for PLA/PBAT, but which is nevertheless double the value reported here. Nofar et al. used a significantly lower molecular weight PLA and a higher molecular weight PBAT in their study.

### 4.4.3 Miscibility

In order to examine the state of miscibility in PLA/L-PBAT blends, TMDSC tests were carried out on samples with 10-30 and 70-90 vol.% of L-PBAT. The main advantage of the

TMDSC technique over dynamic mechanical analysis (DMA) is that the test can be performed on the samples taken right after mixing without any further sample preparation step and, therefore, can better represent the miscibility state of the phases during processing. Figure 4.6(a) shows the variation of the *Tgs* of the PLA and L-PBAT phases.

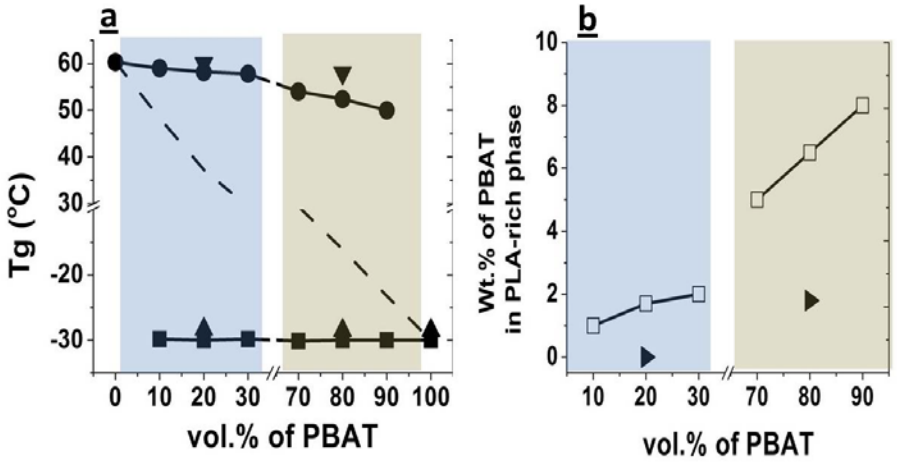


Figure 4.6. (a) Glass transition temperatures of PLA and PBAT phases in the blend samples determined from TMDSC results: (■) L-PBAT phase in PLA/L-PBAT blends; (●) PLA-rich phase in PLA/L-PBAT blends; (▲) H-PBAT in PLA/H-PBAT blends; (▼) PLA-rich phase in PLA/H-PBAT blends. (b): wt.% of PBAT in PLA-rich phase determined from the Fox equation: (□) wt.% of L-PBAT in PLA-rich phase in PLA/L-PBAT blends; (►) wt.% of H-PBAT in PLA-rich phase in PLA/H-PBAT blends. The dashed line in (a) shows the Tg of a miscible blend based on the Fox equation.

As can be seen, after melt-mixing, the Tg of the L-PBAT phase remains unchanged, but the Tg of the PLA phase decreases considerably which indicates the presence of L-PBAT in the PLA phase. Since the Tg of the L-PBAT phase did not change, these results point to a limited one-way partial miscibility of L-PBAT in the PLA phase and therefore, the PLA phase will be referred to as the PLA-rich phase hereafter in this paper. The composition of L-PBAT in the PLA-rich phase can be determined using the Fox equation:

$$\frac{1}{Tg} = \frac{W_1}{Tg_1} + \frac{(1 - W_1)}{Tg_2}$$

where $Tg$, $Tg_1$ *and* $Tg_2$ are the $Tg$s of the PLA-rich phase, the neat PBAT phase, and the neat PLA phase, respectively. Moreover, $W_1$ is the weight percent of PBAT in the PLA-rich phase. The calculated compositions of L-PBAT in the PLA-rich phase are shown in Figure 4.6(b).

Interestingly, as can be seen in Figure 4.6 (a), the one-way partial miscibility of L-PBAT in the PLA-rich phase is dramatically reduced by increasing the molecular weight of the PBAT phase. The miscibility state in a mixture is determined by the enthalpy of mixing and the entropy gain due to mixing. Considering the identical molecular structure of L-PBAT and H-PBAT, the observed decrease in the partial miscibility of PBAT by increasing its molecular weight cannot be due to the change in the enthalpy of mixing. On the other hand, considering the much smaller degree of polymerization (DP) of L-PBAT compared with PLA, Table 4-1, the observed one-way partial miscibility of L-PBAT in PLA can be attributed to the higher mobility of L-PBAT chains and/or the larger entropic gain due to mixing of L-PBAT molecules in the PLA-rich phase. In previous work, Marin et al. [24] showed that PC/PMMA blends demonstrate a classic partial miscibility after melt processing. The materials used in that work were of substantially larger viscosities than the materials used in the present study. This strongly suggests that kinetic barriers to the inter-diffusion of polymer chains due to the absolute viscosities of the base polymers are not responsible for the one-way partial miscibility phenomenon observed in the current work.

To further understand the origin of the observed limited one-way partial miscibility of PBAT in PLA, the solubility parameters of PLA and PBAT were estimated by the group contribution method. Using this approach, the solubility parameters of PLA and PBAT were determined as 21.9 and 22.2 $MPa^{1/2}$. Although the solubility parameter of PBAT has not yet been measured experimentally in the literature, the estimated solubility parameter for PLA is in good agreement with the literature data [36]. The almost identical estimated solubility parameters of PLA and PBAT clearly support the hypothesis of a very small enthalpy of mixing for these two polymers. Under such conditions, it is possible that small changes in the entropy of mixing could affect the miscibility state of the system and result in partial miscibility. Roland et al. [37] reported a similar observation in 1,4 polyisoprene and poly(vinylethylene) blends. They showed that although these polymers do not have any specific interactions, the blends show miscibility even at the high molecular weight of 330000 g/mol. They showed that the enthalpy of mixing was also very small and they estimated the Flory-Huggins interaction parameter to be less than 0.004. At such a small enthalpy of mixing, they concluded that even a small value of the entropy of mixing

can favour the miscibility. Similar behavior has also been reported for the blend of polystyrene and poly(α-methyl styrene) which has a very small positive enthalpy of mixing (Flory-Huggins interaction parameter ~ $3\times10^{-5}$ [38]) and shows miscibility even at the molecular weight of 70000 g/mol of PS [39]. That system also showed a relatively strong dependence of miscibility/partial miscibility to the molecular weight of the components [40].

Considering all of the above, it can be concluded that the near equivalent cohesive energy density between PLA and PBAT leads to a negligible energy change and a very small enthalpy of mixing when replacing a PLA segment in a PLA rich environment with a PBAT segment. Consequently, small changes in the combinational entropy can favour the observed limited partial miscibility in this system. The observed one-way nature of the partial miscibility in PLA/L-PBAT can be attributed to the larger entropic gain of mixing L-PBAT molecules in the PLA-rich phase compared with mixing PLA molecules in the L-PBAT phase. Furthermore, the entropic gain of mixing H-PBAT with PLA is significantly reduced as the molecular weight of these two polymers is very similar. This work is important as it indicates a potential strategy for controlling the level of partial miscibility for systems demonstrating close to zero enthalpy of mixing. One could envisage the addition of small quantities of low molecular weight fractions to a higher molecular weight material that could potentially allow for the tailoring of interfacial properties while maintaining the advantages of high molecular weight materials for mechanical property enhancement.

### 4.4.4 Morphological Characterization of PLA/L-PBAT Blends

Figure 4.7 compares the morphology of PLA/L-PBAT blends of different compositions determined using two different FE-SEM detectors (LEI and LABE) and an AFM technique. As can be seen, phase contrast in the images taken by the LEI detector is poor and no phase can be distinguished in the LEI image of PLA/L-PBAT(50/50). This is due to the small topographical contrast between the phases in the microtomed surfaces of these samples. On the other hand, the LABE detector, due to its position and size, can detect the backscattered electrons with low scattering angles, which significantly enhances the contrast between phases. In Figure 4.7, the LABE detector presents the PBAT phase as the brighter phase while PLA is the darker phase [41]. This allows one to distinguish the phases even in the co-continuous region, which is not generally possible in images taken by SEM without selective extraction of either phase. Note that

due to the very similar solubility parameter of PLA and PBAT selective solvent extraction is not a possibility here. On the other hand, the LABE detector works at higher current and voltage and the scan needs to be done quickly at high magnifications to avoid burning of the surface of the samples due to the high energy of the incident electron beam.

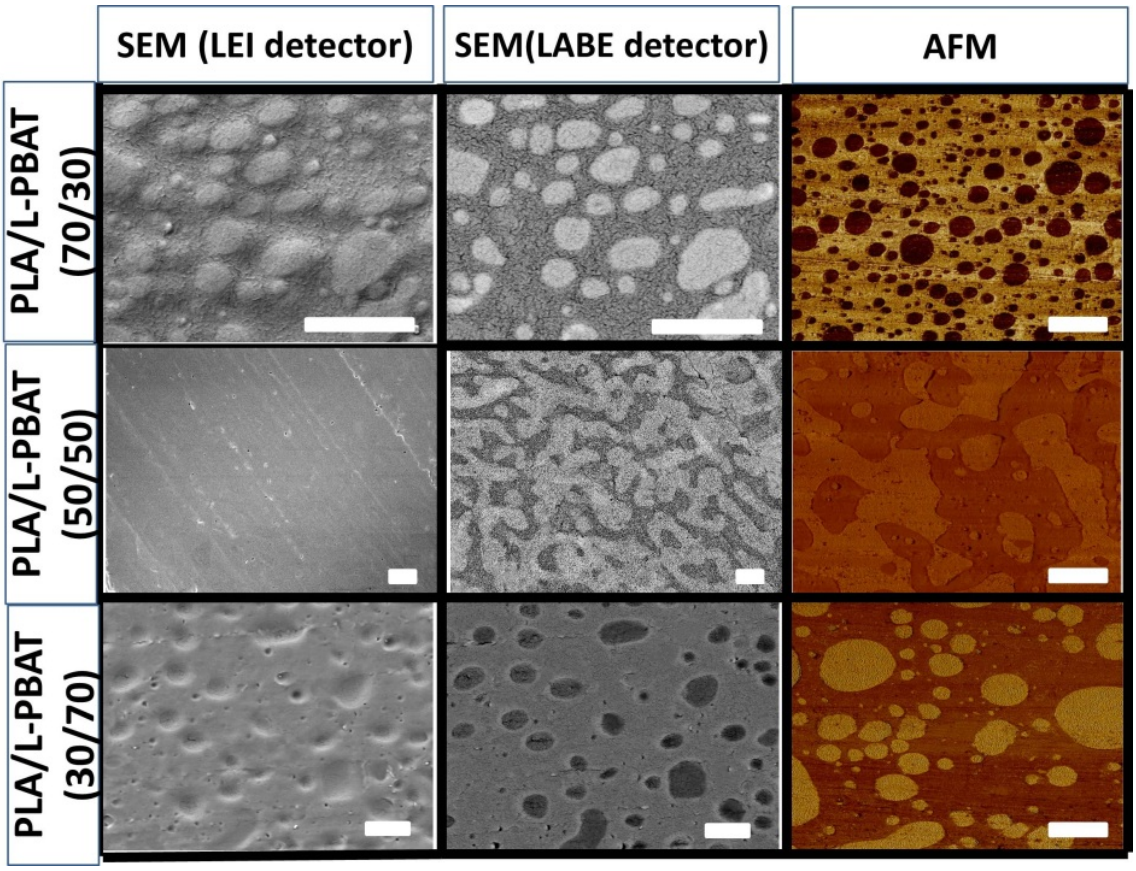


Figure 4.7. Comparison between different microscopy techniques in the analysis of the morphology of PLA/L-PBAT blends with different compositions. All the white scale bars indicate 5 μm.

Atomic force microscopy (AFM) is also a powerful imaging technique that has been successfully used in studying the morphology of polymer blends with complex morphologies [42]. Although it has some inconveniences such as long scan time, limited scan area and great care required in the sample preparation, AFM can provide images with high resolution and phase contrast at nano-metric scales (lateral resolution > 10 nm, height resolution > 1 nm). Such high resolution and phase contrast can be seen in Figure 4.7 where very fine dispersed phase domains in the order of 200 nm can be seen in 30 μm×30 μm AFM images. The AFM technique will be used as the

principal microscopic technique to characterize the morphology of the microtomed samples in this paper.

As previously established by Li et al. [23] and Bhadane et,al [25], the dispersed phase in low interfacial tension systems typically exists in the form of fibers rather than droplets. The formation of the fibrillar morphology in these systems is due to the very long breakup time of the dispersed phase fibers, which originates from their low interfacial tension. Therefore, the type of the morphology of PLA/L-PBAT needs to be determined before any further morphological analysis. Cryo-fractured surfaces of polymer blends with 1, 10, 20, 80, 90 and 99 vol.% of L-PBAT were studied using FE-SEM and the results are shown in Figure 4.8. It can be seen that the dispersed phase exists in the form of stable fibers even at very low compositions of 1 vol.% of the dispersed phase. This fiber-like morphology across the composition range is in line with previous studies and is a direct result of the low interfacial tension resulting from the partial miscibility of the system.

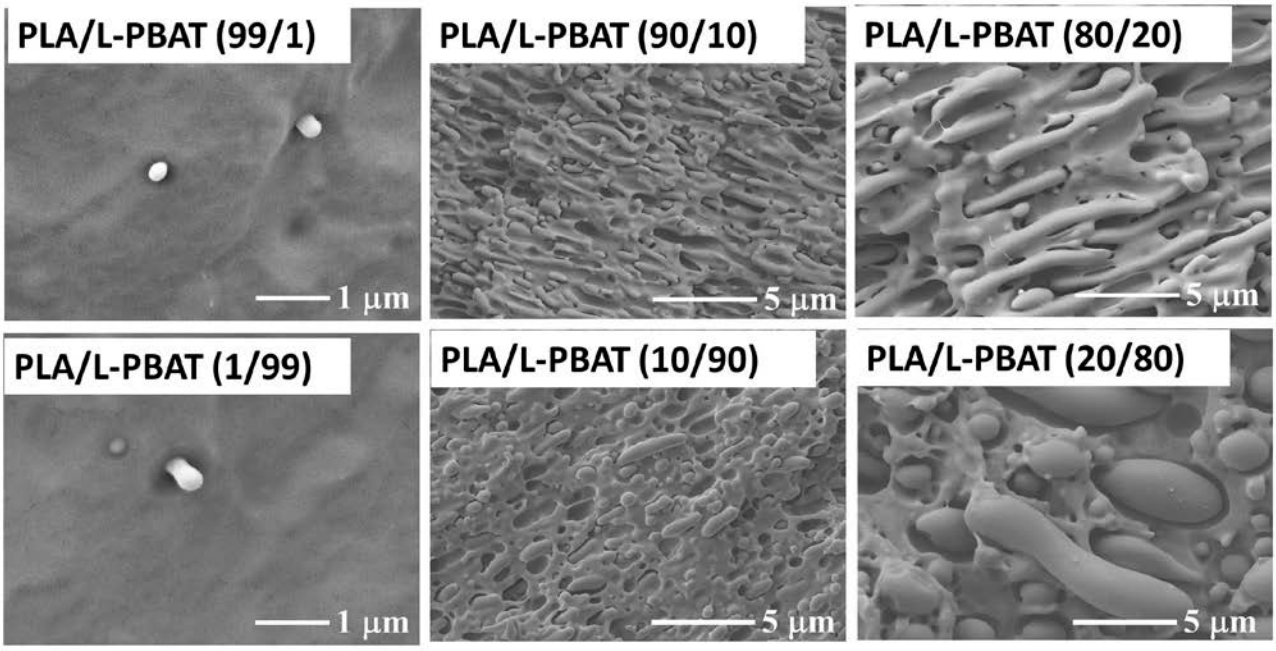


Figure 4.8. FE-SEM images of the fractured surfaces of PLA/L-PBAT blends with different compositions showing the fibrillar morphology of blend samples.

#### 4.4.4.1 The Effect of Composition

The effect of composition on the morphology of PLA/PBAT is shown by AFM imaging in Figure 4.9. Although the dispersed phase in Figure 4.9 appears to be spherical, this is an anomaly due to the cutting of the microtome as discussed in the Experimental. As discussed above, the dispersed phase in PLA/PBAT exists in an elongated/fibrillar state. At low composition of L-PBAT, L-PBAT fibers are dispersed in the PLA-rich matrix and increasing the composition of L-PBAT increases the diameter of these fibers. By further increasing the composition, the co-continuous morphology can be clearly seen in samples with 40 and 50 vol.% of L-PBAT. Although the co-continuous structure in the sample with 60 vol.% of L-PBAT is not as clearly observed as in 40 and 50 vol.% of L-PBAT, the large and elongated structure of PLA-rich phase in this sample nevertheless indicates a high level of continuity of the PLA-rich phase. The continuity development in this blend will be discussed later in this paper. At 70 vol.% of L-PBAT, an evident phase inversion has occurred as the darker phase, L-PBAT, clearly dominates as the matrix. The dispersed PLA-rich phase also shows a fiber diameter dependence with composition. Figure 4.10 shows the average dispersed fiber diameter as a function of L-PBAT composition in these blend samples. Considering that coalescence is generally negligible at 1%, a dashed line can be extrapolated from that point to represent the “no-coalescence” baseline. Therefore, the difference between that baseline and the determined fiber diameters at higher compositions represents the extent of the coalescence in the blend samples with different compositions. It is clear there that, although PLA/L-PBAT has a very low interfacial tension, its morphology shows a considerable coalescence effect with increasing blend composition. This result differs with the results of Li et al. [23] who showed that an immiscible low interfacial tension polymer blend typically demonstrates a phase size that is almost independent of the blend composition. On the other hand, Bhadane et al. [25] observed an increase in phase size with composition in low interfacial tension PP/EPDM blends which they attributed to the partially miscible nature of the blend in the melt state. Marin et al. [24] also observed an increase in the dispersed PMMA phase size with composition in partially miscible PMMA/PC blends. This was related to the reduced miscibility of PMMA in PC phase by increasing the composition. The observed increase in the dispersed fiber phase size with composition in PLA/L-PBAT is thus clearly related to the partially miscible nature of this system.

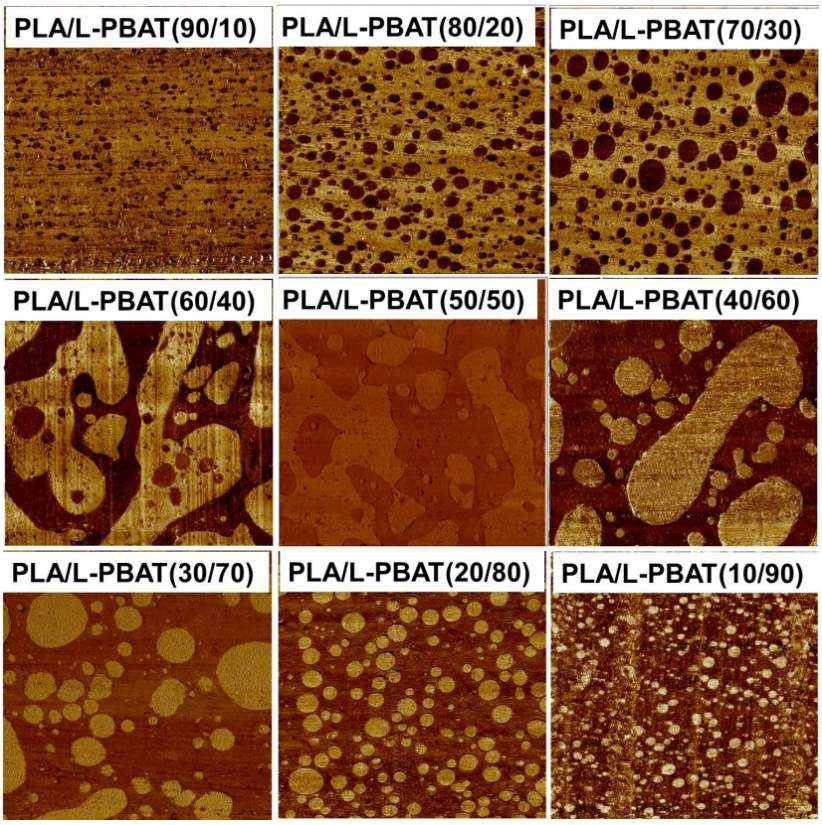


Figure 4.9. AFM images of PLA/L-PBAT blends at different blend compositions. The darker phase is the L-PBAT phase and the brighter phase is the PLA phase in all images. All the micrographs are 30 μm×30 μm.

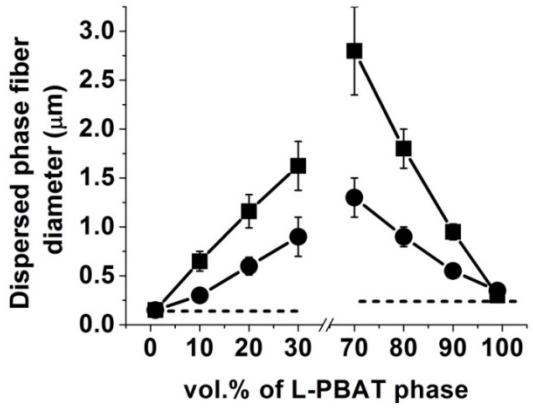


Figure 4.10. The volume average (■) and number average (●) fiber diameter in PLA/L-PBAT blends with different L-PBAT compositions. The dashed lines show the “no-coalescence” baseline. The error bars show the standard deviation of the measured dispersed fiber diameters.

When one compares the left side of Figure 4.10 with the right side, it can be observed that the phase size for PLA in PBAT is always larger at the same composition than for PBAT in PLA. This effect is even observed for 1% PLA in PBAT which has a fiber diameter of 300 ± 60 nm as compared to 150±40 nm for 1% PBAT in PLA. Based on the miscibility data alone, this result is intuitively unexpected since Figure 4.6 indicates that partial miscibility is enhanced when PLA is in a PBAT matrix. Furthermore, the effect is not explained by correcting for the true PLA-rich concentration determined from the Fox equation as that did not result in significant changes to the concentration values. An important factor than can affect the morphology of polymer blends is the viscosity ratio between the dispersed phase and the matrix. From the data in Figure 4.3, the viscosities of PLA and L-PBAT at the shear rate of 25 $s^{-1}$ are determined as 1140 and 346 Pa.s respectively. Therefore, when L-PBAT is the minor phase, the viscosity ratio of dispersed L-PBAT to the PLA matrix is 0.3. On the other side of the composition diagram, the viscosity ratio of the dispersed PLA phase to the L-PBAT matrix will be 3.3. This indicates that after phase inversion, the viscosity ratio of the dispersed phase to the matrix increased by 11 fold. Bhadane et al. [25] studied the effect of viscosity ratio on the dispersed phase size in low interfacial tension blends of PP/EPDM and found that, although small changes in the viscosity ratio does not considerably affect the morphology, increasing the viscosity ratio by a factor of 8 could increase the dispersed phase size by a factor of 3-4 in their system. Hence, it is quite reasonable to expect that an 11 fold larger viscosity ratio for PLA in PBAT can explain the differences in the domain size as compared to PBAT in PLA blends observed in Figure 4.10.

#### 4.4.4.2 Co-continuity Development in PLA/L-PBAT Blends

The co-continuity development in a polymer blend is a key morphological feature of the system and to date, this has not been closely studied in PLA/PBAT systems. Typically, the most simple and reliable method to determine co-continuity quantitatively is by selective gravimetric solvent extraction. In that procedure either phase is extracted using its selective solvent and the ratio of the extracted weight to the initial weight of the phase in the blend is defined as the percent of continuity of that phase. However, as discussed earlier, PLA and PBAT have very similar solubility parameters and selective solvent extraction is impossible in this blend. Therefore, other

methods will need to be employed to determine the co-continuity region in the PLA/L-PBAT system.

Weis et al.[43] and Omonov et al. [44] studied the droplet relaxation in polymer blends with different blend compositions using a Palierne approach. They proposed that the limits of co-continuity can be determined as the compositions where the droplet relaxation shifts to very low frequencies and cannot be observed in the rheological analysis. This is based on the knowledge that increasing the size of droplets in a viscoelastic emulsion results in a shift of the relaxation time of the droplets to lower frequencies. When a 3-D continuous network forms, the relaxation time of the network shifts to very long times or very low frequencies which cannot be observed experimentally.

The storage modulus (*G'*) of polymer blends at different compositions can be used to determine the co-continuity region in PLA/L-PBAT blends using the droplet relaxation approach. The storage modulus of PLA/L-PBAT blends with different compositions are shown in Figure 4.11.

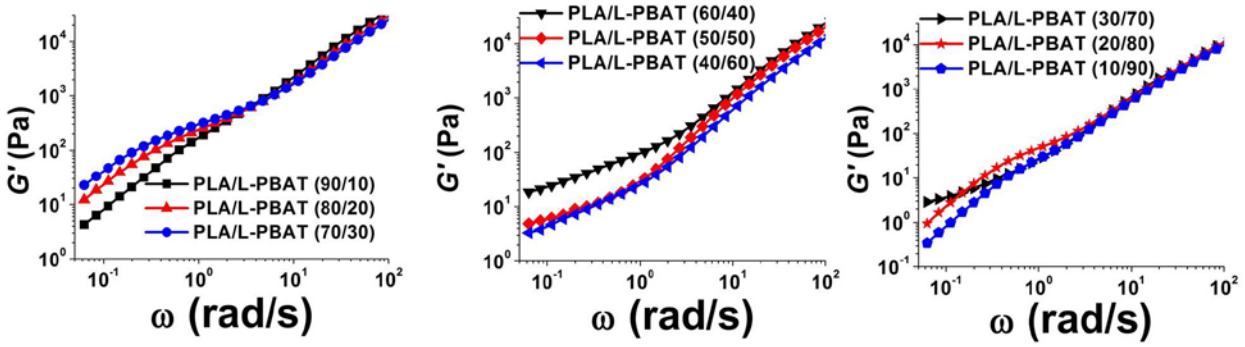


Figure 4.11. Storage modulus (G') as a function of frequency in PLA/L-PBAT blends with different blend compositions at 180$^{o}$C.

As can be seen, the storage modulus of the samples with 10, 20, 30 and 80 to 90 vol.% of L-PBAT clearly shows a shoulder and a terminal zone at low frequencies which is attributed to the droplet relaxation in these samples. In other words, the dispersed phase in these samples has not formed a 3-D continuous structure and is able to relax during the rheological measurements. On the other hand, such relaxation phenomena cannot be observed clearly in the samples with 40 to 70 vol.% of L-PBAT. The droplet relaxation phenomenon can also be shown using the plot of the imaginary component of complex viscosity (η") versus its real component (η') in the form of a

Cole-Cole plot[30]. Figure 4.12 shows the Cole-Cole plot of PLA/L-PBAT blends with different compositions.

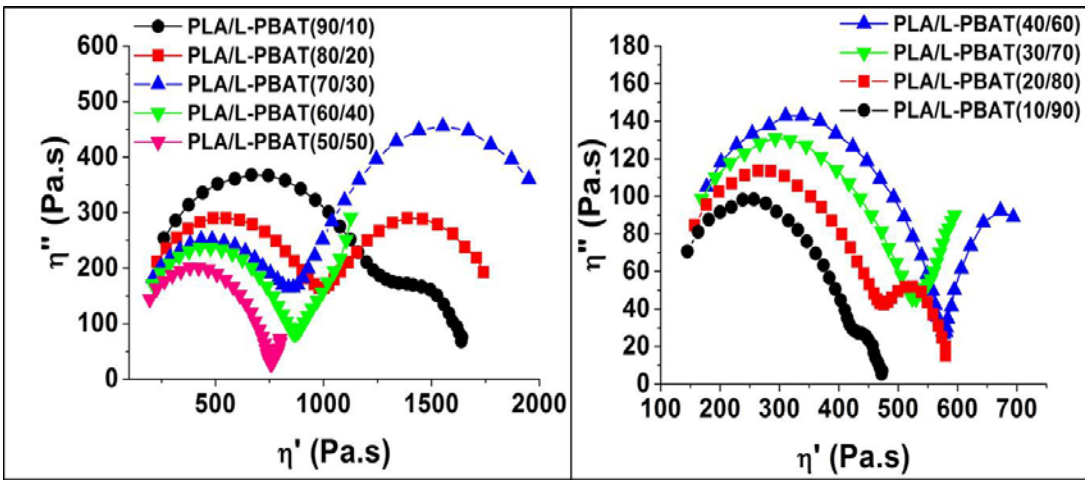


Figure 4.12. Cole-Cole plot of PLA/L-PBAT blends with different blend compositions at 180 ℃.

Two arcs in the Cole-Cole plots of polymer blends represent the relaxation phenomena in the blend samples. The arc on the left side of the plots shows the relaxation of polymer chains while the arc on the right side is attributed to the droplet relaxation phenomenon [30]. The droplet relaxation arcs can be seen clearly in the blend samples with L-PBAT content up to 30 vol.% but at 40 vol.%, the droplet relaxation arc disappears. The droplet relaxation arc was also not observed in the samples with 50 and 60 vol.% of L-PBAT. These results confirm that a 3-D structure of L-PBAT exists in these samples between 30/40-50/60 which is in agreement with AFM images shown in Figure 4.9. It should be noted that, although the shoulder for the droplet relaxation could not be clearly seen in the storage modulus of PLA/L-PBAT(30/70) in Figure 4.11, the maximum peak of the droplet relaxation arc can be clearly seen in the Cole-Cole plot of this sample at low frequencies. These results show that although the domain sizes in PLA/L-PBAT(30/70) are large, they have not formed a 3D continuous structure. Thus, the rheological analysis indicates a wide, symmetric co-continuity region for PLA/L-PBAT extending from 30-40% vol% to 60-70 vol%. Very wide regions of co-continuity have been observed previously for low interfacial tension systems. The co-continuity development in such systems occurs by fiber-fiber coalescence due to the dispersed fibrillar morphologies. These low interfacial tension systems form co-continuous systems at low compositions on both sides of the

composition diagram due to the fiber-fiber coalescence mechanism[25] which results in a wide range of co-continuity.

## 4.5 Conclusions

In this work, the morphology and miscibility of PLA/PBAT blends was examined by a variety of microscopic techniques and by thermal and rheological analysis. The interfacial tension between PLA and low molecular weight PBAT (L-PBAT) was determined as 0.60 ±0.15 mN/m by fitting Palierne's model to the rheological data of the blend at 20 vol.% of L-PBAT. The miscibility of PLA/ PBAT blends was studied by temperature-modulated DSC and the results show a one-way partial miscibility of PBAT in the PLA-rich phase. Increasing the molecular weight of the PBAT phase reduces its partial miscibility in the PLA-rich phase dramatically. Since the solubility parameters of PLA and PBAT are virtually identical, the driving force for this partial miscibility is attributed to the entropy of mixing. This also explains the limited one-way miscibility of PBAT in PLA since changes to the entropy of mixing would be significantly less important for PLA in PBAT. The morphology of the blend samples reveals that the dispersed phase in PLA/L-PBAT blends exists in the form of fibers even at low compositions of 1 vol.% of the dispersed phase. This fiber formation is attributed to the very low interfacial tension of the blend system. AFM images were used to study the influence of composition on dispersed fiber diameter over the entire composition range. Although PLA/L-PBAT has a very low interfacial tension, its morphology shows a considerable coalescence effect with increasing blend composition. Furthermore, the AFM images indicate an inversion of phases at compositional limits of 30/70 and 70/30. It is shown that the larger phase size for PBAT in PLA as compared to PLA in PBAT is due to an 11 fold difference in the viscosity ratio. The co-continuity region for this blend was quantitatively determined for the first time using rheological analysis and it was shown that PLA/L-PBAT has a wide symmetric co-continuous region which is located between 30-40 and 60-70 vol.% of L-PBAT. This result confirms the morphological observation of phase inversion.

## 4.6 Acknowledgements

The authors would like to gratefully acknowledge the NSERC Network for Innovative Plastic Materials and Manufacturing Processes (NIPMMP) for the funding of this work. The authors also would like to thank Dr. Amirhossein Maani, Patricia Moraille and Philippe Plamondon for their help in the rheological measurements, AFM and FE-SEM analysis.

## 4.7 References

1. Yu L, Dean K, and Li L. Progress in Polymer Science 2006;31(6):576-602.
2. Avérous L. Journal of Macromolecular Science, Part C 2004;44(3):231-274.
3. Anderson KS, Schreck KM, and Hillmyer MA. Polymer Reviews 2008;48(1):85-108.
4. Wu D, Lin D, Zhang J, Zhou W, Zhang M, Zhang Y, Wang D, and Lin B. Macromolecular Chemistry and Physics 2011;212(6):613-626.
5. Shin BY, Cho BH, Hong KH, and Kim BS. Polymer-Korea 2009;33(6):588-595.
6. Jiang L, Liu B, and Zhang JW. Industrial & Engineering Chemistry Research 2009;48(16):7594-7602.
7. Coltelli MB, Della Maggiore I, Bertold M, Signori F, Bronco S, and Ciardelli F. Journal of Applied Polymer Science 2008;110(2):1250-1262.
8. Gu S-Y, Zhang K, Ren J, and Zhan H. Carbohydrate Polymers 2008;74(1):79-85.
9. Lee S, Lee Y, and Lee J. Macromolecular Research 2007;15(1):44-50.
10. Li K, Peng J, Turng L-S, and Huang H-X. Advances in Polymer Technology 2011;30(2):150-157.
11. Lin S, Guo W, Chen C, Ma J, and Wang B. Materials & Design 2012;36(0):604-608.
12. Sarath Kumara PH, Nagasawa N, Yagi T, and Tamada M. Journal of Applied Polymer Science 2008;109(5):3321-3328.
13. Shahlari M and Lee S. Polymer Engineering & Science 2012;52(7):1420-1428.
14. Weng Y-X, Jin Y-J, Meng Q-Y, Wang L, Zhang M, and Wang Y-Z. Polymer Testing 2013;32(5):918-926.

15. Xiao H, Lu W, and Yeh J-T. Journal of Applied Polymer Science 2009;112(6):3754-3763.

16. Yeh J-T, Tsou C-H, Huang C-Y, Chen K-N, Wu C-S, and Chai W-L. Journal of Applied Polymer Science 2010;116(2):680-687.

17. Zhang N, Wang Q, Ren J, and Wang L. Journal of Materials Science 2009;44(1):250-256.

18. Zhang N, Zeng C, Wang L, and Ren J. Journal of Polymers and the Environment 2013;21(1):286-292.

19. Kumar M, Mohanty S, Nayak SK, and Rahail Parvaiz M. Bioresource Technology 2010;101(21):8406-8415.

20. Al-Itry R, Lamnawar K, and Maazouz A. Rheologica Acta 2014;53(7):501-517.

21. Jiang L, Wolcott MP, and Zhang J. Biomacromolecules 2005;7(1):199-207.

22. Ravati S and Favis BD. Polymer 2013;54(13):3271-3281.

23. Li J, Ma PL, and Favis BD. Macromolecules 2002;35(6):2005-2016.

24. Marin N and Favis BD. Polymer 2002;43(17):4723-4731.

25. Bhadane PA, Champagne MF, Huneault MA, Tofan F, and Favis BD. Polymer 2006;47(8):2760-2771.

26. Bousmina M, Ait-Kadi A, and Faisant JB. Journal of Rheology 1999;43(2):415-433.

27. Favis BD and Chalifoux J-P. Polymer Engineering & Science 1987;27(21):1591-1600.

28. Saltikov S. The Determination of the Size Distribution of Particles in an Opaque Material from a Measurement of the Size Distribution of Their Sections. In: Elias H, editor. Stereology: Springer Berlin Heidelberg, 1967. pp. 163-173.

29. Palierne JF. Rheologica Acta 1990;29(3):204-214.

30. Graebling D, Muller R, and Palierne JF. Macromolecules 1993;26(2):320-329.

31. Ditmars D, Ishihara S, Chang S, Bernstein G, and West E. J. Res. Natl. Bur. Stand 1982;87(2):159-163.

32. Fox TG and Flory PJ. The Journal of Physical Chemistry 1951;55(2):221-234.

33. Colby RH, Fetters LJ, and Graessley WW. Macromolecules 1987;20(9):2226-2237.

34. Vega JF, Muñoz-Escalona A, Santamaría A, Muñoz ME, and Lafuente P. Macromolecules 1996;29(3):960-965.

35. Nofar M, Maani A, Sojoudi H, Heuzey MC, and Carreau PJ. Journal of Rheology (1978-present) 2015;59(2):317-333.

36. Siemann U. European Polymer Journal 1992;28(3):293-297.

37. Roland CM. Macromolecules 1987;20(10):2557-2563.

38. Kim JK, Lee HH, Son HW, and Han CD. Macromolecules 1998;31(24):8566-8578.

39. Saeki S, Cowie JMG, and McEwen IJ. Polymer 1983;24(1):60-64.

40. Widmaier J-M and Mignard G. European Polymer Journal 1987;23(12):989-992.

41. Jalali Dil E, Carreau PJ, Ravati S, and Favis BD. Morphology of Poly(lactic acid)/Poly(butylene adipate-co-terephthalate) Blends and Its Composite with Spherical Silica Particles. Society of Plastic (ANTEC). Orlando, 2012.

42. Bhadane PA, Tsou AH, Cheng J, Ellul M, and Favis BD. Polymer 2011;52(22):5107-5117.

43. Weis C, Leukel J, Borkenstein K, Maier D, Gronski W, Friedrich C, and Honerkamp J. Polymer Bulletin 1998;40(2-3):235-241.

44. Omonov TS, Harrats C, Moldenaers P, and Groeninckx G. Polymer 2007;48(20):5917-5927.

# CHAPTER 5 ARTICLE 2: LOCALIZATION OF MICRO- AND NANO-SILICA PARTICLES IN HETEROPHASE POLY(LACTIC ACID)/ POLY(BUTYLENE ADIPATE-CO-TEREPHTHALATE) BLENDS*

*Ebrahim Jalali Dil, Basil D. Favis*

*CREPEC, Department of Chemical Engineering, École Polytechnique de Montréal, Montreal, Québec, H3C3A7, Canada.*

## 5.1 Abstract

This work studies the thermodynamic and kinetic parameters influencing the localization of micro- and nano-silica particles in multiphase mixtures of poly (lactic acid), (PLA), and poly(butylene adipate-co-terephthalate), PBAT. The surface energies of PLA and PBAT were measured at ambient and high temperature using contact angle and pendant drop techniques respectively. Based on this data, as well as that for silica, Young's model, which estimates the preferred lowest surface energy condition, predicts that silica particles should be located in the PBAT phase. Atomic force microscopy and scanning electron microscopy results confirm that when micro- or nano-silica particles are added to a PLA/PBAT melt, the silica particles are selectively localized in the PBAT phase irrespective of the PLA phase viscosity. The preferential encapsulation of silica particles by PBAT is shown to occur at the early stages of mixing. However, when micro- or nano-silica is initially distributed into the PLA melt prior to PLA/PBAT mixing, two distinct morphological behaviors are observed that persist over long mixing times. Nano-silica in PLA locates perfectly at the PLA/PBAT interface independently of the PLA viscosity while micro-silica locates at the interface with low viscosity PLA and stays distributed within the PLA when it is of high viscosity. It will be shown that the observed localization of micro- and nano- silica particles at the interface is due to the slow migration velocity of the particles at the interface that originates from the very low interfacial tension in this system. The localization of micro-silica particles in high viscosity PLA is related to the slow PLA film draining step close to the PLA-PBAT interface.

*Accepted in *Polymer*

***Keywords:*** *Localization, Polymer blends, nano-silica.*

## 5.2 Introduction

The addition of solid inclusions to polymer blends is a common method to achieve a balance between toughness and stiffness [1-3, 67]. Recently, the addition of conductive solid particles to polymer blends to achieve semi-conductive materials has also received much attention [4, 5]. It is apparent that controlling the localization of solid inclusions in a multiphase polymer system is crucial to achieving the desired mechanical and/or electrical properties. Although the effects of the thermodynamic interactions of solid particles with polymeric phases[1, 6-26] and the effects of kinetic parameters such as the sequence of addition of components [7, 9, 10, 13, 17-22, 24-33], mixing time [12-14, 20, 29, 30, 33], viscosity [7, 24, 25, 31] and shear rate [23, 34] have been studied in the literature, the fundamental mechanisms of migration and localization of solid particles in multiphase systems are still not understood.

Considering the high viscosity of polymers, the diffusion and Brownian motion of solid particles are not effective mechanisms of the migration in polymer blends [20, 25, 35]. Shear-induced migration is one of the mechanisms that has been proposed to explain the migration of solid particles in multiphase systems. In this mechanism, solid particles move under the hydrodynamic force applied by the shear flow field and collide with the interface. This will eventually result in the transfer of the solid particles from one phase to another phase. The frequency of collision of mono-dispersed spherical particles moving in a shear flow field can be estimated as [25]:

$$C = \frac{8}{\pi}\dot{\gamma}\varphi \qquad \text{Eqn.1}$$

where $\dot{\gamma}$ and φ are the shear rate and the volume fraction of the particles. As can be seen, the shear-induced migration mechanism predicts that increasing the shear rate increases the frequency of collision of the particles with the interface and, consequently, should enhance the migration of solid particles. This is in agreement with the observed enhancement effect of shear rate on the migration of solid particles in polymer blends [23, 34]. However, this mechanism

cannot explain the effects of other kinetic parameters such as mixing strategy, viscosity, particle size and aspect ratio of solid particles. Moreover, this mechanism only considers the migration of the solid particles in the bulk of the phases and does not take into account the migration at the interface.

Goldel et al. [21] proposed a mechanism called “Slim-Fast mechanism (SFM)” to explain the effect of the aspect ratio of solid particles on their migration velocity at the interface. The proposed mechanism is based on the assumption that the driving force for the particle migration at the interface is the interface curvature due to the presence of the particles. According to this mechanism, the transfer of spherical particles through the interface is slower since by moving a spherical particle through the interface, the interface curvature decreases rapidly which reduces the driving force for the migration of the particles. On the other hand, when a rod-like particle migrates perpendicularly through the interface, the interface curvature does not change and therefore, they concluded that, rod-like particles migrate faster at the interface.

Goldel et al. and Fenouillot et al. [20, 35] suggested that the trapping of solid particles between two colliding dispersed phase droplets can also result in the migration of solid particles from the matrix phase to the dispersed phase.

As can be seen, a comprehensive understanding of the parameters and mechanisms governing solid particle migration and localization in multiphase polymer systems is lacking in the literature. In many cases, this difficulty can be attributed to the complexity of the morphological structures that are often achieved. In order to study the effects of the thermodynamic and kinetic parameters on the migration and localization of solid particles in multiphase systems, a model system comprised of poly (lactic acid), PLA; poly (butylene adipate-co-terephthalate), PBAT; and micro- and nano-spherical silica particles was chosen in this study. The PLA/PBAT system also provides the advantage of studying silica localization in a system of very low interfacial tension (0.6 mN/m [36]).

The aim of this article is to examine the effects of thermodynamic and kinetic parameters on the localization of micro- and nano- silica particles in PLA/PBAT blends. The effects of mixing strategy, viscosity of the PLA phase, shear rate and the particle size of silica on the localization and migration of silica particles in PLA/PBAT blends will be studied in detail. The fundamental mechanisms responsible for the observed effects will be examined as well.

## 5.3 Experimental

### 5.3.1 Materials

PLA 2003D and 3001D (Natureworks, Cargil) were purchased from NatureWorks LLC and will be referred hereafter as H-PLA and L-PLA respectively. H-PLA and L-PLA refer to high viscosity and low viscosity PLA. PBAT (Ecoflex FBX 7011) was purchased from BASF. Micro- and nano- spherical silica particles, SEAHOSTAR KE-P30 and KE-P10, were purchased from Nippon Shokubai, Japan. The average diameters of the individual spherical silica particles for micro- and nano-silica are 300 nm and 100 nm, respectively. The silica particles were synthesized by the sol-gel method which results in a narrow particle size distribution. All the materials were dried under vacuum at 60 ℃ overnight before being used in the experiments.

### 5.3.2 Surface tension measurements

To determine the surface energy of PLA and PBAT, thin sheets of the polymers were prepared by compression moulding. Ethanol and distilled water were used to remove any contamination from the surface of the sheets. Finally, the sheets were dried at 60 ℃ for 6 h in a vacuum oven. The surface energy of solid polymers then was determined by measuring the contact angles of water, glycerol and diiodomethane, as liquid probes, on the polymer sheets. The Owens-Wendt [37] approach was used to determine the surface energy as well as its dispersive and polar components. The total surface energies of the PLA and PBAT melts at 180 ℃ were determined using the pendant drop technique under nitrogen atmosphere. The apparatus and the operation description can be found elsewhere [38]. The melt densities of PLA and PBAT at 180 ℃ were measured as 1.1 g/cm$^3$ and 1.06 g/cm$^3$ using a high pressure piston-type dilatometer (PVT-100, ThermoHaake). The polar ($\gamma^p$) and dispersive ($\gamma^d$) components of the surface energy of PLA and PBAT melts at 180 ℃ were determined using the assumption that the polarity (the ratio of the polar component to the total surface energy) is independent of temperature [39-41]. The interfacial tension between PLA and PBAT was estimated using the Harmonic Mean Approach[39]:

$$\gamma_{12} = \gamma_1 + \gamma_2 - 4\left(\frac{\gamma_1^d \gamma_1^d}{\gamma_1^d + \gamma_1^d} + \frac{\gamma_1^p \gamma_1^p}{\gamma_1^p + \gamma_1^p}\right) \qquad \text{Eqn.2}$$

and the interfacial tensions between PLA/Silica and PBAT/Silica were calculated using the Geometric Mean Approach[39]:

$$\gamma_{12} = \gamma_1 + \gamma_2 - 2\left(\sqrt{\gamma_1^d \gamma_1^d} + \sqrt{\gamma_1^p \gamma_1^p}\right) \quad \text{Eqn.3}$$

The Harmonic Mean approach is more accurate in the estimation of the interfacial tensions between low surface energy materials while the Geometric Mean equation can predict the interfacial tensions between low and high surface energy materials more accurately [39].

### 5.3.3 Blend preparation

All samples were prepared using an internal batch mixer (Plasti-Corder DDR501, Brabender) with the total mixing chamber volume of 30 $cm^3$ at 180 ℃ under a nitrogen blanket. The average shear rate at the mixing speeds of 50 and 100 RPM, used in this study, were estimated as 25 $s^{-1}$ and 47 $s^{-1}$, respectively [42]. The two following mixing strategies were employed to prepare the samples:

**Pr1**: The addition of silica particles after melting of PLA and PBAT (one-step process).

**Pr2**: Premixing of silica particles with the PLA phase followed by mixing with PBAT (two-step process).

After 10 minutes of mixing, the chamber was opened and the samples were rapidly frozen in ice-water to freeze-in the morphology and localization of silica particles. All the prepared blend samples contain 70 vol.% of PLA phase and 30 vol.% of PBAT phase. The wt.% of silica particles added to the blends is based on the total weight of the blend.

In L-PLA/PBAT blends prepared by Pr1 at short mixing time, the mixing was stopped 30 s after the addition of nano-silica particles to L-PLA/PBAT melt.

### 5.3.4 Atomic force microscopy (AFM)

The samples were cut and microtomed under liquid nitrogen using a microtome (Leica-Jung RM 2165). The AFM machine was equipped with a scanning probe microscope Dimension 3100 with a Nanoscope IVa controller from Veeco Instruments. Silicon tips, model ACTA-W from AppNano, with the tip radius less than 10 nm were used in this study. The morphologies of the samples were determined by Tapping mode AFM in air. Because of the difference in the modulus of PLA and PBAT, tapping phase AFM is used to determine the morphology of the blend samples. The localization of silica particles in the blends samples was determined using both height and phase images obtained from AFM analysis.

### 5.3.5 Field emission scanning electron microscopy (FE-SEM)

In order to determine the morphology and the localization of silica particles, samples from the internal batch mixer were fractured in liquid nitrogen then the sample surface was coated with gold and the morphology was observed with the Field Emission Scanning Electron Microscope (FE-SEM, JSM 7600F, JEOL).

### 5.3.6 Image analysis

To quantify the localization of silica particles, the locations of 110 to 200 silica particles, depending on the blend structure, were counted in AFM images.

### 5.3.7 Rheological analysis

All the samples were compression moulded at 180 ℃ and at 300 kPa in the form of 1.2 mm thick disks of 25 mm diameter under a nitrogen blanket. The rheological analysis was done using a controlled-stress rheometer (Physica MCR 301, Anton Paar) with 25 mm parallel plate geometry at a 1 mm gap at 180 ℃ under nitrogen atmosphere. All the samples were kept at 180 ℃ for 5 minutes in the rheometer before performing the rheological tests. The stability of L-PLA, H-PLA and PBAT was studied under the test conditions using a time sweep test and a less than 7% drop

in the complex viscosity and storage modulus was observed in the experimental time scale of 40 minutes. Moreover, the linear viscoelastic region was determined using strain sweep tests for the neat polymers at different frequencies. According to the obtained results, the frequency sweep tests were performed at strains of 5%.

### 5.3.8 Temperature-modulated dynamic scanning calorimetry (TMDSC)

TMDSC was employed to determine the miscibility state of PLA/PBAT blends by studying the glass transition temperature (*Tg*) of the polymeric phases. TMDSC tests were performed using a DSC Q1000 machine (TA Instruments) in the temperature range of -60 to 70 ℃. In all of the TMDSC experiments, oscillation amplitude of ±1.27 ℃ and oscillation period of 60 s were used with a heating rate of 2℃/min. The *Tgs* of the phases were determined from the inflection points in the reversible heat flux curves of TMDSC results. The reported values are an average of three different measurements. Due to the high accuracy of TMDSC, the error in the measured *Tgs* was always less than 0.8% (~ 0.4 ℃).

## 5.4 Results and Discussion

### 5.4.1 Rheological Characterization and Surface Tension Measurements of Neat Materials

Figure 5.1 shows the viscosities of the neat polymers. Both PLA and PBAT follow the Cox-Merz rule [43, 44]. All the neat polymers show a Newtonian plateau and liquid-like behaviour at low shear rates. The viscosities of L-PLA, H-PLA and PBAT at the shear rate of 25 $s^{-1}$ were determined as 1140 Pa.s, 2930 Pa.s and 340 Pa.s, respectively. The viscosities of L-PLA, H-PLA and PBAT at the shear rate of 47 $s^{-1}$ were determined as 1030 Pa.s, 2430 Pa.s and 310 Pa.s.

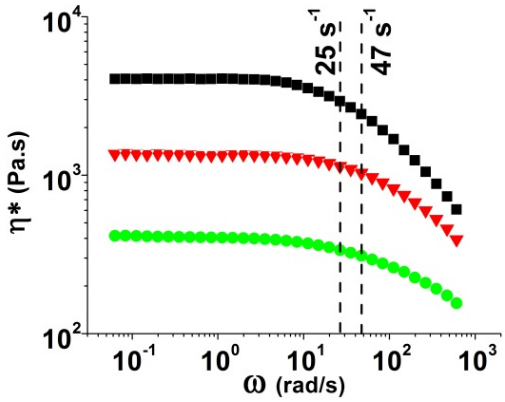


Figure 5.1. The complex viscosity of polymer components as a function of angular frequency: (■) H-PLA; (▼) L-PLA; (●) PBAT. The dashed lines show the angular frequencies which correspond to the shear rates of 25$s^{-1}$ and 47 $s^{-1}$.

The measured surface energies of the neat PLA and PBAT at both room and processing temperatures are reported in Table 5-1. The difference between the measured surface energies of H-PLA and L-PLA was within the margin of the error of the measurements and therefore an average of their surface energies is reported as the surface energy of PLA.

Table 5-1. Surface energy data of PLA, PBAT and silica at 25 and 180 ℃ and the estimated interfacial tensions between the components at the processing temperature.

| | $\gamma$ (mN/m) | $\gamma^d$ (mN/m) | $\gamma^p$ (mN/m) | $\gamma$ (mN/m) | $\gamma^d$ (mN/m) | $\gamma^p$ (mN/m) | Interfacial tension | | |
|---|---|---|---|---|---|---|---|---|---|
| | at 25 ℃ | | | at 180 ℃ | | | PLA | PBAT | Silica |
| PLA | 39.4 | 33.6 | 5.8 | 28 | 23.9 | 4.1 | - | 0.03[a] | 155.3[b] |
| PBAT | 38.4 | 32.1 | 6.3 | 27.6 | 23.1 | 4.5 | 0.03[a] | - | 153[b] |
| Silica[c] | 519.8 | 72.8 | 447 | 242.8 | 34 | 208.8 | 155.3[b] | 153[b] | - |

a: Calculated from the Harmonic Mean Approach

b: Calculated from the Geometric Mean Approach

c: Estimated from the adsorption energy data of Papirer et al.[45, 46].

The surface energy of silica was estimated from the literature data. Papirer et al. [45] used inverse gas chromatography and reported the dispersive component of the surface energy of hydrophilic silica at 110 ℃ as 52 mJ/m$^2$. Using their reported thermal coefficient of -0.25 mJ/(m$^2$K), the dispersive component of the surface energy of hydrophilic silica at 180 ℃ can be estimated as 34 mJ/m$^2$. In this study, the polar component of the surface energy of silica was estimated using the method presented by Das et al. [47]. In that method, the polar component of the surface energy can be estimated from the free energy of the adsorption in inverse gas chromatography measurements of a mono-acidic probe such as dichloromethane and a mono-basic probe such as ethyl acetate. Using the free energies of adsorption reported for hydrophilic silica by Papirer [46] and the characteristics of the dichloromethane and ethyl mono-acetate as mono-acidic and basic the liquid probes [48], the polarity of silica was estimated as 0.86. Using the estimated polarity and the dispersive component of the surface energy, the polar component of the surface energy of silica was estimated at both room and processing temperatures. The estimated surface energies of silica and the interfacial tensions between the components are listed in Table 5-1.

### 5.4.2 Thermodynamics of Localization of Silica Particles in PLA/PBAT Blends

The thermodynamic equilibrium localization of solid particles in a polymer blend can be predicted by the Young's model [35]:

$$\omega = \frac{\gamma_{1s}-\gamma_{2s}}{\gamma_{12}} \qquad \text{Eqn.4}$$

Where ω, $\gamma_{1s}$, $\gamma_{2s}$ and $\gamma_{12}$ are the wetting parameter, the interfacial tensions between: polymer 1 and solid; polymer 2 and solid; and polymer 1 and 2. If ω in Equation 4 is greater than 1, then the localization of solid particles in phase 2 is thermodynamically preferred while for ω < -1, the thermodynamic equilibrium localization of solid particles should be in phase 1. When -1<ω< 1, the localization of solid particles at the interface is thermodynamically preferred. Taking PLA as phase 1 and PBAT as phase 2 and using the estimated interfacial tensions in Table 5-1, ω can be calculated as 76.7 for PLA/PBAT/Silica mixture. Considering the unavoidable errors in the contact angle measurements (such as the roughness of the surface of the solid polymers, the

purity of liquid probes and the resolution of droplet images), the estimated interfacial tension of 0.03 mN/m for PLA/PBAT is within the margin of the experimental error. If the interfacial tension of 0.6 mN/m determined using a rheological technique in the previous study [36] is used in the calculations, ω in PLA/PBAT/silica system can be estimated as 3.8. As both rheological and surface energy approaches estimate a wetting parameter (ω) greater than 1, the thermodynamic equilibrium localization of the silica particles should be in the PBAT phase.

In order to confirm the Young's model prediction, 1 wt.% of micro-silica was added to the L-PLA/PBAT melt according to Pr1 (see Experimental for description of Pr1 and Pr2). Figure 5.2 (a,c) and line 1 in Table 5-2 show the localization of micro-silica particles in this sample. As can be seen, 97% of micro-silica particles are selectively localized in the PBAT phase which is in agreement with Young's model.

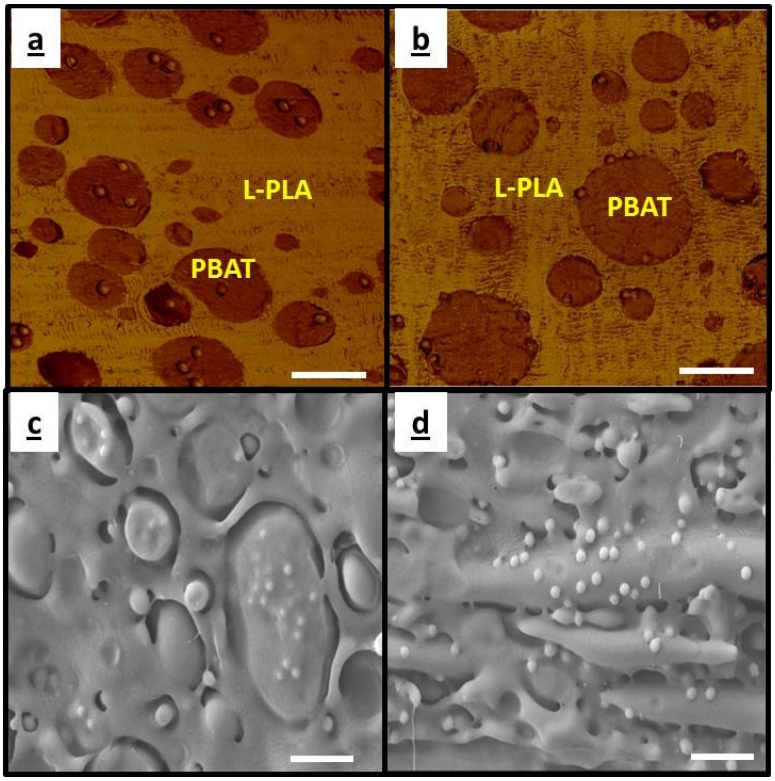


Figure 5.2. Localization of micro-silica particles in L-PLA/PBAT (70/30)/ 1 wt.% micro-silica:(a) AFM image of the sample prepared by Pr1, (b) AFM image of the sample prepared by Pr2. (c) and (d) show SEM images of the fracture surfaces of (a) and (b), respectively. The scale bars show 2μm.

Most of the previous studies have shown that the simultaneous mixing of solid particles and polymer components results in the localization of solid particles in the thermodynamically preferred phase [6, 10, 11, 13, 14, 16-22, 26] unless the difference between the melting temperatures of the polymeric phases is considerable. Under those conditions, solid particles were found to be encapsulated by the phase with the lower melting temperature rather than the phase with the higher thermodynamic affinity [8, 24, 25]. In this study, the effect of the difference between the melting temperatures of PLA and PBAT was eliminated by the addition of silica particles to the mixing chamber after complete melting of the PLA and PBAT phases.

Table 5-2. The quantified localizations of micro- and nano-silica particles in PLA/PBAT samples with the associated standard deviation (std).

| | Sample name | Mixing strategy | Shear rate ($s^{-1}$) | % Particles in PBAT phase | % Particles at the interface | % Particles in PLA phase | std |
|---|---|---|---|---|---|---|---|
| 1 | L-PLA/PBAT/micro-silica | Pr1 | 25 | 97 | 0 | 3 | 3.4 |
| 2 | L-PLA/PBAT/micro-silica | Pr2 | 25 | 0 | 95 | 5 | 4.1 |
| 3 | L-PLA/PBAT/nano-silica | Pr1 | 25 | 95 | 0 | 5 | 5 |
| 4 | L-PLA/PBAT/nano-silica | Pr2 | 25 | 9 | 91 | 0 | 6.3 |
| 5 | H-PLA/PBAT/micro-silica | Pr1 | 25 | 91 | 0 | 9 | 4 |
| 6 | H-PLA/PBAT/micro-silica | Pr2 | 25 | 0 | 7 | 93 | 5.2 |
| 7 | H-PLA/PBAT/micro-silica (3 wt.%) | Pr2 | 25 | 0 | 11 | 89 | 4.7 |
| 8 | H-PLA/PBAT/nano-silica | Pr1 | 25 | 95 | 5 | 0 | 4.3 |
| 9 | H-PLA/PBAT/nano-silica | Pr2 | 25 | 8 | 92 | 0 | 4.1 |
| 10 | L-PLA/PBAT/micro-silica | Pr2 | 47 | 7 | 93 | 0 | 3.2 |
| 11 | L-PLA/PBAT/nano-silica | Pr2 | 47 | 27 | 73 | 0 | 7.1 |
| 12 | H-PLA/PBAT/micro-silica | Pr2 | 47 | 0 | 40 | 60 | 6.8 |

In our previous study [36], it was shown that L-PLA/PBAT exhibits a limited one-way partial miscibility of PBAT in the L-PLA phase. The effect of the presence of silica particles on the miscibility of phases should thus be discussed as it could have also an influence on the localization of silica particles in this system. It can be seen from Table 5-3 that the addition of micro-silica particles in L-PLA/PBAT blends prepared by Pr1 and Pr2 did not have a significant effect on the glass transition temperatures as compared to the L-PLA/PBAT system without silica particles reported previously. Similar results were observed for L-PLA/PBAT with nano-silica particles.

Table 5-3. Glass transition temperatures (Tgs) of the neat polymers and polymer blends and composites with 1 wt.% of micro-silica particles.

| | Tg of PLA phase | Tg of PBAT phase |
|---|---|---|
| L-PLA* | 60.3 | - |
| PBAT* | - | -30 |
| L-PLA/PBAT* | 57.8 | -29.8 |
| L-PLA/PBAT/micro-silica-Pr1 | 58 | -30 |
| L-PLA/PBAT/micro-silica-Pr2 | 57.7 | -29.9 |

*from ref.[36]

### 5.4.3 Effect of mixing strategy

Although, the Young's model can predict the thermodynamic equilibrium localization of solid particles in polymer blends, kinetic effects can interrupt the migration of solid particles toward their preferred thermodynamic equilibrium location. Among different kinetic parameters, the effect of the mixing strategy on the migration and localization of solid particles has been studied extensively [7, 9, 10, 13, 17-22, 24-33]. Although some authors did not observe a considerable effect of mixing procedure on the localization of solid particles in polymer blends [19, 20, 24, 49], most of the previous studies showed strong kinetic effects by changing the mixing strategy of the components[13, 14, 17, 18, 29, 30]. The effect of the mixing strategy on the localization of micro-silica particles was studied by preparing the L-PLA/PBAT blend according to Pr2 (silica dispersed initially in a L-PLA melt then mixed with PBAT). As can be seen in Figure 5.2 (b,d) and on line 2 in Table 5-2, it was found that 95% of the micro-silica particles were localized at the interface in this sample. Considering that the micro-silica particles were initially dispersed in the L-PLA phase, this result and the results of the samples prepared by Pr1 confirm the affinity of micro-silica particles to migrate toward the PBAT phase. Interestingly, as shown in Figure 5.3, it

was found that increasing the micro-silica content to 3 wt.% did not change the localization of micro-silica particles in L-PLA/PBAT samples prepared by Pr1 and Pr2. These effects were also found to be independent of mixing time. The same strategies were used to add nano-silica particles to L-PLA/PBAT and the results are shown in Figure 5.4 and line 3 and 4 in Table 5-2. It can be seen that decreasing the particle size of silica from 300 nm to 100 nm did not change the localization of silica particles in L-PLA/PBAT blends prepared by Pr1 and Pr2.

The observed localization of micro- and nano-silica at the interface of the samples prepared by Pr2, shown above, was found to be stable and did not change by increasing the mixing time. This indicates the significant potential of this approach to generate partially wet silica blend structures.

As the thermodynamic equilibrium localization of silica particles was established to be in the PBAT phase, the premixing of silica particles with the PLA phase using Pr2 provides a unique opportunity to rigorously examine the effect of kinetic parameters on the localization and migration of silica particles in PLA/PBAT blends. This will be considered in more detail below.

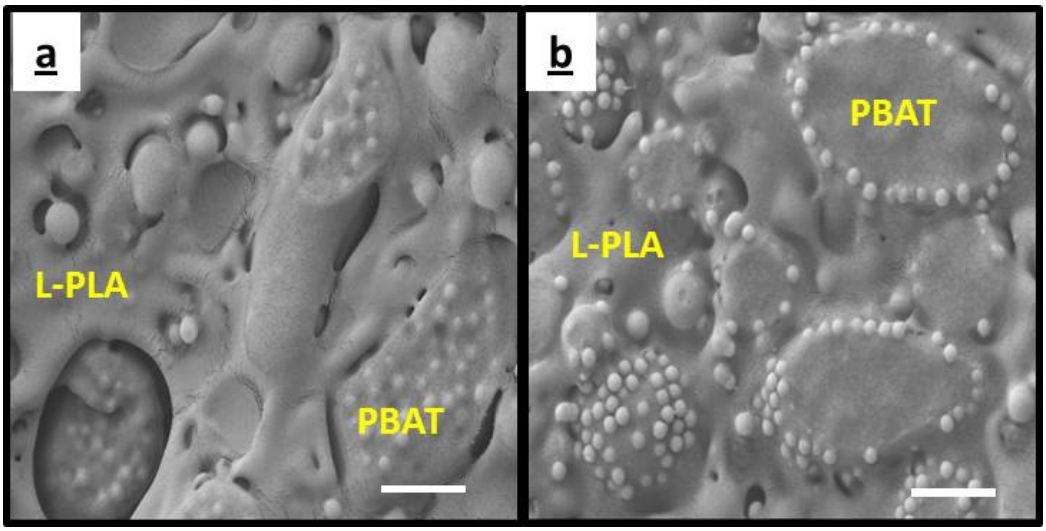


Figure 5.3. Effect of mixing strategy on the localization of micro-silica particles in L-PLA/PBAT (70/30)/ 3 wt.% micro-silica:(a) SEM image of the fracture surface of the sample prepared by Pr1, (b) SEM image of the fracture surface of the sample prepared by Pr2. All the white scale bars show 2μm.

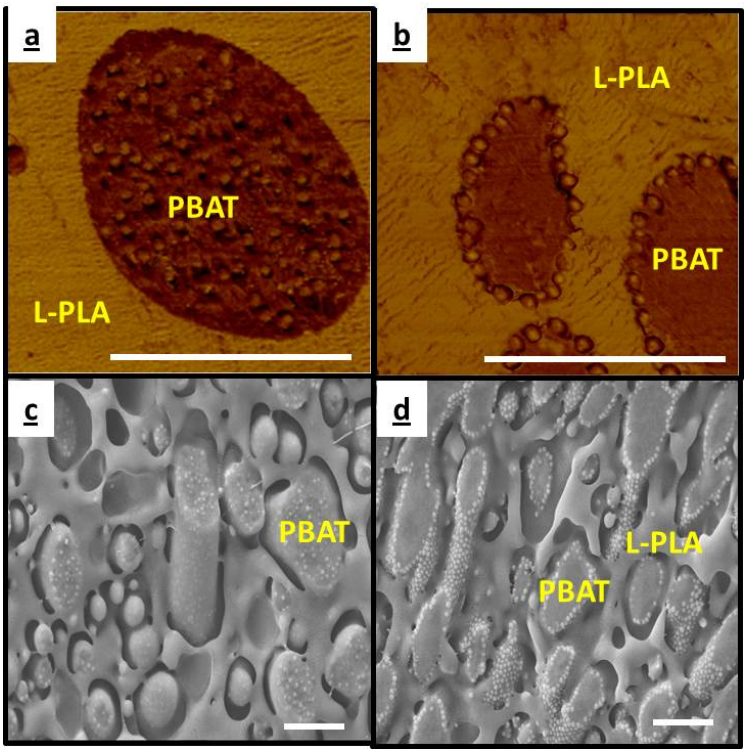


Figure 5.4. Effect of mixing strategy on the localization of nano-silica particles in L-PLA/PBAT (70/30)/ 3 wt.% nano-silica:(a) AFM image of the sample prepared by Pr1, (b) AFM image of the sample prepared by Pr2. (c) and (d) show SEM images of the fracture surfaces of (a) and (b) respectively. The scale bars show 2μm.

### 5.4.4 Effect of the Viscosity of the PLA Phase

The effect of viscosity on the migration of solid particles has been studied by only a few authors. Persson and Bertilsson [31] found that the effect of viscosity is only important in low interfacial tension blends while Feng et al. [50], Elias et al. [25] and Taghizadeh and Favis [23] observed strong effects of viscosity in high interfacial tension blends of PP/PMMA, PP/EVA and thermoplastic starch (TPS)/PCL, respectively.

In order to study the effect of viscosity of the PLA phase, micro- and nano- silica particles were added to the blend samples with a high viscosity PLA (H-PLA) using the Pr1 and Pr2 mixing protocols. The results are shown in Figure 5.5 and on line 5 to 9 in Table 5-2. When the H-PLA/PBAT sample is prepared by Pr1, lines 5 and 8 in Table 5-2, both micro- and nano-silica particles are found to be localized in the PBAT phase.

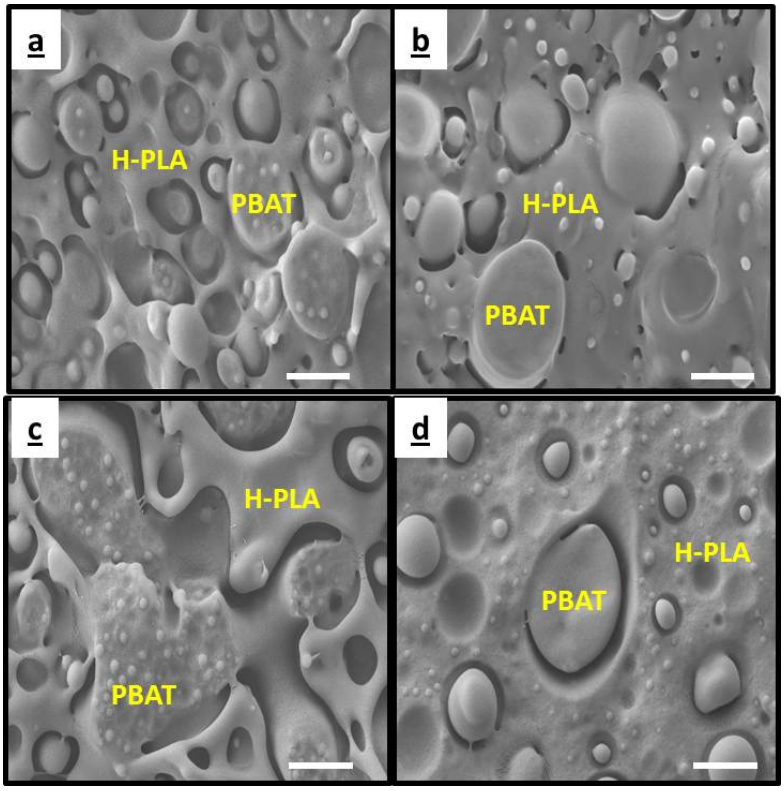


Figure 5.5. SEM images showing the localization of micro-silica particles in H-PLA/PBAT blends containing:(a) 1 wt.% micro-silica prepared by Pr1, (b) 1 wt.% micro-silica prepared by Pr2, (c) 3 wt.% micro-silica prepared by Pr1, (d) 3 wt.% micro-silica prepared by Pr2. The scale bars show 2μm.

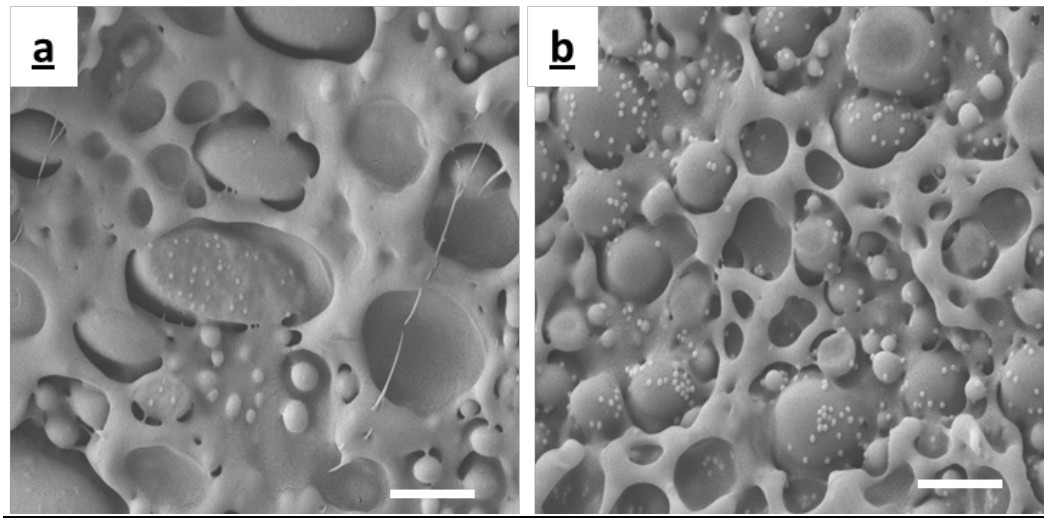


Figure 5.6. The localization of nano-silica particles in H-PLA/PBAT blends containing 1 wt.% nano-silica particles:(a) prepared by Pr1, (b) prepared by Pr2. The scale bars show 2μm.

Comparing these results with the localization of micro- and nano-silica in L-PLA/PBAT blends prepared by Pr1 indicates that the localization of silica particles in the samples prepared by Pr1 does not depend on the viscosity of PLA phase and the particle size of silica. A similar approach was taken by Austin et al.[51] to study the localization of organoclay in blends of polypropylene (PP) and ethylene-propylene rubber graft maleic anhydride (EPR-g-MA). They observed that the addition of organoclay to the melt of PP/EPR-g-MA results in the localization of organoclay particles in the EPR-g-MA phase irrespective of the viscosity of the elastomer phase.

The same localization of nano-silica particles at the interface was also observed in H-PLA/PBAT prepared by Pr2, as shown in Figure 5.5 (b) and on line 9 in Table 5-2. On the other hand, when micro-silica particles were premixed with H-PLA according to Pr2, 93% of the particles were found to be localized in the H-PLA phase (see line 6 in Table 5-2). A similar localization at the interface was observed for the blend sample with 3 wt.% of micro-silica particles (see line 7 in Table 5-2). Therefore, it is can be concluded that the higher viscosity of H-PLA inhibits the migration of micro-silica to the interface in the case where silica is initially added to the H-PLA phase. These effects are stable over long mixing times.

### 5.4.5 Effect of the Shear Rate of Mixing

The shear rate of mixing is another important kinetic parameter that has been shown to enhance the migration of solid inclusions in polymer blends [23, 34].

The effect of the shear rate on the localization of silica particles in PLA/PBAT blends was examined by preparing three samples of: H-PLA/PBAT with 1 wt.% micro-silica; L-PLA/PBAT with 1 wt.% micro-silica; and L-PLA/PBAT with 1 wt.% nano-silica using Pr2 at the shear rate of 47 $s^{-1}$. This is approximately double the shear rate used in the experiments in the sections above. Since it was shown above that Pr2 particularly imposes kinetic effects on the migration of silica particles, this procedure will be focussed on here. The final localizations of silica for the samples prepared at this shear rate are shown in Figure 5.7 and on lines 10 to12 in Table 5-2.

It can be seen that by increasing the shear rate in the H-PLA/PBAT blend, the migration of micro-silica particles to the interface is enhanced and about 40% of micro-silica particles were

found at the interface. On the other hand, in the L-PLA/PBAT blends, increasing the shear rate did not change the localization of micro-silica particles at the interface. In L-PLA/PBAT blend

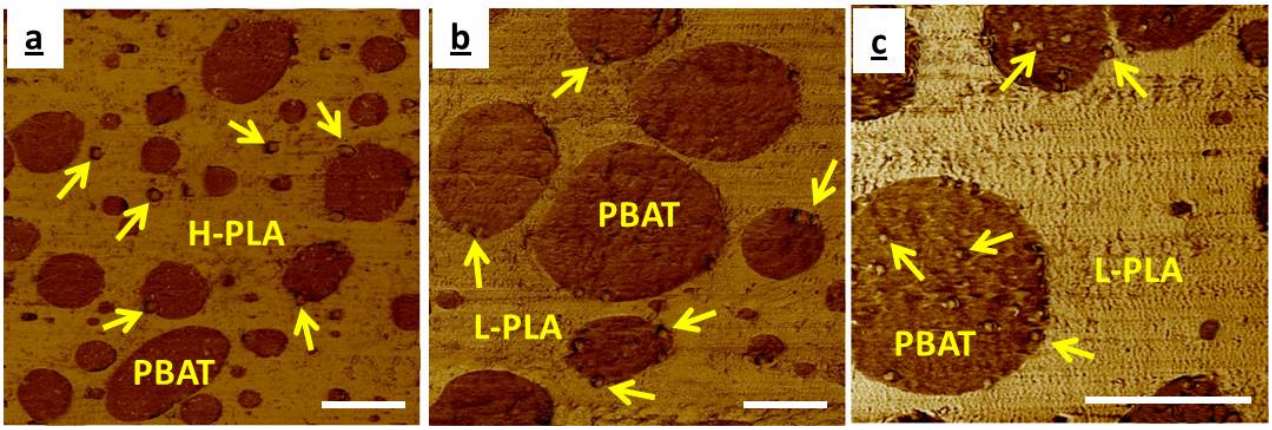


Figure 5.7. The effect of shear rate on the localization of silica particles in the samples prepared by Pr2 at 47 $s^{-1}$, (a) micro-silica particles in H-PLA/PBAT, (b) micro-silica particles in L-PLA/PBAT, (c) nano-silica particles in L-PLA/PBAT. The arrows point to selected micro- and nano-silica particles. The scale bars show 2μm.

with nano-silica particles, increasing the shear rate resulted in the migration of 27% of the nano-silica particles from the interface to PBAT phase. At this point, the work demonstrates that solid inclusion localization kinetic effects are enhanced when solid inclusion addition initially takes place with the phase with which it has the least affinity. Increasing the viscosity of the low affinity phase and using larger solid particles aggravate the kinetic affects. Doubling the shear rate alleviates some of the kinetic issues, but does not eliminate them.

### 5.4.6 Mechanism of Localization of Silica Particles in Pr1

In order to understand the mechanism of the localization of silica particles in the samples prepared by Pr1, a L-PLA/PBAT blend with 1 wt.% of nano-silica was prepared by the addition of silica to a premixed melt of L-PLA and PBAT at a short mixing time of 30 seconds. SEM and AFM images of this sample are shown in Figure 5.8.

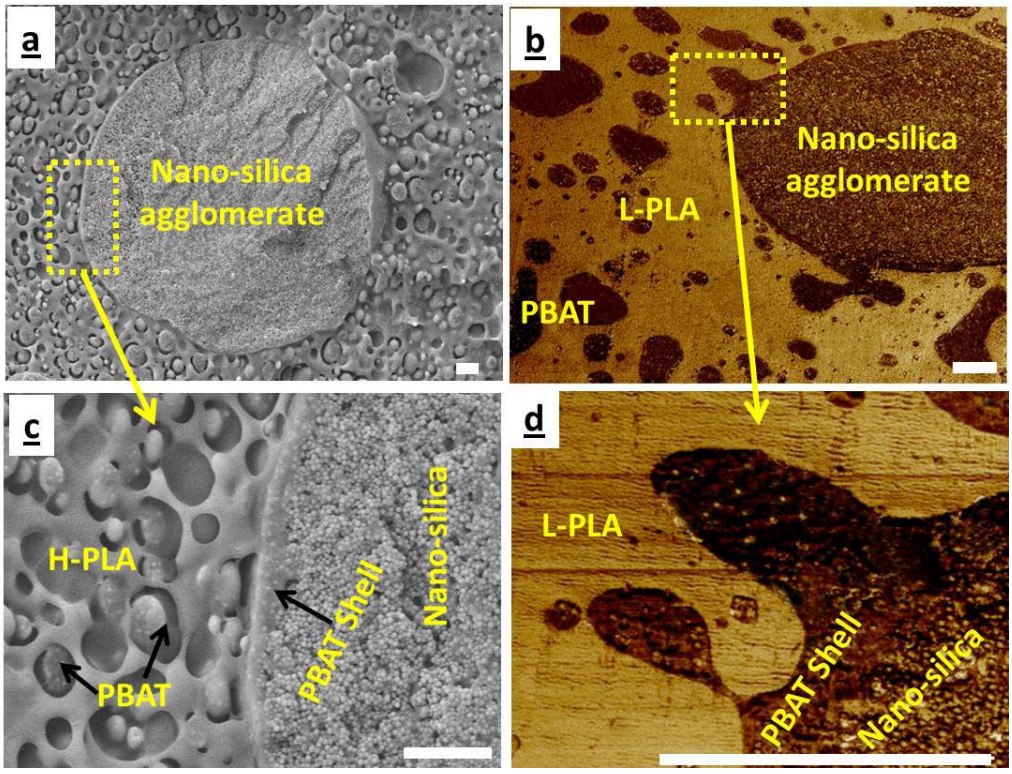


Figure 5.8. Nano-silica agglomerate in L-PLA/PBAT (70/30) blend prepared by Pr1 after 30 s of mixing (a) SEM image of the fracture surface, (b) AFM image of the microtomed surface. (c) and (d) show higher magnifications of the marked areas in (a) and (b) respectively. The scale bars show 2 μm.

As can be seen, a shell of the PBAT phase encapsulates the agglomerate of nano-silica at the early stages of mixing. Using image analysis, the average thickness of the PBAT shell was determined to be 400 nm . Hence, a preferential encapsulation of PBAT around the nano-silica particles occurs at very early stages of the mixing process. Figure 5.8 (d) clearly shows droplets of PBAT/nano-silica subsequently being detached from the encapsulating PBAT shell. Consequently, the detachment of these droplets from the shell results in the selective dispersion of silica particles in the PBAT dispersed phase. The preferential encapsulation of the silica agglomerate by the PBAT phase can be explained by considering that Blake and De Coninck [52] showed that the wetting rate of a solid substrate depends linearly on the interfacial tension between the solid and the liquid phase. Therefore, the observed selective encapsulation of silica agglomerates by the PBAT phase in this work can be attributed to the lower interfacial tension between PBAT/silica as compared with PLA/Silica.

### 5.4.7 Mechanism of Migration of Silica Particles from PLA to PBAT

It was established earlier in this paper that the preferred location for silica in PLA/PBAT blends is in the PBAT phase. With this in mind, the initial dispersion of silica particles into the PLA melt followed by PBAT addition (Pr2) thus offers the possibility to model the important kinetic parameters governing the migration of silica particles from the PLA phase to the PBAT one. This migration process of silica particles can be considered as a three–step process: (a) migration from the bulk of the PLA phase toward the interface, (b) draining of a PLA film between the particle and the interface and (c) migration at the interface. These steps are shown schematically in Figure 5.9.

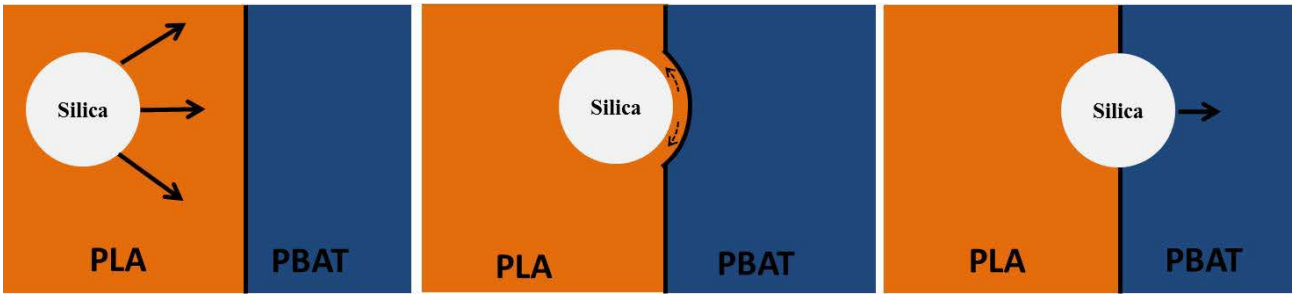


Figure 5.9. The migration mechanism of a silica particle from PLA phase to PBAT phase in the samples prepared by Pr2, (a) migration from the bulk of PLA phase toward the interface, (b) draining of PLA film between the particle and the interface, (c) migration at the interface.

#### *5.4.7.1.1 Bulk Migration*

In this first step, silica particles, that have been initially mixed with the PLA, must migrate in the bulk of the PLA phase far from the interface in order to find the PBAT phase. Eckstein et al.[53] studied the phenomenon of bulk migration experimentally and found that the particle flux in shear-induced migration scales as $\dot{\gamma}R^2$. This result has been confirmed by many others authors since then [54, 55]. The transitional velocity of spherical solid particles in the direction of the flow (flow-induced mechanism) has also been shown to scale as $\dot{\gamma}R$ [56-58].

These equations indicate the well-known conclusions that both shear rate and particle size should significantly influence the particle migration velocity in the bulk. On the one hand, the proportional dependence of the bulk migration velocity to shear rate can potentially explain the

significant increase in the localization of micro-silica particles at the interface in the H-PLA/PBAT blend prepared at the shear rate of 47 $s^{-1}$ (line 12 in Table 5-2) compared with the blend prepared at 25 $s^{-1}$ (line 6 in Table 5-2). However, as will be shown in the section below, shear rate will also influence the contact time at the interface and has a significant influence on film drainage as well. The best way to view the influence of bulk migration is to examine the results of this study with respect to micro- and nano-silica particles. As the particle migration depends on the particle radius, bulk migration should be more difficult for nano-silica than for micro-silica and yet when the particles are mixed initially with H-PLA, it is the nano-particles that are assembled almost perfectly at the interface. Even at an extreme limiting case where micro and nano-silica particles are considered to migrate at the same velocity as the surrounding H-PLA melt, this still does not explain why nano-silica assembles at the interface while micro-silica does not. This result, more than anything else, implies that bulk migration is not a controlling parameter related to the migration of silica particles in this system.

*5.4.7.1.2 Film Draining*

In the next step of migration, when a silica particle approaches the interface, a thin film of PLA phase between the particle and the interface needs to be drained before the particle contacts the other phase. The film draining time ($t_d$) between a spherical solid particle with radius R and a deformable liquid/liquid interface can be estimated as [59]:

$$t_d = \frac{3n^2 \eta A_f^2}{16\pi F_c}\left(\frac{1}{\delta_C^2} - \frac{1}{\delta_o^2}\right) \qquad \text{Eqn.5}$$

Here $F_c$, $\eta$, $A_f$, $\delta_C$ and $\delta_o$ are the contact force, the viscosity of the PLA, the surface area of the PLA film between the particle and the interface ($\sim 2\pi R^2$), the critical film thickness in which the PLA film rupture occurs and the initial PLA film thickness where the film draining process begins, respectively. Moreover, n indicates the mobility of the interfaces and is defined as the number of immobile interfaces in the system. For example, in the present system, n=1 as only one immobile solid/liquid interface contributes in the film draining step. The approaching silica particle remains in contact with the interface for a certain amount of time, which can be called the "contact time". If the film draining time is longer than this contact time, then the silica particle is moved away from the interface by the flow field and cannot reach the interface.

As can be seen in Equation 5, the estimation of the contact force and critical film thickness in Equation 5 is necessary to estimate the film draining time between silica particles and the interface. The contact force acting on a spherical solid particle moving close to a planar interface under simple shear flow has been estimated to be proportional to the shear rate and the inverse of the separation distance between the particle and the interface and the third power of the viscosity ratio [60-62]. However, the values of the predicted forces by the proposed analytical models are found to deviate considerably as the particle approaches the interface and also in systems with a high viscosity ratio of the phases[60]. Therefore, determining an analytical equation to estimate the contact force, $F_c$ in Equation 5, is still a controversial issue. Moreover, at the end of the film draining step, the PLA film rupture occurs by the formation and growth of sinusoidal perturbations at the PLA/PBAT interface similar to the film rupture in polymeric thin films[63]. However, no model has been proposed for the estimation of the critical film thickness between an approaching solid particle and an interface. Despite the difficulties in arriving at analytical numerical values related to film-drainage in the current system, Equation 5 can still provide much insight into the dominant factors influencing film draining at the interface. Equation 5 shows that the PLA film draining time is proportional to the fourth power of the radius of the silica particles and directly proportional to the viscosity of the PLA phase. Therefore, the film draining time is much longer for larger particles and for a more viscous PLA phase. This can explain the enhanced assembly of nano-scale silica particles in the interfacial zone in the blends with H-PLA phase. Considering only the silica particle radius, micro-silica would be expected to take approximately 80 times longer to drain the PLA phase than the nano-silica. For this reason, nano-silica particles, once in contact with the interface, drain the PLA film very effectively and thus are situated at the interface. Enhanced film drainage can also explain the observed effect of the viscosity of the PLA phase on the improved localization of micro-silica particles at the interface when they are initially mixed with L-PLA. As is supported by the experimental data, reducing the particle size is clearly the most effective approach to diminish film drainage time. This results in a virtually perfect assembly of nano-particles at the PLA/PBAT interface when the particles are initially mixed with the PLA phase, Figure 5.4 (b,d).

The shear rate can also influence the film drainage times. Increasing the shear rate increases the frequency of collision of silica particles with the interface and also reduces the film draining time by increasing the contact force in Equation 5. Increased shear rate will, however, also result in a

reduction of the silica particle contact time at the interface. In this study, for the micro-silica in the H-PLA system at higher shear rate (line 12 in Table 5-2), a significantly higher percentage of silica particles locate at the interface. This demonstrates that, on balance, shear rate improved film drainage effects for micro-silica.

*5.4.7.1.3 Migration at the Interface*

At this point in the understanding of the mechanism of silica migration from the PLA phase to PBAT, bulk migration of silica particles in PLA does not appear to be a controlling issue. It has also been shown that film drainage at the interface is expected to be much more of a critical parameter to consider for micro-silica than for nano-silica particles. All these conclusions are corroborated by the experimental results. The main question to consider now is why are nano-particles located in a stable fashion at the PLA/PBAT interface using Pr2? Why do they not move into the PBAT phase, which would be the most stable location from the thermodynamic surface energy perspective? In the third step of migration, for the silica particles initially added to the PLA, the PLA film ruptures between the silica and the interface and the silica particle enters the interface forming a three-phase contact line on the surface of the particle. The three-phase contact line can be clearly seen in Figure 5.10 where a typical micro-silica particle is shown at the interface of L-PLA/PBAT. At this point in the trajectory, the dynamics of silica particle movement towards the PBAT phase is dominated by a migration at the interface phenomenon.

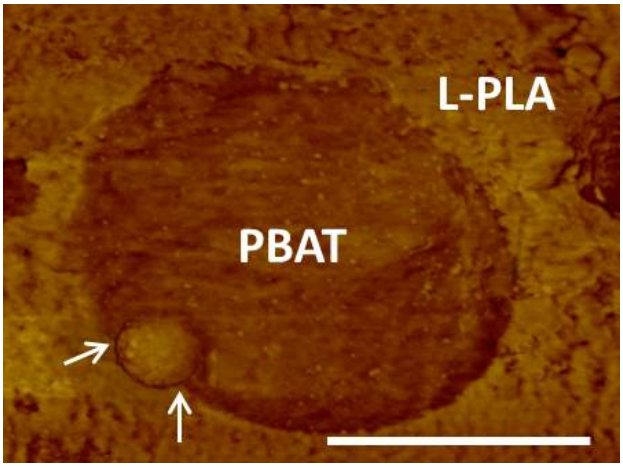


Figure 5.10. AFM image showing a micro-silica particle at L-PLA/PBAT interface in the sample prepared by Pr2. The pointers aim to the three-phase contact line on the surface of silica particle. The scale bar shows 1 μm.

The migration of silica particles at the interface is done by the displacement of the three-phase contact line on the surface of silica. Note that in reality the interface has a certain width to it and it cannot be considered as a simple line. That notion is simplified here to a line in order to more easily model the system. To move the three-phase contact line on the surface of the particle, work must be done to overcome the kinetic barriers against molecular displacement at the three-phase contact line in the preferred direction. This work is provided by the thermodynamic driving force as well as the drag force applied to the particle by either phase. The main difficulty in considering the drag forces in the estimation of the migration velocity at the interface originates from the complexity of determining the direction and magnitude of the drag forces on either side of the interface.For example, a drag force parallel to the interface is likely to move the particle along the interface rather than pushing it through the interface. Plattier et al. [64] tried to determine the relative drag forces applied to a particle at the interface by assuming that both drag forces in either phase always tend to pull the particle out of the interface during the mixing. Moreover, they assumed that the magnitudes of the drag force close to the interface are the same as the one in the bulk and ignored the effect of the interface on the drag forces and flow field. In fact, determining the effect of the drag forces on the migration at the interface requires the knowledge of the flow field close to the interface which is a complex issue and is outside of the scope of this paper. Therefore, in this work, that aspect will not be considered.

The velocity of the displacement of the three-phase contact line on the surface of a silica particle can be estimated by considering dynamic wetting phenomena. In the dynamic wetting of a solid substrate by a liquid phase, the displacement velocity of the three-phase contact line can be estimated as [52, 65]:

$$V = \frac{F}{\xi L} \qquad \text{Eqn. 6}$$

Where F is the thermodynamic driving force, L is the length of the three-phase contact line and $\xi$ is the friction coefficient. The thermodynamic driving force originates from the tendency to decrease the interfacial energy of the system by the migration of the particles toward their thermodynamic equilibrium location. This driving force always acts parallel to the surface of silica and depends on the penetration depth of the particle into the PBAT phase. The driving force decreases by approaching the equilibrium location and finally vanishes when the equilibrium state is achieved. The work done by the thermodynamic driving force for displacing the three-

phase contact line can be defined as the change in the interfacial energy of the system with respect to the particle penetration depth in the PBAT phase. The friction coefficient can be defined as proposed by Blake and De Coninck [52] to consider the effect of viscosity of the phases. Using this approach, the migration velocity at the interface can be estimated as:

$$V = \frac{-R\lambda^3\left[\gamma_{2s}-\gamma_{1s}-(1-\frac{x}{R})\gamma_{12}\right]}{\sqrt{x(2R-x)}\left[\eta_1 \nu_1 \exp\left(\frac{W_{1S}\lambda^2}{k_B T}\right)+\eta_2\ \nu_2 \exp(\frac{W_{2S}\lambda^2}{k_B T})\right]} \qquad \text{Eqn.7}$$

where $\gamma_{1s}$, $\gamma_{2s}$ $\gamma_{12}$ are the interfacial tensions between: phase 1 and solid, phase 2 and solid, phase 1 and phase 2, $\eta_i$ is viscosity of the liquids, $\nu_i$ is molecular volume of the liquids, $\lambda$ is length of individual molecule displacement at the three-phase contact line, $W_{iS}$ is the work of adhesion between liquids and solid, T and $k_B$ are the temperature and Boltzmann constant, and *x* is the penetration depth of the silica particle in the PBAT phase. The details of the derivation of Equation 7 can be found in the ANNEX 1. It should be emphasized that in Equation 7, $\lambda$ is the only parameter that cannot be determined experimentally from the molecular and rheological analysis of the individual polymer components. The value for $\lambda$ in Equation 7 depends on the molecular structure of the liquid phases and is shown to be in the order of the molecular size of the wetting liquid phase in small molecule liquids[65].

Equation 7 now allows one to evaluate the influence of various parameters and can model, at least semi-quantitatively, the migration velocity of a silica particle at the interface of PLA/PBAT as a function of the particle penetration depth into the PBAT phase.

The effect of the thermodynamic parameters (the interfacial tension and work of adhesion between the components) as well as the kinetic parameters (the viscosity of the phases) on the migration velocity at the interface can also be modelled semi-quantitatively based on Equation 7. For instance, it predicts that both reducing the interfacial tension between the liquid components and increasing the viscosity of the phases will reduce the migration velocity at the three-phase contact line. In previous work, the interfacial tension between PLA and PBAT was found to very low at 0.6 mN/m[36]. Hence, from the molecular viewpoint, due to the very similar nature of PLA and PBAT molecules, the molecular substitution of PLA with PBAT results in very little change in the interfacial free energy of the system which reduces significantly the tendency of the PBAT molecules to replace PLA molecules at the three-phase contact line and, consequently, results in a very slow migration velocity at the interface. In addition, it should also be underlined

that low interfacial tension systems represent significantly wider interphase regions[66]. Most likely, both the very slow migration velocity at the interface and the necessity to traverse a greater interfacial distance allows for the silica particles to assemble in a quasi-stable fashion at the interface.

## 5.5 Conclusions

In this work, the effects of the most important thermodynamic and kinetic parameters on the localization and migration of micro- and nano-silica particles in a low interfacial tension system of PLA/PBAT were studied in detail. To determine the thermodynamic equilibrium localization of silica particles, surface energies of PLA and PBAT were measured at the ambient and high temperatures using contact angle and pendant drop techniques, respectively. Using the Young's model, the thermodynamic equilibrium localization of silica particles was determined to be in the PBAT phase. It was found that when the silica particles were added to a PLA/PBAT melt (Pr1), silica particles were localized in the PBAT phase irrespective of the viscosity of the PLA phase. By investigating the morphology at short mixing times, it was found that PBAT phase encapsulates silica particles preferentially at the early stages of mixing in these samples. This preferential encapsulation is due to the lower interfacial tension of PBAT/silica compared with PLA/silica.

In order to examine the influence of kinetic effects on silica localization, detailed work was carried out on the case where the silica particles were premixed with PLA (Pr2). This allows one to examine the main factors controlling the migration of silica particles from the PLA phase to the PBAT. When nano-silica particles were premixed with low or high viscosity PLA phases (L-PLA or H-PLA), they were found to be localized at the interface. The same localization was observed by premixing micro-silica particles with the L-PLA phase. A model is proposed to examine the role of different thermodynamic and kinetic parameters on the migration velocity of spherical particles at the interface of a multiphase system and it was shown that the stable localization of micro- and nano-silica particles at the interface in the above samples is due to the slow migration velocity at the interface which originates from the low interfacial tension of the PLA/PBAT system. In addition, the interphase region in low interfacial tension PLA/PBAT blends is likely to be wide which will also increase the silica particle migration time.

On the other hand, when micro-silica particles were premixed with the high viscosity PLA phase (H-PLA), they stayed in the H-PLA phase. It was shown that this localization of micro-silica particles in the PLA phase can be attributed to the long film draining time between the particles and the interface. The film draining time was shown to depend on the fourth power of the radius of the silica particles and directly to the viscosity of the PLA phase. For this reason, micro-silica particles would be expected to experience much longer drainage times as compared to nano-silica particles. It was also shown that increasing the shear rate of mixing enhances the migration of micro-silica particles from the H-PLA phase to the interface and this was also shown to be principally related to film drainage.

These results clearly indicate that in low interfacial tension systems when the solid particles are mixed with the component with which it has the least affinity, the kinetic parameters influencing localization will be dominated by film drainage for micro-silica particles and by migration at the interface for nano-silica. These findings have important implications in the controlled localization of micro- and nano-particles in low interfacial tension polymer blends.

## 5.6 Acknowledgment

The authors would like to gratefully acknowledge the NSERC Network for Innovative Plastic Materials and Manufacturing Processes (NIPMMP) for the funding of this work. The authors would also like to acknowledge Professor Pierre J. Carreau for helpful discussions, as well as Professor Musa Kamal and Dr. Vahid Khoshkava for their help with the surface energy measurements.

## 5.7 References

1. Yoo Y, Cui L, Yoon PJ, and Paul DR. Macromolecules 2009;43(2):615-624.
2. Lee H-s, Fasulo PD, Rodgers WR, and Paul DR. Polymer 2005;46(25):11673-11689.
3. Karger-Kocsis J. Reinforced Polymer Blends. In: D. R. Paul CBB, editor. Polymer Blends, vol. 2. NewYork: John Wiley & Sons, 1999. pp. 395.
4. Sumita M, Sakata K, Hayakawa Y, Asai S, Miyasaka K, and Tanemura M. Colloid and Polymer Science 1992;270(2):134-139.

5. Levon K, Margolina A, and Patashinsky AZ. Macromolecules 1993;26(15):4061-4063.

6. Al-Saleh MH and Sundararaj U. Composites Part A: Applied Science and Manufacturing 2008;39(2):284-293.

7. Wu D, Lin D, Zhang J, Zhou W, Zhang M, Zhang Y, Wang D, and Lin B. Macromolecular Chemistry and Physics 2011;212(6):613-626.

8. Yuan J-K, Yao S-H, Sylvestre A, and Bai J. The Journal of Physical Chemistry C 2012;116(2):2051-2058.

9. Shi Y-y, Yang J-h, Huang T, Zhang N, Chen C, and Wang Y. Composites Part B: Engineering 2013(0).

10. Chen J, Shi Y-y, Yang J-h, Zhang N, Huang T, Chen C, Wang Y, and Zhou Z-w. Journal of Materials Chemistry 2012;22(42):22398-22404.

11. Cardinaud R and McNally T. European Polymer Journal 2013;49(6):1287-1297.

12. Xiong Z-Y, Wang L, Sun Y, Guo Z-X, and Yu J. Polymer 2013;54(1):447-455.

13. Huang J, Mao C, Zhu Y, Jiang W, and Yang X. Carbon 2014;73:267-274.

14. Zhao X, Zhao J, Cao J-P, Wang D, Hu G-H, Chen F, and Dang Z-M. Materials & Design 2014;56:807-815.

15. Tao F, Nysten B, Baudouin A-C, Thomassin J-M, Vuluga D, Detrembleur C, and Bailly C. Polymer 2011;52(21):4798-4805.

16. Katada A, Buys Y, Tominaga Y, Asai S, and Sumita M. Colloid and Polymer Science 2005;284(2):134-141.

17. Baudouin A-C, Bailly C, and Devaux J. Polymer Degradation and Stability 2010;95(3):389-398.

18. Baudouin A-C, Devaux J, and Bailly C. Polymer 2010;51(6):1341-1354.

19. Göldel A, Kasaliwal G, and Pötschke P. Macromolecular Rapid Communications 2009;30(6):423-429.

20. Göldel A, Kasaliwal GR, Pötschke P, and Heinrich G. Polymer 2012;53(2):411-421.

21. Göldel A, Marmur A, Kasaliwal GR, Pötschke P, and Heinrich G. Macromolecules 2011;44(15):6094-6102.

22. Gültner M, Göldel A, and Pötschke P. Composites Science and Technology 2011;72(1):41-48.

23. Taghizadeh A and Favis BD. Carbohydrate Polymers 2013;98(1):189-198.

24. Elias L, Fenouillot F, Majesté JC, Alcouffe P, and Cassagnau P. Polymer 2008;49(20):4378-4385.

25. Elias L, Fenouillot F, Majesté JC, Martin G, and Cassagnau P. Journal of Polymer Science Part B: Polymer Physics 2008;46(18):1976-1983.

26. Elias L, Fenouillot F, Majeste JC, and Cassagnau P. Polymer 2007;48(20):6029-6040.

27. Zou Z-M, Sun Z-Y, and An L-J. Rheologica Acta 2014;53(1):43-53.

28. Dasari A, Yu Z-Z, and Mai Y-W. Polymer 2005;46(16):5986-5991.

29. Gubbels F, Jerome R, Teyssie P, Vanlathem E, Deltour R, Calderone A, Parente V, and Bredas JL. Macromolecules 1994;27(7):1972-1974.

30. Gubbels F, Jerome R, Vanlathem E, Deltour R, Blacher S, and Brouers F. Chemistry of Materials 1998;10(5):1227-1235.

31. Persson AL and Bertilsson H. Polymer 1998;39(23):5633-5642.

32. Tchoudakov R, Breuer O, Narkis M, and Siegmann A. Polymer Engineering & Science 1996;36(10):1336-1346.

33. Cheah K, Forsyth M, and Simon GP. Journal of Polymer Science Part B: Polymer Physics 2000;38(23):3106-3119.

34. Hong JS, Kim YK, Ahn KH, and Lee SJ. Journal of Applied Polymer Science 2008;108(1):565-575.

35. Fenouillot F, Cassagnau P, and Majesté JC. Polymer 2009;50(6):1333-1350.

36. Jalali Dil E, Carreau PJ, and Favis BD. Polymer 2015;68:202-212.

37. Owens DK and Wendt RC. Journal of Applied Polymer Science 1969;13(8):1741-1747.

38. Demarquette NR and Kamal MR. Polymer Engineering & Science 1994;34(24):1823-1833.

39. Wu S. Polymer Interface and Adhesion, 1982.

40. Wu S. The Journal of Physical Chemistry 1970;74(3):632-638.

41. Khoshkava V and Kamal MR. Biomacromolecules 2013;14(9):3155-3163.

42. Bousmina M, Ait-Kadi A, and Faisant JB. Journal of Rheology 1999;43(2):415-433.

43. Cox WP and Merz EH. Journal of Polymer Science 1958;28(118):619-622.

44. Ravati S and Favis BD. Polymer 2013;54(13):3271-3281.

45. Papirer E, Balard H, and C. V. Surface energies of silica investigated by inverse gas chromatoghraphy. In: Papirer E, editor. Adsorption on silica surfaces. New York: Marcel Dekker, 2000. pp. 205-276.

46. Papirer E and Balard H. Inverse Gas Chromatography: A Method for the Evaluation of the Interaction Potential of Solid Surfaces. In: Pefferkorn E, editor. Interfacial Phenomena in Chromatography, vol. 80. New York: Marcel Dekker Inc., 1999. pp. 145.

47. Das A, Mahaling RN, Stöckelhuber KW, and Heinrich G. Composites Science and Technology 2011;71(3):276-281.

48. Jacob PN and Berg JC. Langmuir 1994;10(9):3086-3093.

49. Bailly M and Kontopoulou M. Polymer 2009;50(11):2472-2480.

50. Feng J, Chan C-m, and Li J-x. Polymer Engineering & Science 2003;43(5):1058-1063.

51. Austin JR and Kontopoulou M. Polymer Engineering & Science 2006;46(11):1491-1501.

52. Blake TD and De Coninck J. Advances in Colloid and Interface Science 2002;96(1–3):21-36.

53. Eckstein EC, Bailey DG, and Shapiro AH. Journal of Fluid Mechanics 1977;79(01):191-208.

54. Leighton D and Acrivos A. Journal of Fluid Mechanics 1987;181:415-439.

55. WANG Y, MAURI R, and ACRIVOS A. Journal of Fluid Mechanics 1998;357:279-287.

56. Buyevich YA. Fluid Dynamics of Fine Suspension Flow. In: Siginer DA, De Kee D, and Chhabra RP, editors. Advances in the Flow and Rheology of Non-Newtonian Fluids, Part B. Netherlands: Elsevier, 1999. pp. 1267.

57. Bossis G and Brady JF. The Journal of Chemical Physics 1984;80(10):5141-5154.

58. Liu S. Chemical Engineering Science 1999;54(7):873-891.

59. Hartland S. Chemical Engineering Science 1969;24(6):987-995.

60. POZRIKIDIS C. Journal of Fluid Mechanics 2007;575:333-357.

61. Lee SH and Leal LG. Journal of Fluid Mechanics 1980;98(01):193-224.

62. Yang S-M and Leal LG. Journal of Fluid Mechanics 1984;149:275-304.

63. Reiter G. Langmuir 1993;9(5):1344-1351.

64. Plattier J, Benyahia L, Dorget M, Niepceron F, and Tassin J-F. Polymer 2015;59(0):260-269.

65. Blake TD. Journal of Colloid and Interface Science 2006;299(1):1-13.

66. Helfand E and Tagami Y. The Journal of Chemical Physics 1972;56(7):3592-3601.

67. Liu Y and Kontopoulou M, Polymer 2006; 47:7731

# CHAPTER 6 ARTICLE 3: LOCALIZATION OF MICRO AND NANO-SILICA PARTICLES IN A HIGH INTERFACIAL TENSION POLY(LACTIC ACID)/ LOW DENSITY POLYETHYLENE SYSTEM*

*Ebrahim Jalali Dil, Basil D. Favis*

*CREPEC, Department of Chemical Engineering, École Polytechnique de Montréal, Montréal, Quebec, Canada, H3T 1J4.*

## 6.1 Abstract

This work studies the effects of thermodynamic and kinetic parameters on the localization and migration of micro- and nano-silica particles in the high interfacial tension blend system of poly (lactic acid), (PLA)/ low density polyethylene (LDPE). The surface modification of micro-silica particles from a high to a low energy surface was carried out by the grafting of (2-Dodecen-1-yl) succinic anhydride to the surface of micro-silica particles using a new gas-phase reaction approach. The surface modification was confirmed by X-ray photoelectron spectroscopy analysis and surface energy measurements. Young's model predicts that the thermodynamic equilibrium localization of unmodified and modified silica particles in PLA/LDPE blends should be in the PLA phase and at the PLA/LDPE interface, respectively. Scanning electron microscopy results confirm that when unmodified micro- or nano-silica particles are added to a PLA/LDPE melt, the silica particles are selectively localized in the PLA phase even in the blend sample with only 5 vol.% of PLA. However, modified micro-silica particles were found to be located principally in the LDPE phase. The influence of kinetic parameters was imposed by premixing modified and unmodified micro-silica particles with a high viscosity LDPE phase (H-LDPE). In that case both silica types remain in the H-LDPE phase independent of shear rate and mixing time. When the viscosity of the LDPE phase is reduced, unmodified and modified micro-silica migrate to their thermodynamically predicted locations in the PLA phase and at the PLA/LDPE interface respectively. In the case of unmodified nano-silica particles premixed in the H-LDPE phase, individual well dispersed nano-silica particles migrate to the PLA phase while aggregates remain

* Submitted to *Polymer*

in the H-LDPE phase. These results have important implications in the field of nanocomposites and indicate that the localization of well-dispersed nanoparticles in a high interfacial tension multiphase system will not likely be influenced by kinetic effects. Kinetic effects are much more dominant in micro-scale silica systems and the kinetic effects are found to depend on a film-draining mechanism at the PLA-LDPE interface region.

***Keywords:*** *Localization, Polymer blends, Surface modification*

## 6.2 Introduction

Micro- and nano-particles dispersed in multiphase polymer systems are receiving significant attention as they can provide a wider range of mechanical and/or electrical properties as compared with those based on a single polymer matrix. Controlling the localization of the particles into specific phases or at the interface is one of the key parameters in achieving property control in such multiphase systems [1-6, 51]. It has been shown that the localization of solid particles in a dispersed rubbery phase not only increases the dispersed phase size [7, 8], but also dramatically suppresses the energy dissipation mechanisms [1]. The localization of solid particles in the matrix phase can reduce the dispersed phase size by diminishing coalescence through the formation of a physical barrier between the dispersed phase droplets as well as through an increase in the matrix viscosity [9, 10]. The localization of solid particles at the interface has also been reported to decrease the dispersed phase size by a solid barrier mechanism [11] and can even enhance the interfacial interactions between polymeric phases [12-15]. In conductive polymer blends, it has been found that the localization of solid particles in either phase of a co-continuous system can significantly reduce the conductivity threshold [6]. This latter phenomenon is known as double percolation [6, 16]. The lowest electrical percolation threshold can be achieved when the conductive particles are localized at the interface of co-continuous polymeric phases [5].

It is apparent that controlling the localization of solid inclusions in a multiphase polymer system is crucial to achieving the desired mechanical and/or electrical properties. Despite the numerous studies in the literature on this subject, a comprehensive understanding of the parameters and

mechanisms governing solid particle migration and localization in multiphase polymer systems is lacking.

Among the few mechanisms that have been proposed to explain the migration of solid particles in multiphase polymer systems, shear induced migration is the most mentioned mechanism [10, 17, 18]. In this case the migration of solid particles is assumed to be controlled only by the hydrodynamic forces and the particles are transferred to the other phase as soon as they collide with the interface. The frequency of collision between mono-dispersed particles can be estimated as [10]:

$$C = \frac{8}{\pi}\dot{\gamma}\varphi \qquad \text{Eqn. 1}$$

Where $\dot{\gamma}$ and φ are the shear rate and the volume fraction of the particles respectively. This mechanism, however, does not explain the trapping of solid particles at the interface reported in some previous studies [19, 20]. The Slim Fast mechanism was proposed by Goldel et al. [21] to explain the effect of aspect ratio on the migration of solid particles at the interface. Some authors [10, 17] also suggested that the trapping of solid particles between two colliding dispersed phase droplets can transfer solid particles from the matrix phase to the dispersed phase. Although each of these mechanisms may explain a part of the migration and localization process, they do not provide an overall picture of the surface energy/thermodynamics of the migration process versus the effects of important kinetic parameters such as viscosity, mixing strategy and the particle size of solid inclusions. In a previous study from this group [19], the migration and localization of micro- and nano-silica particles in low interfacial tension blends of poly (lactic acid),PLA, and poly(butylene adipate-co-terephthalate), PBAT, were studied in detail and it was shown that the film draining step, between silica particles and the interface, and the migration velocity at the interface are limiting factors that can cause a non-equilibrium localization of silica particles.

PLA/PE blends are of interest in the study of solid particle localization since they provide the case of a model high interfacial tension system. In addition, the blending of PLA with PE has been shown to improve the elongation at break and impact properties of PLA considerably [22, 23]. For instant, Anderson and Hillmyer [23] found that the addition of 20 wt.% of PE and 5 wt.% of PLA-PE, as the compatibilizer, significantly increased the impact strength of PLA from 20 J/m to 760 J/m.

The main objective of this paper is to study the effect of thermodynamic and kinetic parameters on the migration and localization of mico- and nano- silica particles in PLA/LDPE blends. The effect of the surface energy of polymer components as well as the surface energy of micro-silica particles on the localization of the silica particles will be studied. Moreover, the effect of mixing strategy, viscosity of the LDPE phase, the particle size of silica and shear rate of mixing on the localization of silica particles will be evaluated.

## 6.3 Experimental

### 6.3.1 Materials

PLA 2003D (Natureworks, Cargil) was purchased from NatureWorks LLC. Two types of LDPE (133A and 100.BW) with melt flow indices of 0.25 g/10 min and 2 g/10 min were purchased from Dow Chemicals and ExxonMobil and will be referred to hereafter as H-LDPE and L-LDPE respectively. (2-Dodecen-1-yl) succinic anhydride was purchased from Sigma-Aldrich and was used as received. Spherical micro- and nano-silica particles, SEAHOSTAR KE-P30 and KE-P10, with hydroxyl content of 1mmol/g were received from Nippon Shokubai, Japan. The average diameters of the individual spherical particles for micro- and nano-silica are 300 nm and 100 nm. All the materials were dried under vacuum at 60 ℃ overnight before being used in the experiments.

### 6.3.2 Surface modification of micro-silica particles

A new gas-phase reaction approach was used to modify the surface of micro-silica particles which eliminates the need of using a solvent and the precautions required for controlling the solvent moisture content. To this aim, 3 g of micro-silica powder was placed on a mesh in a desiccator containing 1g of (2-Dodecen-1-yl) succinic anhydride at the bottom of the desiccator. After applying a vacuum of 760 Torr using a vacuum pump, the desiccator was placed in an oven at 160 ℃. After the reaction time, the desiccator was removed from the oven and cooled in the air. To remove the unreacted (2-Dodecen-1-yl) succinic anhydride, the silica powder was washed six times with acetone using a washing cycle of three days, followed by centrifugal separation of

the particles. Finally the obtained powder was dried in a vacuum oven at 60 ℃ overnight. The unmodified micro-silica and modified micro-silica particles will be referred to as U-micro-silica and M-micro-silica respectively in the rest of the paper.

### 6.3.3 Surface energy measurements and interfacial tensions

The surface energy of PLA and unmodified silica were examined in a previous study[19]. To measure the surface energy of L-LDPE and H-LDPE at room temperature, thin sheets of the polymers were prepared by compression moulding. Ethanol and distilled water were used to remove any contamination from the surface of the sheets. Finally, the sheets were dried at 60 ℃ for 6 h in a vacuum oven. The surface energy then was determined by measuring the contact angles of water, glycerol and diiodomethane, as liquid probes, on the polymer sheets. The Owens-Wendt [24] approach was used to determine the surface energy as well as its dispersive and polar components. The pendant drop technique was used to measure the surface energies of L-LDPE and H-LDPE at the processing temperature. The apparatus and the operation description can be found elsewhere [25].The melt densities of L-LDPE and H-LDPE at 180 ℃ were measured as 0.75 g/cm$^3$ using a high pressure piston-type dilatometer (PVT100, ThermoHaake). To determine the surface energy of modified-silica particles, a film of M-micro-silica was formed by casting a suspension of 1 wt.% of M-micro-silica in acetone. The film is a layer of about 20 μm thick that is formed on a substrate so it can keep its integrity. The surface energy of M-micro-silica at room temperature was determined using the contact angle method. The test procedure was the same as the one described for H-LDPE and L-LDPE. The surface energy of M-micro-silica at the processing temperature was estimated using the thermal coefficient of -0.1 mN/m reported for hydrophobic silica in the literature [18, 26]. The interfacial tensions between PLA/LDPE, PLA/M-micro-silica and LDPE/M-micro-silica were calculated using the Harmonic Mean approach[27]:

$$\gamma_{12} = \gamma_1 + \gamma_2 - 4\left(\frac{\gamma_1^d \gamma_2^d}{\gamma_1^d + \gamma_2^d} + \frac{\gamma_1^p \gamma_2^p}{\gamma_1^p + \gamma_2^p}\right) \qquad \text{Eqn.2}$$

and the interfacial tensions between PLA/Silica and LDPE/Silica were estimated using the Geometric Mean equation[27]:

$$\gamma_{12} = \gamma_1 + \gamma_2 - 2\left(\sqrt{\gamma_1^d \gamma_2^d} + \sqrt{\gamma_1^p \gamma_2^p}\right) \quad \text{Eqn.3}$$

In these equations, $\gamma_i$ is the surface energy, $\gamma_i^d$ is the dispersive component and $\gamma_i^p$ is the polar component of surface energy.Note that when the wetting liquid does not change the arrangement of the solid molecules at the interface (does not swell the solid), the interfacial tension and interfacial surface energy terms are identical and interchangeable [28].

### 6.3.4 X-ray photoelectron spectroscopy (XPS)

X-ray photoelectron spectroscopy (XPS) measurements were conducted on a VG ESCALAB 3 MKII spectrometer (VG, Thermo Electron Corporation, UK) with Mg-Kα ray source. Spectra were carried out with 100 eV pass energy for the survey scan and 20 eV pass energy for the high resolution scans. The relative atomic percent was calculated from the relative peak areas corrected by the Wagner sensitivity factors and Shirley background subtraction.

### 6.3.5 Rheological characterization

The samples were compression moulded at 180 ℃ and at 300 kPa in the form of 1.2 mm thick disks of 25 mm diameter under a nitrogen blanket. The rheological measurements were carried out using a stress-controlled rheometer (Physica MCR 301, Anton Paar) with a 25 mm parallel plate geometry at a 1 mm gap at 180 ℃ under nitrogen atmosphere. The stability of the polymer components was examined under the test conditions using a time sweep test. Less than a 7% drop in the complex viscosity and storage modulus was observed in the experimental time scale of 40 minutes.

### 6.3.6 Blend preparation

The blend samples were prepared using a Brabender internal batch mixer (Plasti-Corder DDR501) with a total volume of 30 $cm^3$ at 180 ℃ under a nitrogen blanket. A 70% mixing

chamber fill factor was used. The average shear rate at the mixing speeds of 50 and 100 RPM used in this study were estimated as 25 $s^{-1}$ and 47 $s^{-1}$, respectively [29]. Two different mixing strategies were used to prepare the samples:

Pr1: The addition of silica particles to the PLA/LDPE melt (one-step process).

Pr2: Premixing of silica particles with the LDPE phase followed by mixing with the PLA phase (two-step process).

After 10 minutes of mixing, the mixer was stopped and the samples were taken and frozen in liquid nitrogen to freeze-in the morphology and localization of silica particles. The blend samples, unless otherwise mentioned, contain 80 vol.% of PLA phase and 20 vol.% of the LDPE phase. The wt.% of silica particles added to the blends is based on the total weight of the blend.

### 6.3.7 Field emission scanning electron microscopy (FE-SEM)

In order to determine the localization of silica particles, samples from the internal batch mixer were cut and microtomed under liquid nitrogen using a microtome (Leica-Jung RM 2165). Then the sample surface was coated with gold and the morphology was observed with a Field Emission Scanning Electron Microscope (JSM 7600F, JEOL).

### 6.3.8 Atomic force microscopy (AFM)

The samples were microtomed using the same procedure as mentioned for the FE-SEM samples. The AFM machine was equipped with a scanning probe microscope Dimension 3100 with a Nanoscope IVa controller from Veeco Instruments. Silicon tips, model ACTA-W from AppNano, with a tip radius less than 10 nm were used in this study. The morphologies of the samples were determined by Tapping mode AFM in air.

### 6.3.9 Image analysis

Image analysis software (SigmaScan Pro. V.5, Sigmaplot) was used to determine the average dispersed phase diameter using an average number of 250 measurements for each sample. The Saltikov correction was applied [27] in calculating the dispersed phase diameter to consider the

fact that the droplets are not cut exactly at their equator in the microtomed surface. To quantify the localization of the silica particles, the location of 110 to 320 silica particles, depending on the blend structure, were determined in SEM images.

## 6.4 Results and Discussion

### 6.4.1 Material Characterization

#### 6.4.1.1 Rheological characterization

Figure 6.1 shows the complex viscosities (η*) and storage moduli of the neat polymer components as a function of angular frequency. PLA shows a Newtonian plateau at low angular frequencies but L-LDPE and H-LDPE exhibit shear thinning behaviour even at very low frequencies which indicates the high level of long chain branching in their structure[30]. The key rheological characteristics of the neat polymer components are listed in Table 0-1.

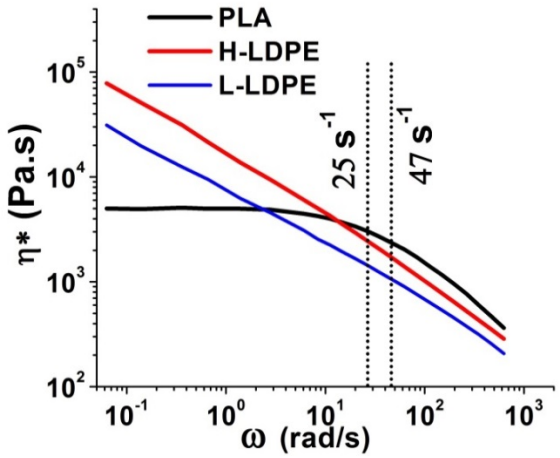


Figure 6.1. Complex viscosities of the neat polymer components. The dashed line represents the average shear rates of mixing [29].

Table 0-1. Rheological characteristics of the neat polymer components

| | Zero shear viscosity (Pa.s) | Power-law index | η* at 25 $s^{-1}$ (Pa.s) | η* at 47 $s^{-1}$ (Pa.s) |
|---|---|---|---|---|
| PLA | 4830 | 0.46 | 2930 | 2430 |
| H-LDPE | - | 0.36 | 2450 | 1690 |
| L-LDPE | - | 0.43 | 1440 | 1015 |

### 6.4.1.2 Modification of the surface of micro-silica particles

The surface modification of micro-silica particles from a high to a low energy surface was carried out by the grafting of (2-Dodecen-1-yl) succinic anhydride to the surface of micro-silica particles using a new gas-phase reaction approach. The evolution of the water contact angle (θ) with reaction time was used to evaluate the extent of the surface modification of the M-micro-silica (modified-silica) particles. Figure 0.2 (a) shows the AFM image of the surface topography of the M-micro-silica film that was used in the water contact angle measurements.

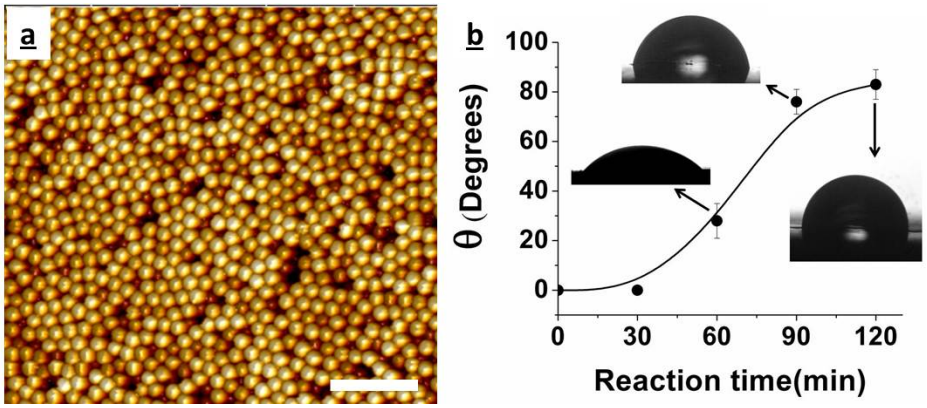


Figure 0.2. (a) AFM image of the surface of the cast M-micro-silica film, the white scale bar shows 2μm. (b) the evolution of the water contact angle (θ) on the M-micro-silica film as a function of reaction time.

The root mean-square ($R_q$) and arithmetic average ($R_a$) roughness of the M-micro-silica film were determined as 69 nm and 54 nm. These values are much smaller than the critical roughness of 500 nm where the surface roughness begins to affect the contact angle results [31, 32].

Complete wetting of the water droplet (θ=0) was observed at short reaction times, but after 60 minutes of the reaction, a water droplet with a contact angle of 22 degrees was formed on the M-micro-silica film. Increasing the reaction time from 90 to 120 minutes only changed the water contact angle from 76 to 83 degrees; therefore, the M-micro-silica particles obtained after 120 minutes of the reaction were used in the experiments. It should also be mentioned that an extra washing cycle of the M-micro-silica particles with acetone did not change the contact angle results which confirms the efficiency of the method used to remove the unreacted (2-Dodecen-1-yl) succinic anhydride.

XPS was used to examine the presence of the (2-Dodecen-1-yl) succinic anhydride molecules on the surface of M-micro-silica particles. The survey scans of the U-micro-silica and M-micro-silica particles are shown in Figure 6.3(a).

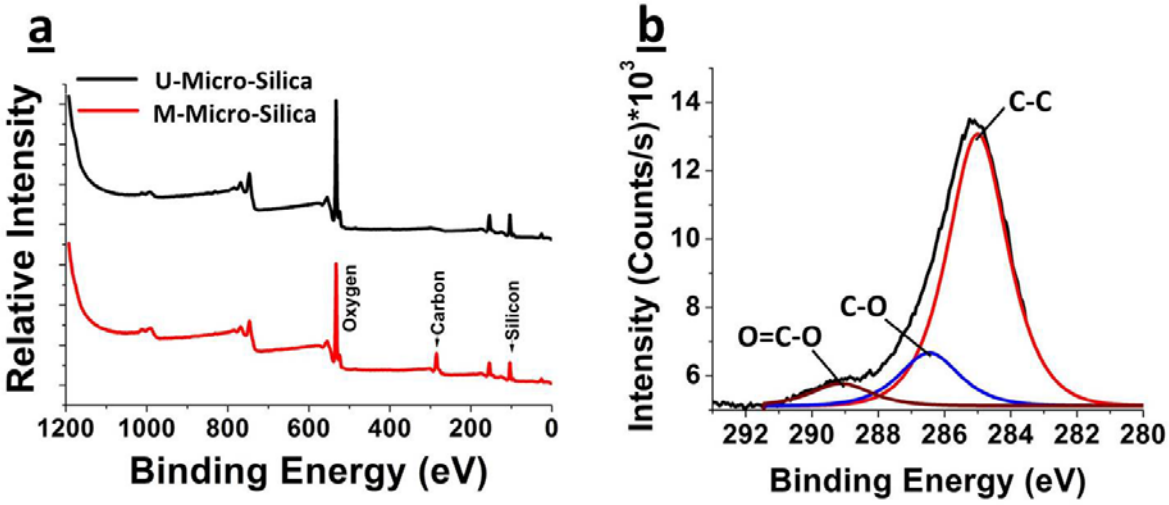


Figure 6.3. (a) XPS survey spectra of U-micro-silica and M-micro-silica particles, (b) High resolution XPS spectra of the carbon regions of M-micro-silica particles

In addition to the peaks of silicon at 103.5 eV and oxygen at 532.8 eV, a carbon peak at 285 eV appears in the M-micro-silica sample which confirms the presence of organic molecules on the silica surface M-micro-silica (modified-silica). The high resolution XPS spectrum of the carbon region in micro-silica and M-micro-silica particles is shown in Figure 6.3(b). The relative atomic % results obtained from the high resolution scans are also presented in Table 6-2.

Table 6-2. The relative atomic% of different groups in the high resolution XPS spectra of U-micro-silica and M-micro-silica particles.

| Element | Identification | Binding Energy (eV) | Relative atomic % | |
|---|---|---|---|---|
| | | | U-micro-silica | M-micro-silica |
| C | C-C | 285 | 0 | 18.9 |
| | C-O | 286.6 | 0 | 3.4 |
| | O=C-O | 289.1 | 0 | 3.1 |
| Si | Si-O | 101.9 | 1.5 | 0 |
| | $SiO_2$ | 103.7 | 31.5 | 17.7 |
| O | Si-OH | 531.2 | 3.7 | 0 |
| | Si-O | 533.1 | 63.3 | 56.9 |

As can be seen for the M-micro-silica, the atomic % of the C-C group is 6.1 times that of the O=C-O group and 5.5 times that for the C-O group. Since the ratio of C-C to O=C-O or C-O in a (2-Dodecen-1-yl) succinic anhydride molecule is 6, the XPS results confirm the presence of (2-Dodecen-1-yl) succinic anhydride molecules on the surface of M-micro-silica particles. The disappearance of the silicon and oxygen peaks of the silanol group after the modification of silica can also be considered as an indication of the reaction of (2-Dodecen-1-yl) succinic anhydride with the silanol groups on the surface of silica particles.

#### 6.4.1.3 Surface energy measurements

The measured surface energies of the components at room temperature and at the processing temperature are listed in Table 0-3. Since the difference between the surface energies of L-LDPE and H-LDPE were found to be within the range of the experimental error, an average value is presented for the surface energy of the LDPE phase. The estimated interfacial tension of 4.1 mN/m between PLA and LDPE at 180$^{o}$C using the Harmonic Mean approach is in good agreement with the interfacial tension of 5 mN/m at 200 $^{o}$C reported previously in the literature [33].

Table 0-3. Surface energies of PLA, LDPE, silica and M-micro-silica particles and the estimated interfacial tensions between the components.

| | at 25$^{o}$ C | | | at 180$^{o}$C | | | Interfacial tension at 180 $^{o}$C (mN/m) | | |
|---|---|---|---|---|---|---|---|---|---|
| | $\gamma$ (mN/m) | $\gamma_d$ (mN/m) | $\gamma_p$ (mN/m) | $\gamma$ (mN/m) | $\gamma_d$ (mN/m) | $\gamma_p$ (mN/m) | PLA | LDPE | Silica |
| PLA* | 39.4 | 33.6 | 5.8 | 28 | 23.9 | 4.1 | - | 4.1 | 155.3 |
| LDPE | 36.4 | 36.4 | 0 | 25.2 | 25.2 | 0 | 4.1 | - | 209.4 |
| Silica* | 519.8 | 72.8 | 447 | 242.8 | 34 | 208.8 | 155.3 | 209.4 | - |
| M-micro-silica | 49.2 | 48 | 1.2 | 33.7 | 33 | 0.7 | 3.6 | 1.8 | - |

* taken from [19]

### 6.4.2 Thermodynamics of the Localization of Silica Particles in PLA/PE Blends

The thermodynamic equilibrium localization of solid particles in a multiphase polymer blend can be predicted by the Young's model[10]:

$$\omega = \frac{\gamma_{1s}-\gamma_{2s}}{\gamma_{12}} \qquad \text{Eqn.4}$$

Where $\gamma_{1s}$, $\gamma_{2s}$ and $\gamma_{12}$ are the interfacial tensions between: polymer 1 and solid, polymer 2 and solid; and polymer 1 and 2. If ω is greater than 1, the localization of silica particles in phase 2 is thermodynamically preferred while for ω < -1, the thermodynamic equilibrium localization of solid particles should be in phase 1. On the other hand, when -1<ω< 1, the localization of solid particles at the interface is thermodynamically preferred. By taking LDPE as phase 1 and PLA as phase 2, ω in PLA/LDPE/unmodified silica mixtures can be estimated as 13.2 which indicates that, at the thermodynamic equilibrium condition, unmodified silica particles should be localized in the PLA phase.

Most of the previous studies have found that the simultaneous mixing of solid particles and polymer components results in the localization of the particles in the thermodynamically preferred phase [17, 21, 34-41]. In order to examine the prediction of the Young's model, blends of PLA/H-LDPE(80/20) with U-micro- and nano-silica particles were prepared using Pr1(addition of silica particles to the PLA/LDPE melt). The SEM images of these samples are shown in Figure 0.4.As quantified in the first line of Table 0-4, 94% of the U-micro-silica (unmodified micro-silica) particles are located in the PLA phase. A similar localization in the PLA phase was observed for nano-silica particles. In order to confirm that the observed localization of silica particles is not due to the higher composition of the PLA phase in the blend, a blend of PLA/H-LDPE (5/95) with 3 wt.% of U-micro-silica (based on the total weight of the blend) was prepared by Pr1. As can be seen in Figure 6.5, even at such a low composition of the PLA phase, U-micro-silica particles were selectively localized in the PLA phase. These results are in agreement with the result of the previous study by this group on low interfacial tension PLA/PBAT blends [19]. In that study, it was shown that when silica particles are added to a melt of PLA/PBAT, the PBAT phase preferentially encapsulates the silica particles at the early stages of mixing irrespective of the particle size of silica due to the lower interfacial tension of PBAT/silica compared to PLA/silica. A similar mechanism is expected to be responsible for the selective localization of silica particles in the PLA phase in this high interfacial tension PLA/LDPE system.

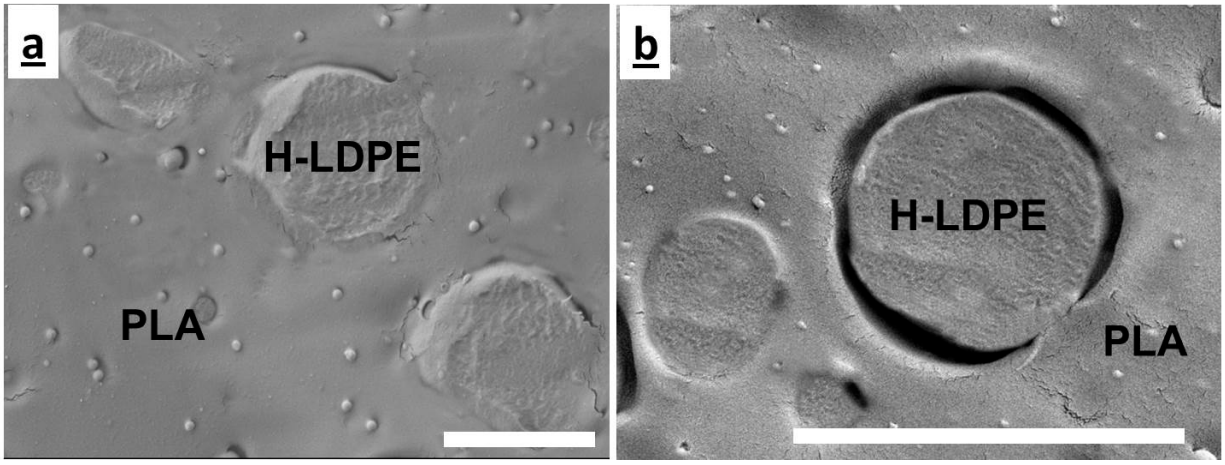


Figure 0.4. The localization of silica particles in the samples prepared by Pr1: (a) PLA/H-LDPE (80/20) with 1 wt.% of U-micro-silica, (b)PLA/H-LDPE with 1 wt.% of nano-silica. The white scale bars show 5 μm.

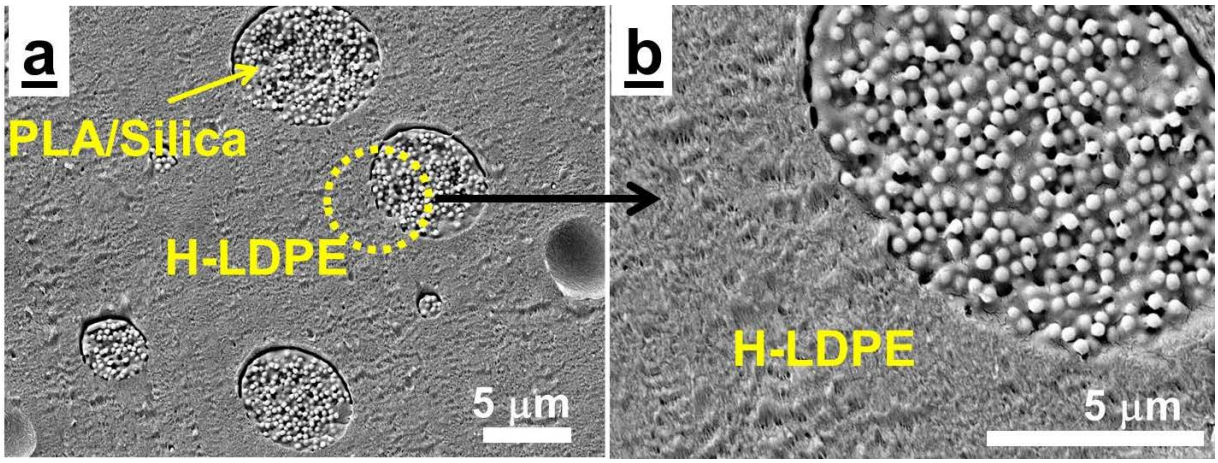


Figure 6.5. The localization of U-micro-silica particles in PLA/H-LDPE (5/95) with 3 wt.% of the silica particles prepared by Pr1.

Table 0-4. The quantified localizations of 1% U-micro-silica, M-micro-silica and nano-silica particles in PLA/LDPE blends with the associated standard deviation (std).

| | Blend sample | Mixing strategy | Silica type | % Silica | | | std |
|---|---|---|---|---|---|---|---|
| | | | | in PLA | at interface | in LDPE | |
| 1 | PLA/H-LDPE (80/20) | Pr1 | U-micro-silica | 94 | 0 | 6 | 4 |
| 2 | PLA/H-LDPE (80/20) | Pr1 | M-micro-silica | 0 | 11 | 89 | 5 |

Table 0-4 Cont'd

| | | | | | | | |
|---|---|---|---|---|---|---|---|
| 3 | PLA/H-LDPE (80/20) | Pr2 | U-micro-silica | 19 | 0 | 81 | 8 |
| 4 | PLA/H-LDPE (80/20) | Pr2 | Nano-silica | 35 | 0 | 65 | 12 |
| 5 | PLA/L-LDPE (80/20) | Pr2 | U-micro-silica | 93 | 0 | 7 | 5 |
| 6 | PLA/L-LDPE (80/20) | Pr2 | M-micro-silica | 0 | 85 | 15 | 7 |
| 7 | PLA/H-LDPE (80/20)* | Pr2* | U-micro-silica | 21* | 0* | 79* | 8 |
| 8 | PLA/H-LDPE (80/20)* | Pr2* | Nano-Silica | 77* | 0* | 23* | 11 |
| 9 | PLA/H-LDPE(90/10) | Pr2 | U-micro-Silica | 15 | 0 | 85 | 8 |
| 10 | PLA/H-LDPE(90/10)** | Pr2 | U-micro-silica | 17 | 0 | 83 | 10 |

* Prepared at the shear rate of 47 $s^{-1}$.
** Contains 3 wt.% of silica

### 6.4.3 Effect of the Surface Energy of Micro-Silica Particles

The effect of the surface energy of solid particles on the localization was examined by the addition of M-micro-silica (modified-silica) particles to PLA/H-LDPE blend by Pr1(addition of silica particles to a PLA/LDPE melt). Using the measured surface energy of M-micro-silica particles reported in Table 0-3, the wetting parameter (ω) from the Young equation is determined as -0.4 which indicates that the thermodynamic equilibrium localization of M-micro-silica particles should be at the PLA/LDPE interface. The localization of M-micro-silica particles in the PLA/H-LDPE blend prepared by Pr1 is shown in Figure 6.6 and on line 2 in Table 0-4. It was found that 89% of the M-micro-silica particles were localized in the H-LDPE phase when processed by Pr1. Comparing these results with the localization of U-micro-silica particles in Figure 6.5, it can be seen that the surface modification treatment of the micro-silica particles completely changed the localization of the silica particles from PLA to H-LDPE in this blend. The encapsulation of M-micro-silica particles by the H-LDPE phase at the early stages of mixing can also be attributed to the lower interfacial tension of H-LDPE/M-micro-silica as compared with PLA/M-micro-silica (see Table 0-3). However, note that the equilibrium localization of M-micro-silica particles, as determined by the Young equation, was predicted to be at the interface. This point will be examined later in this chapter.

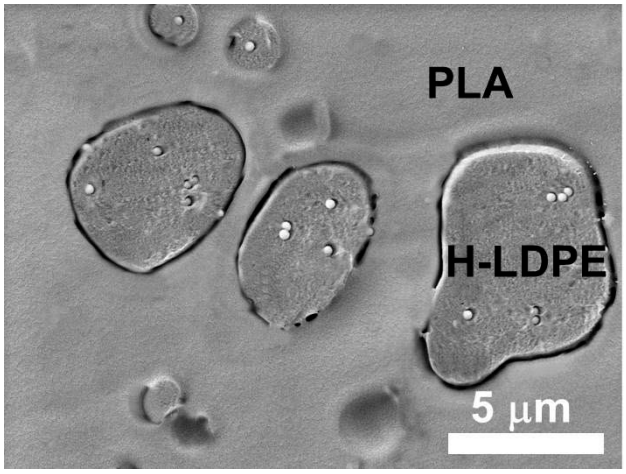


Figure 6.6. The localization of 1 wt.% of M-micro-silica particles in PLA/H-LDPE(80/20) blend prepared by Pr1.

### 6.4.4 Effect of the Mixing Strategy

It has been shown above that the equilibrium localization for the U-micro-silica or nano-silica is in the PLA phase and that this supports the thermodynamic prediction based on surface energies. In this part, the influence of kinetic parameters were imposed on the localization of U-micro-silica (unmodified silica) by premixing U-micro-silica particles with a high viscosity LDPE phase (H-LDPE) before mixing with PLA according to Pr2.

The effect of the Pr2 mixing strategy on the localization of U-micro-silica particles is shown in Figure 6.7 and on line 3 in Table 0-4. This mixing strategy changes the localization of U-micro-silica particles from the PLA phase to the H-LDPE phase. As a result, 81% of the U-micro-silica (unmodified micro-silica) particles are located in H-LDPE indicating strong kinetic barriers against the migration of the particles to the PLA phase. Even increasing the mixing time to 20 minutes did not change the observed localization of U-micro-silica in the H-LDPE phase.

As the localization of unmodified silica particles in the H-LDPE phase is not thermodynamically favoured, premixing of silica particles with the LDPE phase, Pr2, provides a unique opportunity to rigorously examine the effect of kinetic parameters on the localization and migration of silica particles in PLA/LDPE blends. Therefore, Pr2 will be used as the main mixing strategy in the rest of this paper.

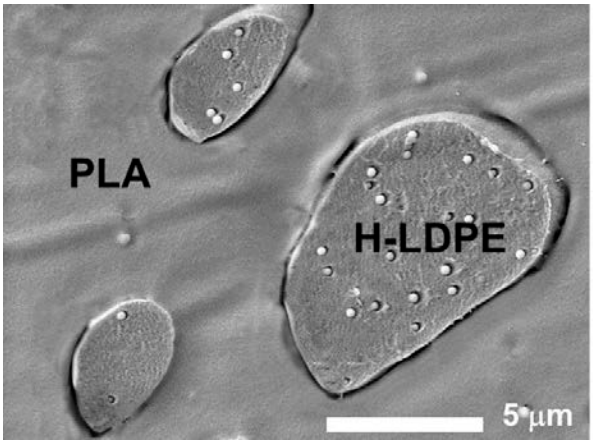


Figure 6.7. The localization of 1 wt.% of U-micro-silica particles in PLA/H-LDPE (80/20) prepared by Pr2.

### 6.4.5 Effect of the Shear Rate

The shear rate of mixing has been shown to enhance the migration of solid inclusions in polymer blends [19, 20, 42]. The effect of increasing the shear rate from 25 $s^{-1}$ to 47 $s^{-1}$ on the localization of U-micro-silica particles in PLA/H-LDPE blends prepared by Pr2 is shown in Figure 0.8 and line 7 in Table 0-4. As can be seen, an almost two fold increase in the shear rate did not have a considerable effect on the localization of micro-silica particles. At the shear rate of $47s^{-1}$, 79% of U-micro-silica particles are still localized in the H-LDPE phase.

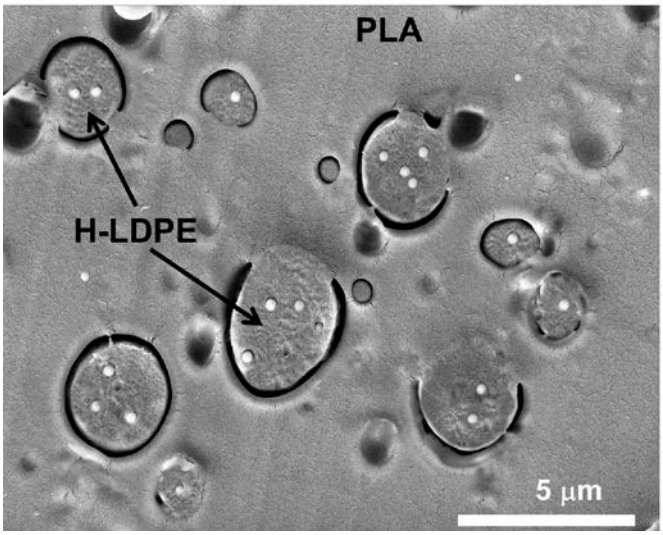


Figure 0.8. The effects of shear rate on the localization of U-micro-silica particles in PLA/H-LDPE (80/20) blend prepared by Pr2 at the shear rate of 47 $s^{-1}$.

Therefore, it can be concluded that the observed localization of U-micro-silica particles in the H-LDPE phase is stable and does not vary with increasing mixing time or shear rate.

### 6.4.6 The Effect of the Viscosity of the LDPE Phase

The high viscosity of polymer melts has been found to interrupt the migration of solid particles toward their thermodynamic equilibrium localizations. Although Persson and Bertilsson [43] mentioned that the effect of viscosity on solid particle localization should only be significant in low interfacial tension blends, other authors such as Feng et al. [44], Elias et al. [18] and Taghizadeh and Favis [20] observed strong viscosity effects on particle migration in high interfacial tension systems.

The effect of viscosity of the LDPE phase on the localization of U-micro-silica particles was examined by preparing PLA/L-LDPE with 1 wt.% of U-micro-silica using Pr2. As can be seen in Figure 0.9 and on line 5 in Table 0-4, decreasing the viscosity of the LDPE phase by a factor of 1.7 results in the migration of 93% of the U-micro-silica particles to the PLA phase, the thermodynamically predicted phase location.

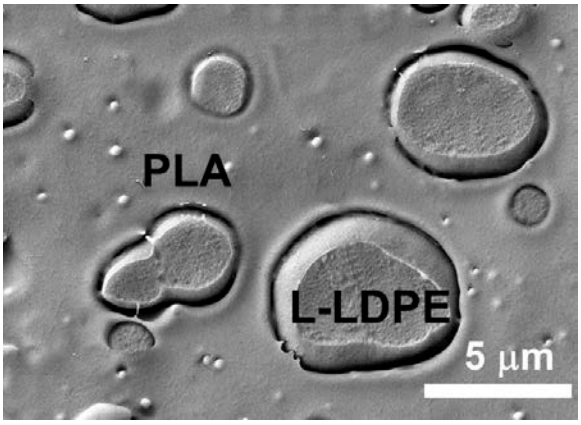


Figure 0.9. The effect of the viscosity of the LDPE phase on the localization of 1 wt.% of U-micro-silica particles in PLA/L-LDPE blend prepared by Pr2.

The effect of viscosity of the LDPE phase on the migration and localization of the surface modified M-micro-silica particles was also examined by preparing the PLA/L-LDPE blend with 1 wt.% of M-micro-silica using Pr2. The localization of the M-micro-silica particles in this sample is shown in Figure 0.10 and on line 6 in Table 0-4. As can be seen, decreasing the

viscosity of the LDPE phase results in the migration of 85% of M-micro-silica particles from the LDPE phase to their thermodynamically predicted localization at the interface. Therefore, it can be concluded that the high viscosity of the H-LDPE phase was also contributing a kinetic barrier that prevented the migration of M-micro-silica particles to the interface in PLA/H-LDPE blends prepared by Pr1 and Pr2.

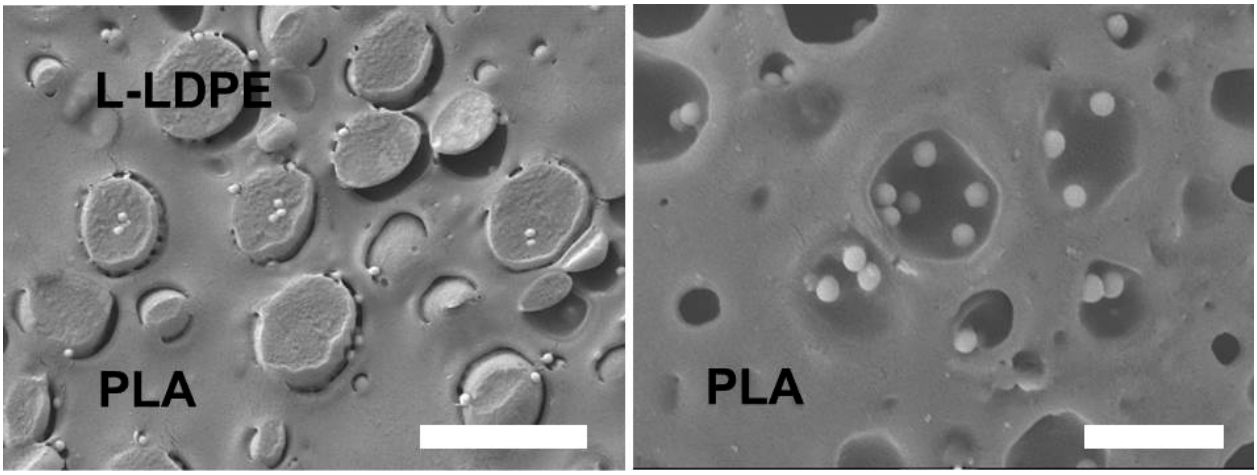


Figure 0.10. The localization of M-micro-silica particles in PLA/L-LDPE (80/20) blends prepared by Pr2: (a) before and, (b) after the extraction of the L-LDPE phase by boiling cyclohexane. The scale bars in (a) and (b) show 5 μm and 2μm respectively.

### 6.4.7 Effect of the Particle Size of Silica

The localization of nano-silica particles in the PLA/H-LDPE blend after premixing with H-LDPE using Pr2 is shown in Figure 6.11 and on line 4 in Table 0-4. Interestingly, it was found that individual well-dispersed nano-silica particles (35%) migrate from the H-LDPE phase to the PLA phase while the majority of the nano-particles (65%) remain localized in the H-LDPE phase in the form of aggregates. The average diameter of these aggregates was estimated as 420 nm using image analysis.

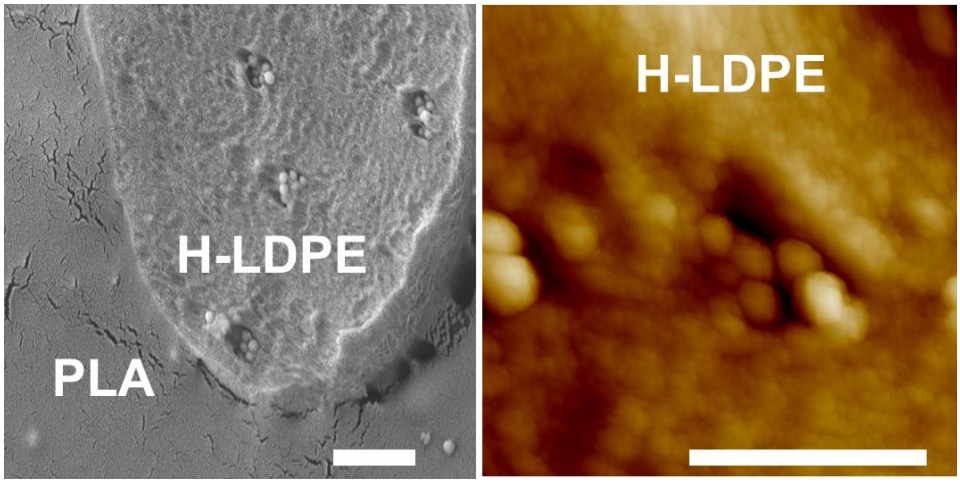


Figure 6.11. The localization of nano-silica particles in PLA/H-LDPE blend prepared by Pr2, (a) SEM image of nano-silica aggregates in H-LDPE, (b) AFM image of nano-silica aggregates in H-LDPE phase. All the white scale bars show 1 μm.

The effect of increasing the shear rate on the localization of nano-silica particles in PLA/H-LDPE blend prepared by Pr2 was also studied and the results are shown in Figure 0.12 and on line 8 in Table 0-4. It can be seen that increasing the shear rate enhanced the dispersion and migration of nano-silica and 77% of nano-silica particles could migrate to the PLA phase. These results, for the first time, clearly show the critical role of dispersion on the localization of nano-particles and indicate that poor dispersion of nano-particles can strongly influence their localization in multi-phase polymer systems.

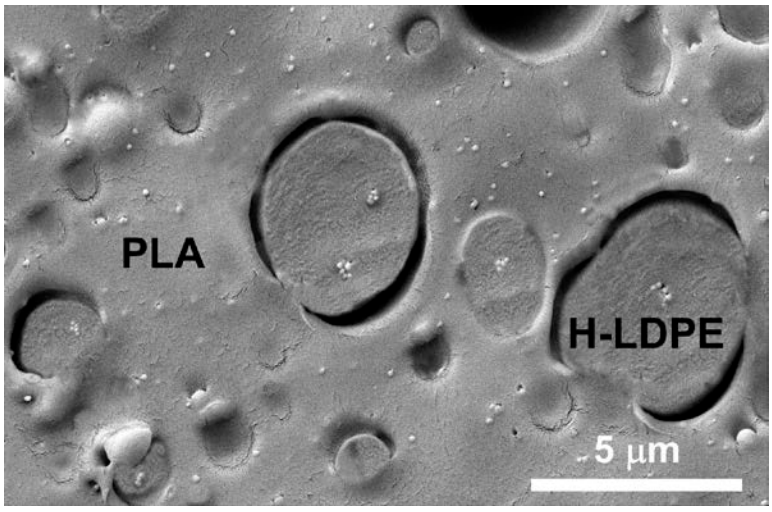


Figure 0.12. The effect of shear rate on the localization of nano-silica particles in PLA/H-LDPE blend prepared by Pr2 at the shear rate of 47 $s^{-1}$.

### 6.4.8 The Mechanism of Migration of Silica Particles

The migration process of silica particles from the LDPE phase to the PLA phase can be considered as a three-step process: (a) migration from the bulk of the LDPE phase toward the interface, (b) draining of the LDPE film between the particle and the interface and (c) migration at the interface. These steps are shown schematically in Figure 0.13 and were discussed previously in an earlier paper from this group [45].

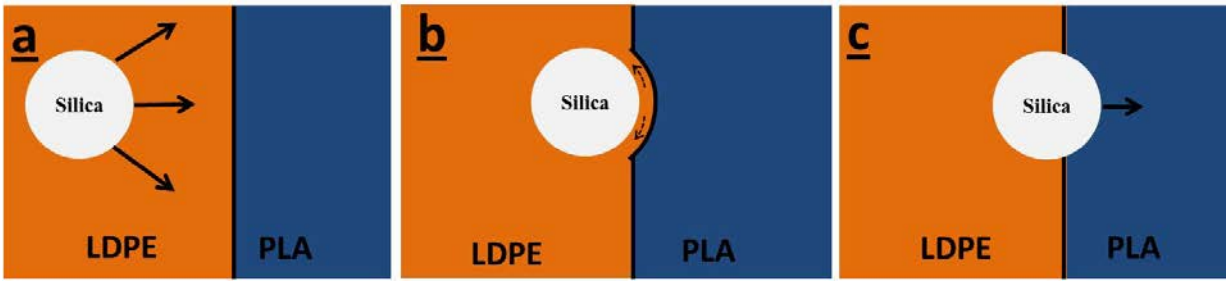


Figure 0.13. The migration mechanism of a silica particle from the LDPE phase to the PLA phase in the samples prepared by Pr2, (a) migration from the bulk of the LDPE phase towards the interface, (b) draining of the LDPE film between the particle and the interface, (c) migration at the interface.

#### 6.4.8.1 Bulk Migration

In the first step of bulk migration, the silica particles need to migrate from inside the LDPE phase to the interface. Figure 6.7 shows that 1 wt.% U-micro-silica particles in PLA/H-LDPE(80/20), prepared by Pr2, are localized in the H- LDPE phase. Figure 6.14 shows that this effect is still observed even when the concentration of H-LDPE is reduced to 10 vol.% and when the concentration of silica particles is increased to 3 wt.%. Decreasing the composition of the H-LDPE phase to 10 vol.% reduces the volume average dispersed H-LDPE diameter by a factor of 2.6. A reduced H-LDPE phase diameter decreases the mean path that a silica particle should migrate to reach the interface and should enhance the bulk migration. However, as can be seen in Figure 6.14 (a), (b) and on lines 9 and 10 in Table 0-4, these changes did not have a significant effect on the localization of U-micro-silica particles.

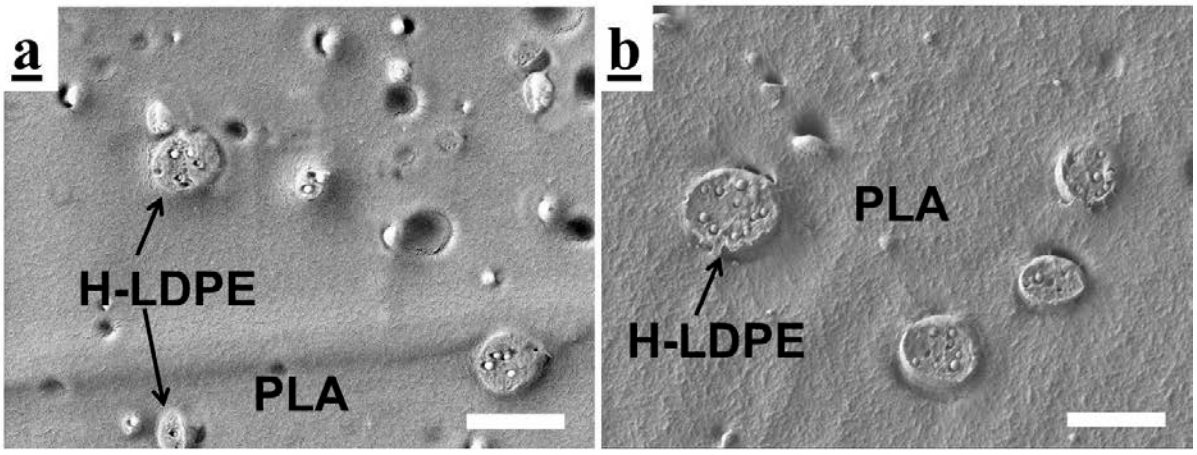


Figure 6.14. The localization of U-micro-silica particles in PLA/H-LDPE(90/10) prepared by Pr2: (a) 1 wt.% of U-micro-Silica, (b) 3 wt.% of U-micro-silica. The white scale bars show 5 μm.

In addition, the shear-induced and transitional migration of a spherical particle under shear flow has been shown to scale as $\dot{\gamma}R^2$ and $\dot{\gamma}R$ respectively [46-49] which indicates that the migration of nano-silica particles should take a longer time compared to micro-silica particles. However, as has been shown in this paper, individual nano-silica particles could migrate from H-LDPE phase to the PLA phase while micro-silica particles remain in H-LDPE phase.

The above mentioned results clearly confirm that the migration of U-micro-silica particles from the bulk of H-LDPE phase toward the interface is not a kinetic barrier that significantly influences the localization of U-micro-silica particles in the H-LDPE phase. A similar conclusion was found for silica localization in a low interfacial tension system in a previous paper from this group [45].

#### 6.4.8.2 Film Drainage

In the film draining step, a silica particle initially dispersed in the LDPE by Pr2 needs to drain a film of the LDPE phase between the particle and the PLA/LDPE interface in order to reach the interface. As discussed in more detail in a previous paper[45], the film draining time between a spherical solid particle with radius R and a deformable liquid/liquid interface can be expressed as[50]:

$$t_d = \frac{3n^2\eta A^2}{16F}\left(\frac{1}{\delta_C^2} - \frac{1}{\delta_o^2}\right) \qquad \text{Eqn.5}$$

where F, A, $\eta$, $\delta_C$ and $\delta_o$ are the contact force, the surface area of the film ($\sim R^2$), the viscosity of the LDPE phase, the critical film thickness in which the LDPE film rupture occurs, and the initial LDPE film thickness where the film draining process begins, respectively. Moreover, n is the number of immobile interfaces such as LDPE/Silica which, in the present system, is equal to one. When a silica particle approaches the interface, it remains in contact with the interface for a certain amount of time which can be called the "contact time". The contact time of a silica particle can be defined as the inverse of the frequency of collision of any particle with the interface. If the film draining time between a particle and the interface is longer than the contact time between the particle and the interface, then the particle will be moved away from the interface by the internal flow field inside the LDPE phase before it can reach the interface. The linear dependency of the film draining time on the viscosity of the LDPE phase in Equation 6 can explain the observed enhancement in the migration of U-micro-silica and M-micro-silica particles by decreasing the viscosity of the LDPE phase. The observed effect of the particle size of silica in the PLA/H-LDPE sample prepared by Pr2 can also be explained by considering the strong dependency of the LDPE film draining time to the silica particle radius in Equation 6 ($t_d \sim R^4$). Such a dependency indicates that decreasing the diameter of silica particles from 300 nm to 100 nm should reduce the film draining time by approximately 80 times which significantly enhances the migration of individual nano-silica particles. On the other hand, as the average diameter of the nano-silica aggregates in H-LDPE phase was determined to be even larger than U-micro-silica particles, the film draining time between these aggregates and the PLA/H-LDPE interface is likely to be even longer than that of individual U-micro-silica particles. These results explain why well-dispersed nano-particles find their way to the predicted thermodynamic location in the PLA phase independently of mixing procedure and phase viscosity. It is worth mentioning that as the shear rate and silica content in the PLA/H-LDPE samples with U-micro-silica and nano-silica were similar, the contact time between silica particles and the interface in those two blends should also be similar.

Increasing the shear rate did not change the localization of U-micro-silica particles in PLA/H-LDPE blends. This can be explained by considering that the shear rate also reduces the contact time between a silica particle and the interface which decreases the chance of the particle to drain the H-LDPE film between the particle and the interface.

#### 6.4.8.3 Migration at the Interface

Since the non- equilibrium localization of U-micro-silica and nano-silica particles at the interface was not observed, the migration at the interface is clearly not a limiting kinetic parameter in the migration of the silica particles in the high interfacial tension PLA/LDPE system.

### 6.4.9 Comparison between the Migration and Localization in Low and High Interfacial Tension Blends

In the previous study [19], the effects of kinetic parameters on the localization of U-micro-silica and nano-silica in low interfacial tension blends of PLA/PBAT were studied in detail. Comparing the obtained results with the present study can provide a general perspective of the migration process in polymer blends.

For both high and low interfacial tension blend systems, when the silica particles are added to a melt of the blend, the nano- and micro-silica particles are encapsulated preferentially by the phase for which they have the lowest interfacial tension independently of the viscosity of the phases.

When the kinetic parameters are imposed by melt mixing of the silica particles with the phase for which it has the least affinity, a number of interesting observations emerge: (a) film draining is a critical step in the migration of micro-silica particles in both low and high interfacial tension blends; (b) the migration of well-dispersed nano-silica particles from the bulk to the interface is not likely to be influenced by kinetic effects in polymer blends; (c) The migration at the interface is a limiting step in the migration of micro- and nano-silica in low interfacial tension blends while it does not affect the localization in the high interfacial tension blend. Table 0-5 shows a summary of the kinetic effects that controls the localization of silica particles in high and low interfacial tension systems.

Table 0-5. The kinetic parameters that control the migration and localization of micro- and nano-silica in high and low interfacial tension polymer blends.

| | High Interfacial tension system | Low interfacial tension system |
|---|---|---|
| Micro-Silica | Film draining step | Film draining step<br>Migration at the interface |
| Nano-Silica | Film draining in the case of aggregation | Migration at the interface |

## 6.5 Conclusions

In this article, the effects of thermodynamic and kinetic parameters on the localization of micro- and nano- silica particles in high interfacial tension blends of poly(lactic acid),PLA,/low density polyethylene(LDPE) were studied. The surface of micro-silica particles was modified by the grafting of (2-Dodecen-1-yl) succinic anhydride to the surface. Using the Young's model, the thermodynamic equilibrium localizations of unmodified and modified silica particles were determined to be in the PLA phase and at the interface respectively. The addition of unmodified micro-silica (U-micro-silica) or nano-silica to a melt of PLA and high viscosity LDPE (H-LDPE) results in the localization of the particles in the PLA phase while modified micro-silica particles (M-micro-silica) are localized in the H-LDPE phase. The observed localizations are attributed to the preferential encapsulation of the particles by the phase which they have the lowest interfacial tension.

The effects of kinetic parameters were studied by premixing of silica particles with H-LDPE phase followed by mixing with PLA. It was shown that U-micro-silica or M-micro-silica particles remain localized in the H-LDPE. By decreasing the viscosity of the LDPE phase, the silica particles migrated to their thermodynamic equilibrium localizations. When nano-silica particles were used, individual nano-silica particles could migrate to the PLA phase while the nano-silica aggregates remain in the H-LDPE phase. These observations can be explained by considering the effect of viscosity and particle size of silica on the film draining time between micro-silica particles and PLA/LDPE interface. Increasing the shear rate did not change the localization of micro-silica particles in the H-LDPE phase but enhanced the migration of nano-silica particles by enhancing their dispersion.

One of the most important outcomes of this work is the conclusion that the equilibrium localization of well dispersed nanoparticles in a high interfacial tension polymer blend system will not be significantly influenced by kinetic effects. This conclusion has important potential implications for nanocomposites and underlines the critical role of controlling dispersion in such systems.

## 6.6 Acknowledgment

The authors would like to gratefully acknowledge the NSERC Network for Innovative Plastic Materials and Manufacturing Processes (NIPMMP) for the funding of this work. The authors also would like to acknowledge Professor Musa Kamal and Dr. Vahid Khoshkava for their help in the contact angle and pendant drop measurements.

## 6.7 References

1. Yoo Y, Cui L, Yoon PJ, and Paul DR. Macromolecules 2009;43(2):615-624.
2. Li Y and Shimizu H. Macromolecules 2008;41(14):5339-5344.
3. Meincke O, Kaempfer D, Weickmann H, Friedrich C, Vathauer M, and Warth H. Polymer 2004;45(3):739-748.
4. Lee SH, Bailly M, and Kontopoulou M. Macromolecular Materials and Engineering 2012;297(1):95-103.
5. Gubbels F, Jerome R, Teyssie P, Vanlathem E, Deltour R, Calderone A, Parente V, and Bredas JL. Macromolecules 1994;27(7):1972-1974.
6. Sumita M, Sakata K, Hayakawa Y, Asai S, Miyasaka K, and Tanemura M. Colloid and Polymer Science 1992;270(2):134-139.
7. Hong JS, Namkung H, Ahn KH, Lee SJ, and Kim C. Polymer 2006;47(11):3967-3975.
8. Dasari A, Yu Z-Z, and Mai Y-W. Polymer 2005;46(16):5986-5991.
9. Lee H-s, Fasulo PD, Rodgers WR, and Paul DR. Polymer 2005;46(25):11673-11689.
10. Fenouillot F, Cassagnau P, and Majesté JC. Polymer 2009;50(6):1333-1350.
11. Si M, Araki T, Ade H, Kilcoyne ALD, Fisher R, Sokolov JC, and Rafailovich MH. Macromolecules 2006;39(14):4793-4801.
12. Elias L, Fenouillot F, Majesté JC, Alcouffe P, and Cassagnau P. Polymer 2008;49(20):4378-4385.
13. Hong J, Kim Y, Ahn K, Lee S, and Kim C. Rheologica Acta 2007;46(4):469-478.
14. Sinha Ray S, Pouliot S, Bousmina M, and Utracki LA. Polymer 2004;45(25):8403-8413.
15. Tao F, Auhl D, Baudouin A-C, Stadler FJ, and Bailly C. Macromolecular Chemistry and Physics 2013;214(3):350-360.
16. Sumita M, Sakata K, Asai S, Miyasaka K, and Nakagawa H. Polymer Bulletin 1991;25(2):265-271.

17. Göldel A, Kasaliwal GR, Pötschke P, and Heinrich G. Polymer 2012;53(2):411-421.

18. Elias L, Fenouillot F, Majesté JC, Martin G, and Cassagnau P. Journal of Polymer Science Part B: Polymer Physics 2008;46(18):1976-1983.

19. Jalali Dil E and Favis BD. To be submitted 2015.

20. Taghizadeh A and Favis BD. Carbohydrate Polymers 2013;98(1):189-198.

21. Göldel A, Marmur A, Kasaliwal GR, Pötschke P, and Heinrich G. Macromolecules 2011;44(15):6094-6102.

22. Wang Y and Hillmyer MA. Journal of Polymer Science Part A: Polymer Chemistry 2001;39(16):2755-2766.

23. Anderson KS, Lim SH, and Hillmyer MA. Journal of Applied Polymer Science 2003;89(14):3757-3768.

24. Owens DK and Wendt RC. Journal of Applied Polymer Science 1969;13(8):1741-1747.

25. Demarquette NR and Kamal MR. Polymer Engineering & Science 1994;34(24):1823-1833.

26. Papirer E, Balard H, and C. V. Surface energies of silica investigated by inverse gas chromatoghraphy. In: Papirer E, editor. Adsorption on silica surfaces. New York: Marcel Dekker, 2000. pp. 205-276.

27. Wu S. Polymer Interface and Adhesion, 1982.

28. Shuttleworth R. Proceedings of the Physical Society. Section A 1950;63(5):444.

29. Bousmina M, Ait-Kadi A, and Faisant JB. Journal of Rheology 1999;43(2):415-433.

30. Gotsis AD. Branched Polyolefins. In: Kontopoulou M, editor. Applied Polymer Rheology: Polymeric Fluids with Industrial Applications. United States: John Wiley & Sons, 2012. pp. 67.

31. Hideo N, Ryuichi I, Yosuke H, and Hiroyuki S. Acta Materialia 1998;46(7):2313-2318.

32. Khoshkava V and Kamal MR. Biomacromolecules 2013;14(9):3155-3163.

33. Wang J, Lessard BH, Maric M, and Favis BD. Polymer 2014;55(16):3461-3467.

34. Cardinaud R and McNally T. European Polymer Journal 2013;49(6):1287-1297.

35. Katada A, Buys Y, Tominaga Y, Asai S, and Sumita M. Colloid and Polymer Science 2005;284(2):134-141.

36. Baudouin A-C, Bailly C, and Devaux J. Polymer Degradation and Stability 2010;95(3):389-398.

37. Baudouin A-C, Devaux J, and Bailly C. Polymer 2010;51(6):1341-1354.

38. Göldel A, Kasaliwal G, and Pötschke P. Macromolecular Rapid Communications 2009;30(6):423-429.

39. Elias L, Fenouillot F, Majeste JC, and Cassagnau P. Polymer 2007;48(20):6029-6040.

40. Kontopoulou M, Liu Y, Austin JR, and Parent JS. Polymer 2007;48(15):4520-4528.

41. Austin JR and Kontopoulou M. Polymer Engineering & Science 2006;46(11):1491-1501.

42. Hong JS, Kim YK, Ahn KH, and Lee SJ. Journal of Applied Polymer Science 2008;108(1):565-575.

43. Persson AL and Bertilsson H. Polymer 1998;39(23):5633-5642.

44. Feng J, Chan C-m, and Li J-x. Polymer Engineering & Science 2003;43(5):1058-1063.

45. Jalali Dil E and Favis BD. Submitted to Polymer 2015.

46. Bossis G and Brady JF. The Journal of Chemical Physics 1984;80(10):5141-5154.

47. Liu S. Chemical Engineering Science 1999;54(7):873-891.

48. Eckstein EC, Bailey DG, and Shapiro AH. Journal of Fluid Mechanics 1977;79(01):191-208.

49. Leighton D and Acrivos A. Journal of Fluid Mechanics 1987;181:415-439.

50. Hartland S. Chemical Engineering Science 1969;24(6):987-995.

51 Liu Y and Kontopoulou M, Polymer 2006; 47:7731

# CHAPTER 7 GENERAL DISCUSSIONS

In this study, first, a detailed study on the morphology and miscibility of PLA/PBAT was carried out. As a hypothesis at the beginning of this research, a PLA/PBAT blend was expected to have a low interfacial tension due to their similar natures. However, previous studies in this group showed that the breaking thread method could not be used to estimate quantitatively the interfacial tension of PLA/PBAT as the thread did not break even after one hour[142]. To determine the interfacial tension, first, the interfacial tension was estimated from the surface energy approach but the error of the estimation was even larger than the estimated interfacial tension value. Finally, rheological approach was undertaken to determine the interfacial tension. The first set of experimental data revealed that drying of the disk sample was necessary to avoid degradation of PLA during the rheological measurements. The degradation of PLA was minimized by drying the disk samples in a vacuum oven at 60 ℃ overnight. The obtained results by this approach indicate much better accuracy and reproducibility.

In this work, the miscibility of PLA/PBAT was studied by examining the shift in Tg of the phases. It was found that the conventional DSC cannot provide a good precision and reproducibility required to determine the miscibility of the phases in this system. In fact, in blend samples with low composition of the dispersed phase, the conventional DSC could not detect the Tg of the dispersed phase. On the other hand, the temperature-modulated DSC could detect Tg clearly, even at 10 vol.% of the dispersed phase. Using this approach, a limited one-way partial miscibility of PBAT in the PLA-rich phase was shown in PLA/PBAT blends. Determining the morphology of PLA/PBAT was another important goal in this project. The most important difficulty in the analysis of the morphology of PLA/PBAT was the very close solubility parameters of PLA and PBAT. This prevents etching and the selective extraction of either phase and makes the morphological characterization very difficult, especially close to the co-continuous region. In this work, SEM with LABE and AFM techniques were used to overcome the limits of the conventional SEM technique in distinguishing phases. The matrix dissolution and filtration of the dispersed phase is a common method in determining the type of the morphology of the dispersed phase (spherical or fibrillar). However, this method was not an option in this system. It was shown that studying the fracture surfaces of the blend sample can provide valuable information regarding the type of the morphology. Using this approach, the morphology of

PLA/PBAT was found to be fibrillar morphology over the full composition range. In addition, determining the co-continuity using selective solvent extraction was not possible in this system. It was shown that studying the droplet relaxation in rheological analysis can be a promising method in determining the limits of co-continuity in this system.

The localization and migration of micro- and nano-silica particles in two blends of PLA/PBAT and PLA/LDPE were also studied. Measuring the surface energy of the silica particles was the most important difficulty in determining the thermodynamic equilibrium localization of silica particles. It was not experimentally possible to measure the surface energy of the particles by the contact angle technique as the liquid probes spread instantly on the surface of silica particles. Even when a droplet of the low viscosity PLA phase was placed on a layer of silica particles at 180$^{o}$C, the PLA droplet spread and formed a film on the surface of silica after 40 minutes. Therefore, the surface energy of silica was estimated from the data in the literature. In the first set of the experiments it was found that when silica particles were used without drying both micro- and nano-silica particles formed aggregates in the samples. The dispersion of the silica particles was significantly enhanced by drying them at 60$^{o}$C under a vacuum overnight before the experiments. Therefore, the moisture content was found to play an important role in achieving a good dispersion of silica particles. To minimize the moisture intake, the PLA, PBAT, LDPE and silica particles required for each experiment were weighted and placed in the vacuum oven. This eliminates the moisture intake during the weighing of the polymers and particles before the experiments. The addition of the particles to a PLA/PBAT or PLA/LDPE melt resulted in the localization of the particles in the phase which has the lowest interfacial tension. The effect of kinetic parameters was studied by premixing particles with the phase which has the lowest thermodynamic affinity. The obtained results indicate the role of film draining in the migration of micro-silica particles. However, quantitative discussions on the effect of kinetic parameters on film draining were not possible due to the lack of a mathematical model to analyze the particle movement close to the interface. The poor dispersion of nano-silica particles was found to be the only kinetic barrier against their migration in PLA/LDPE blends. On the other hand, it was found that the migration of silica particles at the interface of PLA/PBAT is a significant kinetic barrier. By developing a semi-empirical model, it was found that the low interfacial tension between PLA and PBAT results in a slow migration velocity of silica particles at the interface.

# CHAPTER 8 CONCLUSIONS AND RECOMMENDATIONS

## 8.1 Conclusion

In this dissertation, the localization of micro- and nano-silica particles in bioplastic blends of PLA/LDPE and PLA/PBAT were investigated. First, the miscibility and morphology development in PLA/PBAT blends were studied in detail. The interfacial tension between PLA and PBAT was determined to be 0.6±0.15 mN/m, which indicates a very low interfacial tension and high level of compatibility in this system. The miscibility of PLA/PBAT was analyzed by studying the shift in Tg of the phases in the temperature-modulated DSC results. The obtained results point to a limited one-way partial miscibility of PBAT in the PLA-rich phase. The partial miscibility of PBAT in PLA was reduced significantly by increasing the molecular weight of PBAT. Since the enthalpy of mixing in this system is small (due to the similar nature of PLA and PBAT), the observed partial miscibility is attributed to the combinational entropy of mixing. This can also explain the one-way partial miscibility as the entropic gain is much less for mixing PLA molecules in PBAT. SEM images of the fracture surfaces of blend samples with different compositions revealed that the dispersed phase exists in the form of stable fibers in this system. The fiber formation is attributed to the low interfacial tension between PLA and PBAT, which increases the stability of the dispersed phase fibers. The morphology of PLA/PBAT over the full composition range was studied by AFM. A considerable coarsening of the dispersed phase by increasing the composition was observed, which was attributed to the partially miscible nature of PLA/PBAT blends. It was also found that the dispersed PLA phase forms larger fibers in PBAT compared to the dispersed PBAT in PLA. This was attributed to an 11–fold increase in the viscosity ratio by the phase inversion. Using the droplet relaxation peak in Cole-Cole plots of PLA/PBAT blends, the limits of the co-continuity region in this system were determined. The results indicate that PLA/PBAT has a wide symmetric co-continuity region which is located between 30-40 and 60-70 vol.% of PBAT.

The effects of thermodynamic and kinetic parameters on the localization of silica particles in PLA/PBAT blends were studied. It was shown that the addition of silica particles to PLA/PBAT does not affect the partial miscibility in this system. Using the measured surface energy data and

Young's model, the thermodynamic equilibrium localization of the silica particles was predicted to be in the PBAT phase. When the particles were added to a PLA/PBAT melt, both micro- and nano-silica were selectively encapsulated by the PBAT phase due to the lower interfacial tension of PBAT/silica compared to that of PLA/silica. The effect of kinetic parameters was imposed by the premixing of the silica particles with the PLA phase. When micro- and nano-silica were initially dispersed in a low viscosity PLA phase, they were localized at the interface rather than in the PBAT phase. A semi-empirical model is proposed to determine the effects of thermodynamic and kinetic parameters on the migration velocity of the particles at the interface. It was shown that the observed stable localization of the silica particles at the interface of PLA/PBAT pertains to the very low migration velocity of the particles at the interface, which originates from the low interfacial tension of PLA/PBAT. By increasing the viscosity of the PLA phase, nano-silica particles were still localized at the interface but micro-silica particles could not migrate to the interface and remained in the PLA phase. Increasing the shear rate enhanced the migration of micro-silica particles from the high viscosity PLA phase to the interface. These results indicate that the migration of micro-silica particles to the interface is significantly influenced by the film draining time between the particles and the interface.

The migration and localization of micro- and nano-silica particles in a high interfacial tension blend of PLA/LDPE was also studied. The surface of the micro-silica particles was modified by the grafting of (2-Dodecen-1-yl) succinic anhydride using a new gas phase reaction approach. The effect of the reaction time was studied by measuring the water contact angle of the modified powder at different reaction times. It was found that by increasing the reaction time, the surface energy of the particle decreased and reached a plateau after 90 minutes. Surface energy measurements and XPS analysis confirmed the presence of the reactant molecules on the surface of the particles. Using Young's model, the thermodynamic equilibrium localizations of unmodified and modified silica particles were determined to be in the PLA phase and at the interface, respectively. When unmodified silica particles or modified micro-silica particles were added to a melt of PLA and a high viscosity LDPE, the unmodified silica particles were localized into the PLA phase while modified micro-silica particles were located in the LDPE phase. This is due to the preferential encapsulation of the particles by the phase with which they have the lowest interfacial tension. The effects of kinetic parameters were studied by premixing silica particles with the LDPE phase followed by mixing with PLA. Using this mixing strategy, both modified

and unmodified micro-silica particles were localized in the LDPE phase. Decreasing the viscosity of the LDPE phase enhanced the migration of these particles to their thermodynamic equilibrium localizations but increasing the shear rate did not have a considerable effect on their localization. These results indicate that the LDPE film draining between the particles and the interface plays a critical role in inhibiting the migration of unmodified and modified micro-silica particles to their thermodynamic equilibrium localizations. On the other hand, when nano-silica was initially dispersed into the high viscosity LDPE phase, individual well-dispersed nano-silica particles could migrate to the PLA phase under all the conditions studied, while nano-silica aggregates remain in the LDPE phase. Increasing the shear rate enhanced the dispersion and migration of nano-silica particles. These results highlight the importance of achieving a good dispersion in controlling the localization of nanoparticles. Moreover, it can be concluded that the localization of well-dispersed nano-particles in a high interfacial tension polymer blend system is not significantly influenced by the kinetic effects.

Comparing the obtained results in the low (PLA/PBAT) and high (PLA/LDPE) interfacial tension blends suggests that in both systems the addition of silica particles after the melting of the polymers results in the localization of the particles in the phase with which they have the lowest interfacial tension. When micro-silica particles are premixed into the phase with lower affinity, the migration of micro-silica particles to the interface is controlled by the film draining step between the particles and the interface. On the other hand, in both the systems studied, individual well-dispersed nano-silica particles could migrate readily to the interface, irrespective of the viscosity. However, in the low interfacial tension blend, both micro- and nano-silica particles experience a very low migration velocity at the interface, which results in a non-equilibrium thermodynamic localization of the particles at the interface.

## 8.2 Original Contributions

Several major scientific contributions of this work are listed below.

In the first part of this research study:

- For the first time, it was demonstrated that PLA/PBAT exhibits a limited one-way partial miscibility of PBAT in the PLA-rich phase. This partial miscibility was shown to depend strongly on the molecular weight and has a strong entropic nature.

- SEM with a LABE detector was used for the first time in the analysis of the morphology of polymer blends. The results indicate that LABE can provide much higher phase contrast compared to the conventional SEM technique. This provides valuable information, especially in the analysis of blends with a co-continuous morphology.
- It was clearly shown that PLA/PBAT has a fibrillar morphology, even at 1 vol.% of the dispersed phase.
- Using a rheological approach, the limits of the co-continuity region in PLA/PBAT were quantitatively determined for the first time.

In polymer blends containing silica particles:

- The wide range of thermodynamic and kinetic parameters that were studied in this work allowed us to achieve a detailed mechanism of the migration process that can explain clearly the role of different parameters involved in the migration. Such a detailed mechanism was lacking in the literature. The knowledge obtained on the role of these parameters will provide a high level of control in the localization of solid particles, which has not been achieved so far in the literature. As a result, in this work, silica particles could be localized in either phase or at the interface in both studied high and low interfacial tension blends.
- It was found that the addition of solid particles to a melt of polymer blend results in the preferential encapsulation of the particles by the phase with which they have the lowest interfacial tension. This encapsulation occurred at the early stages of mixing irrespective of the viscosity of the phases, particles size and surface energy of silica.
- The critical role of the film draining step between micro-particles and the interface was highlighted in this study for the first time.
- It was shown that the migration of well-dispersed nano-particles in a high interfacial tension blend is not affected by the kinetic parameters. However, achieving a good dispersion can be a limiting factor in controlling the localization of nano-particles.
- It was found that the migration of solid particles at the interface is a significant kinetic barrier in low interfacial tension systems.
- The proposed model for the migration velocity at the interface, to our knowledge, is the only model existing in the literature that can show, at least semi-quantitatively, the relative effects

of thermodynamic and kinetic parameters on the migration velocity of solid particles at the interface of a multiphase system.

- A new gas phase reaction approach was introduced for the modification of silica, which eliminates the difficulties regarding using a solvent in the surface modification of silica.

## 8.3 Recommendations for Future Works

Based on the obtained results in the present study, the following recommendations are proposed for future works:

1. Despite the low interfacial tension of partially miscible blends, increasing the composition results in a considerable coarsening of the dispersed phase in these systems. Further investigations are required to understand the nature of this behavior.
2. The obtained results indicate the possibility of enhancing the compatibility of PLA and PBAT by the addition of a lower molecular weight fraction of the polymer components to the blend. It will be interesting to study this approach in improving the mechanical properties of PLA/PBAT blends.
3. It will be interesting to study the effect of the shape and aspect ratio of solid particles on their migration and localization in polymer blends. However, the selected particles should have similar surface energies to isolate the effect of the kinetic parameters from the differences in the thermodynamic affinity. The two following systems are proposed:
    i. Comparing the localization and migration of spherical nano-silica and unmodified montmorillonite clay: the dispersion of montmorillonite is very difficult due to the strong inter-layer bond in its structure. To overcome this issue, it is proposed to disperse montmorillonite particles in a water-soluble polymer (such as PEO) in water followed by the sonication of the mixture. After the water has evaporated, a highly dispersed mixture of polymer/ montmorillonite will be obtained that can be used in the experiments.
    ii. Comparing the localization and migration of graphene and carbon nanotube: a similar approach as mentioned for montmorillonite can be used to minimize the effect of dispersion on the localization.
4. Although the internal batch mixer can provide much better control during mixing (compared to the extruders) the flow field inside the batch mixer is not a pure shear flow.

To study the effect of shear flow on the migration, it is proposed to study the localization in a blend of two polymers that have much different melting temperatures ($T_m$). For example, studying the migration of hydrophilic silica in PP/EVA could be a good model system. The particles should be premixed in the PP phase (which has a higher $T_m$). A powder of this mixture can be obtained by grinding it in liquid nitrogen. Then, this powder can be added to EVA in a batch mixer at temperatures above the $T_m$ of EVA (but much less than the $T_m$ of PP). This will prevent the melting of the PP phase and, as a result, the particles will remain in the PP phase. The disk samples then can be prepared by compression molding of the blend above the $T_m$ of EVA. The obtained disk samples can then be used to study the migration under pure shear in a rheometer at temperatures above the $T_m$ of the PP phase.

5. Studying the localization and migration of micro- and nano-silica particles in a twin-screw extrusion would be an interesting future work as it would provide information regarding the effect of the processing method (as another controlling tool) on the localization of silica particles.
6. Recent studies revealed the great potential of ternary polymer blends in producing much wider properties compared to binary systems. It will be interesting to study the effect of thermodynamic and kinetic parameters on the localization and migration of solid particles in a ternary polymer blend.

# REFERENCES


[1] L. Yu, K. Dean, and L. Li, "Polymer blends and composites from renewable resources," *Progress in Polymer Science,* vol. 31, pp. 576-602, 6// 2006.

[2] European-Bioplastics, "Bioplastics facts and figures," European Bioplastics2013.

[3] T. H., "Polyesteres III. Applications and commercial products: Polylactides," in *Biopolymers*. vol. 4, A. Steinbüchel, Ed., ed Germany: Wiley VCH, 2002.

[4] H. Liu, F. Chen, B. Liu, G. Estep, and J. Zhang, "Super Toughened Poly(lactic acid) Ternary Blends by Simultaneous Dynamic Vulcanization and Interfacial Compatibilization," *Macromolecules,* vol. 43, pp. 6058-6066, 2010/07/27 2010.

[5] K. S. Anderson and M. A. Hillmyer, "The influence of block copolymer microstructure on the toughness of compatibilized polylactide/polyethylene blends," *Polymer,* vol. 45, pp. 8809-8823, 12// 2004.

[6] K. S. Anderson, K. M. Schreck, and M. A. Hillmyer, "Toughening Polylactide," *Polymer Reviews,* vol. 48, pp. 85-108, 2008/02/01 2008.

[7] Z. Su, Q. Li, Y. Liu, H. Xu, W. Guo, and C. Wu, "Phase Structure of Compatibilized Poly(Lactic Acid)/Linear Low-Density Polyethylene Blends," *Journal of Macromolecular Science, Part B,* vol. 48, pp. 823-833, 2009/07/14 2009.

[8] K. Nuñez, C. Rosales, R. Perera, N. Villarreal, and J. M. Pastor, "Poly(lactic acid)/low-density polyethylene blends and its nanocomposites based on sepiolite," *Polymer Engineering & Science,* vol. 52, pp. 988-1004, 2012.

[9] P. Sarazin, G. Li, W. J. Orts, and B. D. Favis, "Binary and ternary blends of polylactide, polycaprolactone and thermoplastic starch," *Polymer,* vol. 49, pp. 599-609, 1/21/ 2008.

[10] M. B. Coltelli, I. Della Maggiore, M. Bertold, F. Signori, S. Bronco, and F. Ciardelli, "Poly(lactic acid) properties as a consequence of poly(butylene adipate-co-terephthalate) blending and acetyl tributyl citrate plasticization," *Journal of Applied Polymer Science,* vol. 110, pp. 1250-1262, Oct 2008.

[11] S.-Y. Gu, K. Zhang, J. Ren, and H. Zhan, "Melt rheology of polylactide/poly(butylene adipate-co-terephthalate) blends," *Carbohydrate Polymers,* vol. 74, pp. 79-85, 10/1/ 2008.

[12] L. Jiang, M. P. Wolcott, and J. Zhang, "Study of Biodegradable Polylactide/Poly(butylene adipate-co-terephthalate) Blends," *Biomacromolecules,* vol. 7, pp. 199-207, 2006/01/01 2005.

[13] M. Kumar, S. Mohanty, S. K. Nayak, and M. Rahail Parvaiz, "Effect of glycidyl methacrylate (GMA) on the thermal, mechanical and morphological property of biodegradable PLA/PBAT blend and its nanocomposites," *Bioresource Technology,* vol. 101, pp. 8406-8415, 11// 2010.

[14] P. H. Sarath Kumara, N. Nagasawa, T. Yagi, and M. Tamada, "Radiation-induced crosslinking and mechanical properties of blends of poly(lactic acid) and poly(butylene terephthalate-co-adipate)," *Journal of Applied Polymer Science,* vol. 109, pp. 3321-3328, 2008.

[15] S. Lee, Y. Lee, and J. Lee, "Effect of ultrasound on the properties of biodegradable polymer blends of poly(lactic acid) with poly(butylene adipate-co-terephthalate)," *Macromolecular Research,* vol. 15, pp. 44-50, 2007/02/01 2007.

[16] K. Li, J. Peng, L.-S. Turng, and H.-X. Huang, "Dynamic rheological behavior and morphology of polylactide/poly(butylenes adipate-co-terephthalate) blends with various composition ratios," *Advances in Polymer Technology,* vol. 30, pp. 150-157, 2011.

[17] Y.-X. Weng, Y.-J. Jin, Q.-Y. Meng, L. Wang, M. Zhang, and Y.-Z. Wang, "Biodegradation behavior of poly(butylene adipate-co-terephthalate) (PBAT), poly(lactic acid) (PLA), and their blend under soil conditions," *Polymer Testing,* vol. 32, pp. 918-926, 8// 2013.

[18] H. Xiao, W. Lu, and J.-T. Yeh, "Crystallization behavior of fully biodegradable poly(lactic acid)/poly(butylene adipate-co-terephthalate) blends," *Journal of Applied Polymer Science,* vol. 112, pp. 3754-3763, 2009.

[19] J.-T. Yeh, C.-H. Tsou, C.-Y. Huang, K.-N. Chen, C.-S. Wu, and W.-L. Chai, "Compatible and crystallization properties of poly(lactic acid)/poly(butylene adipate-co-terephthalate) blends," *Journal of Applied Polymer Science,* vol. 116, pp. 680-687, 2010.

[20] N. Zhang, Q. Wang, J. Ren, and L. Wang, "Preparation and properties of biodegradable poly(lactic acid)/poly(butylene adipate-co-terephthalate) blend with glycidyl methacrylate as reactive processing agent," *Journal of Materials Science,* vol. 44, pp. 250-256, 2009/01/01 2009.

[21] N. Zhang, C. Zeng, L. Wang, and J. Ren, "Preparation and Properties of Biodegradable Poly(lactic acid)/Poly(butylene adipate-co-terephthalate) Blend with Epoxy-Functional Styrene Acrylic Copolymer as Reactive Agent," *Journal of Polymers and the Environment,* vol. 21, pp. 286-292, 2013/03/01 2013.

[22] Y. Wang and J. F. Mano, "Biodegradable poly(L-lactic acid)/poly(butylene succinate-co-adipate) blends: Miscibility, morphology, and thermal behavior," *Journal of Applied Polymer Science,* vol. 105, pp. 3204-3210, 2007.

[23] H. Eslami and M. R. Kamal, "Effect of a chain extender on the rheological and mechanical properties of biodegradable poly(lactic acid)/poly[(butylene succinate)-co-adipate] blends," *Journal of Applied Polymer Science,* vol. 129, pp. 2418-2428, 2013.

[24] I. Pillin, N. Montrelay, and Y. Grohens, "Thermo-mechanical characterization of plasticized PLA: Is the miscibility the only significant factor?," *Polymer,* vol. 47, pp. 4676-4682, 6/14/ 2006.

[25] O. Martin and L. Avérous, "Poly(lactic acid): plasticization and properties of biodegradable multiphase systems," *Polymer,* vol. 42, pp. 6209-6219, 6// 2001.

[26] R. M. Rasal, A. V. Janorkar, and D. E. Hirt, "Poly(lactic acid) modifications," *Progress in Polymer Science,* vol. 35, pp. 338-356, 3// 2010.

[27] Y. Yoo, L. Cui, P. J. Yoon, and D. R. Paul, "Morphology and Mechanical Properties of Rubber Toughened Amorphous Polyamide/MMT Nanocomposites," *Macromolecules,* vol. 43, pp. 615-624, 2010/01/26 2009.

[28] M. Bailly and M. Kontopoulou, "Preparation and characterization of thermoplastic olefin/nanosilica composites using a silane-grafted polypropylene matrix," *Polymer,* vol. 50, pp. 2472-2480, 5/22/ 2009.

[29] M. Kontopoulou, Y. Liu, J. R. Austin, and J. S. Parent, "The dynamics of montmorillonite clay dispersion and morphology development in immiscible ethylene–propylene rubber/polypropylene blends," *Polymer,* vol. 48, pp. 4520-4528, 7/13/ 2007.

[30] D. Wu, Y. Zhang, M. Zhang, and W. Yu, "Selective Localization of Multiwalled Carbon Nanotubes in Poly(ε-caprolactone)/Polylactide Blend," *Biomacromolecules,* vol. 10, pp. 417-424, 2009/02/09 2009.

[31] F. Fenouillot, P. Cassagnau, and J. C. Majesté, "Uneven distribution of nanoparticles in immiscible fluids: Morphology development in polymer blends," *Polymer,* vol. 50, pp. 1333-1350, 3/6/ 2009.
[32] A. Taguet, P. Cassagnau, and J.-M. Lopez-Cuesta, "Structuration, selective dispersion and compatibilizing effect of (nano) fillers in polymer blends," *Progress in Polymer Science,* 2014.
[33] K. A. Edwards, "BASF Biodegradable Plastics Overview," BASF2010.
[34] L. Avérous, "Biodegradable Multiphase Systems Based on Plasticized Starch: A Review," *Journal of Macromolecular Science, Part C,* vol. 44, pp. 231-274, 2004/12/30 2004.
[35] U. Witt, T. Einig, M. Yamamoto, I. Kleeberg, W. D. Deckwer, and R. J. Müller, "Biodegradation of aliphatic–aromatic copolyesters: evaluation of the final biodegradability and ecotoxicological impact of degradation intermediates," *Chemosphere,* vol. 44, pp. 289-299, 7// 2001.
[36] R. Dell'Erba, G. Groeninckx, G. Maglio, M. Malinconico, and A. Migliozzi, "Immiscible polymer blends of semicrystalline biocompatible components: thermal properties and phase morphology analysis of PLLA/PCL blends," *Polymer,* vol. 42, pp. 7831-7840, 8// 2001.
[37] M. E. Broz, D. L. VanderHart, and N. R. Washburn, "Structure and mechanical properties of poly(d,l-lactic acid)/poly(ε-caprolactone) blends," *Biomaterials,* vol. 24, pp. 4181-4190, 10// 2003.
[38] P. Sarazin, X. Roy, and B. D. Favis, "Controlled preparation and properties of porous poly(l-lactide) obtained from a co-continuous blend of two biodegradable polymers," *Biomaterials,* vol. 25, pp. 5965-5978, 12// 2004.
[39] S. Lin, W. Guo, C. Chen, J. Ma, and B. Wang, "Mechanical properties and morphology of biodegradable poly(lactic acid)/poly(butylene adipate-co-terephthalate) blends compatibilized by transesterification," *Materials & Design,* vol. 36, pp. 604-608, 4// 2012.
[40] M. Shahlari and S. Lee, "Mechanical and morphological properties of poly(butylene adipate-co-terephthalate) and poly(lactic acid) blended with organically modified silicate layers," *Polymer Engineering & Science,* vol. 52, pp. 1420-1428, 2012.
[41] L. Jiang, B. Liu, and J. W. Zhang, "Properties of Poly(lactic acid)/Poly(butylene adipate-co-terephthalate)/Nanoparticle Ternary Composites," *Industrial & Engineering Chemistry Research,* vol. 48, pp. 7594-7602, Aug 2009.
[42] R. Al-Itry, K. Lamnawar, and A. Maazouz, "Rheological, morphological, and interfacial properties of compatibilized PLA/PBAT blends," *Rheologica Acta,* vol. 53, pp. 501-517, 2014/07/01 2014.
[43] Y. Kim, C. Choi, Y. Kim, K. Lee, and M. Lee, "Compatibilization of immiscible poly(l-lactide) and low density polyethylene blends," *Fibers and Polymers,* vol. 5, pp. 270-274, 2004/12/01 2004.
[44] M. H. Abdolrasouli, G. M. M. Sadeghi, H. Nazockdast, and A. Babaei, "Polylactide/Polyethylene/Organoclay Blend Nanocomposites: Structure, Mechanical and Thermal Properties," *Polymer-Plastics Technology and Engineering,* vol. 53, pp. 1417-1424, 2014/09/17 2014.
[45] C. W. Macosko, "Morphology development and control in immiscible polymer blends," *Macromolecular Symposia,* vol. 149, pp. 171-184, 2000.
[46] B. D. Favis, "Factors influencing the morphology of immiscible polymer belnds in melt ptocessing," in *Polymer Blends*. vol. 1, D. R. Paul and C. B. Bucknall, Eds., ed New York: Wiley, 1999.

[47] S. Wu, *Polymer Interface and Adhesion*, 1982.
[48] D. Y. Kwok and A. W. Neumann, "Contact angle measurement and contact angle interpretation," *Advances in Colloid and Interface Science,* vol. 81, pp. 167-249, 9/7/ 1999.
[49] D. Y. Kwok, L. K. Cheung, C. B. Park, and A. W. Neumann, "Study on the surface tensions of polymer melts using axisymmetric drop shape analysis," *Polymer Engineering & Science,* vol. 38, pp. 757-764, 1998.
[50] R.-J. Roe, "Surface tension of polymer liquids," *The Journal of Physical Chemistry,* vol. 72, pp. 2013-2017, 1968/06/01 1968.
[51] N. R. Demarquette and M. R. Kamal, "Interfacial tension in polymer melts. I: An improved pendant drop apparatus," *Polymer Engineering & Science,* vol. 34, pp. 1823-1833, 1994.
[52] B. Favis and D. Therrien, "Factors influencing structure formation and phase size in an immiscible polymer blend of polycarbonate and polypropylene prepared by twin-screw extrusion," *Polymer,* vol. 32, pp. 1474-1481, 1991.
[53] L. A. Girifalco and R. J. Good, "A Theory for the Estimation of Surface and Interfacial Energies. I. Derivation and Application to Interfacial Tension," *The Journal of Physical Chemistry,* vol. 61, pp. 904-909, 1957/07/01 1957.
[54] S. Wu, "Calculation of interfacial tension in polymer systems," *Journal of Polymer Science Part C: Polymer Symposia,* vol. 34, pp. 19-30, 1971.
[55] S. Wu, "Interfacial and Surface Tensions of Polymers," *Journal of Macromolecular Science, Part C,* vol. 10, pp. 1-73, 1974/01/01 1974.
[56] P. Elemans, J. Janssen, and H. Meijer, "The measurement of interfacial tension in polymer/polymer systems: The breaking thread method," *Journal of Rheology (1978-present),* vol. 34, pp. 1311-1325, 1990.
[57] J. F. Palierne, "Linear rheology of viscoelastic emulsions with interfacial tension," *Rheologica Acta,* vol. 29, pp. 204-214, 1990/05/01 1990.
[58] G. I. Taylor, "The Formation of Emulsions in Definable Fields of Flow," *Proceedings of the Royal Society of London. Series A,* vol. 146, pp. 501-523, October 1, 1934 1934.
[59] H. P. Grace, "DISPERSION PHENOMENA IN HIGH VISCOSITY IMMISCIBLE FLUID SYSTEMS AND APPLICATION OF STATIC MIXERS AS DISPERSION DEVICES IN SUCH SYSTEMS," *Chemical Engineering Communications,* vol. 14, pp. 225-277, 1982/03/01 1982.
[60] B. D. Favis and J.-P. Chalifoux, "The effect of viscosity ratio on the morphology of polypropylene/polycarbonate blends during processing," *Polymer Engineering & Science,* vol. 27, pp. 1591-1600, 1987.
[61] J. Janssen and H. Meijer, "Droplet breakup mechanisms: Stepwise equilibrium versus transient dispersion," *Journal of Rheology (1978-present),* vol. 37, pp. 597-608, 1993.
[62] G. Wildes, H. Keskkula, and D. R. Paul, "Morphology of PC/SAN blends: effect of reactive compatibilization, SAN concentration, processing, and viscosity ratio," *Journal of Polymer Science Part B: Polymer Physics,* vol. 37, pp. 71-82, 1999.
[63] P. A. Bhadane, M. F. Champagne, M. A. Huneault, F. Tofan, and B. D. Favis, "Continuity development in polymer blends of very low interfacial tension," *Polymer,* vol. 47, pp. 2760-2771, Apr 2006.
[64] U. Sundararaj and C. W. Macosko, "Drop Breakup and Coalescence in Polymer Blends: The Effects of Concentration and Compatibilization," *Macromolecules,* vol. 28, pp. 2647-2657, 1995/04/01 1995.

[65] B. D. Favis and J. M. Willis, "Phase size/composition dependence in immiscible blends: Experimental and theoretical considerations," *Journal of Polymer Science Part B: Polymer Physics,* vol. 28, pp. 2259-2269, 1990.
[66] P. Pötschke and D. R. Paul, "Formation of Co-continuous Structures in Melt-Mixed Immiscible Polymer Blends," *Journal of Macromolecular Science, Part C,* vol. 43, pp. 87-141, 2003/01/04 2003.
[67] J. Li, P. L. Ma, and B. D. Favis, "The Role of the Blend Interface Type on Morphology in Cocontinuous Polymer Blends," *Macromolecules,* vol. 35, pp. 2005-2016, 2002/03/01 2002.
[68] R. C. Willemse, "Co-continuous morphologies in polymer blends: stability," *Polymer,* vol. 40, pp. 2175-2178, 4// 1999.
[69] C. Cerclé and B. D. Favis, "Generalizing interfacial modification in polymer blends," *Polymer,* vol. 53, pp. 4338-4343, 9/12/ 2012.
[70] R. Fayt, R. Jérôme, and P. Teyssié, "Molecular design of multicomponent polymer systems. XIV. Control of the mechanical properties of polyethylene–polystyrene blends by block copolymers," *Journal of Polymer Science Part B: Polymer Physics,* vol. 27, pp. 775-793, 1989.
[71] C. Harrats, R. Fayt, and R. Jérôme, "Effect of block copolymers of various molecular architecture on the phase morphology and tensile properties of LDPE rich (LDPE/PS) blends," *Polymer,* vol. 43, pp. 863-873, 2// 2002.
[72] L. A. Utracki, "Compatibilization of Polymer Blends," *The Canadian Journal of Chemical Engineering,* vol. 80, pp. 1008-1016, 2002.
[73] M. Matos, B. D. Favis, and P. Lomellini, "Interfacial modification of polymer blends—the emulsification curve: 1. Influence of molecular weight and chemical composition of the interfacial modifier," *Polymer,* vol. 36, pp. 3899-3907, // 1995.
[74] B. D. Favis, "Polymer alloys and blends: Recent advances," *The Canadian Journal of Chemical Engineering,* vol. 69, pp. 619-625, 1991.
[75] R. Al-Itry, K. Lamnawar, and A. Maazouz, "Improvement of thermal stability, rheological and mechanical properties of PLA, PBAT and their blends by reactive extrusion with functionalized epoxy," *Polymer Degradation and Stability,* vol. 97, pp. 1898-1914, 10// 2012.
[76] Q. K. Meng, M. C. Heuzey, and P. J. Carreau, "Effects of a Multifunctional Polymeric Chain Extender on the Properties of Polylactide and Polylactide/Clay Nanocomposites," *International Polymer Processing,* vol. 27, pp. 505-516, 2012/11/01 2012.
[77] K. S. Anderson, S. H. Lim, and M. A. Hillmyer, "Toughening of polylactide by melt blending with linear low-density polyethylene," *Journal of Applied Polymer Science,* vol. 89, pp. 3757-3768, 2003.
[78] Y. Wang and M. A. Hillmyer, "Polyethylene-poly(L-lactide) diblock copolymers: Synthesis and compatibilization of poly(L-lactide)/polyethylene blends," *Journal of Polymer Science Part A: Polymer Chemistry,* vol. 39, pp. 2755-2766, 2001.
[79] H.-s. Lee, P. D. Fasulo, W. R. Rodgers, and D. R. Paul, "TPO based nanocomposites. Part 1. Morphology and mechanical properties," *Polymer,* vol. 46, pp. 11673-11689, 11/28/ 2005.
[80] J. Karger-Kocsis, "Reinforced Polymer Blends," in *Polymer Blends*. vol. 2, C. B. B. D. R. Paul, Ed., ed NewYork: John Wiley & Sons, 1999, p. 395.

[81] S. H. Lee, M. Bailly, and M. Kontopoulou, "Morphology and Properties of Poly(propylene)/Ethylene-Octene Copolymer Blends Containing Nanosilica," *Macromolecular Materials and Engineering,* vol. 297, pp. 95-103, 2012.

[82] Y. Liu and M. Kontopoulou, "The structure and physical properties of polypropylene and thermoplastic olefin nanocomposites containing nanosilica," *Polymer,* vol. 47, pp. 7731-7739, 10/18/ 2006.

[83] M. Sumita, K. Sakata, Y. Hayakawa, S. Asai, K. Miyasaka, and M. Tanemura, "Double percolation effect on the electrical conductivity of conductive particles filled polymer blends," *Colloid and Polymer Science,* vol. 270, pp. 134-139, 1992/02/01 1992.

[84] K. Levon, A. Margolina, and A. Z. Patashinsky, "Multiple percolation in conducting polymer blends," *Macromolecules,* vol. 26, pp. 4061-4063, 1993/07/01 1993.

[85] A. Göldel, G. Kasaliwal, and P. Pötschke, "Selective Localization and Migration of Multiwalled Carbon Nanotubes in Blends of Polycarbonate and Poly(styrene-acrylonitrile)," *Macromolecular Rapid Communications,* vol. 30, pp. 423-429, 2009.

[86] Y. Li and H. Shimizu, "Conductive PVDF/PA6/CNTs Nanocomposites Fabricated by Dual Formation of Cocontinuous and Nanodispersion Structures," *Macromolecules,* vol. 41, pp. 5339-5344, 2008/07/01 2008.

[87] O. Meincke, D. Kaempfer, H. Weickmann, C. Friedrich, M. Vathauer, and H. Warth, "Mechanical properties and electrical conductivity of carbon-nanotube filled polyamide-6 and its blends with acrylonitrile/butadiene/styrene," *Polymer,* vol. 45, pp. 739-748, 2// 2004.

[88] L. Elias, F. Fenouillot, J. C. Majeste, and P. Cassagnau, "Morphology and rheology of immiscible polymer blends filled with silica nanoparticles," *Polymer,* vol. 48, pp. 6029-6040, 9/21/ 2007.

[89] A.-C. Baudouin, C. Bailly, and J. Devaux, "Interface localization of carbon nanotubes in blends of two copolymers," *Polymer Degradation and Stability,* vol. 95, pp. 389-398, 3// 2010.

[90] A.-C. Baudouin, J. Devaux, and C. Bailly, "Localization of carbon nanotubes at the interface in blends of polyamide and ethylene–acrylate copolymer," *Polymer,* vol. 51, pp. 1341-1354, 3/11/ 2010.

[91] L. Elias, F. Fenouillot, J. C. Majesté, G. Martin, and P. Cassagnau, "Migration of nanosilica particles in polymer blends," *Journal of Polymer Science Part B: Polymer Physics,* vol. 46, pp. 1976-1983, 2008.

[92] J.-K. Yuan, S.-H. Yao, A. Sylvestre, and J. Bai, "Biphasic polymer blends containing carbon nanotubes: Heterogeneous nanotube distribution and its influence on the dielectric properties," *The Journal of Physical Chemistry C,* vol. 116, pp. 2051-2058, 2012.

[93] M. Sumita, K. Sakata, S. Asai, K. Miyasaka, and H. Nakagawa, "Dispersion of fillers and the electrical conductivity of polymer blends filled with carbon black," *Polymer Bulletin,* vol. 25, pp. 265-271, 1991/02/01 1991.

[94] A. Katada, Y. Buys, Y. Tominaga, S. Asai, and M. Sumita, "Relationship between electrical resistivity and particle dispersion state for carbon black filled poly (ethylene-co-vinyl acetate)/poly (L-lactic acid) blend," *Colloid and Polymer Science,* vol. 284, pp. 134-141, 2005/11/01 2005.

[95] S. A. Hosseini Pour, B. Pourabbas, and M. Salami Hosseini, "Electrical and rheological properties of PMMA/LDPE blends filled with carbon black," *Materials Chemistry and Physics,* vol. 143, pp. 830-837, 1/15/ 2014.

[96] E. Papirer, H. Balard, and V. C., "Surface energies of silica investigated by inverse gas chromatoghraphy," in *Adsorption on silica surfaces*, E. Papirer, Ed., ed New York: Marcel Dekker, 2000, pp. 205-276.
[97] R. M. Kooshki, I. Ghasemi, M. Karrabi, and H. Azizi, "Nanocomposites based on polycarbonate/poly (butylene terephthalate) blends effects of distribution and type of nanoclay on morphological behavior," *Journal of Vinyl and Additive Technology*, vol. 19, pp. 203-212, 2013.
[98] D. Dharaiya and S. C. Jana, "Thermal decomposition of alkyl ammonium ions and its effects on surface polarity of organically treated nanoclay," *Polymer*, vol. 46, pp. 10139-10147, 11/14/ 2005.
[99] A. H. Barber, S. R. Cohen, and H. D. Wagner, "Static and Dynamic Wetting Measurements of Single Carbon Nanotubes," *Physical Review Letters*, vol. 92, p. 186103, 05/07/ 2004.
[100] S. Nuriel, L. Liu, A. Barber, and H. Wagner, "Direct measurement of multiwall nanotube surface tension," *Chemical Physics Letters*, vol. 404, pp. 263-266, 2005.
[101] R. Menzel, A. Lee, A. Bismarck, and M. S. Shaffer, "Inverse gas chromatography of as-received and modified carbon nanotubes," *Langmuir*, vol. 25, pp. 8340-8348, 2009.
[102] K. H. Nam and W. H. Jo, "The effect of molecular weight and polydispersity of polystyrene on the interfacial tension between polystyrene and polybutadiene," *Polymer*, vol. 36, pp. 3727-3731, // 1995.
[103] M. R. Kamal, R. Lai-Fook, and N. R. Demarquette, "Interfacial tension in polymer melts. Part II: Effects of temperature and molecular weight on interfacial tension," *Polymer Engineering & Science*, vol. 34, pp. 1834-1839, 1994.
[104] A. Taghizadeh and B. D. Favis, "Carbon nanotubes in blends of polycaprolactone/thermoplastic starch," *Carbohydrate Polymers*, vol. 98, pp. 189-198, 10/15/ 2013.
[105] M. Gültner, A. Göldel, and P. Pötschke, "Tuning the localization of functionalized MWCNTs in SAN/PC blends by a reactive component," *Composites Science and Technology*, vol. 72, pp. 41-48, 12/6/ 2011.
[106] J. Chen, Y.-y. Shi, J.-h. Yang, N. Zhang, T. Huang, C. Chen, *et al.*, "A simple strategy to achieve very low percolation threshold via the selective distribution of carbon nanotubes at the interface of polymer blends," *Journal of Materials Chemistry*, vol. 22, pp. 22398-22404, 2012.
[107] Y. Liu and M. Kontopoulou, "Effect of filler partitioning on the mechanical properties of TPO/nanosilica composites," *Journal of Vinyl and Additive Technology*, vol. 13, pp. 147-150, 2007.
[108] R. Cardinaud and T. McNally, "Localization of MWCNTs in PET/LDPE blends," *European Polymer Journal*, vol. 49, pp. 1287-1297, 2013.
[109] A. Göldel, G. R. Kasaliwal, P. Pötschke, and G. Heinrich, "The kinetics of CNT transfer between immiscible blend phases during melt mixing," *Polymer*, vol. 53, pp. 411-421, 2012.
[110] A. Göldel, A. Marmur, G. R. Kasaliwal, P. Pötschke, and G. Heinrich, "Shape-dependent localization of carbon nanotubes and carbon black in an immiscible polymer blend during melt mixing," *Macromolecules*, vol. 44, pp. 6094-6102, 2011.
[111] J. R. Austin and M. Kontopoulou, "Effect of organoclay content on the rheology, morphology, and physical properties of polyolefin elastomers and their blends with polypropylene," *Polymer Engineering & Science*, vol. 46, pp. 1491-1501, 2006.

[112] M. H. Al-Saleh and U. Sundararaj, "An innovative method to reduce percolation threshold of carbon black filled immiscible polymer blends," *Composites Part A: Applied Science and Manufacturing,* vol. 39, pp. 284-293, 2// 2008.

[113] J. Huang, C. Mao, Y. Zhu, W. Jiang, and X. Yang, "Control of carbon nanotubes at the interface of a co-continuous immiscible polymer blend to fabricate conductive composites with ultralow percolation thresholds," *Carbon,* vol. 73, pp. 267-274, 2014.

[114] D. Wu, D. Lin, J. Zhang, W. Zhou, M. Zhang, Y. Zhang, *et al.*, "Selective Localization of Nanofillers: Effect on Morphology and Crystallization of PLA/PCL Blends," *Macromolecular Chemistry and Physics,* vol. 212, pp. 613-626, 2011.

[115] X. Zhao, J. Zhao, J.-P. Cao, D. Wang, G.-H. Hu, F. Chen, *et al.*, "Effect of the selective localization of carbon nanotubes in polystyrene/poly (vinylidene fluoride) blends on their dielectric, thermal, and mechanical properties," *Materials & Design,* vol. 56, pp. 807-815, 2014.

[116] L. Elias, F. Fenouillot, J. C. Majesté, P. Alcouffe, and P. Cassagnau, "Immiscible polymer blends stabilized with nano-silica particles: Rheology and effective interfacial tension," *Polymer,* vol. 49, pp. 4378-4385, 9/23/ 2008.

[117] T.-W. Lee and Y. G. Jeong, "Enhanced electrical conductivity, mechanical modulus, and thermal stability of immiscible polylactide/polypropylene blends by the selective localization of multi-walled carbon nanotubes," *Composites Science and Technology,* vol. 103, pp. 78-84, 10/28/ 2014.

[118] A. L. Persson and H. Bertilsson, "Viscosity difference as distributing factor in selective absorption of aluminium borate whiskers in immiscible polymer blends," *Polymer,* vol. 39, pp. 5633-5642, 11// 1998.

[119] J. Feng, C.-m. Chan, and J.-x. Li, "A method to control the dispersion of carbon black in an immiscible polymer blend," *Polymer Engineering & Science,* vol. 43, pp. 1058-1063, 2003.

[120] J. Plattier, L. Benyahia, M. Dorget, F. Niepceron, and J.-F. Tassin, "Viscosity-induced filler localisation in immiscible polymer blends," *Polymer,* vol. 59, pp. 260-269, 2/24/ 2015.

[121] F. Gubbels, R. Jerome, P. Teyssie, E. Vanlathem, R. Deltour, A. Calderone, *et al.*, "Selective Localization of Carbon Black in Immiscible Polymer Blends: A Useful Tool To Design Electrical Conductive Composites," *Macromolecules,* vol. 27, pp. 1972-1974, 1994/03/01 1994.

[122] J. S. Hong, Y. K. Kim, K. H. Ahn, and S. J. Lee, "Shear-induced migration of nanoclay during morphology evolution of PBT/PS blend," *Journal of Applied Polymer Science,* vol. 108, pp. 565-575, 2008.

[123] H. Rumpf, "The strength of granules and agglomerates," in *Agglomeration*, W. A. Knepper, Ed., ed New York: Wiley, 1962, pp. 379-418.

[124] F. Tao, B. Nysten, A.-C. Baudouin, J.-M. Thomassin, D. Vuluga, C. Detrembleur, *et al.*, "Influence of nanoparticle–polymer interactions on the apparent migration behaviour of carbon nanotubes in an immiscible polymer blend," *Polymer,* vol. 52, pp. 4798-4805, 9/29/ 2011.

[125] G. Filippone, N. T. Dintcheva, F. P. La Mantia, and D. Acierno, "Using organoclay to promote morphology refinement and co-continuity in high-density polyethylene/polyamide 6 blends – Effect of filler content and polymer matrix composition," *Polymer,* vol. 51, pp. 3956-3965, 8/4/ 2010.

[126] G. Wu, B. Li, and J. Jiang, "Carbon black self-networking induced co-continuity of immiscible polymer blends," *Polymer,* vol. 51, pp. 2077-2083, 2010.
[127] J. S. Hong, H. Namkung, K. H. Ahn, S. J. Lee, and C. Kim, "The role of organically modified layered silicate in the breakup and coalescence of droplets in PBT/PE blends," *Polymer,* vol. 47, pp. 3967-3975, 5/17/ 2006.
[128] A. Nuzzo, E. Bilotti, T. Peijs, D. Acierno, and G. Filippone, "Nanoparticle-induced co-continuity in immiscible polymer blends – A comparative study on bio-based PLA-PA11 blends filled with organoclay, sepiolite, and carbon nanotubes," *Polymer,* vol. 55, pp. 4908-4919, 9/15/ 2014.
[129] M. Kong, Y. Huang, G. Chen, Q. Yang, and G. Li, "Retarded relaxation and breakup of deformed PA6 droplets filled with nanosilica in PS matrix during annealing," *Polymer,* vol. 52, pp. 5231-5236, 10/13/ 2011.
[130] B. B. Khatua, D. J. Lee, H. Y. Kim, and J. K. Kim, "Effect of Organoclay Platelets on Morphology of Nylon-6 and Poly(ethylene-ran-propylene) Rubber Blends," *Macromolecules,* vol. 37, pp. 2454-2459, 2004/04/01 2004.
[131] S. Sinha Ray, S. Pouliot, M. Bousmina, and L. A. Utracki, "Role of organically modified layered silicate as an active interfacial modifier in immiscible polystyrene/polypropylene blends," *Polymer,* vol. 45, pp. 8403-8413, 11// 2004.
[132] S. H. Lee, M. Kontopoulou, and C. B. Park, "Effect of nanosilica on the co-continuous morphology of polypropylene/polyolefin elastomer blends," *Polymer,* vol. 51, pp. 1147-1155, 3/2/ 2010.
[133] E. Moghbelli, H.-J. Sue, and S. Jain, "Stabilization and control of phase morphology of PA/SAN blends via incorporation of exfoliated clay," *Polymer,* vol. 51, pp. 4231-4237, 8/19/ 2010.
[134] R. Aveyard, B. P. Binks, and J. H. Clint, "Emulsions stabilised solely by colloidal particles," *Advances in Colloid and Interface Science,* vol. 100–102, pp. 503-546, 2/28/ 2003.
[135] M. Trifkovic, A. T. Hedegaard, M. Sheikhzadeh, S. Huang, and C. W. Macosko, "Stabilization of PE/PEO Cocontinuous Blends by Interfacial Nanoclays," *Macromolecules,* 2015/06/19 2015.
[136] R. J. g. Lopetinsky, J. h. Masliyah, and Z. Xu, "Solid stabilized emulsions," in *Colloidal particles at liquid interfaces*, B. P. Binks and T. S. Horozov, Eds., ed Canbridge: Cambridge University Press 2006.
[137] Y. S. Lipatov, "Phase Separation in Filled Polymer Blends," *Journal of Macromolecular Science, Part B,* vol. 45, pp. 871-888, 2006/10/01 2006.
[138] Z. Fang, Y. Xu, and L. Tong, "Effect of clay on the morphology of binary blends of polyamide 6 with high density polyethylene and HDPE-graft-acrylic acid," *Polymer Engineering & Science,* vol. 47, pp. 551-559, 2007.
[139] G. I. Taylor, "The Viscosity of a Fluid Containing Small Drops of Another Fluid," *Proc. R. Soc. Lond. A 1,* vol. 138, p. 41, 1932.
[140] R. Salehiyan, Y. Yoo, W. J. Choi, and K. Hyun, "Characterization of Morphologies of Compatibilized Polypropylene/Polystyrene Blends with Nanoparticles via Nonlinear Rheological Properties from FT-Rheology," *Macromolecules,* vol. 47, pp. 4066-4076, 2014/06/24 2014.
[141] H. Gramespacher and J. Meissner, "Interfacial tension between polymer melts measured by shear oscillations of their blends," *Journal of Rheology (1978-present),* vol. 36, pp. 1127-1141, 1992.

[142] E. Jalali Dil, P. J. Carreau, S. Ravati, and B. D. Favis, "Morphology of Poly(lactic acid)/Poly(butylene adipate-co-terephthalate) Blends and Its Composite with Spherical Silica Particles," presented at the Society of Plastic (ANTEC), Orlando, 2012.

# ANNEX 1 SUPPORTING INFORMATION FOR ARTICLE 1

## A.1.1. Migration Velocity at the Interface

In the dynamic wetting phenomena, the displacement velocity of the three-phase contact line can be estimated as [1, 2]:

$$\boldsymbol{V = \frac{F}{\xi L}} \qquad \text{Eqn. 1}$$

Where F is the thermodynamic driving force, L is the length of the three-phase contact line (which is shown as the red line in the Figure A.1.1 (b)) and ξ is the friction coefficient.

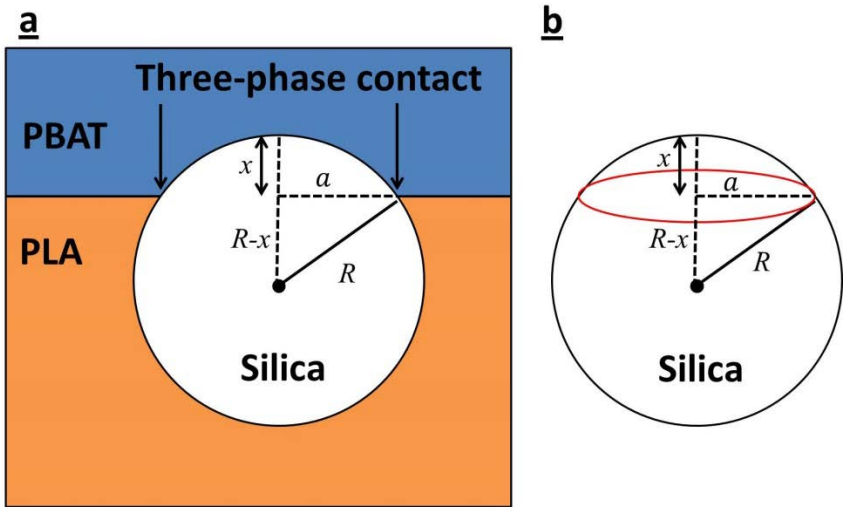


Figure 1.1. (a) 2D and (b) 3D schematic of the geometry of a spherical particle at the interface, The red line in (b) shows the three-phase contact line on the surface of silica. x is the penetration depth of the particle into the PBAT phase and $a=\sqrt{x(2R-x)}$

The work done by the thermodynamic driving force in displacing the three-phase contact line is equal to the change in the interfacial free energy of the system:

$$dW = -dG = F(x) \times dx \qquad \text{Eqn. 2}$$

Where W is the work done by the thermodynamic driving force at the three-phase contact line, dG is the change in the interfacial free energy of the system, F is the thermodynamic driving force and x is the penetration depth in the PBAT phase (shown in Figure A.1.1).

The negative sign for dG in Equation 2 is due to the fact that the movement of the particle toward the thermodynamic equilibrium location reduces the interfacial free energy of the system. The thermodynamic driving force then can be defined as:

$$\boldsymbol{F(x) = -\frac{dG}{dx}} \qquad \text{Eqn.3}$$

The interfacial free energy of a system with a spherical particle of radius R at the interface can be written as[3]:

$$\mathbf{G = \gamma_{1S}.A_{1S} + \gamma_{2S}.A_{2S} - \gamma_{12}.A_{12*}} \qquad \text{Eqn.4}$$

Here, $A_{1s}$, $A_{2s}$ and $A_{12*}$ are the interfacial areas between: polymer 1 and solid, polymer 2 and solid and the subtracted interfacial area from the interface of polymer 1 and 2 due to the presence of the solid particle at the interface. In the case of spherical particles at the interface, as can be seen in Figure A.1.1, the geometry of the part of the particle located in either phase represents a "spherical cap" and therefore the values of $A_{1S}$, $A_{2S}$ and $A_{12*}$ can be calculated as:

$$\mathbf{A_{1S} = 4\pi R^2 - 2\pi Rx} \qquad \text{Eqn.5}$$

$$\mathbf{A_{2S} = 2\pi Rx} \qquad \text{Eqn.6}$$

$$\mathbf{A_{12*} = \pi(2Rx - x^2)} \qquad \text{Eqn.7}$$

Substituting these values into equation 4 results in:

$$\boldsymbol{G = 2\pi R\left[(2R - x)\gamma_{1s} + x.\gamma_{2s} - (x - \frac{x^2}{2R})\gamma_{12}\right]} \qquad \text{Eqn.8}$$

According to Equation 2, the thermodynamic driving force (F(x)) can then be determined by differentiating Equation 8 with respect to x:

$$\boldsymbol{F(x) = -2\pi R\left[\gamma_{2s} - \gamma_{1s} - (1 - \frac{x}{R})\gamma_{12}\right]} \qquad \text{Eqn.9}$$

The thermodynamic driving force per the length of the three-phase contact line (F/L in Equation 1) at any penetration depth ($x$) then can be determined as:

$$\frac{F(x)}{L(x)} = \frac{F(x)}{2\pi\sqrt{x(2R-x)}} = \frac{-R}{\sqrt{x(2R-x)}}\left[\gamma_{2s} - \gamma_{1s} - (1 - \frac{x}{R})\gamma_{12}\right] \quad \text{Eqn.10}$$

where $2\pi\sqrt{x(2R-x)}$ is the length of the three-phase contact line at any $x$. To estimate the friction coefficient ($\xi$) in Equation 1, the theory of Blake and De Conick [1, 2] for the friction coefficient in dynamic wetting can be extended to consider the effect of viscosity and surface energy of the second liquid phase as another energy dissipation mechanism at the three-phase contact line:

$$\xi = \frac{\eta_1\ \nu_1}{\lambda^3}\exp\left(\frac{W_{1S}\lambda^2}{k_BT}\right) + \frac{\eta_2\ \nu_2}{\lambda^3}\ \exp(\frac{W_{2S}\lambda^2}{k_BT}) \quad \text{Eqn. 11}$$

where $\eta$, $\nu$, $\lambda$, $W_{LS}$, T and $k_B$ are the viscosity of the liquid phases, molecular volume of the liquid phases, the length scale of individual molecule displacement at the three-phase contact line, the work of adhesion between the liquid phases and solid, temperature and the Boltzmann constant. The migration velocity at the interface can then be estimated by substituting Equations 10 and 11 into Equation 1:

$$V = \frac{-R\lambda^3\left[\gamma_{2s}-\gamma_{1s}-(1-\frac{x}{R})\gamma_{12}\right]}{\sqrt{x(2R-x)}\left[\eta_1\ \nu_1\exp\left(\frac{W_{1S}\lambda^2}{k_BT}\right)+\eta_2\ \nu_2\exp(\frac{W_{2S}\lambda^2}{k_BT})\right]} \quad \text{Eqn.12}$$

### A.1.2. References


1. Blake TD. Journal of Colloid and Interface Science 2006;299(1):1-13.
2. Blake TD and De Coninck J. Advances in Colloid and Interface Science 2002;96(1–3):21-36.
3. Tiwari RR and Paul DR. Polymer 2011;52(4):1141-1154.

# ANNEX 2 EFFECTS OF DIFFERENT LOCALIZATIONS OF MICRO- AND NANO- SILICA PARTICLES ON MORPHOLOGY, RHEOLOGY AND MECHANICAL PROPERTIES OF POLY(LACTIC ACID)/POLY(BUTYLENE ADIPATE-CO-TEREPHTHALATE) BLENDS*

## A.2.1. Introduction

The addition of solid inclusions to polymer blends has been shown as an effective method to achieving a balance between toughness and stiffness [1-6, 38]. Moreover, with systems that display double and multiple percolation phenomena, the addition of conductive solid particles to polymer blends to achieve a semi-conductive material has also received much attention [7, 8]. Nanoparticles, in particular, have significant potential to improve the mechanical and/or electrical properties at much lower solid contents due to their much higher specific surface area.

The localization of nanoparticles is one of the key parameters in achieving property control in multiphase systems incorporating nanoparticles [1, 2, 9-11]. It has been shown that the localization of solid particles in a dispersed rubbery phase increases the dispersed phase size due to increasing the viscosity and elasticity of the dispersed phase [5, 12, 13]. At higher solid contents, the localization of the solid particles in the dispersed phase can promote the continuity of the dispersed phase by the formation of a 3D network of solid particles [14-17]. The localization of solid particles in the matrix phase has also been shown to reduce the dispersed phase size by diminishing coalescence through increasing the viscosity of the matrix and a solid barrier mechanism [2, 6, 18]. In the solid barrier mechanism, solid particles in the matrix that are trapped between two colliding droplets act as a solid barrier and prevent the coalescence of the droplets. The localization of solid particles at the interface of polymer blends has particularly received much attention [8, 19]. It has been reported that the localization of solid particles at the interface in polymer blends reduces significantly the dispersed phase size by the solid barrier mechanism [20, 21] and can even enhance the interfacial interactions between polymeric phases [22-26]. Moreover, the localization of solid particles at the interface has been shown to affect the rheological behaviour of polymer blends [27, 28].

*In preparation for *ACS Applied Materials and Interfaces*.

In the previous study [29], the effects of thermodynamic and kinetic parameters on the localization of micro- and nano- silica particles in a low interfacial tension blend of poly(lactic acid), PLA,/poly(butylene-adipate-co-terephthalate), PBAT, were studied and using different mixing strategies, viscosity of the PLA phase and the particle size of silica, different localizations of micro- and nano-silica particles could be achieved. In this study, the effects of different localizations of silica particles on the morphology, rheology and mechanical properties of PLA/PBAT will be studied. To this aim, the morphology and rheology of PLA/PBAT blends with micro- and nano-silica particles localized in the PBAT phase and at the interface were examined. In addition, the rheology and morphology of the blend with micro-silica localized into the PLA phase was studied. The effect of different localizations on the morphology and rheology was discussed in detail. Finally, mechanical properties of PLA/PBAT blends with nano-silica particles localized into the PBAT phase and at the interface were examined.

## A.2.2. Experimental

### *A.2.2.1. Materials*

PLA 3001D and PLA 2003D (Natureworks) were purchased from Cargil and will be referred hereafter as L-PLA and H-PLA respectively. PBAT (Ecoflex FBX 7011) was purchased from BASF. Spherical micro- and nano- silica particles, SEAHOSTAR KE-P30 and KE-P10, were purchased from Nippon Shokubai, Japan. The average diameters of the individual spherical silica particles for micro- and nano-silica are 300 nm and 100 nm, respectively. All the materials were dried under vacuum at 60 $^{O}$C overnight before being used in the experiments.

### *A.2.2.2. Blend preparation*

All samples were prepared using an internal batch mixer (Plasti-Corder DDR501, Brabender) with the total mixing chamber volume of 30 $cm^3$ at 180 $^{o}$C under a nitrogen blanket. The average shear rate at the mixing speed of 50 RPM used in this study was estimated as 25 $s^{-1}$ [30]. Two mixing strategies were used:

Pr1) the addition of the particles to a PLA/PBAT melt (one step process)

Pr2) premixing silica particles with PLA followed by mixing with PBAT (two-step process).

After 10 minutes of mixing, the chamber was opened and the samples were rapidly frozen in ice-water to freeze-in the morphology and localization of silica particles. The wt.% of silica particles added to the blends is based on the total weight of the blend.

*A.2.2.3. Atomic force microscopy (AFM)*

The samples were cut and microtomed under liquid nitrogen using a microtome (Leica-Jung RM 2165). The AFM machine was equipped with a scanning probe microscope Dimension 3100 with a Nanoscope IVa controller from Veeco Instruments. Silicon tips, model ACTA-W from AppNano, with the tip radius less than 10 nm were used in this study. The morphologies of the samples were determined by Tapping mode AFM in air. Because of the difference in the modulus of PLA and PBAT, tapping phase AFM is used to determine the morphology of the blend samples. The localization of silica particles in the blends samples was determined using both height and phase images obtained from AFM analysis.

*A.2.2.4. Field emission scanning electron microscopy (FE-SEM)*

In order to determine the morphology and the localization of silica particles, samples from the internal batch mixer were fractured in liquid nitrogen then the sample surface was coated with gold and the morphology was observed with the Field Emission Scanning Electron Microscope (FE-SEM, JSM 7600F, JEOL).

*A.2.2.5. Image analysis*

In order to determine the average dispersed PBAT fiber diameter, commercial image analysis software (SigmaScan Pro. V.5, Sigmaplot) was used. The average dispersed PBAT fiber size was determined from an average number of 200 dispersed phase fibers in AFM images. To consider the effect of fiber alignment on the observed cross-section of PBAT fibers, a new approach based on the measuring of the smallest diameter of the cross-section of PBAT fibers in the microtomed surface was used [31].

*A.2.2.6. Rheological analysis*

All the samples were compression moulded at 180 $^{o}$C and at 300 kPa in the form of 1.2 mm thick disks of 25 mm diameter under a nitrogen blanket. The rheological analysis was done using a constant stress rheometer (Physica MCR 301, Anton Paar) with 25 mm parallel plate geometry at a 1 mm gap at 180 $^{o}$C under nitrogen atmosphere. All the samples were kept at 180$^{o}$C for 5 minutes in the rheometer before performing the rheological tests. The stability of L-PLA, H-PLA and PBAT was studied under the test conditions using a time sweep test and a less than 7% drop in the complex viscosity and storage modulus was observed in the experimental time scale. Moreover, the linear viscoelastic region was determined using strain sweep tests for the neat polymers and the polymer blend samples at different frequencies. According to the obtained results, the frequency sweep tests for neat polymers and polymer blends were performed at strains of 5% and 1% respectively.

*A.2.2.7. Tensile properties*

Samples were prepared using compression moulding at 180$^{o}$C and 300 kPa under nitrogen atmosphere. The samples were conditioned for 24h at 22$^{o}$C and 50% humidity. Tensile tests were performed according to ASTM D638 on an Instron 3365 tensile machine equipped with 5kN load cell at a cross-head speed of 50mm/min. An average and standard error based on 10 measurements are reported for each sample.

*A.2.2.8. Notched impact strength*

Samples were prepared and conditioned as of the tensile test samples. The samples dimensions were 64×12×3.4 mm. The tests were performed using an Izod impact pendulum (Ceast 6545) according to ASTM D256. The reported values are based on seven measurements for each sample.

## A.2.3. Results and Discussion

### A.2.3.1.Rheological Characterization

Figure A.2.1 shows the complex viscosity and the storage modulus of L-PLA, H-PLA, PBAT and their mixtures with micro- and nano-silica particles. As can be seen, all neat polymers show Newtonian plateau at low frequencies. The addition of 4.3 wt.% of micro-silica to the H-PLA phase slightly increased the zero-shear viscosity but did not change the viscosity at the processing condition.

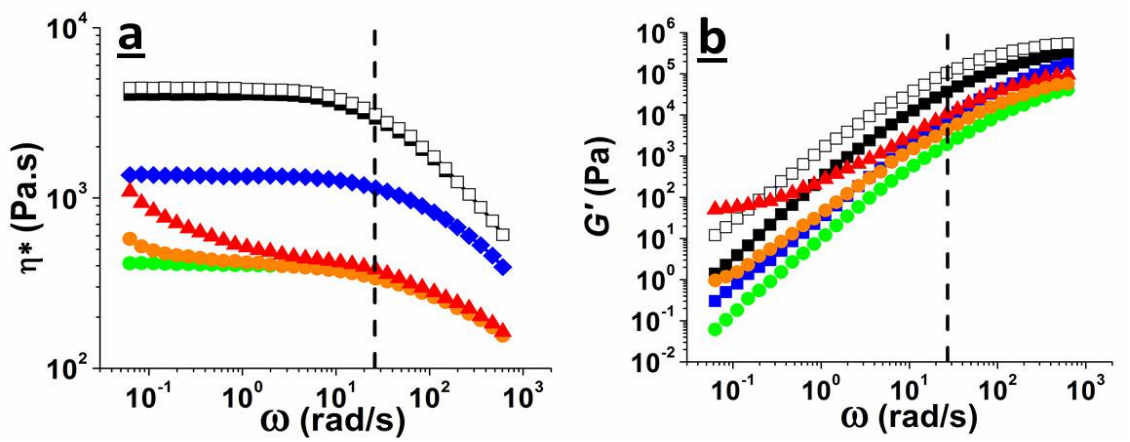


Figure A.2.1. The complex viscosity and storage modulus of H-PLA, L-PLA, PBAT and their mixtures with micro- and nano-silica: (■) H-PLA, (□) H-PLA with 4.3 wt.% micro-silica, (◆) L-PLA, (●) PBAT, (●) PBAT/10 wt.% micro-silica, (▲) PBAT/10 wt.% nano-silica

However, 10 wt.% of micro-silica particles in the PBAT phase increased the viscosity and resulted in a non-terminal behaviour at low frequencies. The upturn in the viscosity and non-terminal behaviour were much pronounced when nano-silica was added to the PBAT phase. These results point to the formation of a structure of micro- or nano-silica in the PBAT phase at 10 wt.% of silica.

### A.2.3.1. Localization of Silica Particles

In the previous study[32], using the measured surface energies of the polymer components and the estimated surface energy of the silica particles, thermodynamic equilibrium localization of silica particles was well-established to be in the PBAT phase. However, different localizations of micro- and nano-silica particles could be achieved by changing the mixing strategy and the viscosity of the PLA phase. Figure A.2.2 shows the different localizations of micro- and nano-silica obtained in the previous study.

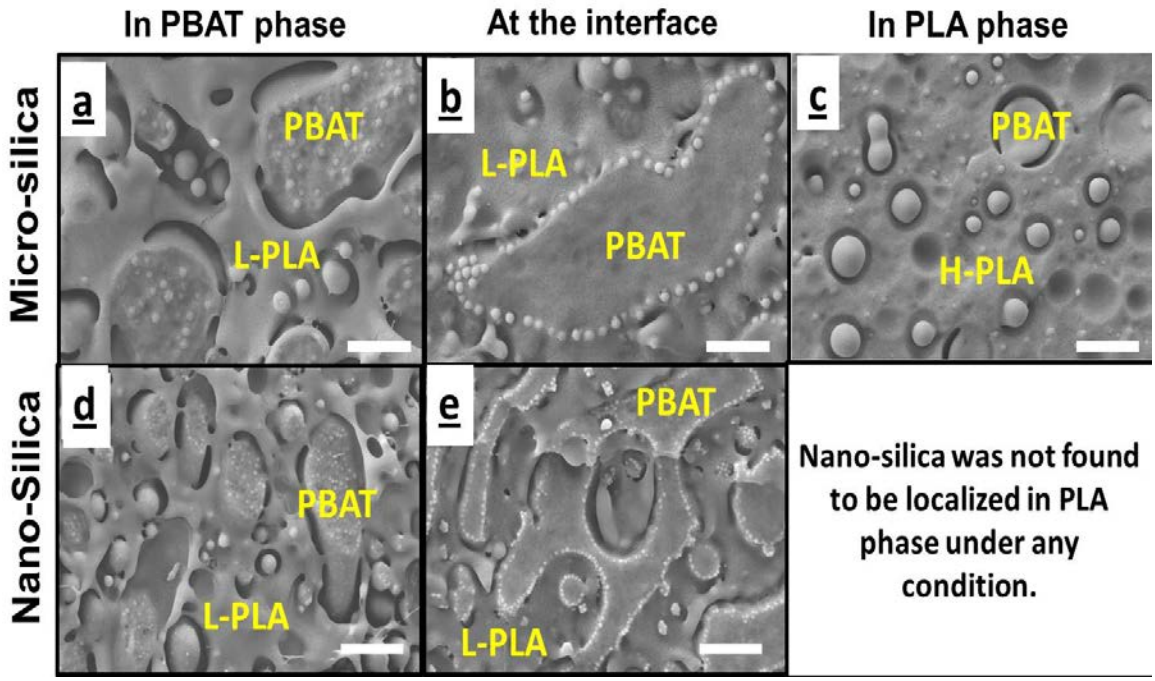


Figure A.2.2. Different localizations of micro- and nano-silica particles in PLA/PBAT (70/30).

As can be seen, micro-silica could be localized in either phase or at the interface but nano-silica could only be localized in the PBAT phase and at the interface.

**A.2.3.2. Effect of the Localization of Micro-silica in the PLA Phase**

By premixing micro-silica with H-PLA phase, the particles remained in the H-PLA phase, Figure A.2.2(c). Figure A.2.3 compares the morphology of H-PLA/PBAT(70/30) blend and the blend with micro –silica prepared by Pr2.

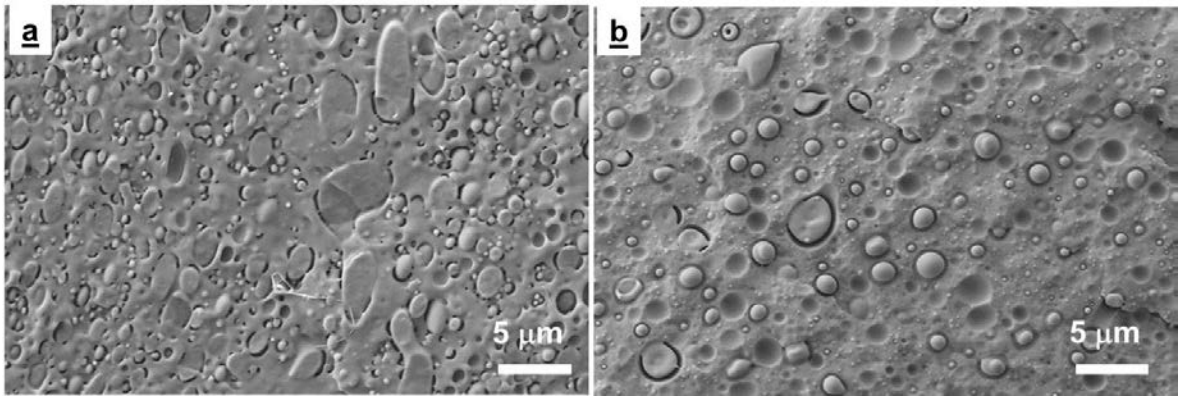


Figure A.2.3. The effect of the localization of micro-silica particles in the PLA phase on the morphology of H-PLA/PBAT(70/30): (a) 0 wt.% of micro-silica, 3 wt.% of micro-silica.

As can be seen in Figure A.2.2(c), the micro-silica particles in this system are selectively localized in the PLA phase. Comparing the continuity of the PBAT phase in these samples can help to better understand their morphologies. However, due to the very similar solubility parameters of PLA and PBAT, the solvent extraction is not an option in determining the continuity of the PBAT phase. In the previous study on the morphology of PLA/PBAT blend [31], the rheological analysis was shown to be a promising method in distinguishing a dispersed/matrix morphology from a co-continuous morphology in PLA/PBAT. Figure A.2.4 shows the rheological properties of H-PLA/PBAT with micro-silica localized in the PLA phase.

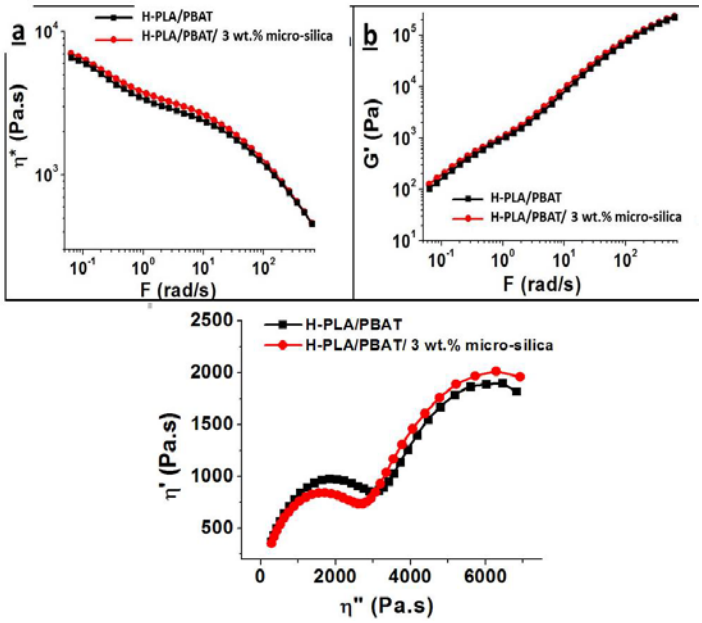


Figure A.2.4. The effect of localization of micro-silica particles in the H-PLA phase on the rheological properties of H-PLA/PBAT (70/30) (■) and H-PLA/PBAT (70/30) with 3 wt.% of micro-silica(●).

As can be seen, the localization of micro-silica particles in the H-PLA phase did not considerably change the rheological behavior of H-PLA/PBAT. The storage modulus of the neat H-PLA/PBAT(70/30) blend shows a clear shoulder at low frequencies which is attributed to the droplet relaxation of the PBAT dispersed phase. The droplet relaxation can be better seen in Cole-Cole plot of these samples which plots the imaginary component of the complex viscosity (η”) versus its real component (η’). The arc on the left side in Cole-Cole plots shows the

relaxation of polymer chains and the one on the right side is related to the droplet relaxation of the dispersed PBAT phase [33].The droplet relaxation peak can be seen in both samples with and without micro-silica particles which indicates that the morphology of this blend is a matrix/dispersed morphology. However, the results of the image analysis indicate that the addition of micro-silica reduced the PBAT fiber diameter from 2.3 μm to 1.5 μm. As the presence of micro-silica in the H-PLA phase does not change the viscosity of H-PLA considerably, Figure A.2.1, therefore the observed reduction in the PBAT phase size should be attributed to the solid barrier effect of the particles.

### A.2.3.2. Localization of Micro- and Nano-silica in the PBAT Phase

Figure A.2.5 shows the effect of localization of 3 wt.% of micro- and nano-silica in the PBAT phase in L-PLA/PBAT(70/30) blends. The localization of micro- and nano-silica in these samples are shown in Figure A.2.2 (a,d).

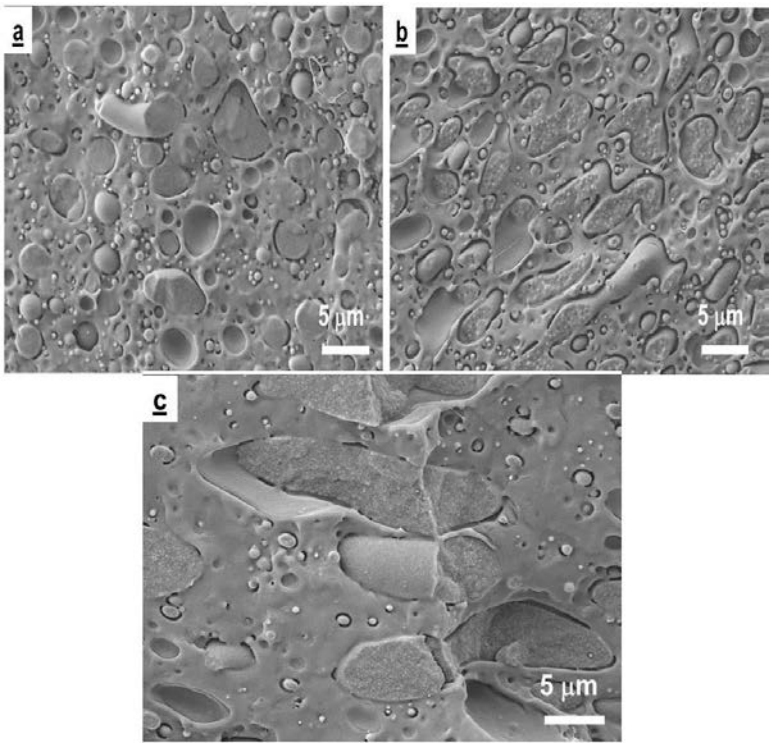


Figure A.2.5. The effect of the selective localization of micro- and nano-silica in the PBAT phase in L-PLA/PBAT (70/30): (a) the neat blend, (b) the blend with 3 wt.% of micro-silica, (c) the blend with 3 wt.% of nano-silica.

As can be seen, the localization of micro- and nano-silica particles in the PBAT phase increases the PBAT phase size. This effect is much more pronounced for the system with nano-silica. As the larger PBAT phase size in these samples cannot be attributed to the effect of particles on the viscosity at the processing condition, Figure A.2.1, the observed coarsening of the dispersed phase is attributed to the retardation of the breakup of dispersed phase in the presence of solid particles [16, 34].

Figure A.2.6 shows the rheological properties of L-PLA/PBAT blend and the blend with micro- and nano-silica localized into the PBAT phase. As can be seen, the selective localization of micro- and nano-silica particles in the PBAT phase slightly increased the viscosity, Figure A.2.6(a), and shifted the droplet relaxation in Cole-Cole plot to lower frequencies, Figure A.2.6 (c). However, the droplet relaxation peak can still be observed which indicates that the PBAT phase exists in the form of separated domains rather than a continuous structure.

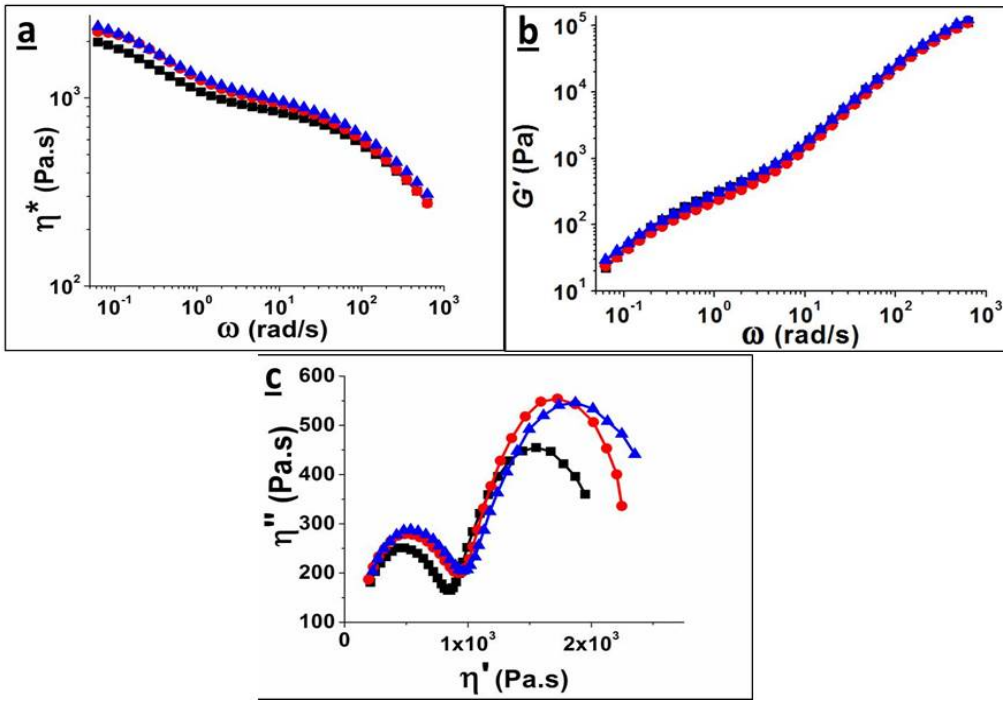


Figure A.2.6. The effect of the localization of micro- and nano-silica in the PBAT phase on the rheological properties of L-PLA/PBAT (70/30) blend. (■) the neat blend, (●) the blend with 3 wt.% of micro-silica, (▲) the blend with 3 wt.% of nano-silica.

### A.2.3.2. Localization of Micro- and Nano-silica at the Interface

The morphology of L-PLA/PBAT(70/30) blend and the blend with micro- and nano-silica particles localized at the interface are shown in Figure A.2.7. As can be seen, a matrix/dispersed morphology can be seen in the sample with micro-silica but the sample containing nano-silica shows a co-continuous morphology. The rheological analysis can be again used to compare the continuity level of the PBAT phase in these samples. The rheological properties of the blend samples with 3 wt.% of micro- and nano- silica particles are shown in Figure A.2.8.

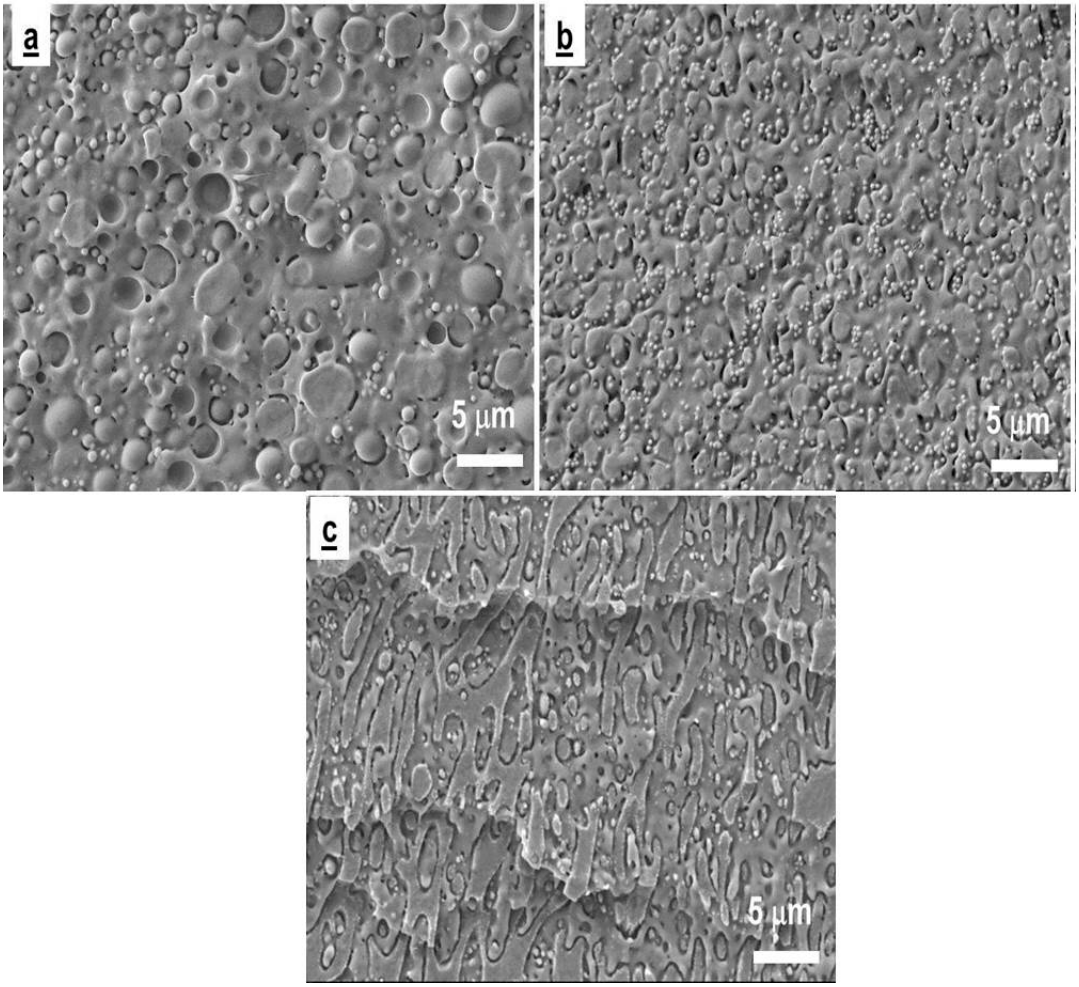


Figure A.2.7. The localization of micro- and nano-silica in PLA/PBAT(70/30): (a) neat blend, (b) 3 wt.% of micro-silica, (c) 3 wt.% of nano-silica.

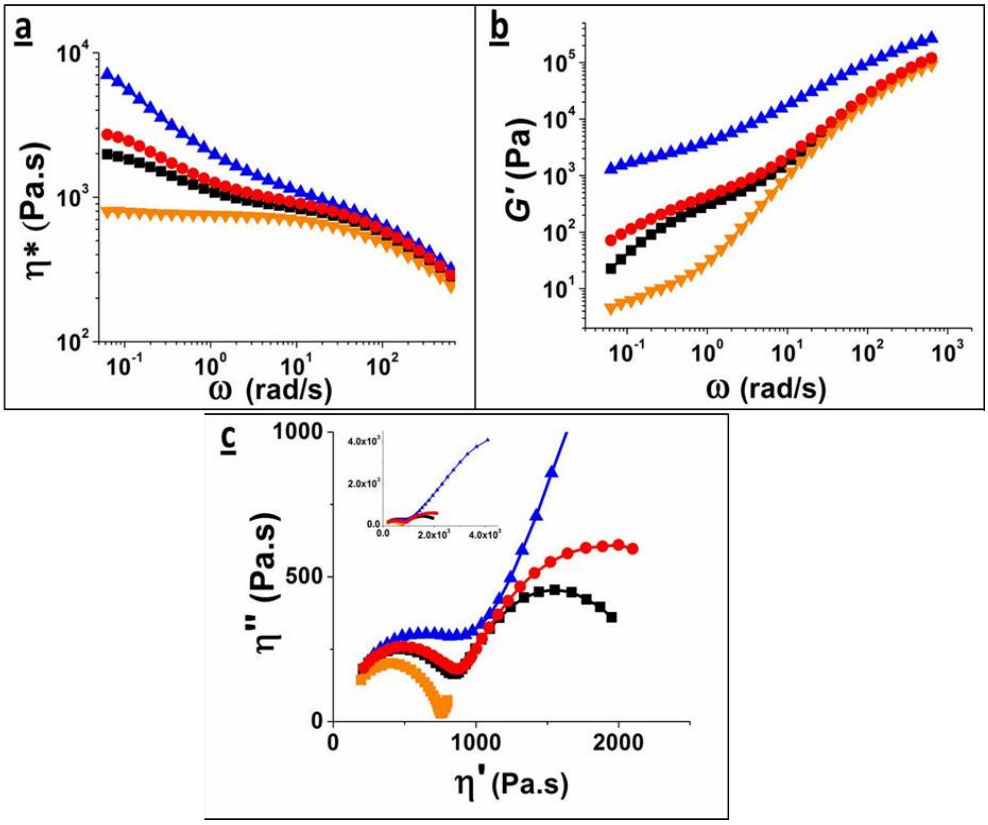


Figure A.2.8. The rheological analysis of L-PLA/PBAT(70/30) blends with micro- and nano-silica particles localized at the interface, (a) complex viscosity, (b) storage modulus, (c) Cole-Cole plot. (■)L-PLA/PBAT(70/30) blend,(●)the blend with 3 wt.% of micro-silica, (▲)the blend with 3 wt.% of nano-silica, (▼) L-PLA/PBAT(50/50). The subplot in (c) shows the full range of the data.

The storage modulus of L-PLA/PBAT(70/30) shows a clear shoulder at low frequencies which is attributed to the droplet relaxation of the PBAT dispersed phase. The droplet relaxation arc can be clearly seen in Cole-Cole plot of L-PLA/PBAT(70/30) which confirms the matrix/dispersed morphology in this sample. Despite the presence of the droplet relaxation arc in the blend with micro-silica particles, this arc was clearly shifted toward lower frequencies. This indicates that the presence of micro-silica at the interface retarded the PBAT droplet relaxation. In the blend sample with nano-silica particles at the interface, the droplet relaxation arc was disappeared in Cole-Cole plot and a gel-like behaviour was observed in the complex viscosity and storage modulus of the sample. Both SEM image (Figure A.2.7c) and the disappearance of the droplet

relaxation point to the formation of a continuous structure of the PBAT phase in this sample. The rheological properties of L-PLA/PBAT(50/50), which was shown to have a co-continuous morphology[31], is also shown in Figure A.2.8. It can be seen that by the formation of the continuous PBAT structure in L-PLA/PBAT(50/50), the droplet relaxation arc was disappeared in Cole-Cole plot; however, no gel-like behaviour was observed in the complex viscosity and storage modulus of this sample. Therefore, the formation of a 3D continuous structure of the PBAT phase cannot be responsible for the observed gel-like behaviour in the L-PLA/PBAT(70/30) blend with 3 wt.% of nano-silica localized at the interface. These results indicate that the observed gel-like behaviour should be attributed to the formation of a 2D network of nano-silica particles at the PLA/PBAT interface.

In the previous study[31], it was found that the limits of co-continuity in L-PLA/PBAT are located between 30-40 and 60-70 vol.% of PBAT. Therefore, the addition of nano-silica particles to L-PLA/PBAT(70/30) has shifted the limit of co-continuity in this sample. However, as the particles are localized at the interface, the observed shift cannot be attributed to the shift in the composition of the PBAT phase. Moreover, in the previous section, it was shown that even the selective localization of nano-silica in the PBAT phase did not result in the formation of a continuous PBAT structure in the blend. The effect of nano-silica particles on shifting the limit of continuity of the PBAT phase to lower compositions can be attributed to the stabilization mechanism of nano-silica particles. Figure A.2.9 shows the proposed stabilization mechanism for nano-silica particles.

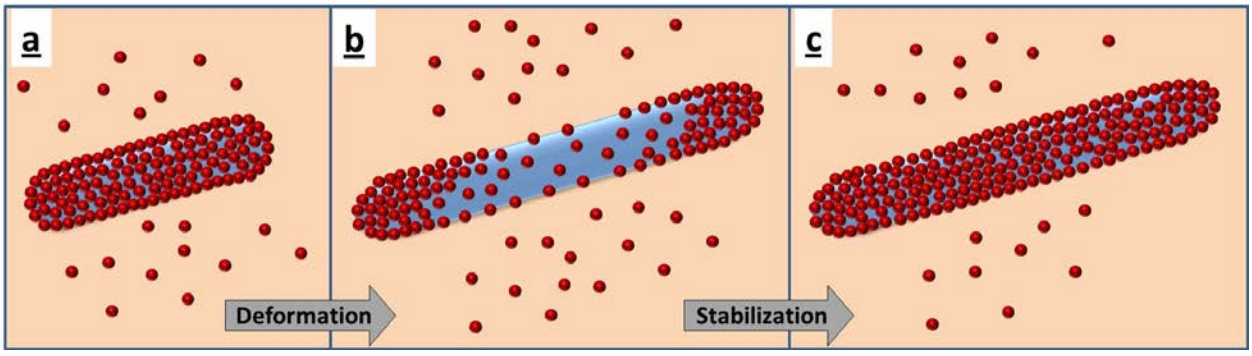


Figure A.2.9. Stabilization mechanism of the PBAT dispersed phase in the blend with nano-silica localized at the interface: (a) a PBAT fiber with nano-silica at the interface, (b) deformation of the PBAT fiber by hydrodynamic forces, (c) stabilization of the deformed PBAT fiber by migration of nano-silica from PLA.

In this mechanism, a new PLA/PBAT interface is created due to the deformation of the PBAT phase by the hydrodynamic forces. The long relaxation and breakup time of the dispersed phase in low interfacial tension PLA/PBAT [35, 36] allows nano-silica particles to migrate and stabilize the newly created interface. This will result in the stabilization of the elongated PBAT thread and prevents its retraction and breakup. As this process repeats, it results in the formation of a highly elongated stabilized PBAT phase. Eventually the coalescence of these highly elongated dispersed PBAT fibers results in the formation of a continuous PBAT structure at lower compositions.

### A-2.3.3. Effect of different Localizations of Nano-silica Particles on the Mechanical Properties

Figure A.2.10 and Table A.2.1 show the effect of different localizations of nano-silica particles on the tensile properties of L-PLA/PBAT(70/30) blends.

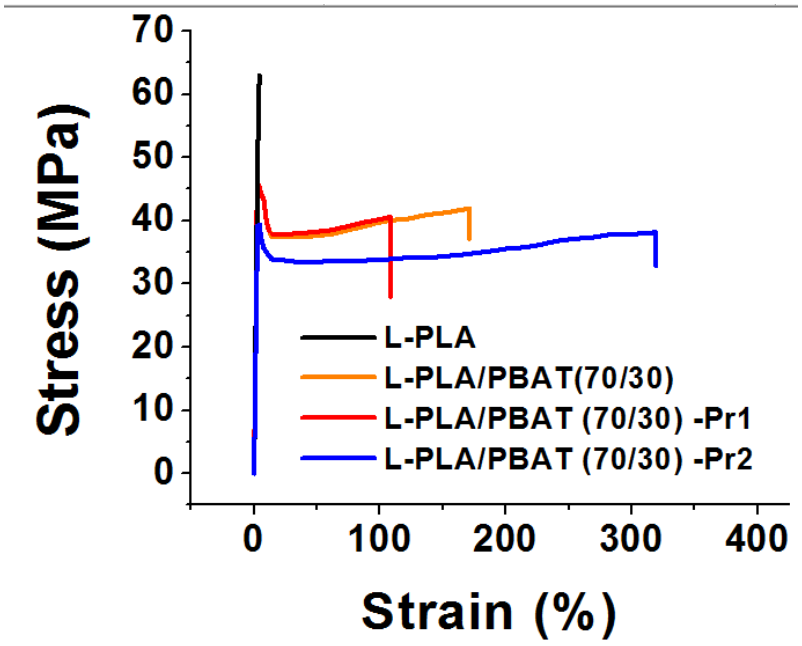


Figure A.2.10. The effect of different localizations of nano-silica particles on the tensile stress-strain curve of L-PLA/PBAT(70/30).

Table A.2.1. The effect of different localizations of nano-silica on the mechanical properties of L-PLA/PBAT(70/30)

| Sample | Tensile Modulus (MPa) | Tensile Strength(MPa) | Elongation at Break (%) | Izod impact strength (J/m) |
|---|---|---|---|---|
| L-PLA | 2040±36 | 62.5±2.3 | 4.2± 1 | 22±5 |
| L-PLA/PBAT | 1643±53 | 45.7±4.1 | 171±18 | 55±8 |
| L-PLA/PBAT-Pr1 | 1724±28 | 47±3.5 | 108±24 | 38±7 |
| PLA/PBAT-Pr2 | 1135±47 | 38±2.7 | 319±42 | 260±18 |

It can be seen that blending PLA with PBAT improved the elongation at break and impact strength but, at the same time, it reduced the modulus and tensile strength. The localization of nano-silica particles in the PBAT phase increased slightly the modulus and tensile strength but reduced the elongation at break and impact strength. The localization of the particles at the interface reduced the tensile modulus and strength compared to the blend but improved significantly the elongation at break and impact properties. These results can be attributed to the formation of a highly continuous structure of PBAT in the blend sample as in highly continuous structures, both phases fully contribute to the tensile properties of the sample [37]. Interestingly, the localization of nano-silica particles at the interface increased the impact strength by a factor of 4.7 compared with the neat blend. The observed increase in the impact properties can be attributed to the formation of 3D network of PBAT phase. In addition, the localization of silica particles at the interface increases the work of adhesion between the phases. This can also improve the stress transfer and impact strength in this blend.

### A-2.4. Conclusion

The effect of different localizations of micro- and nano-silica particles on the morphology and rheology of PLA/PBAT(70/30) was studied. The results indicate that the localization of micro-silica in the PLA phase reduced the dispersed phase size but did not affect the rheological properties. The localization of micro- and nano-silica particles in the PBAT phase promoted the formation of a continuous PBAT structure in the blend. This was attributed to the effect of the particles on the viscosity of PBAT and also on the retardation of the relaxation and breakup of the PBAT phase. When the particles were localized at the interface, micro-silica particles only shifted the droplet relaxation, however, no droplet relaxation was observed in the blend with nano-silica particles at the interface. Moreover, a gel-like behaviour was observed in the complex

viscosity and storage modulus of this sample. These results point to the formation of a continuous PBAT structure in this sample. This observation was attributed to the stabilization effect of the nano-silica particles which prevents the retraction and breakup of the PBAT phase. This results in the formation of a highly elongated PBAT phase which promotes the development of the continuity of PBAT. The formation of the co-continuous morphology of PLA/PBAT improves the elongation at elongation and impact properties significantly. This can be attributed to the formation of 3D network of PBAT phase and also increase in the interfacial adhesion due to the localization of nano-silica particles at the interface.

### A-2.5. References


1. Yoo, Y., et al., *Morphology and Mechanical Properties of Rubber Toughened Amorphous Polyamide/MMT Nanocomposites.* Macromolecules, 2009. **43**(2): p. 615-624.
2. Lee, H.-s., et al., *TPO based nanocomposites. Part 1. Morphology and mechanical properties.* Polymer, 2005. **46**(25): p. 11673-11689.
3. Karger-Kocsis, J., *Reinforced Polymer Blends*, in *Polymer Blends*, C.B.B. D. R. Paul, Editor. 1999, John Wiley & Sons: NewYork. p. 395.
4. Lee, S.H., M. Bailly, and M. Kontopoulou, *Morphology and Properties of Poly(propylene)/Ethylene-Octene Copolymer Blends Containing Nanosilica.* Macromolecular Materials and Engineering, 2012. **297**(1): p. 95-103.
5. Kontopoulou, M., et al., *The dynamics of montmorillonite clay dispersion and morphology development in immiscible ethylene–propylene rubber/polypropylene blends.* Polymer, 2007. **48**(15): p. 4520-4528.
6. Bailly, M. and M. Kontopoulou, *Preparation and characterization of thermoplastic olefin/nanosilica composites using a silane-grafted polypropylene matrix.* Polymer, 2009. **50**(11): p. 2472-2480.
7. Sumita, M., et al., *Double percolation effect on the electrical conductivity of conductive particles filled polymer blends.* Colloid and Polymer Science, 1992. **270**(2): p. 134-139.
8. Levon, K., A. Margolina, and A.Z. Patashinsky, *Multiple percolation in conducting polymer blends.* Macromolecules, 1993. **26**(15): p. 4061-4063.
9. Göldel, A., G. Kasaliwal, and P. Pötschke, *Selective Localization and Migration of Multiwalled Carbon Nanotubes in Blends of Polycarbonate and Poly(styrene-acrylonitrile).* Macromolecular Rapid Communications, 2009. **30**(6): p. 423-429.
10. Li, Y. and H. Shimizu, *Conductive PVDF/PA6/CNTs Nanocomposites Fabricated by Dual Formation of Cocontinuous and Nanodispersion Structures.* Macromolecules, 2008. **41**(14): p. 5339-5344.
11. Meincke, O., et al., *Mechanical properties and electrical conductivity of carbon-nanotube filled polyamide-6 and its blends with acrylonitrile/butadiene/styrene.* Polymer, 2004. **45**(3): p. 739-748.
12. Hong, J.S., et al., *The role of organically modified layered silicate in the breakup and coalescence of droplets in PBT/PE blends.* Polymer, 2006. **47**(11): p. 3967-3975.

13. Dasari, A., Z.-Z. Yu, and Y.-W. Mai, *Effect of blending sequence on microstructure of ternary nanocomposites.* Polymer, 2005. **46**(16): p. 5986-5991.
14. Filippone, G., et al., *The role of organoclay in promoting co-continuous morphology in high-density poly(ethylene)/poly(amide) 6 blends.* Polymer, 2008. **49**(5): p. 1312-1322.
15. Filippone, G., et al., *Using organoclay to promote morphology refinement and co-continuity in high-density polyethylene/polyamide 6 blends – Effect of filler content and polymer matrix composition.* Polymer, 2010. **51**(17): p. 3956-3965.
16. Nuzzo, A., et al., *Nanoparticle-induced co-continuity in immiscible polymer blends – A comparative study on bio-based PLA-PA11 blends filled with organoclay, sepiolite, and carbon nanotubes.* Polymer, 2014. **55**(19): p. 4908-4919.
17. Wu, G., B. Li, and J. Jiang, *Carbon black self-networking induced co-continuity of immiscible polymer blends.* Polymer, 2010. **51**(9): p. 2077-2083.
18. Fenouillot, F., P. Cassagnau, and J.C. Majesté, *Uneven distribution of nanoparticles in immiscible fluids: Morphology development in polymer blends.* Polymer, 2009. **50**(6): p. 1333-1350.
19. Gubbels, F., et al., *Selective Localization of Carbon Black in Immiscible Polymer Blends: A Useful Tool To Design Electrical Conductive Composites.* Macromolecules, 1994. **27**(7): p. 1972-1974.
20. Si, M., et al., *Compatibilizing Bulk Polymer Blends by Using Organoclays.* Macromolecules, 2006. **39**(14): p. 4793-4801.
21. Baudouin, A.-C., et al., *Polymer blend emulsion stabilization using carbon nanotubes interfacial confinement.* Polymer, 2011. **52**(1): p. 149-156.
22. Elias, L., et al., *Immiscible polymer blends stabilized with nano-silica particles: Rheology and effective interfacial tension.* Polymer, 2008. **49**(20): p. 4378-4385.
23. Hong, J., et al., *Interfacial tension reduction in PBT/PE/clay nanocomposite.* Rheologica Acta, 2007. **46**(4): p. 469-478.
24. Sinha Ray, S., et al., *Role of organically modified layered silicate as an active interfacial modifier in immiscible polystyrene/polypropylene blends.* Polymer, 2004. **45**(25): p. 8403-8413.
25. Tao, F., et al., *Influence of Multiwall Carbon Nanotubes Trapped at the Interface of an Immiscible Polymer Blend on Interfacial Tension.* Macromolecular Chemistry and Physics, 2013. **214**(3): p. 350-360.
26. Salehiyan, R., et al., *Characterization of Morphologies of Compatibilized Polypropylene/Polystyrene Blends with Nanoparticles via Nonlinear Rheological Properties from FT-Rheology.* Macromolecules, 2014. **47**(12): p. 4066-4076.
27. Elias, L., et al., *Morphology and rheology of immiscible polymer blends filled with silica nanoparticles.* Polymer, 2007. **48**(20): p. 6029-6040.
28. Filippone, G., G. Romeo, and D. Acierno, *Role of Interface Rheology in Altering the Onset of Co-Continuity in Nanoparticle-Filled Polymer Blends.* Macromolecular Materials and Engineering, 2011. **296**(7): p. 658-665.
29. Jalali Dil, E. and B.D. Favis, *Localization of Micro- and Nano- Silica Particles in Heterophase Poly(lactic acid)/ Poly(butylene adipate-co-terephthalate) Blends* To be submitted, 2015.
30. Bousmina, M., A. Ait-Kadi, and J.B. Faisant, *Determination of shear rate and viscosity from batch mixer data.* Journal of Rheology, 1999. **43**(2): p. 415-433.

31. Jalali Dil, E., P.J. Carreau, and B.D. Favis, *Morphology, miscibility and continuity development in poly(lactic acid)/poly(butylene adipate-co-terephthalate) blends.* Polymer, 2015. **68**: p. 202-212.
32. Jalali Dil, E. and B.D. Favis, *Localization of Micro- and Nano- Silica Particles in Heterophase Poly(lactic acid)/ Poly(butylene adipate-co-terephthalate) Blends.* Submitted to Polymer, 2015.
33. GRAEBLING, D., R. MULLER, and J. PALIERNE, F., *Linear viscoelasticity of incompatible polymer blends in the melt in relation with interfacial properties.* J. Phys. IV France, 1993. **03**(C7): p. C7-1525-C7-1534.
34. Kong, M., et al., *Retarded relaxation and breakup of deformed PA6 droplets filled with nanosilica in PS matrix during annealing.* Polymer, 2011. **52**(22): p. 5231-5236.
35. Li, J., P.L. Ma, and B.D. Favis, *The Role of the Blend Interface Type on Morphology in Cocontinuous Polymer Blends.* Macromolecules, 2002. **35**(6): p. 2005-2016.
36. Bhadane, P.A., et al., *Continuity development in polymer blends of very low interfacial tension.* Polymer, 2006. **47**(8): p. 2760-2771.
37. Pötschke, P. and D.R. Paul, *Formation of Co-continuous Structures in Melt-Mixed Immiscible Polymer Blends.* Journal of Macromolecular Science, Part C, 2003. **43**(1): p. 87-141.
38 Liu Y. and Kontopoulou M., Polymer 2006; 47:7731
39 Lee S.H, Kontopoulou M., Park C. B., Polymer 2010;51:1147

# ANNEX 3 COMPATIBILIZATION OF PLA-PBAT INTERFACE BY SOLID STATE SHEAR PULVERIZATION (SSSP)

According to the previous studies in the literature, the addition of PBAT to PLA enhances the elongation at break but does not improve the impact properties considerably[1-4]. For instant, Jiang et al. [1] showed that the addition of 20 wt.% of PBAT increased the elongation at break of PLA from 4% to more than 200% but could only enhance the impact strength by a factor of 1.7. These results indicate that despite the low interfacial tension between PLA and PBAT, the interfacial adhesion between them is not high enough to withstand the high deformation rates in the impact tests. The addition of comnpatibilizers is a well-known method to enhance the interfacial adhesion and impact strength in multiphase systems [5]. However, due to the very similar nature of PLA and PBAT, finding a compatibilizer that can be effectively situated at PLA-PBAT interface is challenging. The best choice for the compatibilizer is obviously the block copolymer of PLA and PBAT but this copolymer has not been synthesized yet. Solid state shear pulverization (SSSP) is a method in which two polymers are pulverized at the temperature much lower than their melting point. The applied mechanical forces results in the chain scission and formation of radicals on the surface of polymer powder particles. It has been shown that due to collision of polymer powder particles of two different polymers, the radicals on their surface can react and form a block or segmented copolymer of the polymers [6]. Due to its simplicity and low final cost, comparing with the synthesis of a new copolymer, researchers have been motivated to apply this method to compatibilize the interfaces between synthetic polymers[7, 8] and even the interfaces of polymers with solid particles [9-11]. The formation of the copolymers in this method has been experimentally proven but there is not much knowledge about controlling the final structure of the formed copolymer. Twin screw extruders with specific screw configurations are usually used in SSSP method but some authors have also used freezer mills[12] and showed that despite the lower efficiency of freezer mills, they still can be used as a simple method to produce block copolymers via SSSP. In this work, the SSSP method was employed to improve the interfacial adhesion between PLA (3001D) and PBAT (Ecoflex 7011 FBX). To this aim, two different strategies were used:

(Procedure1) SSSP of PLA and PBAT granules separately.

(Procedure2) Simultaneous SSSP of PLA and PBAT granules.

SSSP was done by a freezer/mill (6870, Spex SamplePrep) in a liquid nitrogen bath. The granules were milled in 15 cycles of 2 minutes long with 2 minutes of the cooling step after each cycle. The impact rate of 15 cps was used to prepare the samples. The obtained powders then were melt mixed with an internal batch mixer (Plasti-Corder DDR501, Brabender). All the blend samples contain 60 vol.% of PLA and 40 vol.% of PBAT. Rheological properties of PLA and PBAT powders after SSSP were found to be almost the same as the polymer granules.

Figure A.3.1 shows the morphology of PLA/PBAT (60/40) prepared by the above mentioned strategies.

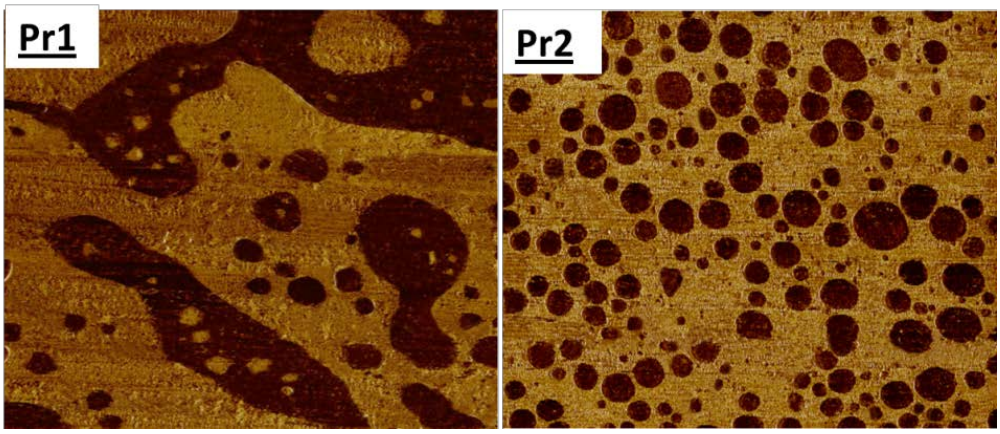


Figure A.3.1. The effect of different SSSP strategy on the morphology of PLA/PBAT(60/40): a) Procedure1, (b)Procedure 2

Comparing the morphology of these two samples reveals that, the morphology changed from a co-continuous morphology to a dispersed-matrix morphology. Note that the morphology of PLA/PBAT(60/40) was shown to be a co-continuous morphology in the previous study[13]. Considering the negligible change in the rheological properties of individually pulverized polymers, the obtained results indicate the suppression of coalescence after SSSP process. This can be attributed to the formation of PLA-PBAT copolymer at the interface reduces the coalescence rate in these systems.

These results indicate the potential of SSSP process as an economic and effective method in enhancing the interfacial adhesion and improving the mechanical properties in the systems with similar components such as PLA/PBAT.

### A-3.1. Conclusion

Solid state shear pulverization (SSSP) was used as a method to enhance the interfacial adhesion between PLA and PBAT. It was found that the simultaneous pulverization of both PLA and PBAT granules changed the morphology from a co-continuous morphology to the matrix dispersed morphology. These results indicate that SSSP process could successfully be employed to compatibilize the interface of PLA/PBAT.

## A-3.2. References


1. Jiang, L., M.P. Wolcott, and J. Zhang, *Study of Biodegradable Polylactide/Poly(butylene adipate-co-terephthalate) Blends.* Biomacromolecules, 2005. **7**(1): p. 199-207.
2. Lin, S., et al., *Mechanical properties and morphology of biodegradable poly(lactic acid)/poly(butylene adipate-co-terephthalate) blends compatibilized by transesterification.* Materials & Design, 2012. **36**(0): p. 604-608.
3. Zhang, N., et al., *Preparation and properties of biodegradable poly(lactic acid)/poly(butylene adipate-co-terephthalate) blend with glycidyl methacrylate as reactive processing agent.* Journal of Materials Science, 2009. **44**(1): p. 250-256.
4. Zhang, N., et al., *Preparation and Properties of Biodegradable Poly(lactic acid)/Poly(butylene adipate-co-terephthalate) Blend with Epoxy-Functional Styrene Acrylic Copolymer as Reactive Agent.* Journal of Polymers and the Environment, 2013. **21**(1): p. 286-292.
5. Lacasse, C. and B.D. Favis, *Interface/morphology/property relationships in polyamide-6/ABS blends.* Advances in Polymer Technology, 1999. **18**(3): p. 255-265.
6. Furgiuele, N., et al., *Novel Strategy for Polymer Blend Compatibilization: Solid-State Shear Pulverization.* Macromolecules, 1999. **33**(2): p. 225-228.
7. Lebovitz, A.H., K. Khait, and J.M. Torkelson, *In Situ Block Copolymer Formation during Solid-State Shear Pulverization: An Explanation for Blend Compatibilization via Interpolymer Radical Reactions.* Macromolecules, 2002. **35**(26): p. 9716-9722.
8. Lebovitz, A.H., K. Khait, and J.M. Torkelson, *Stabilization of Dispersed Phase to Static Coarsening: Polymer Blend Compatibilization via Solid-State Shear Pulverization.* Macromolecules, 2002. **35**(23): p. 8672-8675.

9. Masuda, J.i. and J.M. Torkelson, *Dispersion and major property enhancements in polymer/multiwall carbon nanotube nanocomposites via solid-state shear pulverization followed by melt mixing.* Macromolecules, 2008. **41**(16): p. 5974-5977.
10. Iwamoto, S., et al., *Solid-state shear pulverization as effective treatment for dispersing lignocellulose nanofibers in polypropylene composites.* Cellulose, 2014. **21**(3): p. 1573-1580.
11. Wakabayashi, K., et al., *Polymer-graphite nanocomposites: effective dispersion and major property enhancement via solid-state shear pulverization.* Macromolecules, 2008. **41**(6): p. 1905-1908.
12. Henry, M.F., *Solid-State Compatibilization of Immiscible Polymer Blends: Cryogenic Milling and Solid-State Shear Pulverization*. 2010, Bucknell University.
13. Jalali Dil, E., P.J. Carreau, and B.D. Favis, *Morphology, miscibility and continuity development in poly(lactic acid)/poly(butylene adipate-co-terephthalate) blends.* Polymer, 2015. **68**: p. 202-212.

# ANNEX 4 EFFECT OF MICRO-SILICA PARTICLES ON THE MORPHOLOGY OF PLA/H-LDPE BLENDS*

The effects of the selective localization of micro-silica particles in the PLA phase on the morphology of PLA/H-LDPE blends are shown in Figure A.4.1. All the samples were prepared by the addition of micro-silica to the PLA/PBAT melts. In all samples, silica content is based on the PLA phase. The continuity diagrams of PLA/H-LDPE blends with different micro-silica contents are also shown in Figure A.4.2.

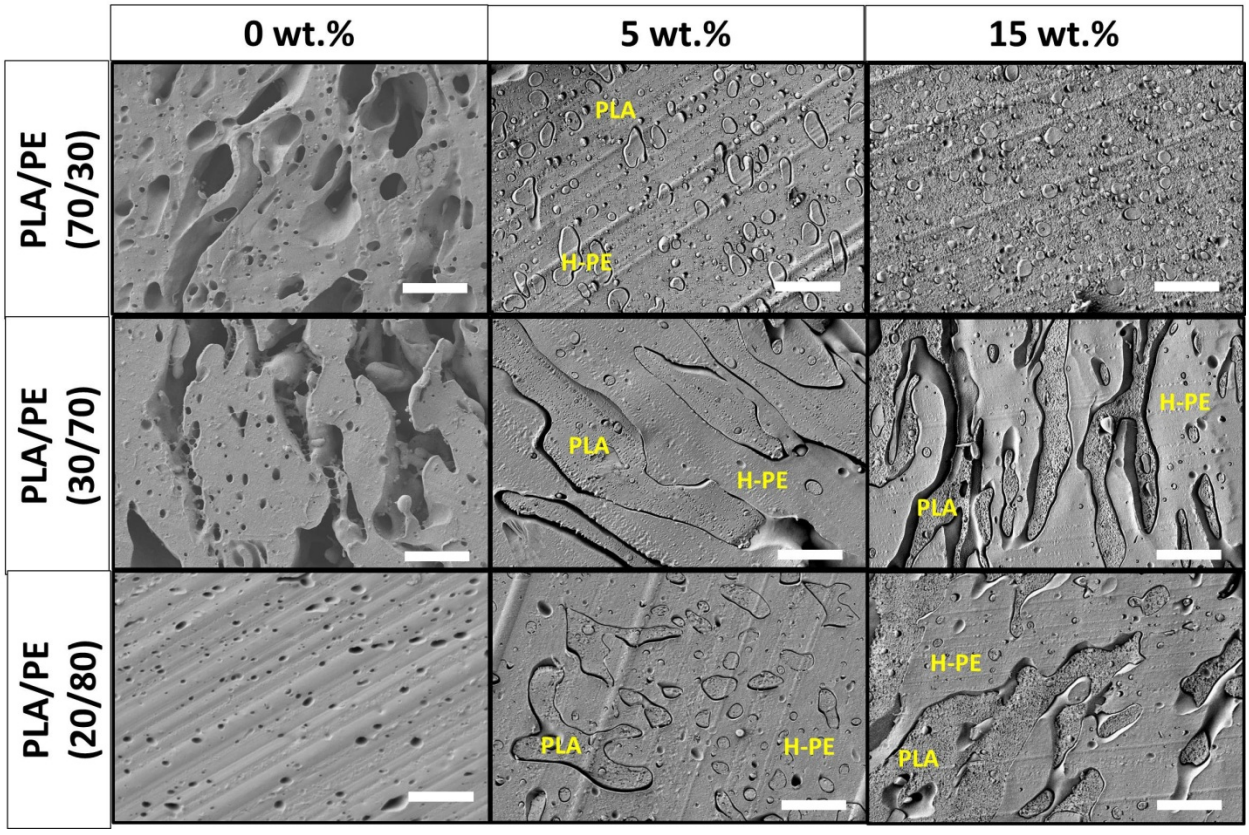


Figure A.4.1. The effect of the selective localization of micro-silica in the PLA phase at different silica contents on the morphology of PLA/H-LDPE blends. The silica contents are shown on the headers of the columns. The H-LDPE phase was extracted in PLA/H-LDPE(70/30); the PLA phase was extracted in PLA/H-LDPE(30/70) and (20/80). The white scale bars show 20 μm.

*In preparation for *Polymer Communication*

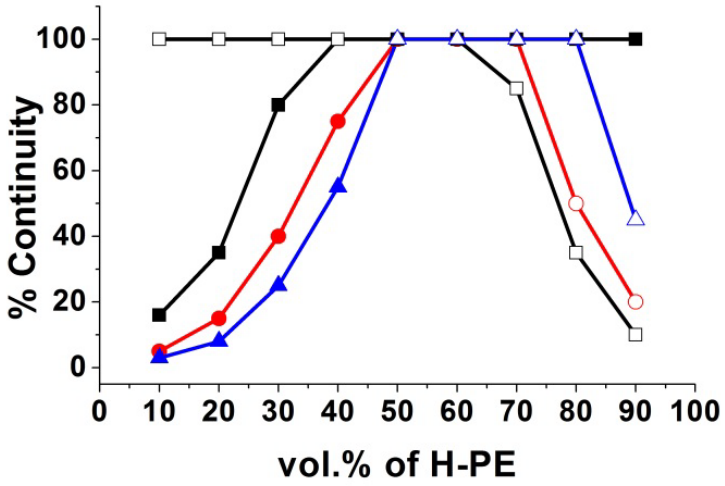


Figure 4.2. The continuity development diagram in PLA/H-LDPE blends with different micro-silica contents: (■)H-LDPE phase in the neat blend,(●) H-LDPE in the blend with 5 wt.% of micro-silica, (▲) H-LDPE in the blend with 15 wt.% of micro-silica, (□)PLA in the neat blend, (○) PLA in the blend with 5 wt.% of micro-silica, (△) PLA in the blend with 15 wt.% of micro-silica.

The localization of 5 wt.% of micro-silica in the PLA phase reduced the H-LDPE phase size and dropped the continuity level from 80% to 40%. Further increase in the micro-silica content decreased the continuity of H-LDPE phase to 25%. The reduction in the dispersed phase size by the localization of solid particles in the matrix has been attributed to two main mechanisms: (i) altered viscosity of the matrix and (ii) the solid barrier effect[1].

The increase in the viscosity of the matrix, due to the presence of the solid particles, increases significantly the film draining time between two dispersed phase droplets and, consequently, reduces the coalescence rate and the dispersed phase size[1, 2]. In the solid barrier mechanism, the coalescence of the dispersed phase droplets is prevented by the formation of a physical barrier of the particles between the colliding droplets [1-5].

The rheological properties of neat polymers and polymer/silica composites are shown in Figure A.4.3. As can be seen, the addition of even 15 wt.% of micro-silica particles to the PLA phase did not change considerably the viscosity and elasticity of this phase at the processing condition.

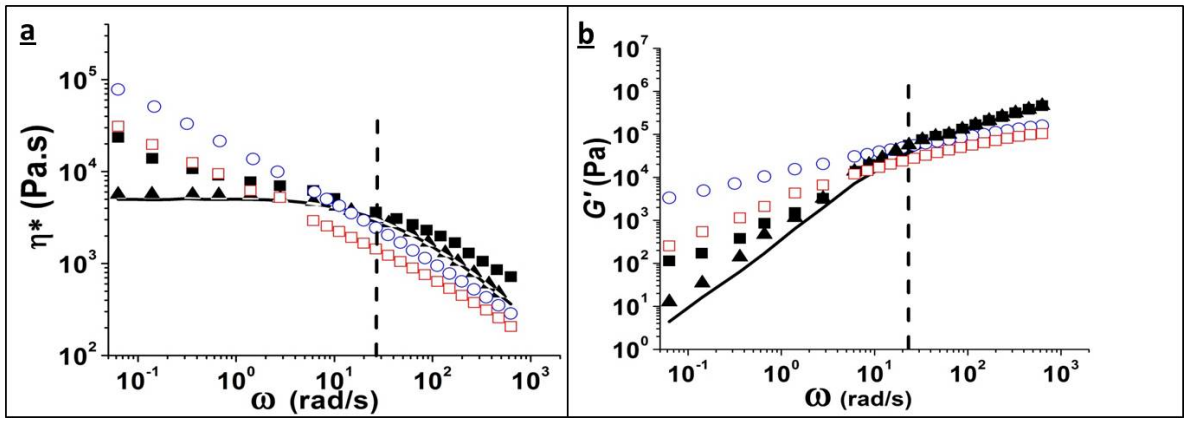


Figure A.4.3. Complex viscosities and storage moduli of the neat polymer components and PLA/micro-silica mixtures at 180°C: (-) neat PLA, (▲)PLA with 5 wt.% of micro-silica, (■) PLA with 15 wt.% of micro-silica, (□) L-PE, (○) H-PE. The dashed line represents the average shear rate of mixing at 25 $s^{-1}$[6].

Therefore, the most plausible explanation for the observed reduction in the H-LDPE phase continuity is the solid barrier mechanism.

In the complementary blend of PLA/H-LDPE(30/70), the addition of 5 wt.% of micro-silica promoted the continuity development of the PLA phase and resulted in the formation of a co-continuous morphology in this sample. Increasing the micro-silica content in this sample was found to reduce the size of the co-continuous structure. Similar effect of silica particles on the size of the co-continuous morphology of PP/polyolefin elastomer (POE) blends was previously reported by Lee et al. [7] and was attributed to the enhanced dispersed POE droplet deformation and breakup due to the confined flow between silica domains in the PP matrix. However, as the authors mentioned, confirming the confined flow mechanism is very difficult experimentally [8].

The effect of silica particles on the formation of continuous network of PLA phase can be better seen by studying the morphology of PLA/H-LDPE (20/80) blend. As can be seen in Figure A.4.2, the addition of 5 wt.% of micro-silica to this sample increased the continuity level of the PLA phase from 35% to 50%. Further increase in the silica content results in the formation of a co-continuous structure at 15 wt.% of micro-silica particles. The increase in the continuity and phase size of the dispersed phase due to the localization of solid particles has been attributed to the increase in the viscosity and elasticity of the dispersed phase which reduces the deformation and

breakup of the dispersed phase [2, 9-11]. However, as the localization of micro-silica particles in the PLA phase does not change the viscosity and elasticity considerably, this mechanism cannot explain the observed improvement in the continuity development of the PLA phase.

The SEM image of the morphology of PLA/H-LDPE(10/90) containing 15 wt.% of micro-silica, Figure A.4.4, reveals a highly elongated fibrillar morphology of PLA/micro-silica phase in this sample.

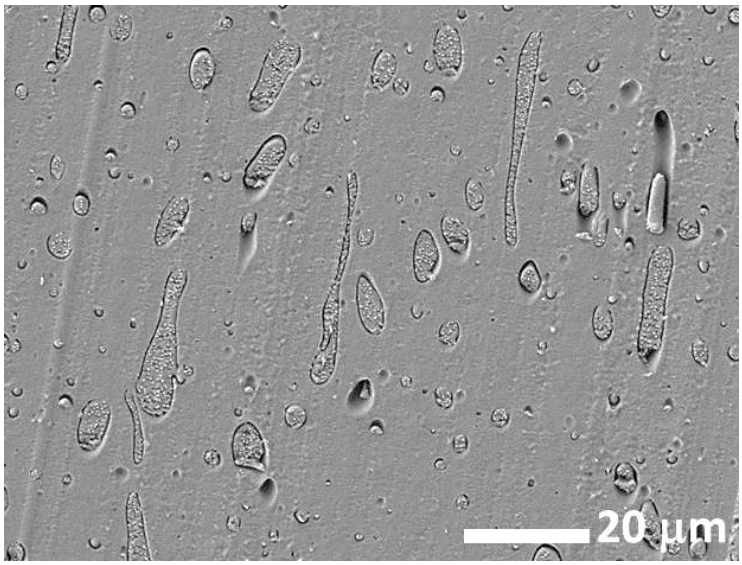


Figure A.4.4. SEM image of PLA/H-LDPE (10/90) with 15 wt.% of micro-silica

The observed elongated morphology in this sample can be attributed to the retarded relaxation and breakup of the dispersed PLA phase due to the presence of micro-silica particles. Kong et al.[12] used the breaking thread method and clearly showed that the presence of silica particles in the dispersed polyamide (PA6) phase retarded considerably the relaxation and breakup of PA6 threads in the PS matrix. The formation of stable and highly elongated domains shifts the continuity limit of the dispersed phase to a lower compositions and broadens the co-continuity region[13, 14]. These are in agreement with the shift and broadening of the co-continuity region observed in this study. The formation of highly elongated stable PLA/silica threads in these samples can also explain the observed finer co-continuous structure of PLA/H-LDPE(30/70) blends containing micro-silica particles.

### A-4.1. Conclusions

The effect of selective localization of micro-silica particles in the PLA phase on the morphology of PLA/H-LDPE phase was studied. The results show that the selective localization of the particles in the PLA phase shifts and broadens the continuity diagram in this blend. These results are shown to be due to the retardation of the relaxation and breakup of the dispersed PLA/silica compared to the dispersed PLA.

### A-4.2. References


1. Fenouillot, F., P. Cassagnau, and J.C. Majesté, *Uneven distribution of nanoparticles in immiscible fluids: Morphology development in polymer blends.* Polymer, 2009. **50**(6): p. 1333-1350.
2. Kontopoulou, M., et al., *The dynamics of montmorillonite clay dispersion and morphology development in immiscible ethylene–propylene rubber/polypropylene blends.* Polymer, 2007. **48**(15): p. 4520-4528.
3. Khatua, B.B., et al., *Effect of Organoclay Platelets on Morphology of Nylon-6 and Poly(ethylene-ran-propylene) Rubber Blends.* Macromolecules, 2004. **37**(7): p. 2454-2459.
4. Austin, J.R. and M. Kontopoulou, *Effect of organoclay content on the rheology, morphology, and physical properties of polyolefin elastomers and their blends with polypropylene.* Polymer Engineering & Science, 2006. **46**(11): p. 1491-1501.
5. Bailly, M. and M. Kontopoulou, *Preparation and characterization of thermoplastic olefin/nanosilica composites using a silane-grafted polypropylene matrix.* Polymer, 2009. **50**(11): p. 2472-2480.
6. Bousmina, M., A. Ait-Kadi, and J.B. Faisant, *Determination of shear rate and viscosity from batch mixer data.* Journal of Rheology, 1999. **43**(2): p. 415-433.
7. Lee, S.H., M. Kontopoulou, and C.B. Park, *Effect of nanosilica on the co-continuous morphology of polypropylene/polyolefin elastomer blends.* Polymer, 2010. **51**(5): p. 1147-1155.
8. Lee, S.H., M. Bailly, and M. Kontopoulou, *Morphology and Properties of Poly(propylene)/Ethylene-Octene Copolymer Blends Containing Nanosilica.* Macromolecular Materials and Engineering, 2012. **297**(1): p. 95-103.
9. Filippone, G., et al., *The role of organoclay in promoting co-continuous morphology in high-density poly(ethylene)/poly(amide) 6 blends.* Polymer, 2008. **49**(5): p. 1312-1322.
10. Wu, G., B. Li, and J. Jiang, *Carbon black self-networking induced co-continuity of immiscible polymer blends.* Polymer, 2010. **51**(9): p. 2077-2083.
11. Nuzzo, A., et al., *Nanoparticle-induced co-continuity in immiscible polymer blends – A comparative study on bio-based PLA-PA11 blends filled with organoclay, sepiolite, and carbon nanotubes.* Polymer, 2014. **55**(19): p. 4908-4919.
12. Kong, M., et al., *Retarded relaxation and breakup of deformed PA6 droplets filled with nanosilica in PS matrix during annealing.* Polymer, 2011. **52**(22): p. 5231-5236.

13. Li, J., P.L. Ma, and B.D. Favis, *The Role of the Blend Interface Type on Morphology in Cocontinuous Polymer Blends.* Macromolecules, 2002. **35**(6): p. 2005-2016.
14. Pötschke, P. and D.R. Paul, *Formation of Co-continuous Structures in Melt-Mixed Immiscible Polymer Blends.* Journal of Macromolecular Science, Part C, 2003. **43**(1): p. 87-141.

# ANNEX 5 LOCALIZATION OF COPPER NANO-WIRES IN POLY(LACTIC ACID)/LOW DENSITY POLYETHYLENE BLENDS*

### A.5.1. Summary

In this part, the effect of kinetic parameters on controlling the localization of copper nanowire (CuNW) in poly(lactic acid), PLA,/Low density polyethylene (LDPE) were studied. The effect of mixing strategy on the localization of the particles was examined by premixing CuNW particles in either phase. In addition, the effect of shear rate and mixing time on the localization and migration of the particles was discussed. Finally, the effect of different localizations of the particles on the morphology of the blend was studied.

## A.5.2.Experimental

### A.5.2.1. Materials

PLA 2003D (Natureworks, Cargil) was purchased from NatureWorks LLC. LDPE (133A) with melt flow indices of 0.25 g/10 min was purchased from Dow Chemicals. All the materials were dried under vacuum at 60 $^{O}$C overnight before being used in the experiments. CUNW particles were synthesized and provided by Prof. Sundararaj's group.

### A.5.2.2. Blend preparation

Masterbatches of PLA/CuNW and LDPE/CuNW were provided by Prof. Sundararaj;s group. The blend samples were prepared using a Brabender internal batch mixer (Plasti-Corder DDR501) with a total volume of 30 cm$^3$ at 180 $^{o}$C under a nitrogen blanket. A 70% mixing chamber fill factor was used. The average shear rate at the mixing speeds of 50 and 100 RPM used in this study were estimated as 25 s$^{-1}$ and 47 s$^{-1}$, respectively [1]. Two different mixing strategies were used to prepare the samples:

*In preparation for *Polymer Communication*

**Pr2:** The addition LDPE/CuNW matsrebatch to PLA.

After mixing, the mixer was stopped and the samples were taken and frozen in liquid nitrogen to freeze-in the morphology and localization of silica particles. All blend samples contain 70 vol.% of PLA phase and 30 vol.% of the LDPE phase. The mentioned wt.% of CuNW particles is based on the total weight of the blend.

### A.5.2.3. Rheological characterization

The samples were compression moulded at 180 $^{o}$C and at 300 kPa in the form of 1.2 mm thick disks of 25 mm diameter under a nitrogen blanket. The rheological measurements were carried out using a stress-controlled rheometer (Physica MCR 301, Anton Paar) with a 25 mm parallel plate geometry at a 1 mm gap at 180 $^{o}$C under nitrogen atmosphere. The stability of the polymer components was examined under the test conditions using a time sweep test. Less than a 7% drop in the complex viscosity and storage modulus was observed in the experimental time scale of 40 minutes.

### A.5.2.4.Transmission electron microscopy (TEM)

The transmission electron microscopy (TEM) analysis of the blend nanocomposites was performed on cryo-ultramicrotomed sample sections using a Tecnai TF20 G2 FEG-TEM (FEI, Hillsboro, USA) at a 200 kV acceleration voltage with the standard single-tilt holder. The images were captured on a Gatan UltraScan 4000 CCD (Gatan, Pleasanton, USA) at 2048×2048 pixels. The samples were cryo-ultramicrotomed to sections of ~70 nm using a Leica EM UC6.

### A.5.2.5. Field emission scanning electron microscopy (FE-SEM)

In order to determine the localization of silica particles, samples from the internal batch mixer were cut and microtomed under liquid nitrogen using a microtome (Leica-Jung RM 2165). Then the sample surface was coated with gold and the morphology was observed with a Field Emission Scanning Electron Microscope (JSM 7600F, JEOL).

### A.5.2.6. Continuity measurements

The continuity level of the phases in the blend samples was determined by cutting three samples of approximately 8×10×5 $mm^3$ and weighing about 0.4–0.5 gm, from each blend sample. Then either the PE or PLA phase was extracted from these samples using boiling cyclohexane or chloroform, respectively. The continuity level of the extracted phase (A) was determined as:

$$\%\textbf{Continuity of A} = \frac{\textbf{Extracted weight from the sample}}{\textbf{Initial weight of A in the sample}} \times \mathbf{100}$$

The reported values are an average of the three different measurements.

## A.5.3. Results and Discussion:

### A.5.3.1. Material characterization:

Figure A.5.1 shows the synthesized CuNW particles. The synthesized nanowires had averages diameter and length of 30 nm and 1.5µm, respectively.

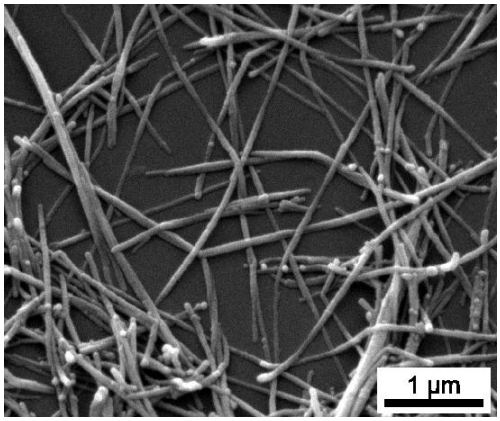


Figure A.5.1. SEM image of the CuNW particles.

### A.5.3.2. Rheological Properties of PLA and LDPE and PLA/CuNW and LDPE/CuNW mixtures

Figure A.5.2 shows the complex viscosity of PLA/CuNW and LDPE/CuNW mixtures as a function of the angular frequency.

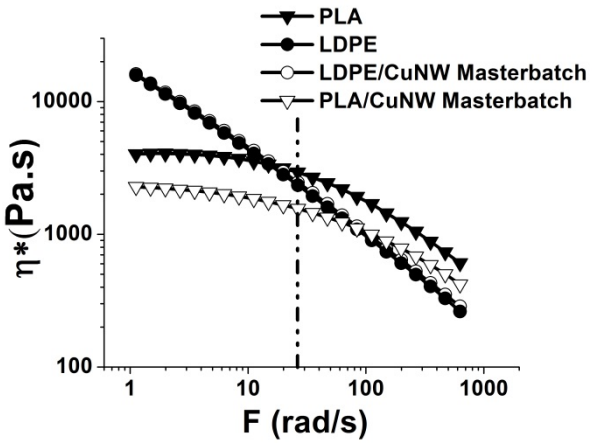


Figure 5.2. The complex viscosities of PLA, LDPE and their composites with CuNW particles. The dashed line represents the average shear rate of mixing[1].

PLA shows a Newtonian plateau at low angular frequencies but LDPE exhibit shear thinning behavior even at very low frequencies which is associated with the high level of long chain branching in its structure [2]. The viscosity of PLA/CuNW masterbatch is less than the neat PLA which can be attributed to the decrease in the molecular weight due to the sonication during masterbatch preparation [9]. The rheological properties of LDPE/CuNW were found to be almost identical to LDPE. To better understand these results, the dispersion of CuNW particles in PLA/CuNW and LDPE/CuNW masterbatches were studied by TEM and the results are shown in Figure A.5.3.

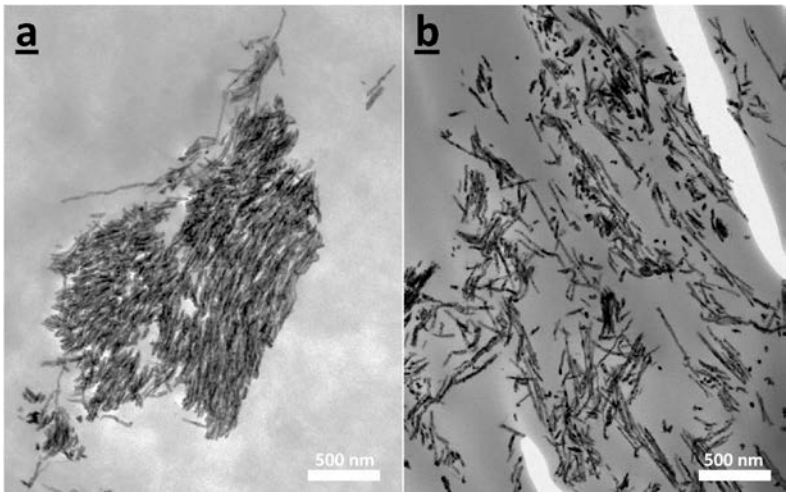


Figure 5.3. Dispersion of CuNW particles in: (a) LDPE/ 4 wt.% CuNW masterbatch, (b) PLA/1.2 wt.% CuNW masterbatch.

As can be seen, CuNW particles exist in the form of agglomerates in LDPE/CuNW. Such poor dispersion of CuNW particles in LDPE can explain why the addition of 4 wt.% of CuNW could not influence its rheological behavior. On the other hand, a good dispersion of CuNW particles in PLA was observed which indicates better interaction of PLA and CuNW particles.

### A.5.3.2. Thermodynamics of Localization of CuNW Particles in PLA/LDPE Blends

The thermodynamic localization of solid inclusions in multiphase systems can be predicted by the Young's equation:

$$\boldsymbol{\omega} = \frac{\boldsymbol{\gamma_{1s}-\gamma_{2s}}}{\boldsymbol{\gamma_{12}}} \qquad \text{Eqn.1}$$

Where $\gamma_{1s}$, $\gamma_{2s}$ and $\gamma_{12}$ are the interfacial tensions between: polymer 1 and solid, polymer 2 and solid; and polymer 1 and 2. If ω is greater than 1, the localization of silica particles in phase 2 is thermodynamically preferred while for ω < -1, the thermodynamic equilibrium localization of solid particles should be in phase 1. On the other hand, when -1<ω< 1, the localization of solid particles at the interface is thermodynamically preferred.

The interfacial tensions between components can be estimated using the surface energy data of the components. However, determining the surface energy of metals such as copper is very challenging. For instant, the surface energy of solid and liquid copper at the melting point (1083 ℃) were experimentally determined as 1.52 and 1.295 $J.m^{-2}$ respectively[3]. Using molecular dynamic simulation, Jia et al. [4] estimated the surface energy of copper at 180 ℃ as 1.77 $J.m^{-2}$. Considering that most of polymer melts have surface energy in order of 30 $mJ/m^{-2}$ at this temperature[5, 6] indicates the high surface energy of copper. Moreover, to estimate the interfacial tension between the components, the dispersive and polar contributions to the surface energy are required which has not been reported for copper yet. This clearly indicates the inapplicability of Young's equation in the systems containing high surface energy metals.

### A.5.3.3. Effect of Mixing Strategy on the Localization of CuNW particles in PLA/LDPE

In the previous studies, changing the mixing strategy was shown to be an effective method to study the migration and localization of solid inclusions. The localization of CuNW particles in PLA/LDPE prepared by Pr1 and Pr2 are shown in Figure A.5.4.

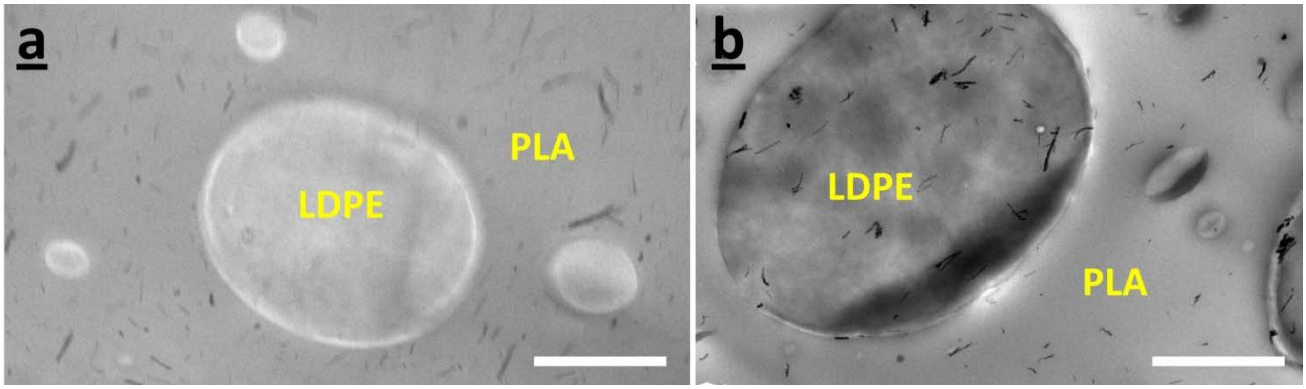


Figure 5.4. TEM image of PLA/LDPE (70/30) blend prepared by: (a) Pr1, (b) Pr2. The white scale bars show 2μm.

As can be seen, when CuNW particles were premixed with PLA phase, they were found to remain localized in the PLA phase and no CuNW particle was observed in the PE phase. However, when CuNW particles were initially dispersed in the LDPE phase, the particles were found to be localized in both PLA and LDPE phase. Comparing these results clearly indicate that the particle tend to migrate from LDPE to PLA phase. This can be attributed to the higher polarity of PLA compared to LDPE. The presence of some CuNW particles in the LDPE phase in the sample prepared by Pr2 can be attributed to the kinetic effects. It was previously shown that increasing the shear rate and mixing time can enhance the migration of solid inclusions from one phase to the other. The effect of these parameters will be investigated below.

### A.5.3.4. Effect of Shear Rate and Mixing Time on the Localization of CuNW Particles in PLA/LDPE

To examine the effect of shear rate on the migration of CuNW particles, LDPE/CuNW masterbatch was melt mixed with PLA (according to Pr2) at 100 RPM. Figure A.5.5 shows the localization of CuNW particles in this sample.

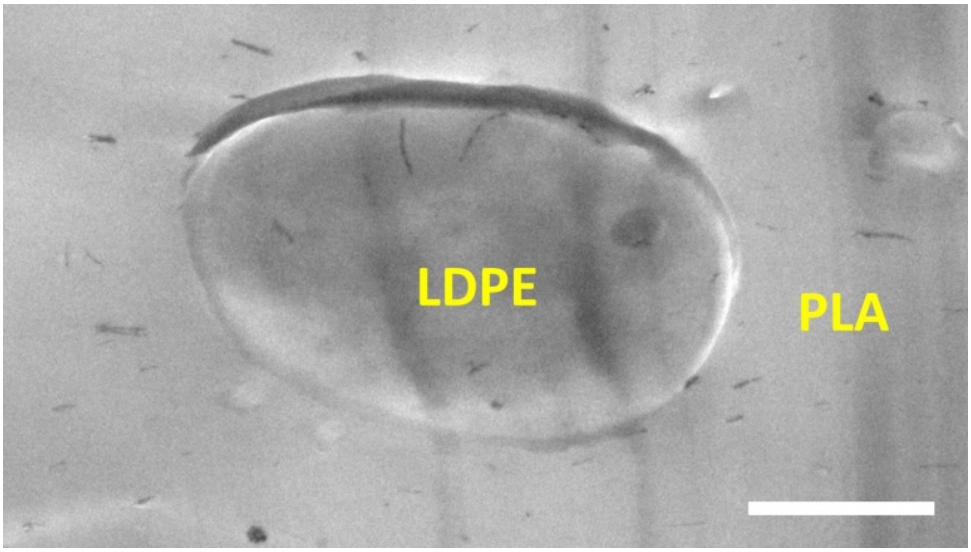


Figure A.5.5. The localization of CuNW particles in PLA/LDPE (70/30) prepared by P2 at 100 RPM. The white scale bar shows 2μm.

As can be seen, increasing the shear rate by a factor of almost 2 clearly enhanced the migration of CuNW particles and only few particles can be seen in the LDPE phase. Increasing the mixing time has also been shown to enhance the migration of solid inclusions. To study the effect of mixing time, PLA/LDPE(70/30) /CuNW was prepared according to Pr2 at 20 minutes. The results are shown in Figure A.5.6. Again, it can be seen that increasing the mixing time by a factor of 2 resulted in the migration of more CuNW particles from the LDPE phase to PLA.

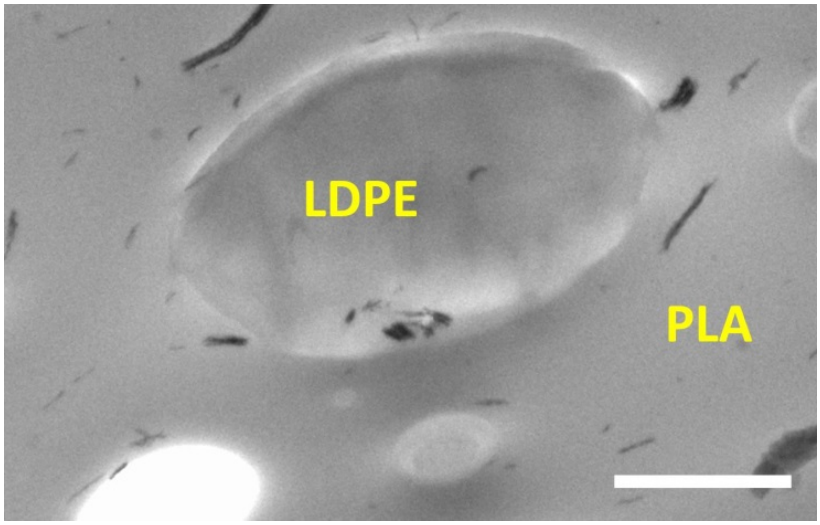


Figure A.5.6. The effect of mixing time on the localization of CuNW particles in PLA/LDPE(70/30)/CuNW prepared by Pr2 at 20 min of mixing.

### A.5.3.5. Effect of Different Localizations of CuNW Particles on the Morphology of PLA/LDPE Blends

The effect of different localizations of CuNW particles on the morphology of PLA/LDPE (70/30) is shown in Figure A.5.7.

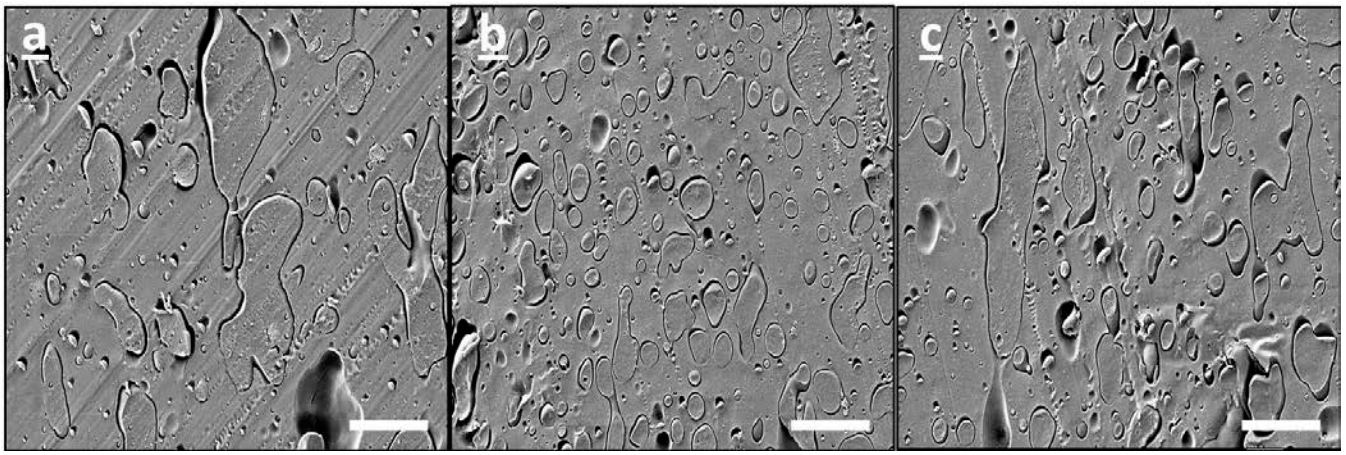


Figure A.5.7. The effect of different localization of CuNW particles on the morphology of PLA/LDPE(70/30): (a) No CuNW, (b) 1 wt.% CuNW in PLA phase (prepared by Pr1), (c) CuNW in the PLA and LDPE phase (prepared by Pr2). The white scale bars show 10 μm.

It can be seen that the localization of CuNW particles in the PLA matrix reduced the LDPE phase size. To quantify this effect, continuity of LDPE phase in these samples was determined using selective extraction of LDPE using boiling cyclohexane. It was found that when CuNW particles were initially distributed in the LDPE phase, the continuity of LDPE was reduced to 70% compared to 85% of the blend without CuNW particles. However, when the particles are only localized in the PLA phase, the continuity of LDPE phase dropped to 43%. These results indicate that the presence of CuNW particles in the matrix phase reduced the coalescence of the dispersed LDPE phase. The reduced phase size of the dispersed phase by the localization of solid inclusions in the matrix has been attributed to the increase in the viscosity of the matrix and solid barrier effect[7, 8]. Considering the rheological properties of PLA/CuNW, Figure A.5.2, it can be seen that the viscosity of PLA/CuNW is even lower than the neat PLA phase. Therefore, the increase in the viscosity could not be the effective mechanism of the phase reduction. Consequently, the observed decrease in the LDPE continuity can only be attributed to the solid barrier effect.

### A.5.4.Conclusion

The effects of kinetic parameters on the localization of CuNW particles in PLA/LDPE blends were studied. It was found that when the particles were initially dispersed into the PLA phase, the particles remained in the PLA phase but when they were dispersed in the LDPE phase, some particles migrated to the LDPE phase. These results indicate a higher affinity of the particles to the PLA phase. Increasing the shear rate and mixing time were also found to enhance the migration of CuNW particles from the LDPE phase to PLA. It was also found that the localization of CuNW particles in the PLA phase reduced the LDPE phase continuity due to the solid barrier effect.

### A.5.5.References


1. Bousmina M, Ait-Kadi A, and Faisant JB. Journal of Rheology 1999;43(2):415-433.
2. Gotsis AD. Branched Polyolefins. In: Kontopoulou M, editor. Applied Polymer Rheology: Polymeric Fluids with Industrial Applications. United States: John Wiley & Sons, 2012. pp. 67.
3. Sander D and Ibatch H. Physics of Covered Solid Surfaces. In: Bonzel HP, editor. Physics of Covered Solid Surfaces, vol. 42. Berlin: Springer, 2002. pp. 4.4.-1.
4. Ming J, Yanqing L, Zhongliang T, and Yexiang L. Modelling and Simulation in Materials Science and Engineering 2009;17(1):015006.
5. Wu S. Journal of Colloid and Interface Science 1969;31(2):153-161.
6. Wu S. The Journal of Physical Chemistry 1970;74(3):632-638.
7. Fenouillot F, Cassagnau P, and Majesté JC. Polymer 2009;50(6):1333-1350.
8. Taguet A, Cassagnau P, and Lopez-Cuesta J-M. Progress in Polymer Science 2014.
9 Reich G., European Journal of Pharmaceutics and Biopharmaceutics 1998, 45:165.